12. SITE 1118[1]

Shipboard Scientific Party[2]

SITE 1118

Hole 1118A (RCB):
   9°35.110'S, 151°34.421'E; 2303.6 mbsl
   0–205.0 mbsf drilled without coring; 205.0–926.6 mbsf cored;
   466.21 m recovered (65%)

Site 1118 is 1.8 km north of a major south-dipping normal fault system that is antithetic to, and bounds the rift basin above, the low-angle fault dipping north from Moresby Seamount. The location was selected in order to drill through the thick synrift section onlapping the northern margin and to penetrate an angular unconformity into north-dipping reflectors deep in the inferred prerift forearc basin sequence. The site is ~9 km due south of Site 1109 and has similar objectives in common to it and Site 1115, namely to determine (1) the sedimentology, biostratigraphy, and vertical-motion history of the northern margin, and (2) the nature of the forearc basin and basement sequence.

Results from Site 1118 record the progressive subsidence of a lower Pliocene, subaerially eroded and tropically weathered, landmass. A conglomerate of dolerite with minor basalt was recovered and imaged with FMS below 873 mbsf. Iron oxides and well-rounded clasts reveal that the dolerite, similar to that encountered at Site 1109 (although locally more pegmatitic), was exposed to subaerial alteration. Shearing and veining fragmented and partially brecciated the dolerite, which was deposited as a poorly sorted, probably fluvial conglomerate mixed with various clasts and sediment, including paleosols.

The dolerite conglomerate is overlain to 857 mbsf by a sequence of lower Pliocene limestones, calcareous paraconglomerates, and a volcaniclastic sandstone that was deposited in a marine lagoon with abundant calcareous algae. This sequence is well marked in the geophysical logs and by highs in the $CaCO_3$ profile of >80 wt%. A VSP shows that the

dolerite-limestone section corresponds to a strong reflector at the base of the sedimentary sequence that mantles underlying northward-dipping reflectors, which were not penetrated.

The Gauss/Gilbert Chron boundary (3.58 Ma), occurring at 846–850 mbsf, dates an upward-fining sequence disconformably above the limestones as all middle Pliocene and younger, in agreement with paleontological data (Biozones N20–N21 and NN16A–NN19A through the top of the cored sequence at 205 mbsf). The lower sedimentary section records a significant terrestrial input, including wood fragments, confirmed by the C/N ratio, which indicates a mixed-marine and terrigenous source of organic carbon. The whole sequence records turbiditic and hemipelagic sedimentation. It comprises mixed volcaniclastic sandstones, siltstones, and minor claystones, and then mostly siltstones and claystones interbedded with turbiditic sandstones and siltstones that decrease in proportion upward. The orientations of the subhorizontal maximum axes of the ellipsoids of magnetic susceptibility (corrected for bedding dip and core orientation) between 490 and 680 mbsf suggest an east-southeast–west-northwest–directed paleocurrent during sedimentation, almost perpendicular to the present-day slope.

The sedimentation rate from 3.58 to 2.58 Ma (387.5 mbsf) was 479 m/m.y., the highest encountered during Leg 180, with benthic foraminifers revealing an upper bathyal (150–500 m) paleowater depth. Between 2.58 and 1.95 Ma (288 mbsf), the sedimentation rate decreased to 155 m/m.y., and the paleodepth was middle bathyal (500–2000 m) to at least 205 mbsf. Apparently, rapid subsidence since 3.6 Ma was accompanied by sufficient sediment supply to limit deepening of the seafloor until 2.6 Ma. High porosities slowly decreasing from 50%–60% at 205 mbsf to 40%–50% at 800 mbsf likely reflect underconsolidation related to the observed high sedimentation rates.

Volcanic ash and volcaniclastic sands are ubiquitous throughout the Pliocene sedimentary section, but especially so in the portion dated to between 3.0 and 3.6 Ma in which a predominance of rhyodacitic glass reflects explosive acidic volcanism probably associated with rifting of the continental arc.

Most of the sedimentary section is undeformed with nearly horizontal beds and shows compaction-related minor faults as well as common slump folds. The abundance of synsedimentary features on such a nearly level seafloor suggests an unstable area periodically shaken by earthquakes and affected by mass movement.

As seen in other northern sites drilled during Leg 180, the variations in interstitial water constituents reflect the oxidation of organic matter mediated by microbial activity and the concomitant early diagenesis of biogenic carbonates. Volcanic alteration and authigenesis are important processes, particularly in the lower part of the hole. The abundance of volcaniclastic sands and the higher porosities in the lower part of the hole, when combined with the high temperature gradient (~63°C·km^{-1}), greatly influence the pore-water chemistry. In particular, the dissolved silica, lithium, and strontium show higher concentrations than might otherwise be expected. In addition, temperature measurements in the open hole during a logging run suggest migration of warm fluids at 700–800 mbsf.

Both methane and ethane, whose ratio is between ~5000 and ~1600, are present down to ~700 mbsf, below which ethane is not detected. The highest concentrations in these two volatile hydrocarbons occur where sulfate disappears from the interstitial water, attesting to a biogenic origin.

Bacteria population numbers and dividing and divided cells decrease rapidly with increasing depth and conform to the general model for their distribution in marine sediments. In extending their known distribution to 842 mbsf at this site, the deepest samples so far obtained, there is an indication that numbers are decreasing more rapidly than the model predicts, resulting in a sigmoidal depth distribution in these sediments.

OPERATIONS

Hole 1118A (ACE-1C)

During the ~11.5-nmi transit from Site 1117, a rotary core barrel (RCB) bottom hole assembly (BHA) with drilling jars and a mechanical bit release (MBR) was assembled and run down to the seafloor. After the positioning beacon was deployed (1830 hr on 28 July 1998), Hole 1118 was spudded at 2030 hr on 28 July. A seafloor depth of 2303.6 meters below sea level (mbsl) was determined by reduction in drill-string weight. This was 3.0 m shallower than the 3.5-kHz precision depth recorder (PDR) depth. With a center bit in place, we drilled without coring to 205.0 meters below seafloor (mbsf) with an average rate of penetration (ROP) of 51.3 m/hr.

Once the center bit was retrieved and the hole circulated with a 20-bbl gel mud sweep, RCB coring began at 0330 hr on 29 July (Table **T1**). Cores 1R through 73R were taken from 205.0 to 897.5 mbsf (Table **T2**). When the driller raised the bit off bottom to recover Core 73R, he observed 30,000-lb overpull, high torque, high pump pressure, and 3.0 m of fill in the bottom of the hole. Core 74R also had similar overpull and fill. Coring was stopped after reaching 926.6 mbsf (Core 76R) to allow enough time for a wiper trip, hole conditioning, and a full wireline logging program. Overall ROP for the cored portion of the hole was 15.3 m/hr. Total recovery for the hole was 466.21 m (65%). After circulating the hole clean with a 40-bbl pill of bentonite gel mud, a wiper trip was conducted up to 98.6 mbsf. When the bit was lowered back down, 36.0 m of fill was encountered in the bottom of the hole. We decided not to take the time to clean out the fill and released the bit at 892.6 mbsf. In preparation for logging, the hole was displaced with 300 bbl of sepiolite mud and the drill string raised up to 98.6 mbsf. Overpulls of 20,000–30,000 lb were required to pull the pipe from 491.6 to 434.6 mbsf; therefore, an additional 20-bbl pill of 10.5-ppg mud was spotted in the pipe before continuing up to logging depth.

We began rigging up for logging at 1030 hr on 3 August. The first logging run was with the triple-combo tool and was able to reach 887.6 mbsf, which was 5.0 m above where the bit was released. The loggers requested that the pipe be raised 20 m to log more of the shallow section, but this was rejected because the pipe was experiencing up to 30,000-lb overpull. A second pass was made with the triple combo to get more detailed temperature data, and the tool was stopped for 10 min each at 410.0, 620.0, and 830.0 mbsf.

After the triple combo run was finished, the Formation MicroScanner (FMS) sonic tool string was run and also reached 887.6 mbsf. The lowermost 50.0 m of the hole was logged twice and the logs were collected up to the pipe depth (98.6 mbsf). Caliper data from the FMS-sonic tool indicated some tight spots (4–5 in diameter) as far down as 298.6 mbsf. During the FMS-sonic run, the drill string began taking weight (10,000–

Table T1. Site 1118 coring summary, **p. 163.**

Table T2. Site 1118 coring summary by section, **p. 165.**

20,000 lb) and overpull of 10,000–20,000 lb. After the FMS-sonic run was finished and it was in the pipe being retrieved, the pipe was raised slightly but could only be lowered back down to within 6 in of the dual-elevator stool even with slow circulation (higher circulation could not be used with the logging tool inside the drill pipe). We decided to pull back up about 1.0 m with the pipe hung off the elevator bales and retrieve the FMS-sonic tool string by pulling it through the blocks. Once the tools were laid down, the top drive was picked up and the pipe lowered back down to 309.6 mbsf; however, no resistance was encountered and the pipe was pulled back to 107.6 mbsf in preparation for the vertical seismic profile (VSP) logging with the well seismic tool (WST). The WST was run in the hole but could not pass 691.6 mbsf (because of its light weight). A total of 20 stations were occupied between 691.6 and 107.6 mbsf. The WST was retrieved and logging was completed at 1845 hr on 4 August.

The drill string was lowered to 395.6 mbsf and the hole was displaced with 144 bbl of 10.5 ppg mud. After the drill pipe was retrieved and the BHA taken apart and secured, the positioning beacon was recovered at 0337 hr on 5 August. At 0430 hr on 5 August the vessel began the transit to Sydney, Australia. After the 6.04-day transit (1524 nmi), Leg 180 ended with the first line ashore in Sydney, Australia, at 0530 hr on 11 August 1998.

LITHOSTRATIGRAPHY

Within the ~926.6-m-thick succession drilled at Site 1118 eight lithostratigraphic units were recognized on the basis of sediment or rock type, grain size, sedimentary structures, color, smear slides, thin sections, bulk mineralogy (X-ray diffraction [XRD]), and carbonate content, aided by geophysical logs (Fig. **F1**). Smoothed grain-size trends are shown in Figure **F2**. No coring took place in Hole 1118A until 205.0 mbsf. However, part of this missing interval (100.0–205.0 mbsf), reconstructed by using geophysical logs, was found to be mainly muddy sediments with rare thin (<15 cm), more sandy layers (see **"Downhole Measurements,"** p. 45). The Formation MicroScanner (FMS) images show that the basal unit recovered is a sedimentary conglomerate rather than in situ igneous rock as initially inferred from the limited recovery. Details of the lithostratigraphic units present are as follows:

Lithostratigraphic Unit I

Description: silty claystone and clayey siltstone interbedded with
    sandstone and siltstone
Interval: Cores 180-1118A-1R through 18R
Depth: 205.0–377.8 mbsf
Age: late Pliocene to Pleistocene?

From 205.5 to 255 mbsf RCB recovery was minimal. Beneath this, recovery was good to excellent (see the core description forms, or "barrel sheets," in the **"Core Descriptions"** contents list).

Lithostratigraphic Unit I is characterized by a relatively homogenous succession of mainly greenish and grayish silty claystone and clayey siltstones interbedded with graded sandstones and siltstones. Carbonate values of the fine-grained sediments of Unit I vary between 2.4 and 16.2 wt% with a few more calcareous samples being present (35.5

F1. Lithology of Hole 1118A, **p. 55.**
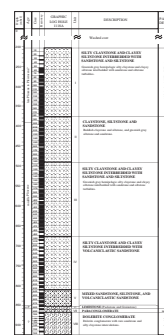
F2. Grain-size trend in units observed in Hole 1118A, **p. 56.**
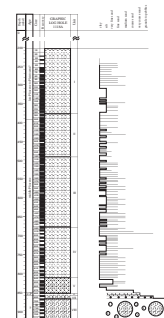
and 72.5 wt% in Cores 7R and 8R; see "CaCO₃, Sulfur, Organic Carbon, and Nitrogen," p. 40). In general, claystones, grayish siltstones, greenish siltstones, and paler siltstones alternate every few centimeters to tens of centimeters. Colors are mainly greenish or grayish in the upper part of the unit. Graded sandstones/siltstones tend to be darker green and greenish gray in color (e.g, Section 12R-5) than the clayey siltstones and silty claystones that are typically pale shades of the same colors. Slightly reddish intervals appear from the middle part of the unit downward (~310 mbsf).

The following lithologies are present:

Bioturbated Silty Claystone and Clayey Siltstone

Greenish gray silty claystone and clayey siltstone form much of the background sediment. Typically, these sediments are calcareous and contain volcanic glass and detrital grains, scattered foraminifers, and rare small (several millimeters) shell fragments. The silty claystones are mainly moderately to highly bioturbated. Small *Chondrites* burrowing predominates, but larger *Zoophycos* burrowing is locally present (Fig. F3). Many of the small (<5 mm) burrows are lensoidal in shape. In addition, sulfide reduction spots (with reduction halos) and color mottling are visible.

Smear slides reveal the presence of common nannofossils and planktonic foraminifers together with feldspar, biotite, volcanic glass, and accessory minerals, particularly hornblende (see "Site 1118 Smear Slides," p. 92). The XRD analysis of the fine-grained sediment component (claystone and silty claystone) revealed mainly plagioclase, calcite, pyroxene and minor amphibole, illite, smectite?, chlorite, and possible mixed-layer clays. Dolomite and pyrite are found sporadically (Table T3). Below 290 mbsf calcite, plagioclase, and quartz predominate in most samples with minor amounts of clay minerals (i.e., chlorite and illite).

Reddish Silty Claystone

These are similar to the above sediments, but tend to be well laminated, reddish, and exhibit little or no burrowing (Section 9R-1). These intervals range from several centimeters to tens of centimeters in thickness and become relatively numerous below 335.0 mbsf (e.g., interval 180-1118A-14R-7, 79–90 cm), although the reddish colors are always subordinate within Unit I. Smear slides contain nannofossils and planktonic foraminifers together with feldspar, biotite, volcanic glass, and accessory minerals, including inorganic calcite (see "Site 1118 Smear Slides," p. 92).

Siltstone-Silty Claystone

Very thin beds and laminae of dark greenish gray siltstones occur throughout the unit. Typically, each has a structureless or laminated silty base several millimeters thick overlain by almost homogenous dark silty claystone. The tops of individual beds are commonly burrowed. Elsewhere, the siltstone is extensively burrowed, obscuring much of the primary structure. The burrows are infilled with clayey siltstone. Smear slides are seen to be similar in composition to the lithologies discussed above (see "Site 1118 Smear Slides," p. 92).

F3. Bioturbated silty claystone with *Zoophycos* burrows, p. 57.
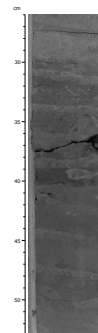

Table T3. XRD analysis of bulk fine-grained sediments, p. 178.

Sandstone-Siltstone-Clayey Siltstone

Throughout the unit there are occurrences of normally graded sandstone as very thin beds and laminae ranging from 0.5 through 3.5 cm thick (average 2 cm). Colors range from dark greenish gray to dark gray. Most beds begin with scoured bases. These bases are mainly subplanar, but are locally irregular. Rarely, isolated fine- to medium-grained sandstone is present in small lobes at the base of individual sandstone beds (e.g., interval 180-1118A-6R-6, 125 cm). In many cases the overlying sandstone bed was not recovered. Where recovered, the fine sandstone grades upward to clayey siltstone, which is usually structureless. Occasionally, planar lamination, ripple, or wavy lamination is present (e.g., interval 180-1118A-6R-1, 38–38.5 cm). This sediment is typically burrowed such that bedding is commonly obscured.

In smear slides the following poorly sorted grains were observed: nannofossils, planktonic foraminifers, sponge spicules, quartz, plagioclase, biotite, calcite, pyrite, accessory minerals (e.g., hornblende), volcanic rock fragments, and detrital organic matter (see "Site 1118 Smear Slides," p. 92). Also, rare carbonaceous detritus was noted at the base of a few fine-grained, graded beds. In addition, one impregnated thin section of sandstone revealed quartz, plagioclase, planktonic foraminifers, biotite, basaltic grains (flow banded), glassy basalt, and rare benthic foraminifers set in a clay-rich matrix. Occasional burrows are pyrite filled (see "Site 1118 Thin Sections"). XRD analysis also indicates pyrite in several samples (Table T3).

Soft-Sediment Deformation

Soft-sediment deformation was observed in parts of Unit I (see Fig. F4). These structures are intraformational and adjacent to undeformed beds. This contrasts with faulting, folding, and other structural features that follow deposition and partial lithification (see "Structural Geology," p. 28). The inferred soft-sediment deformation features were first seen as locally inclined lamination sharply overlain by subhorizontal laminae (e.g., intervals 180-1118A-9R-3, 33–34 cm, and 13R-5, 80–104 cm). Soft-sediment deformation structures then become larger and more extensively developed downhole (Sections 14R-1 through 14R-5; 250–340 mbsf). Fold axes are subhorizontal, and the deformed interval includes several small faults (i.e., interval 180-1118A-14R-1, 60–149 cm). Several of the deformed zones are overlain by small injection structures (intervals 180-1118A-14R-2, 15–45 cm, and 14R-3, 60–95 cm). The highly deformed and folded intervals are separated by less deformed inclined beds of laminated silty claystone and clayey siltstone (Fig. F5). Beneath the zone of deformation, beds are less deformed but show some evidence of sediment dewatering (interval 180-1118A-4R-5, 35–49 cm). In addition, fluid escape pipes were also noted in intervals 180-1118A-15R-3, 46–57 cm, and 16R-6, 51–59 and 82–87 cm.

Interpretation

Unit I accumulated during late Pliocene (to Pleistocene?) time in an inferred middle bathyal water depth (500–2000 m) at an estimated average sedimentation rate of 155 m/m.y. (see "Sediment Accumulation Rate," p. 33). The succession was mainly deposited by low-density turbidity currents alternating with hemipelagic mudstone. Flute casts formed by erosion at the head of a turbidity current, or load structures

F4. Contorted and deformed silty claystone and siltstone, p. 58.
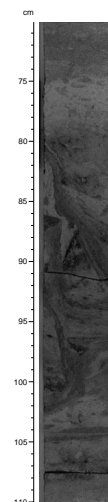
F5. Graded siltstones and clayey siltstone, p. 59.
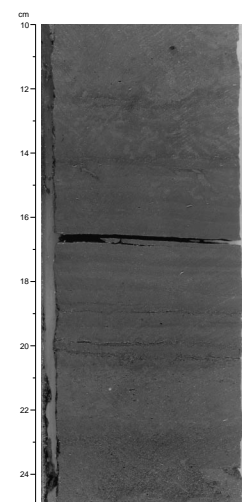
caused by differential compaction of sand and clay, are occasionally preserved at the base of individual beds. The bottom sediment was well oxidized, judging from the common bioturbation. A single interval of high carbonate content (72.5 wt%) combined with elevated organic carbon and sulfur is interpreted as a bioclast-rich interval associated with abundant pyrite (see "Discussion," p. 38, in "Inorganic Geochemistry"). These bioclasts were possibly formed in a shallower water (but still pelagic) setting and then redeposited by turbidity currents. Below 330.0 mbsf the rare reddish, less burrowed intercalations are similar to more extensive reddish sediment found in Unit II (see "Lithostratigraphic Unit II," p. 7) and may indicate times of relatively oxidizing bottom-water conditions. The mineralogy and petrography indicate relatively constant provenance from a basic-acidic volcanic terrain, based on the abundance of plagioclase and feldspar and small lithoclasts of basic volcanic rock seen in thin section. Tectonic instability, manifested by slumping, peaked at ~330.0–340.0 mbsf.

The geophysical logs (triple combo) reveal large-scale trends and variation in the succession (see "Downhole Measurements," p. 45). Above the cored interval (0–205 mbsf) alternating clay-rich and more sandy intervals are present. The geophysical logs suggest that the upper interval of minimal recovery (200.0–255.0 mbsf) is relatively clay rich, mainly based on the combined gamma-ray log and neutron porosity logs. The diameter of the borehole decreased here, suggesting the presence of abundant swelling clay. Some mixed-layer clay was detected in the adjacent interval lower in the succession that was recovered. Beneath 205.0 mbsf there is a relatively dense (calcareous?) clay-rich unit, followed from 291.5 to 289.8 mbsf by a more bedded, still clay-rich succession. Possible slumps or slides are imaged on the FMS from 285.5–290.5 mbsf, marked by apparently deformed bedding inclined in variable directions. Below 292.0 mbsf the succession apparently becomes generally more sandy with a pronounced sandy interval ~20 cm thick at 297.0 mbsf. More possible slumps or slides are seen from 308 to 309 mbsf on the FMS images. Below 347.0 mbsf, the succession becomes more clay rich with a carbonate-rich bed (<30 cm) at 363.0 mbsf. A large increase in the K/Th ratio at 376.5 mbsf suggests the presence of sandy volcaniclastic sediment at this level.

Lithostratigraphic Unit II

Description: reddish claystones and siltstones, and greenish gray siltstones and sandstones
Interval: Sections 180-1118A-19R-1 through 30R-7
Depth: 377.8–492.35 mbsf
Age: middle Pliocene to late Pliocene (>2.5 Ma)

Lithostratigraphic Unit II is defined by the presence of distinctive intercalations of reddish silty claystone and clayey siltstone within greenish gray silty claystone, clayey siltstone, siltstone, and sandstone. In addition, some graded sandstone intervals are thicker (>5 cm) than those of Unit I. Furthermore, intervals of soft-sediment deformation were only rarely observed in Unit II. Calcium carbonate values in fine-grained sediment vary from 0.45 to 16.5 wt% and show no systematic variation downhole in Unit II (see "CaCO$_3$, Sulfur, Organic Carbon, and Nitrogen," p. 40). Otherwise, the lithologies present are very similar to those of Unit I and will be summarized only briefly.

The following lithologies are present in Unit II:

Reddish or Brownish Silty Claystone and Clayey Siltstone

Typically, the intervals in which the dominant color is reddish or reddish brown, range from tens of centimeters to several meters thick. Commonly, these intervals are well laminated with relatively little or no bioturbation (Fig. F6). The reddish intervals are interbedded with grayish to greenish sandstones, siltstones, and some claystones (see "Dark Greenish or Grayish Clayey Siltstones," p. 8). Individual laminae are thin to thick and defined by subtle color changes. Very rare foraminifers are present. Good examples of well-laminated intervals are as follows: intervals 180-1118A-19R-4, 0–55 cm, and 22R-1, 0–30 cm; Sections 22R-2 and 3; intervals 180-1118A-23R-3, 25–35 cm; 23R-5, 0–89 cm; 24R-7, 20–66 cm; 25R-1, 22–25 cm; 25R-6, 68–124 cm; 25R-7, 0–49 cm; 25R-CC, 0–12 cm; and 26R-1, 0–23 cm; Section 27R-6; and interval 180-1118A-28R-1, 0–108 cm. In addition, Cores 28R and 29R include a number of reddish brown finely laminated intervals 5–20 cm thick.

Examination of smear slides reveals nannofossils, foraminifers, quartz, feldspar, mica, volcanic glass, volcanic rock fragments, and accessory minerals (e.g., hornblende; see "Site 1118 Smear Slides," p. 92). Pyrite is relatively rare compared to the darker greenish gray sediments. The XRD analysis of the fine-grained sediment revealed a very constant composition of calcite, plagioclase with minor amphibole, pyroxene, pyrite, and clay minerals (mainly chlorite and illite). Minor mixed-layer clay may also be present (Table T3).

Dark Greenish or Grayish Clayey Siltstones

These intervals are subordinate, estimated at 15%–25% of the recovered sedimentary rocks within this unit. Individual beds begin with planar-laminated, ripple- or wavy-laminated siltstone. Locally, starved ripples are present (interval 180-1118A-26R-4, 70–72 cm). The bed bases are sharp and commonly scoured. The upper parts of individual beds are homogeneous, dark gray or greenish gray, grading into silty claystone. The tops of individual beds are burrowed, and burrowing locally extends into the body of the bed above.

Rarely, fluidization and small fluid-escape pipes were noted in the siltstone. These features take the form of thin (<1 mm), wispy vertical linear veins just above the base of individual siltstones. The individual vertical linear vein structures are ~3–5 cm long and ~2–4 mm apart (e.g., interval 180-1118A-25R-3, 60–66 cm). These structures are unusual and were not noted in similar sediments in other holes during Leg 180.

Smear slides of this facies revealed quartz, feldspar, biotite, volcanic rock fragments, accessory minerals (e.g., hornblende), calcite, pyrite, nannofossils, and mainly planktonic foraminifers (see "Site 1118 Smear Slides," p. 92).

Graded Sandstone/Siltstone

From 415.0 mbsf normally graded sandstones are rarely more than a few centimeters thick. However, occasional thicker beds are present. For example, in interval 180-1118A-23R-4, 0–62 cm, a single sandstone bed (the lower 7 cm) grades into fine-grained sandstone (25 cm thick; Fig. F7), then into siltstone (30 cm thick). Sole marks (flutes and loads) are present at the base of some of these beds (e.g., interval 180-1118A-23R-6, 20–21 cm) and, in addition, low-angle ripple lamination (e.g., intervals 180-1118A-27R-5, 23–25 and 84–86 cm, and 27R-6, 90–92 cm), and wavy

F6. Laminated silty claystone and clayey siltstone, p. 60.
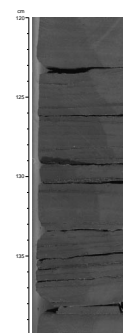
F7. Normal-graded beds with flutes mark at base, p. 61.
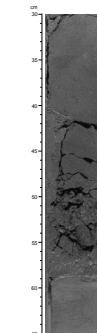
lamination (interval 180-1118A-27R-6, 96–98 cm) are locally present in the lower parts of individual beds. The sandstone rarely also shows evidence of fluid injection into overlying siltstone.

Smear slides reveal essentially the same compositions as within the generally finer grained sediments described above (see "Site 1118 Smear Slides," p. 92). In addition, thin sections of very fine grained sandstone from the base of normal-graded units revealed the following composition: angular grains of quartz, plagioclase, biotite, rare palagonite, planktonic foraminifers, fresh basaltic grains (with flow-banded feldspar microphenocrysts), rare chloritic grains, and common pyrite, especially within burrows, and planktonic foraminifer tests (Fig. F8; see "Site 1118 Thin Sections").

Soft-Sediment Deformation

A zone of inclined lamination and folding was noted in interval 180-1118A-21R-4, 121–131 cm, and a small interval with dewatering structures was observed higher in the same core (Fig. F9) and again in intervals 180-1118A-21R-5, 21–34 and 78–83 cm. A further short interval of contorted and overturned bedding is seen in interval 180-1118A-27R-1, 93–106 cm.

Interpretation

Unit II, of mainly middle Pliocene age, records a continuation of very similar turbiditic and hemipelagic sediment as in Unit I. However, the sedimentation rate was substantially higher at ~435 m/m.y. and the depth of accumulation was reduced to upper bathyal (150–500 m; see "Sediment Accumulation Rate," p. 33). Unit II was recognized mainly on the presence of distinctive reddish, mainly fine-grained intervals that are finely laminated and lack all but incipient bioturbation. These intervals are interpreted to record times when bottom waters were relatively oxidizing, resulting in combustion of organic matter, and thus, a relatively unsuitable substrate for benthic fauna. Strong bottom-current activity might have inhibited benthic activity. An alternative explanation is that these sediments were relatively enriched in iron oxide when initially deposited and lacked nutrients. By contrast, the intercalated more greenish gray turbidites and hemipelagic sediments are rich in pyrite, especially in burrows and foraminifers, indicating that subsurface anoxia was developed. Rapid deposition of Unit II is consistent with the presence of fluid-escape structures, although these could have been tectonically triggered.

The XRD and smear-slide data indicate that there is little systematic difference in the provenance of the different sediment types discussed above, or any significant change from Unit I in this regard. The abundance of quartz, plagioclase, and basic volcanic rock fragments points to a mainly volcaniclastic origin, including basaltic rocks. In addition, acidic volcanic glass is a minor component of Unit II. Seafloor conditions were more stable than during the accumulation of Unit I, based on the rarer occurrence of soft-sediment deformation structures.

The geophysical logs indicate a continuation of a very similar muddy succession as in Unit I, including rare medium thickness (<15 cm) sandstone beds, based mainly on the natural gamma-ray and neutron porosity responses (see "Downhole Measurements," p. 45). At 287.5 mbsf there is a marked increase in resistivity seen on the FMS images as a bright blotchy image that may reflect increased calcium carbonate con-

F8. Fine-grained volcaniclastic sandstone with a silty clay matrix, p. 62.
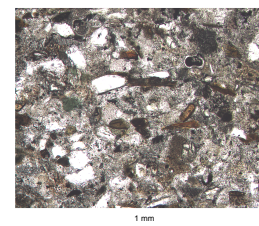
F9. Contorted and deformed fine-grained sediments, p. 63.
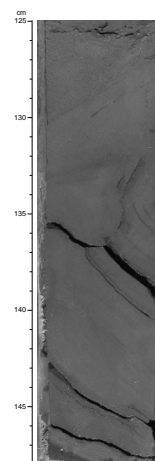
tent in view of the increased photoelectric response. This enhanced photoelectric effect response might also relate to the increased presence of iron oxide that imparts the distinctive reddish color to Unit II. From 402.0 to 411.0 mbsf an inferred sand interval shows a high Th/K ratio that is interpreted as three main volcaniclastic turbidites (each ~30 cm thick), based on the FMS images. Beneath this, the succession is well bedded, corresponding to the turbiditic deposits cored. At 437 mbsf the succession apparently becomes more claystone rich, but still with sandstone intercalations marked by high thorium, uranium, and potassium log responses.

Lithostratigraphic Unit III

Description: silty claystone and clayey siltstone interbedded with sandstone and siltstone
Interval: Sections 180-1118A-30R-CC through 50R-3
Depth: 492.35–679.27 mbsf
Age: middle Pliocene

Lithostratigraphic Unit III is marked by a return to a mainly grayish green succession of sandstones, siltstones, and hemipelagic sediments similar to those of Unit I. Calcium carbonate analyses indicate a downward trend of generally increasing carbonate content from ~3 to 25 wt%. Occasional volcanic ash layer samples exhibit much lower values, and some intervals between 610.0 and 635.0 mbsf have values of 30–35 wt% (see **"CaCO$_3$, Sulfur, Organic Carbon, and Nitrogen,"** p. 40). The lithologies are as follows:

Silty Claystone and Clayey Siltstone

As in Units I and II, silty claystones and clayey siltstones constitute the background sedimentation. These sediments are typically greenish to grayish, burrowed, with rare foraminifers and small shell fragments. The sediments are typically paler colored (e.g., see Section 37R-5) than the two main types of graded sandstones as discussed below. The silty claystone and clayey siltstone are mainly structureless, but are rarely thinly laminated to thinly bedded. Some thin beds and laminae exhibit sharp bases, but some bed bases are diffuse, even where not affected by burrowing (e.g., Section 43R-6). Occasionally, large burrows are elliptical (intervals 180-1118A-42R-6, 78–80 and 86–88 cm). The XRD analysis of the fine-grained sediment revealed a remarkably constant composition with calcite, plagioclase, quartz, also minor amphibole, pyroxene, chlorite, illite, smectite?, and pyrite (Table **T3**).

Siltstone/Silty Claystone Couplets

Interbeds of siltstone/silty claystone 5–15 cm thick are found throughout Unit III. Typically, several such interbeds are present per section, but up to 10 per section were observed in certain cores (e.g., Section 44R-5). Beds typically begin with several millimeters of well-sorted siltstone and pass up into dark greenish gray structureless, or parallel-wavy-laminated siltstone (Fig. **F10**), locally with common planktonic foraminifers (e.g., interval 180-1118A-35R-4, 13–50 cm). Most of these very thin beds lack burrowing. Locally, near the top of the unit, some thin-bedded (<3 cm) sandstones are dark reddish brown as in Unit II (e.g., Section 31R-1 and interval 180-1118A-31R-2, 43–65 cm). The tops of individual beds are

F10. Siltstone-claystone couplets, **p. 64.**
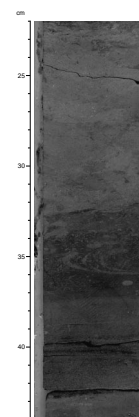
strongly burrowed (mainly *Chondrites* type). The burrows are infilled with silty claystone or sandstone rich in ferromagnesian mineral grains. Near the base of the unit, siltstones are occasionally dark yellowish brown (e.g., interval 180-1118A-44R-7, 22–29 cm). Below 640 mbsf graded siltstone/silty claystone couplets become less numerous, whereas thicker bedded, graded sandstones/siltstones increase in relative abundance (see "Sandstone/Siltstone," p. 11). Smear slides reveal compositions effectively identical to that of the sandstone/siltstone (see following section; also see "Site 1118 Smear Slides," p. 92).

Sandstone/Siltstone

The sandstones/siltstones range from medium to fine grained and thin to medium bedded with erosional bases. They are structureless, exhibit normal grading, parallel, wavy (e.g., interval 180-1118A-33R-2, 99–103 cm, and Section 34R-3), or ripple laminated (intervals 180-1118A-33R-1, 104 cm; 37R-2, 28–31 and 75–87 cm). Approximately seven graded sandstone beds occur per core section (e.g., Section 44R-5). Most of the beds are greenish gray; however, near the top of the unit a few sandstone beds are dark reddish brown (e.g., Sections 31R-5 and 6; and intervals 180-1118A-33R-3, 126–139 cm, and 33R-4, 87–89 cm).

In detail, some individual thin beds have a scoured base followed by beds of planar lamination (Fig. F11), followed by beds of ripple lamination (5–7 cm), then followed by structureless siltstone and claystone. Rarely, climbing-ripple lamination is observed with a high angle of climb (Fig. F12). Small (1 cm) basal flutes or load casts are occasionally present (e.g., interval 180-1118A-35R-5, 14–16 cm). A few beds exhibit convolute lamination (e.g., interval 180-1118A-46R-3, 140–144 cm), or small water-escape structures (Fig. F13). The tops of beds are commonly bioturbated, and the tops of the individual graded units are often obscured by intense burrowing. Up to 6–10 graded beds were observed per section in some cores (e.g., Section 36R-5).

Near the base of the unit the thickness of the individual sandstone/siltstone couplets increases to a maximum of ~35 cm. Such sandstones show planar and cross lamination and grade up into silty claystone and siltstone (e.g., interval 180-1118A-45R-6, 53–94 cm). The upper parts of the beds are composed of dark siltstone that is variably burrowed, making the top of individual beds hard to recognize. In addition, near the base of the unit there are occasional intervals of bed amalgamation, including normal-graded sandstone, small-scale climbing-ripple lamination, and clayey intercalations (e.g., interval 180-1118-47R-6, 40–145 cm). Individual cross laminations show differing dip orientations within single core sections.

Many of the sandstone beds are rich in volcaniclastic detrital grains. Also, carbonaceous grains are locally abundant. Smear slides reveal the presence of nannofossils, mainly planktonic foraminifers, quartz, feldspar, plagioclase, mica, volcanic rock fragments, volcanic glass, calcite, and pyrite (see "Site 1118 Smear Slides," p. 92). Seven thin sections of fine- to coarse-grained sandstone showed very similar compositions (see "Site 1118 Thin Sections"). Most of the sandstones are relatively well sorted with angular to subrounded grains in different thin sections. Normal grading is clearly seen in some cases. Mineral grains are mainly plagioclase and quartz, with biotite, amphibole, and pyroxene. Rock fragments are abundant mainly of basic volcanic rocks with flow-banded feldspar microphenocrysts, variable occurrences of fresh colorless volcanic glass, also rare palagonite, acidic and chloritic volcanic

F11. Sand/siltstone graded bed, p. 65.
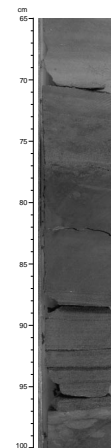
F12. Climbing-ripple lamination and parallel lamination, p. 66.
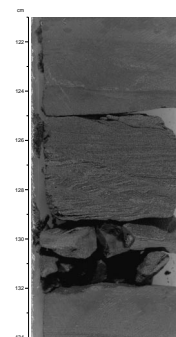
F13. Water-escape structure within a clayey siltstone, p. 67.
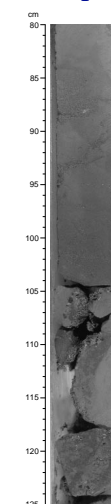
grains, rare calcite grains (micrite and microspar), and a few shell fragments (Fig. F14). Pyrite is unusually abundant within the matrix as well as in the foraminifers. The matrix is largely fine-grained carbonate.

The basic volcanic rocks are commonly present as small clasts, transitional to matrix (e.g., interval 180-1118A-35R-1, 140–143 cm). In several cases (e.g., interval 180-1118A-34R-3, 61–63 cm) individual laminae are packed with broken and intact planktonic foraminifers and form discrete laminae (interval 180-1118A-44R-4, 29–30 cm). One sample is a mixed carbonate-volcaniclastic sandstone with most of the above mineral and rock grains mixed with abundant derived micritic grains and mainly planktonic foraminifers (interval 180-1118A-43R-7, 63–64 cm). Individual foraminifer tests (commonly pyrite filled) are coated with fine calcite spar.

Volcanic Ash

Thin beds of light gray volcanic ash are found sporadically (e.g., intervals 180-1118A-32R-4, 99–99.5 cm, and 37R-4, 52–57 cm). Most of these ash beds are distinguished by a relatively uniform fine grain size, light gray to yellowish brown color, and low calcium carbonate content (<3 wt%). A further four thin beds (1–5 cm) of sandstone to siltstone were identified as crystal-rich volcanic ash (interval 180-1118A-43R-60, 52–62 cm). Thin volcanic ash laminae also are present in interval 180-1118A-44R-2, 103–112 cm. Smear slides mainly reveal abundant colorless volcanic ash. In addition, one thin section in interval 180-1118A-38R-3, 128–130 cm, was found to comprise bubble-wall colorless glass shards in an isotropic fine glass-rich matrix (Fig. F15, see also "Site 1118 Thin Sections").

Soft-Sedimentary Deformation Structures

These features are rare in Unit III. For example, a small interval of inclined to recumbent folding within structureless silty claystone and overlying planar-laminated sandstone is seen in interval 180-1118A-31R-2, 56–64 cm (Fig. F16). The top of this convolute interval is capped by small dewatering or flame structures (several millimeters long). Additional very small convolute, folded intervals with flame structures are seen in the same section at intervals 180-1118A-31R-2, 71–73, 78–80, 93–97, 109–110, 22–123, and 137–138 cm. Another short interval of inclined lamination was observed in interval 180-1118A-39R-1, 53–56 cm. In one instance, an interval of soft-sediment deformation is marked by "plastically" deformed clasts of silty claystone, including very coarse grained to granule sandstone and shell and organic fragments (interval 180-1118A-40R-1, 105–120 cm). Small sand-injection structures were also noted in interval 180-1118A-47R-6, 63–77 cm.

Interpretation

Unit III accumulated in the middle Pliocene at upper bathyal water depths (150–500 m) at an estimated very rapid average sedimentation rate of 479 m/m.y. In detail, Unit III spans two intervals when accumulation rates are determined as 435 and 485 m/m.y. (see "Sediment Accumulation Rate," p. 33). The unit records further turbiditic and hemipelagic sedimentation. However, near the base of the unit (below 640 mbsf) few turbidites are identifiable. In contrast to Unit II, reddish thinly laminated intervals are not developed. Although still sporadic

F14. Fine-grained volcaniclastic sandstone with a silty clay matrix, **p. 68.**
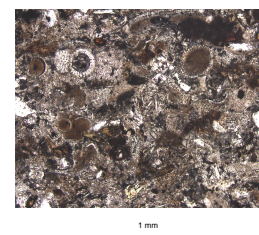
F15. Crystal vitric tuff with pipe-vesicle glass shards, **p. 69.**
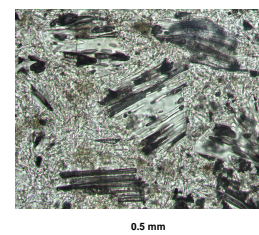
F16. Deformed laminated sandstone bed, **p. 70.**
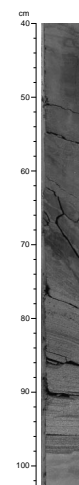
throughout the unit, volcanic glass is more abundant than in Unit II. The provenance of the turbiditic sandstone/siltstone remains little changed from Unit II. However, some sandstones are extremely rich in lithic clasts derived from basic volcanic rocks. Also, some sandstones contain calcium carbonate grains and concentrations of planktonic foraminifers that were probably redeposited from an upslope but still pelagic setting.

In addition, the geophysical logs suggest that much of Unit III is more sandy than above. Individual intervals 1–2 m thick are composed of inferred "radioactive" (i.e., volcaniclastic) sandstone. From 587.0 to 613.0 mbsf the combined density, neutron porosity, and (low) photoelectric log responses suggest the presence of sand that is "nonradioactive" in contrast to that above. Several different provenances of volcaniclastic sandstone are implied (see "Downhole Measurements," p. 45). The FMS shows that this interval is well bedded.

Lithostratigraphic Unit IV

Description: silty claystones, clayey siltstones, graded sandstone/
    siltstone, volcaniclastic sandstone, clayey sandy siltstone, and
    sandy silty claystones
Interval: Section 180-1118A-50R-4 through interval 180-1118A-
    64R-1, 14 cm
Depth: 679.27–810.84 mbsf
Age: middle Pliocene

Lithostratigraphic Unit IV is marked by the disappearance of regular-graded couplets and the appearance of more variably bedded volcaniclastic sandstones, siltstones, mixed sediments (e.g., sandy silty claystone), and common volcanic ash. Ash-poor fine-grained sediments contain ~20–30 wt% calcium carbonate, whereas volcanic ash is strongly depleted in calcium carbonate and in organic carbon (<4%) (see "CaCO₃, Sulfur, Organic Carbon, and Nitrogen," p. 40). The following lithologies are present in Unit IV:

Silty Claystone and Clayey Siltstone

Silty claystones and clayey siltstone differ from counterparts in the overlying units in that they are less regularly bedded and commonly contain admixtures of detrital volcaniclastic grains and volcanic ash (i.e., sandy silty claystone; e.g., Section 56R-5). Some bed bases are diffuse and ill defined (e.g., interval 180-1118A-57R-1, 0–16 cm). Most of the silty claystones and clayey siltstones have a uniform olive green color (dark gray to greenish gray; Fig. F17). In places these sediments contain scattered bioclasts, shell fragments, planktonic foraminifers, and fragments of terrestrial organic matter. Burrows are typically small *Chondrites* and larger *Zoophycos* as seen elsewhere. These sedimentary rocks are mainly sparsely burrowed, in contrast to the very strong bioturbation seen in the overlying units (although some intervals are strongly burrowed; Fig. F17). Some burrows are infilled with fine- to medium-grained volcaniclastic sandstone.

Graded Sandstone/Siltstone

Sandstones/siltstones are well developed between 730.0 and 790.0 mbsf. Up to six discrete normal-graded sandstone/siltstone beds occur

F17. Bioturbated silty claystone and clayey siltstone, p. 71.
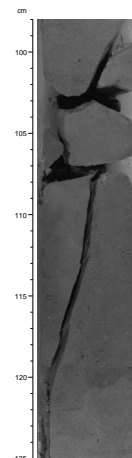
per section (Fig. F18). The sandstones and siltstones rarely exhibit parallel lamination or wavy lamination (e.g., interval 180-1118A-59R-2, 24–48 cm). Individual beds are mainly sharp based and erosional (e.g., interval 180-1118A-60R-2, 53–56.5 cm), but a few have diffuse bases not only owing to bioturbation (e.g., interval 180-1118A-50R-4, 24–27 cm). The sandstones are medium to fine grained, with concentrations of volcaniclastic grains, including dark ferromagnesian mineral grains (hornblende and biotite) and scattered shell fragments. The sandstone mainly changes abruptly into silty claystone. Some graded beds exhibit parallel, ripple, and wavy lamination (interval 180-1118A-59R-2, 24–48 cm). Also, small (1 cm) load casts are locally present at the base of some beds (e.g., interval 180-1118A-63R-5, 98–98.5 cm). Some of the graded sandstones are very rich in volcanic glass, although they differ from the more homogenous volcanic ash described below. In these sandstones the distinction between volcaniclastic sandstone and volcanic ash becomes difficult.

Three thin sections of sandstone (see "Site 1118 Thin Sections") contain common angular grains of quartz, plagioclase (including large zoned crystals), hornblende, rare pyroxene, common lithoclasts of flow-banded basalt, vesicular colorless glass, and rare acidic extrusive grains. Individual fragments of volcanic glass include (co-magmatic) phenocrysts of hornblende and biotite, planktonic foraminifers, rare fragments of calcareous algae, and shell fragments. Foraminifers are lined with calcite spar overgrowths. One sample (interval 180-1118A-58R-3, 38–40 cm) is rich in biotite laths defining lamination.

Clayey Sandy Siltstone and Sandy Silty Claystone

This unit comprises numerous variable, intermixed sediment types. Occasional interbeds are greenish clay-rich siltstone with scattered planktonic foraminifers concentrated near the tops of individual beds (e.g., interval 180-1118A-50R-5, 0–24 cm). The sandy siltstone includes admixed detrital grains, foraminifers, and bioclast fragments. In addition, the sandy silty claystone has a high concentration of detrital sand grains most abundant near the base of individual beds (e.g., interval 180-1118A-57R-3, 52.5–73 cm). Sandy silty claystones are also locally rich in bioclasts and foraminifers (interval 180-1118A-63R-5, 101–122 cm). Some beds are sharp based and graded, but others are nearly homogenous with diffuse bed tops and bases, especially where disrupted by burrowing (e.g., interval 180-1118A-57R-1, 124–130 cm).

Smear slides contain quartz, feldspar, plagioclase, biotite, volcanic rock fragments, volcanic ash, calcite, pyrite, nannofossils, foraminifers, and sponge spicules (see "Site 1118 Smear Slides," p. 92). In addition, XRD analysis reveals common calcite, plagioclase, quartz, and minor illite, pyrite, amphibole, and chlorite (see Table T3).

Volcanic Ash

Common volcanic ash layers are distinguished by a distinctive pale buff color and are present as laminae to thin beds. Some of the volcaniclastic sandstones are very rich in volcanic glass, as mentioned above. Grain size ranges from very fine through medium to rarely coarse grained. Most have sharp bases and are graded. Some beds are graded and exhibit well-developed parallel lamination (intervals 180-1118A-59R-5, 59–62 cm, and 59R-6, 53–55 cm). Many beds begin with medium, fine, or very fine grained sandstone and pass into siltstone that becomes

F18. Volcaniclastic sandstone under parallel-laminated volcaniclastic sand, p. 72.
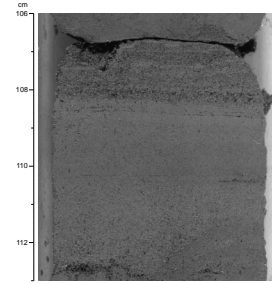
darker upward merging with greenish silty claystone. Burrowing in the volcanic ash is relatively minor except at the top of some thin beds (Fig. F19).

Examples of very fine grained volcanic ash laminae are seen in intervals 180-1118A-53R-1, 92 cm; 54R-1, 46–47 cm; 56R-1, 34–44.5 cm; 56R-1, 70–70.5 cm; and 56R-5, 26–29 cm. Seven discrete beds of volcanic ash up to 9 cm thick are present in Section 57R-4. Lower in the succession (below 745.0 mbsf) some ash layers are crystal rich (e.g., interval 180-1118A-58R-1, 123–126 cm). Thin beds of volcanic ash in interval 180-1118A-58R-5, 50–51.5 cm, exhibit sharp bases and tops. Volcanic ash is also conspicuous in Sections 59R-5 (as three thin interbeds) and 63R-5 (as five very thin beds), and in intervals 180-1118A-62R-3, 73–75 cm, and 63R-4, 0–9 cm. Furthermore, a small number of composite glass-rich intervals are present as repeated thin beds and laminae showing repeated grading and parallel lamination (e.g., interval 180-1118A-63R-4, 0–9 cm).

Two thin sections of volcanic ash revealed a mixed glassy and detrital origin. In addition to abundant angular shards of colorless volcanic glass and grains of plagioclase, quartz, biotite, and hornblende, lithoclasts of basic and acidic volcanics were observed. Individual fragments of volcanic glass again include phenocrysts of hornblende and biotite (Fig. F20; see "Site 1118 Thin Sections").

Soft-Sediment Deformation Structures

In Unit IV these are restricted to small elongate, subvertical sand-filled dewatering structures (e.g., interval 180-1118A-63R-5, 100–122 cm).

## Interpretation

Unit IV accumulated in the middle Pliocene at upper bathyal water depths (150–500 m) at an estimated sedimentation rate of ~485 m/m.y. (see "Sediment Accumulation Rate," p. 33). Unit IV marks a significant change from the mainly hemipelagic and turbiditic sediments of Units I through III to generally coarser grained sediments with more variable sedimentary structures. Although some beds still show clear evidence of deposition from turbidity currents (grading, partial Bouma sequences, and sharp bases; see above), many others exhibit contrasting features, including sharp bed tops. These features are suggestive of reworking by currents other than turbidites. In addition, there is a relatively greater input of calcium carbonate mainly in the form of micritic matrix and micritic clasts. A number of laminae very rich in planktonic foraminifers were probably redeposited from further upslope, based on the textural evidence. Pelagic carbonate was also redeposited as micritic clasts.

Acidic volcanic glass is abundant in Unit IV. This glass is comagmatic with biotite and hornblende phenocrysts. Similar crystals associated with volcanic glass fragments are present in abundance in the interbedded volcaniclastic sandstones and siltstones. Thus, the volcanic ash layers and the glass-rich clastic sediments are inferred to relate to the same episode of contemporaneous volcanism.

The geophysical logs must be interpreted with caution because the caliper indicates markedly larger borehole diameter in the lower part of the unit (beneath 740.0 mbsf). However, the logs indicate that Unit IV is sandy, more so than Unit III. From 682.0 to 735.0 mbsf, an interval of very poor recovery, sands of "nonradioactive type" appear to be

F19. Volcaniclastic sandstone with volcanic ash laminae, p. 73.
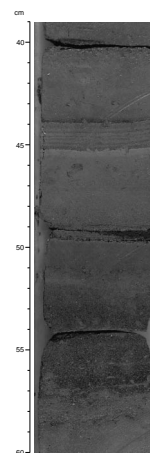
F20. Crystal vitric tuff and mineral crystals, p. 74.
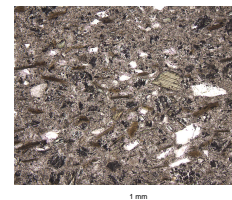
present, based on the low K/Th ratio. The sandstone intervals show up as "fuzzy" on the FMS, in addition, interbedded with several thin, more claystone-rich intervals. From 735.0 mbsf the succession appears to become more muddy, alternating with more sandstone intervals down to 839.0 mbsf. The sandstone remains of "nonradioactive type" (with low thorium and potassium; see "Downhole Measurements," p. 45).

Lithostratigraphic Unit V

Description: mixed sandstones, siltstones, and volcaniclastic sandstone
Interval: intervals 180-1118A-64R-1, 14 cm, through 68R-3, 115 cm
Depth: 810.84–857.1 mbsf
Age: middle Pliocene to latest early Pliocene at the base

Lithostratigraphic Unit V is characterized by variably interbedded, poorly sorted, mixed sandy and silty claystones, siltstones, and cemented sandstones with local lithic fragments. Coarse-grained sandstones rich in bioclasts are present in the lowermost 10 m of the unit. By contrast with Unit IV, primary volcanic ash is minimal. Calcium carbonate values are mainly high, ranging from 10 to 33 wt% (see "CaCO3, Sulfur, Organic Carbon, and Nitrogen," p. 40). The following lithologies are present:

Sandy Silty Claystone (Mixed Sediment)

This is greenish gray, burrowed, with scattered volcaniclastic grains. Bedding is irregular with sharp bases and tops to individual beds. Small lithoclasts (<1 cm) of volcanic rock are rarely present (e.g., interval 180-1118A-64R-1, 50–53 cm; and Sections 66R-3 and 67R-CC. Fragments of wood were noted occasionally (intervals 180-1118A-65R-1, 109.5–111 cm; 66R-1, 101.5 and 138.5 cm; 66R-2, 60 cm; and 66R-CC, 6–27 cm). Common concentrates of quartz, feldspar, and ferromagnesian grains are present. Burrows include possible rare *Zoophycos* (Section 66R-4). Locally, the claystone is admixed with detrital volcaniclastic grains and volcanic ash (Fig. F21). In one case, claystone (rich in volcanic ash) is thickly interlaminated with medium- to coarse-grained volcaniclastic sandstone (Section 66R-CC).

Silty Claystone and Siltstone

These sediments are moderately to strongly burrowed with scattered shell fragments, detrital grains, and planktonic foraminifers (Fig. F22). Burrows are infilled with siltstone or sandstone, as seen in overlying units. The bases of individual beds are commonly diffuse, and overall, bedding is weakly defined (Section 67R-1). Rare intervals of reverse grading are typically disrupted by burrowing. Elliptical burrows and minor pyrite were observed locally (e.g., interval 180-1118A-65R-4, 99 cm). Lower in the unit (from ~825.0 mbsf) silty claystone is interbedded with fine- to medium-grained sandstone with diffuse intergradational boundaries (e.g., Section 65R-CC). Some beds show sharp bases as well as tops (e.g., interval 180-1118A-66R-5, 14–21 cm).

Sandstone/Siltstone

This sediment is medium to thick bedded, with sharp, scoured bases (e.g., interval 180-1118A-64R-2, 9–12 cm). Colors range from greenish

F21. Hornblende and plagioclase-phyric basalt with glassy matrix, **p. 75.**
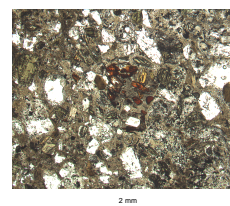
F22. Bioturbated silty claystone and clayey siltstone, **p. 76.**
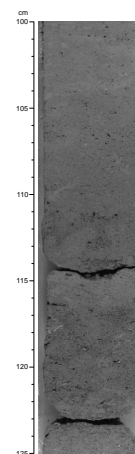
gray to dark gray. Burrowing is extensive with individual burrows being locally infilled with pyritic sandstone. Numerous lithic clasts and bioclasts are present, including foraminifers and shelly fragments. The latter include cross sections of complete thin-shelled bivalves (Section 65R-5). Sparse carbonaceous grains are also present (e.g., Section 64R-1). Parallel and wavy lamination were noted. Sandstone-siltstone commonly grade into siltstone and claystone at the top of individual beds (e.g., interval 180-1118A-64R-2, 9–12 cm), but the contact is often diffuse as a result of extensive burrowing. Commonly, the base of individual graded units was not recovered. The sandstone is mainly well cemented with calcite spar.

In general, the sandstone is mainly fine to medium grained in the upper part of the unit, but is locally coarse grained in the lower part (below ~850 mbsf). This sandstone shows only a very weak bedding. Sand grains are angular, but relatively well sorted (e.g., Section 67R-5).

Mixed Bioclastic/Volcaniclastic Sandstone

This is restricted to near the base of the unit. It is dominated by poorly sorted, medium-grained, rarely normally graded, weakly bioturbated calcareous sandstone with common, but scattered, bioclasts including thin shell fragments, planktonic and benthic foraminifers, coralline algae, and coral fragments (e.g., interval 180-1118A-68R-2, 117–118.5 cm; Fig. F23). Granule-sized clay-rich clasts (0.8 cm × 0.2 cm × 0.3 cm) were observed subparallel to each other (e.g., interval 180-1118A-68R-1, 54–74 cm). The orientation of bioclasts defines a weak horizontal bedding. The sandstone locally passes downward into finer grained, more muddy sediment (interval 180-1118A-68R-3, 40–60 cm). A small number of subrounded to rounded pebbles of basic volcanics were noted at the base of the unit (interval 180-1118A-68R-3, 110–115 cm).

A thin section of heterogeneous laminated sandstone (interval 180-1118A-64R-1, 49–61 cm) consists of laminae of different composition (see "Site 1118 Thin Sections"). Graded volcaniclastic laminae are composed of volcanic glass, quartz, feldspar, biotite, and hornblende in a calcite spar matrix. In addition, intercalated laminae are rich in micrite with particles of volcanic glass (as globular fragments).

The above bioclastic-rich sandstone is interbedded with much less calcareous, darker, well-cemented planar-laminated, coarse-grained sandstone, composed of angular quartz, feldspar, and ferromagnesian mineral grains (e.g., interval 180-1118A-68R-3, 60–64 cm). Only rare small bioclasts are present in this sandstone (Fig. F24).

Claystone

Olive green, weakly calcareous homogenous silty claystone forms a very minor amount of Unit V (e.g., within interval 180-1118A-64R-1, 36–38 cm). The XRD analysis of this fine-grained sediment indicates the presence of calcite, plagioclase, quartz, illite, and minor pyrite and amphibole (Table T3).

Soft-Sediment Deformation Structures

Local small-scale subvertical sand-injection structures are present (e.g., interval 180-1118A-64R-1, 60–63 cm). In one case the injected sandstone directly underlies the base of a sandstone bed (e.g., interval

F23. Sandstone with mineral grains and shell fragments, p. 77.
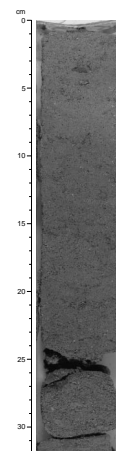
F24. Bioclastic sandstone overlain by a coarse-grained sandstone, p. 78.
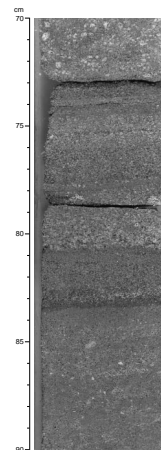
180-1118A-64R-1, 21.5–23 cm). In another case, possible sand injection up a small, steeply inclined fault plane was observed (interval 180-1118A-64R-1, 108–120 cm; see **"Structural Geology,"** p. 28).

Interpretation

Unit V accumulated mainly in the middle Pliocene. However, the lowest part of the unit (Section 68R-3) accumulated in the latest early Pliocene. Upper bathyal depths are inferred from benthic foraminifers. The sedimentation rate remains high, averaging about 480 m/m.y. (see **"Sediment Accumulation Rate,"** p. 33). Unit V is inferred to record well-oxygenated, mixed hemipelagic and turbiditic sediments, but the succession was also influenced by traction currents within a slope setting adjacent to a landmass. The presence of irregular bedding and sharp tops to many units specifically attest to a traction current influence. A vegetated adjacent landmass is inferred from the presence of sporadic wood fragments. A relatively higher input of neritic bioclasts (including coral fragments, coralline algae, and benthic foraminifers) near the base of the unit is indicative of proximity to a carbonate margin.

In addition, the geophysical logs of this short interval suggest that it is sandy, especially toward the base (below 851.0 mbsf), based on the resistivity and gamma logs and that this material is not "radioactive," similar to the sands in Unit III above. A very resistant inferred medium bed of sandstone (<30 cm) is seen on the FMS at 815.0 mbsf (see **"FMS Images,"** p. 49). Finally, around 850.0 mbsf there was a marked input of very "radiogenic" sand, as also seen in Unit VI (see **"Lithostratigraphic Unit VI,"** p. 18).

Lithostratigraphic Unit VI

Description: limestone (packstone/grainstone)
Interval: intervals 180-1118A-68R-3, 115 cm, through 69R-1, 15 cm
Depth: 857.1–859.15 mbsf
Age: early Pliocene or latest Miocene

Lithostratigraphic Unit VI is dominated by a thin interval of packstone/grainstone rich in bioclasts of shallow-water carbonate. The upper contact is marked by an irregular contact between pale packstone/grainstone below and well-cemented calcareous sandstone of Unit V above. The base of the unit is marked by a gradational change from packstone/grainstone to conglomerate in Section 69R-1 (see **"Lithostratigraphic Unit VII,"** p. 19). Two calcium carbonate analyses yielded values of ~82 and 91 wt% (see **"CaCO$_3$, Sulfur, Organic Carbon, and Nitrogen,"** p. 40). The following lithology is present:

Limestone (Packstone/Grainstone)

This is made up of poorly sorted bioclastic fragments (up to 2.5 cm long), including calcareous algae, coral, echinoderm debris, bivalve shells, and benthic foraminifers. The material is well cemented by calcite spar. In places intact rhodoliths are present. The limestone includes wispy, irregular laminae composed of silty clay with detrital grains (Fig. **F25**). Sand-sized detrital grains are also scattered through the packstone/grainstone as a whole. In addition, rare siliciclastic granules or small pebbles of dolerite and basalt are locally present (e.g., interval

F25. Packstone and grainstone overlain by mixed sandstone, **p. 79.**
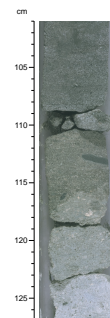
180-1118A-69R-1, 0–9 cm). There are also intervals with rare angular, to subrounded, to rounded pebbles of basalt/dolerite with bioclastic fragments giving rise to ill-defined beds (e.g., Section 69R-1). Some of the bioclasts, especially those composed of aragonite (e.g., coral), are dissolved to form secondary solution porosity.

Thin sections reveal that texturally the limestones are packstone/ grainstone (see "Site 1118 Thin Sections"). The main biogenic components are calcareous algae, shell fragments, benthic foraminifers, bryozoans, echinoderm debris, occasional coral fragments (dissolved), and rare small planktonic foraminifers (globigerines). In addition, scattered detrital grains are present (quartz, plagioclase [zoned], hornblende, and biotite). Lithic grains are aphyric basalt, basalt with large feldspar phenocrysts, rare felsic and rare chloritized grains, and micritic clasts. Bryozoans are locally encrusted with calcareous algae. Remnants of a micritic matrix are also present together with a pyrite-calcite spar cement. Pyrite is locally abundant.

Interpretation

Unit VI accumulated during early Pliocene, or earlier, and included reworked benthic foraminifers (see "Benthic Foraminifers," p. 32). This limestone is a shallow-water carbonate with coralline algae, coral fragments, echinoderm debris, benthic foraminifers, and other bioclasts. The matrix was originally micritic, but was later dissolved and replaced by calcite spar. This evidence, and the state of preservation of delicate algal material (e.g., as original algal mats) shows that the bioclastic material originally accumulated in a relatively low energy setting, probably a lagoon or embayed area open to marine circulation. In addition, a coastal setting is suggested by admixing with detrital lithoclastic grains of basalt/dolerite. However, there is little evidence of coeval volcanism, in contrast to the overlying units (see sections above).

The geophysical logs, especially the photoelectric effect log, confirm that it is a very carbonate rich interval ~3 m thick from 857 to 860 mbsf. This indicates that the recovered packstone/grainstone is about one-half of that present. Limestone is present down to 860.2 mbsf, followed by sandstone, based on the gamma-ray log. This sandstone corresponds to an interval of very radiogenic sand (with a Th/K ratio of up to 10; see "Lithologic Analysis," p. 46).

Lithostratigraphic Unit VII

Description: carbonate-rich paraconglomerate
Interval: intervals 180-1118A-69R-1, 15 cm, through 70R-1, 87 cm
Depth: 859.15–873.1 mbsf
Age: undated

Lithostratigraphic Unit VII is defined by the presence of poorly sorted paraconglomerate composed of basic igneous rock clasts set in a matrix of neritic bioclastic carbonate. The upper contact is seen to be gradational on the FMS log (see paragraph below). The lower contact is a sharp, subhorizontal, planar surface separating sandy limestone above from dolerite below. The measured calcium carbonate content varies from 67 to 84 wt% (see "CaCO$_3$, Sulfur, Organic Carbon, and Nitrogen," p. 40). The following lithologies are present:

Paraconglomerate

This is a pebbly, mixed sediment with bioclastic debris, as described above, mixed with mainly subrounded to rounded granules and pebbles of basalt and dolerite together with common quartz, feldspar, and ferromagnesian detrital grains. There is well-developed calcite spar cement. The largest pebble recovered is 6 cm in length (Fig. F26). A small number of intact rhodoliths are preserved (e.g., Section 69R-2). The largest pebbles are preserved in the middle part of the unit (interval 180-1118A-69R-3, 35–65 cm). None of the clast-rich intervals define a clast-supported texture. In addition, individual pebbles exhibit pale alteration rims and are coated with calcium carbonate (Fig. F27).

All of the bioclasts exhibit secondary solution porosity that is not seen in more sandy material. Rare vugs are present (<1 cm × 1 cm) with a lining of drusy calcite. Rare coral fragments are preserved only as internal molds (e.g., Section 69R-CC).

Limestone/Calcareous Sandstone

Coarse, to very coarse grained, mixed sandy limestone and calcareous sandstone dominate the lower 1 m of the unit. This includes common poorly sorted, but well-rounded pebbles and granules of dolerite and basalt together with neritic bioclasts, notably calcareous algae, rhodoliths, coral, and shell fragments (Fig. F28). In addition, well-sorted calcareous bioclast-rich medium-grained limestone <10 cm thick rests directly on dolerite beneath (interval 180-1118A-70R-1, 80–87 cm). Several thin layers of wavy-laminated, disrupted algal micrite are present (interval 180-1118A-70R-1, 3–12 cm). Also, just above the contact with the underlying basic igneous rock, two intact pieces of homogenous calcareous algae were recovered (interval 180-1118A-70R-1, 70–80 cm).

Thin sections contain abundant fragments of calcareous algae (locally rounded), shell fragments, benthic foraminifers, echinoderm plates, also rare echinoderm debris, bryozoans, and coral fragments together with rounded fresh aphyric basalt granules, rare chloritized basic and acidic extrusive igneous rock, and detritus, including grains of quartz and feldspar (see "Site 1118 Thin Sections"). Echinoderm spines are lined with prismatic calcite spar. There is a cement composed of blocky calcite spar (Fig. F29). Several thin sections show evidence of a primary micritic matrix replaced mainly by calcite spar.

In addition, XRD analysis of the sandstone contains calcite and subordinate plagioclase, quartz, amphibole, and illite (Table T3).

Interpretation

Unit VII lacks age-diagnostic fossils and can only be said to have accumulated in early Pliocene time, or earlier (see "Biostratigraphy," p. 31). This is a mixed sediment composed of detritus of shallow-water carbonate material as in Unit VI (see "Lithostratigraphic Unit VI," p. 18), mixed with rounded pebbles and granules of basalt and dolerite, as seen in Unit VIII (see "Lithostratigraphic Unit VIII," p. 21). The igneous clasts are inferred to have been rounded and then mixed with shallow-water carbonate. In view of the presence of underlying inferred river conglomerate (see "Lithostratigraphic Unit VIII," p. 21) it is likely that the conglomerate was supplied fluvially. The probable setting is a coastal area affected by waves or currents. However, the algal mats and a primary micritic matrix is suggestive of a relatively low

F26. Paraconglomerate with well-rounded pebbles, p. 80.
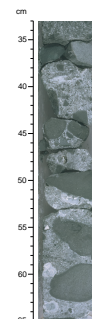
F27. Plagioclase and clinopyroxene-phyric basalt within a paraconglomerate, p. 81.
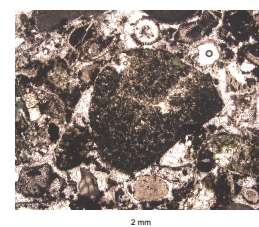
F28. Calcareous sandstone with abundant fragments, p. 82.
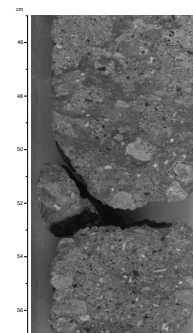
F29. Grainstone comprised of abundant fragments, p. 83.
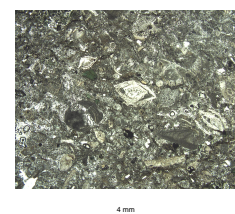
energy setting, possibly a marine lagoon or embayed area, as inferred for Unit VII. During diagenesis much of this micritic matrix was replaced by sparry calcite. In addition, the base of the unit is marked by a sharp planar, slightly inclined (6°–7°) contact of the unit between well-washed shallow-water carbonate and dolerite. This contact may represent a wave-cut platform (Fig. F30), although FMS interpretation suggests that, alternatively, it may be an artefact of drilling.

The FMS logs confirm that much of Unit VII is conglomeratic, corresponding to the paraconglomerate recovered. The logs additionally show that major spikes in gamma ray, thorium, potassium, photoelectric effect, and velocity are present at 860.2–816.7 mbsf. These are interpreted as a "radioactive" volcaniclastic sandstone. Below 865 mbsf the gamma log was not available, making interpretation more tentative (see "Downhole Measurements," p. 45). However, the combined neutron porosity, photoelectric logs, and FMS resistivity logs indicate the presence of a carbonate-rich interval near the base of the unit (869.2–873.1 mbsf) in agreement with the material recovered.

Lithostratigraphic Unit VIII

Description: dolerite with rare granule conglomerate, sandstone, and silty claystone intercalations
Interval: interval 180-1118A-70R-1, 87 cm, through Section 76R-1
Depth: 873.1–929.6 mbsf
Age: indeterminate

Lithostratigraphic Unit VIII is mainly dolerite as described in "Unbrecciated Dolerite," p. 26. However, a small number of thin sedimentary intercalations are present. The FMS images are critical in showing that at least from 890 mbsf upward a very coarse conglomerate is present with no intact dolerite (Fig. F30). Details of the recovery are as follows:

Material from within the Uppermost Interval of Basalt/Dolerite (Section 180-1118A-70R-2)

Sandstone

Well-lithified calcite-cemented sandstone is found as two pieces ~60 cm beneath the highest location of basalt/dolerite (i.e., within interval 180-1118A-70R-2, 0–14 cm). This sandstone comprises well-rounded bioclastic grains, including calcareous algae together with angular to rounded lithoclasts of basalt/dolerite and black breccia (see paragraph below). The breccia lithoclast has angular grains of basalt/dolerite in a matrix of well-cemented, black, fine-grained sandstone with scattered granules. The lithology of this clast is the same as that of the black breccia described below. A thin section reveals poorly sorted, rounded grains of basalt/dolerite and rare large, altered plagioclase grains set in a chloritic silty matrix (see "Site 1118 Thin Sections").

Material from Lower within the Basalt/Dolerite (below Section 180-1118A-70R-2)

Black Siltstone Breccia with Basalt/Dolerite Clasts

This material is present ~60 cm lower in the recovered succession beneath clasts of breccia. The black breccia is composed of subangular to subrounded clasts of relatively fresh dolerite/basalt, plus a few out-

F30. Dolerite/basalt overlain by various carbonates and sandy paraconglomerates, p. 84.
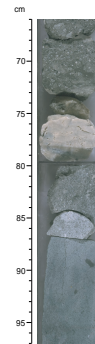
standing orange, weathered clasts set in a matrix of well-lithified black siltstone with subangular granules of basalt/dolerite. Additional very similar fragments of black breccia and sandstone are seen in the underlying interval (interval 180-1118A-70R-3, 0–50 cm).

In addition, a few pieces of polymict breccia were recovered in the underlying core (intervals 180-1118A-71R-1, 13–15 and 51–61 cm). A thin section of this rock revealed subrounded lithoclasts of basalt and dolerite in very variable states of alteration in a matrix of volcaniclastic silt (derived from basalt), sand-sized basalt and dolerite grains, and rare pyroxene and green chloritic material (Fig. **F31;** see also **"Site 1118 Thin Sections"**). A few calcite grains are also present. XRD analysis revealed plagioclase quartz, K-feldspar, and smectite? (Table **T3**). Another thin section (interval 180-1118A-71R-1, 29–31 cm) is dominated by subrounded granules of very variably altered basalt/dolerite in a matrix of greenish chloritic material (see **"Site 1118 Thin Sections"**). In Section 72R-1 three intervals of polymict breccia were noted (Fig. **F32**). Core 74R includes pieces of weathered dolerite that in some cases appear to be derived from conglomerate as the fragments are subangular to rounded. Furthermore, within Section 74R-3 a number of isolated dolerite pieces are present, which are inferred to represent clasts within conglomerate that were disaggregated by drilling.

Material from Low in the Basalt/Dolerite (below Core 180-1118A-74R)

Additional clasts and sediments were recovered in Core 180-1118A-75R, as follows:

Basalt Coated with Silty Sandstone

Several individual pieces of basalt are cut by small (2–3 mm) fissures infilled with orange brown sandy siltstone (interval 180-1118A-75R-1, 114–115.5 cm).

Granule Conglomerate

Several pieces were recovered of poorly sorted dark brown angular granules of basalt/dolerite with a matrix of sand grains and granules (up to 3 mm in size). These grains show variable weathering and alteration (interval 180-1118A-75R-1, 80–85 cm).

Matrix-Supported Breccia

This was encountered as a piece (interval 180-1118A-75R-2, 0.3 cm) of angular to subangular to locally rounded breccia with pebbles and granules of mainly basalt and dolerite in a dark brown clayey siltstone matrix. In addition, three pieces of matrix-supported breccia were recovered lower in the succession (interval 180-1118A-76R-1, 40–57 cm). The matrix-supported breccia contains angular to subrounded clasts of dolerite/basalt within a orange brown sandy and silty matrix showing very variable degrees of weathering of individual grains. The clasts include coarse-grained sandstone composed of subrounded grains and granules (i.e., second-cycle conglomerate clasts). Some of the derived clasts in the primary conglomerate include fragments of basalt/dolerite that have undergone onion-skin weathering and alteration. The matrix of the breccia is cut by small calcite veins.

Sandstone-Coated Pebbles

Several pieces of basalt/dolerite coated with poorly sorted sandy siltstone were recovered (interval 180-1118A-75R-2, 3–10 cm).

F31. Plagioclase- and clinopyroxene-phyric basalt fragment in a silty matrix, **p. 85.**
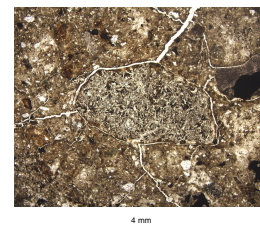
F32. Polymict breccia of basalt/dolerite within a matrix of sandstone, **p. 86.**
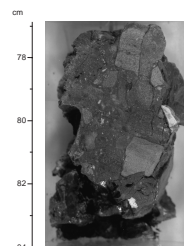
Mud-Filled Fissure

One piece of weathered basalt/dolerite was recovered including a mud-filled fissure (interval 180-1118A-75R-2, 28–43 cm). This is infilled with dark brown sandy silty claystone, including scattered small basalt/dolerite clasts in variable states of alteration. In addition, the adjacent basalt/dolerite is very strongly weathered and fissured. Individual fissures (weathering cracks) are infilled with mud. Another piece (interval 180-1118A-76R-2, 113–119 cm) of very weathered dolerite is fissured with an infilling siltstone, sandstone, and granules of orange weathered basalt/dolerite.

Silty Claystone

The lowest sediment to be recovered (interval 180-1118A-76R-2, 113–119 cm) comprises small pieces (i.e., a drilling breccia) of very altered orange brown silty claystone with small clasts (sand and granule sized) of very weathered basalt/dolerite. Some of these clasts are very well rounded.

Interpretation

An interpretation of Unit VIII is heavily dependent on interpretation of the FMS log data. Also, there is an (excessive) offset between FMS depths and triple-combo depths that complicates comparisons. The gamma-ray log is not available and the neutron porosity log ends at 872 mbsf. Conglomerate appears at 873.1 mbsf. There is a fairly sharp contact between inferred large (tens of centimeters), rounded clasts of basalt/dolerite and overlying limestone at the base of Unit VII. In the cores a sharp planar contact between a piece of grainstone and a piece of basalt/dolerite was observed. This contact was initially interpreted as an original subhorizontal planar contact between dolerite and limestone (i.e., a wave-cut platform?), based on the core recovery alone. The FMS image did not reveal any such planar-sharp contact, but nevertheless, confirms that an abrupt contact exists between conglomerate and limestone.

From 873.5 to 890.0 mbsf the FMS images reveal a poorly sorted conglomerate composed of mainly rounded clasts up to 0.5 m thick. The interstices between these rounded clasts are infilled with smaller (<5 cm) angular to subangular clasts and dark, resistive, presumably finer grained material. In some areas, the conglomerate appears to be matrix supported, but overall this interval is clast supported. The lowest 40 m of the succession, which includes pieces of dolerite and minor sedimentary rock, was not imaged.

Taking account of the critical FMS images, Unit VIII is inferred to represent deposits from a fluvial channel at least 30 m thick draining a hinterland of substantial relief (hundreds of meters at least). The conglomerate was almost entirely derived from basalt/dolerite (locally pegmatitic; see "Igneous and Metamorphic Petrology," p. 25). This implies that at least locally, large outcrops of basalt/dolerite existed in the area.

All the clastic material between the recovered dolerite is interpreted as original primary sediment intercalations, including some sediment that filtered into cracks within individual clasts. This material initially accumulated in a highly oxidizing climate, resulting in variable reddening and alteration. Specifically, the fine-grained and poorly sorted sandy sediment with strongly oxidized material is inferred to represent paleosol. Surface oxidation rather than later alteration in response to

fluid flow is the probable cause of this oxidation. This, however, excludes the minor hydrothermal veining that took place prior to incorporation of the basalt/breccia as clasts in the conglomerate. Later, the texturally less mature, less oxidized, black breccia and sand were deposited between larger clasts. Finally, the conglomerate was transgressed, resulting in interfingering with neritic grainstone over a narrow interval (~1 m) directly below Unit VII.

Depositional History

Site 1118 was initially part of a tropically weathering landmass with basalt/dolerite locally outcropping (Unit VIII). A rugged hinterland was drained by a river giving rise to a conglomerate-filled channel at least 50 m thick. Weathered volcaniclastic material filtered into interstices and cracks within the conglomerate. Alternatives are that this was part of the Paleogene ophiolitic basement related to the Papuan Ophiolitic Belt, part of the Miocene Trobriand forearc (emergent prior to early Pliocene time), or magmatic rocks related to rifting of the Woodlark Basin. Initially, the interstitial material was lateritic, essentially reworked paleosol, followed by less altered more angular dolerite/breccia debris. Later the conglomerate was transgressed by the sea, resulting in minor interfingering of conglomerate and limestone.

Conglomeratic material derived from the landmass was reworked probably in a coastal setting and mixed with shallow-water-derived carbonate as paraconglomerate (Unit VII). The FMS data suggest that the conglomerate fines upward, presumably as transgression advanced. Corals grew either as fringing reefs or near-coastal patch reefs, although little is preserved at Site 1118. The rhodolithic algae and algal mats developed in a relatively protected shallow-water area, possibly an open-marine lagoon or embayed area. With further transgression in early Pliocene time, terrigenous input diminished and a pure limestone accumulated, still in a shallow, semi-enclosed setting (Unit VI).

The base of the overlying mixed sandstone, siltstone, and volcaniclastic sandstone accumulated in the early-middle Pliocene already at upper bathyal depths (150–500 m). This implies that sudden subsidence took place ushering in very rapid sedimentation (~479 m/m.y.). However, the contact between Units VI and V is sharp and irregular, and it is possible that intervening slope facies were deposited but then removed by currents or slumping. The overlying interval (Unit IV) contains much reworked pelagic carbonate, and it is possible that this too was reworked from a slope setting but at a later time. The mixed sandstone, siltstone, and volcaniclastic sandstone (Unit V) reveals the combined activity of turbidity currents and traction currents. Shallow-water detritus was still being supplied from a neighboring carbonate platform and wood drifted from a landmass.

During the middle Pliocene, at a time of continuing very rapid deposition, subsidence carried the basin to well below wave base and turbiditic and hemipelagic sedimentation ensued (Unit IV). This was a time of explosive volcanic activity, alternatively related to rifting of the preexisting Trobriand Arc or to (classical) continental rifting to form the Woodlark Basin. Both fine-grained air-fall tuffs and coarser grained redeposited crystal tuff accumulated, related to coeval acidic volcanism.

In all, ~500 m of turbidites and hemipelagic sediments accumulated, initially at upper bathyal depths (Units II, III, and IV) and then at middle bathyal depths (500–2000 m) under very similar conditions (Unit I) during the middle Pliocene to late Pliocene to Pleistocene. However,

this was broken by an interval (Unit III) that includes reddish, finely laminated, little-bioturbated sediments that could record an episode of more oxidizing bottom-water conditions, if not simply increased input of oxidized iron. Sporadic input of air-fall tuff continued, but the dominant input of volcaniclastic sediment switched to a copious supply of fresh basic volcanic rock. This epiclastic sediment was derived either from Woodlark rift-related extrusives or from the earlier (Miocene) Trobriand Arc. Associated mixed-layer clay was possibly derived from the Papua New Guinea landmass or the D'Entrecasteaux Islands, as discussed for the nearby Site 1108 (see "Site 1108" chapter). During late Pliocene time deposition slowed from ~435 m/m.y. to ~155 m/m.y., paralleling the trend at the other sites determined during Leg 180. The little-cored initial interval of Unit I may represent muddy sediment rich in swelling clay, based on the geophysical logs and reports of the change in hole diameter through time. Finally, the geophysical logs also suggest that the noncored interval of upper Pliocene? to Pleistocene records continued turbiditic and hemipelagic deposition, as recovered at Site 1109.

Finally, drilling of Hole 1118A revealed additional important information on the nature and history of contemporaneous volcanism related to genesis of the Woodlark Basin as summarized in Figure F33. Analysis of the visual core descriptions shows that volcanic ash has a cumulative thickness of 20.1 m. The total number of ash layers recovered is 611. Of these, 41 are interpreted as primary air-fall tuff and 570 as volcaniclastic sand and silt layers. The latter category includes both reworked contemporaneous volcanic ash and crystal tuff, and also epiclastic (older) volcanic rock debris. The majority of the ash layers are found from 695 to 811 mbsf (Cores 180-1118A-51R through 63R). These are considered to relate to rifting of the Woodlark Basin during the middle Pliocene, but determining whether from Trobriand Arc volcanism and/or from rift volcanism will require shore-based geochemical analysis.

IGNEOUS AND METAMORPHIC PETROLOGY

A fractured dolerite unit (Unit VIII) was first encountered within Section 180-1118A-70R-3, at 869 mbsf, below a packstone/grainstone unit with scattered rounded basaltic clasts and fragments from a lagoonal environment and a paraconglomerate containing basalt and dolerite clasts set in a calcareous matrix (Units VI and VII; refer to "Lithostratigraphic Unit VI," p. 18, and "Lithostratigraphic Unit VII," p. 19). The FMS images show that at least the upper part of Unit VIII is also a conglomerate (see "Log Unit L9," p. 48), although it was originally interpreted as a fractured dolerite with cracks infilled with sedimentary material. Clasts in the conglomerate reach a large size; several unbroken pieces of dolerite were recovered that were tens of centimeters in length. Fifty-eight meters of this conglomerate were cored from 869 to 920 mbsf of which 13.6 m (23.4%) were recovered (Fig. F34). The rocks range from slightly altered, unbrecciated dolerite clasts (Fig. F35) to pervasively altered breccia rocks. The recovered breccia rocks contain angular dolerite clasts within a dark brown to black, clay-sized, iron oxide–rich matrix thought to be derived from extensive weathering of dolerite (Fig. F36). Among the clasts recovered, brecciation occurs in zones (see "FMS Images," p. 49, for spatial attitudes and trends of brecciation).

F33. Volcanogenic ash layers and thickness per core, p. 87.
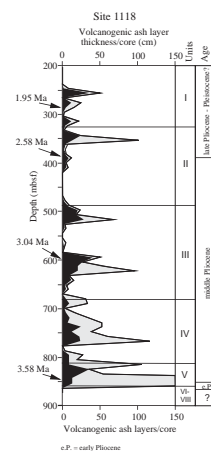
F34. Diagram of recovery and rock types, p. 88.
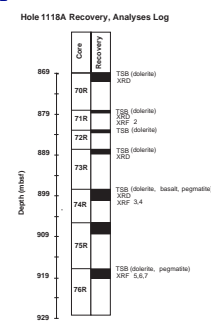
F35. Granular dolerite crosscut by a fracture, p. 89.
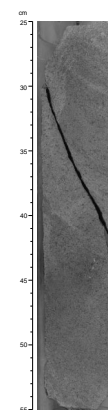
Lithologic Description

Conglomerate

The clasts within the conglomerate have varying degrees of subaerial iron oxide weathering and brecciation that create a dark brown, dolerite- derived matrix. Angular clasts of dolerite were recovered, some within this brown matrix, others without matrix (see "Domain III: Dolerite," p. 30). Many of the angular clasts within the matrix material have onion-skin iron oxide weathering, which indicates weathering of the clasts before incorporation into the conglomerate. One particular example shows a clast with a network of iron oxide weathering separating angular zones within a dolerite (see "Structural Geology," p. 28). This most likely represents a partially brecciated and weathered dolerite clast, intermediate between the two types observed. The close association of iron oxide weathering to fractures suggests that fluid flowing within these veins is a likely agent of weathering. Thin-section analysis shows veins filled with calcite and zeolite with iron oxide weathering on the inside, suggesting that weathering may be associated with the fluids responsible for calcite precipitation (Fig. F37). Many slickensided surfaces can be seen on chips of this clay-sized, brown matrix material, which suggests that the unit has undergone some degree of faulting (refer to "Structural Geology," p. 28).

Unbrecciated Dolerite

Apart from the degree of weathering and brecciation, there is no mineralogical difference between fractured and unfractured dolerite rocks within this unit. The rocks are generally slightly to moderately altered and fine- to medium-grained with a granular to ophitic texture. Mineralogy includes largely fresh clinopyroxene and partially sausseritized plagioclase, often intergrown along with dendritic magnetite, iron oxide, and less commonly, pyrite. Chlorite occasionally replaces clinopyroxene (Fig. F38) but also occurs interstitially, possibly replacing interstitial glass. Clusters of greenish layer silicates ("iddingsite") represent pseudomorphed olivine at least in some cases, but this never makes up more than ~5% of the rock. Grain size varies moderately throughout zones within cores, but no systematic change can be noted with increasing depth. Mineralogy of the dolerite at this site is similar to that at Sites 1109, 1114, and 1117, although there are textural and grain-size variations, and the small amount of gabbro recovered at Site 1117 has appreciable amounts of quartz, which was not seen except in occasional small amounts in the gabbro rocks from the other sites. Two pegmatitic zones occur at intervals 180-1118A-74R-2 (Piece 5, 120–149 cm; 900.24–900.53 mbsf) and 76R-2 (Pieces 11 and 12, 77–89 cm; 917.71–917.83 mbsf), which have dendritic magnetite crystals even better developed than those at Site 1117 (Fig. F39). Very fine grained (basaltic) clasts, similar to the chilled margin described in the Site 1109 dolerite are also present in interval 180-1118A-74R-1 (Piece 1, 124–126 cm; Fig. F40). There is no significant difference in primary mineralogy between the pegmatite and the dolerite, and no sharp contact can be observed between the rock types.

F36. Brecciated and altered dolerite, p. 90.
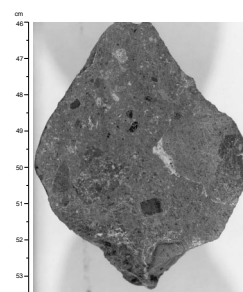
F37. Vein filled with calcite and zeolite crosscutting dolerite, p. 91.
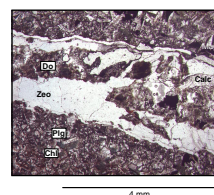
F38. Altered dolerite, p. 92.
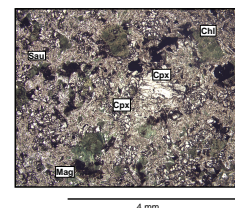
F39. Dendritic magnetite in pegmatitic dolerite, p. 93.
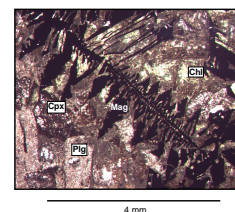
F40. Variolitic groundmass containing plagioclase and clinopyroxene, p. 94.
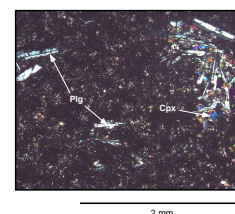
Chemistry

X-ray fluorescence (XRF) analyses are reported in Tables T4 and T5. One sample is from a basaltic pebble in the overlying Unit VII. Compositions generally resemble those of other dolerites and gabbros from Leg 180, but there is significantly more variation than reported at Site 1109, although this is largely due to the presence of a pegmatitic patch (analysis 5 in Table T4). Variation is shown in Figure F41 where some elements are plotted against the iron/magnesium ratio, showing a general pattern to be expected from igneous fractionation: alkalis and Ce rise, MgO, Ni, and Cr fall, although Ba and SiO_2 are equivocal. The latter, in particular, generally show a slight rise with increasing differentiation, although the pegmatite is anomalous with high Fe*/MgO and a relatively low silica content. Possibly, processes other than crystal fractionation that also involve volatiles can account for this anomaly.

The precise nature of the dolerite body is not entirely agreed upon (see, e.g., "Domain III: Dolerite," p. 30) and the chemistry may shed some light on the problem. It is clear from the data in Tables T4 and T5 that dolerite compositions are not randomly distributed. The most primitive compositions are at the top and bottom, the more evolved compositions toward the middle. This is consistent with the samples coming from a single dolerite sheet rather than clasts in a conglomerate, but analyses would need to be more numerous to give a definitive answer.

Interpretation

Our preliminary interpretation is that this is a conglomerate body consisting largely of dolerite and subordinate basaltic clasts in a matrix composed largely of weathered dolerite-derived material, most of which was probably not recovered (see "Downhole Measurements," p. 45). The latter type of clast may be samples of the dolerite chilled margin, although the relatively large amount of fine-grained basalt in these overlying units suggest that there were lava flows in the hinterland as well as dolerite.

The dolerite clasts have been fractured and subjected to subaerial alteration, most likely aided by fluid circulation within fractures and prior to incorporation in the conglomerate, although this may have taken place along cracks and fissures in a dolerite body. The interpretation of the overall nature of the unit relies heavily on FMS logging data, which extends down to Core 180-1118A-72R and suggests that the dolerite clasts recovered from Cores 70R to 72R are part of a large conglomerate unit from which only minimal matrix material has been recovered. However, no FMS data is available below Core 72R, and the dolerite recovered below may either be part of the same conglomerate or could be in situ brecciated dolerite. The alternative interpretation (i.e., it is a fractured dolerite body) cannot be ruled out and is, in fact, supported to some extent by the chemical data.

The mineralogy and chemistry suggest that dolerite clasts within this breccia are similar to those of the dolerite unit encountered at Site 1109. Further comparison of petrological and chemical evidence, such as mineral chemistry, trace element and isotope geochemistry, and radiometric dating between Sites 1109 and 1118 from the hanging wall and Sites 1114 and 1117 from the footwall of this fault system, will be required to clarify the relationship between rocks from each site and to determine the tectonic settings in which these rocks were formed.

F41. Major and trace elements from Site 1118, p. 95.
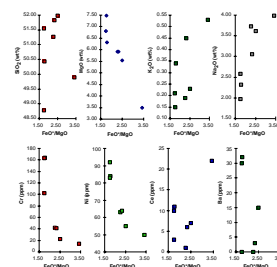
STRUCTURAL GEOLOGY

The 722-m-thick section cored below 205 mbsf at Site 1118 is composed of a 664-m-thick sedimentary succession, Pleistocene–early Pliocene in age (see "Biostratigraphy," p. 31) that overlies a dolerite at 869 mbsf described in "Igneous and Metamorphic Petrology," p. 25, and subsidiary sedimentary rocks (see "Lithostratigraphy," p. 4).

The sedimentary section is composed of seven lithostratigraphic units described in "Lithostratigraphy," p. 4. It is subdivided into three structural domains. Domain I is characterized by undeformed zones or zones with soft-sediment disturbances only. Domain II extends throughout the lower part of the sequence and exhibits brittle fault zones. The dolerite at the bottom of the hole comprises Domain III and is sheared, brecciated, and veined. In the following, the depth of the sections refers to their top.

Domain I

Domain I constitutes most of Hole 1118A (~90% of the total thickness). It includes undeformed zones (Subdomain Ia) and two types of soft-sediment deformation zones (Subdomains Ib and Ic) that alternate along the section. The deformed zones are between 272.1 and 583.7 mbsf (Core 180-1118A-8R to Section 40R-3; lithostratigraphic Units I, II, and III).

Subdomain Ia

Subdomain Ia comprises five undeformed zones where bedding dip is consistently <10° (Figs. F42, F43). Minor normal faulting is rarely observed in intervals 180-1118A-30R-4, 116–120 cm (488.76 mbsf), and 33R-2, 9–15 cm (514.27 mbsf; Fig. F42).

Subdomain Ib

Subdomain Ib shows soft-sediment deformations that are fully described in "Soft-Sediment Deformation," p. 6. They are principally developed within two relatively narrow zones at 320.3–335.2 mbsf (Sections 180-1118A-13R-1, to 14R-4), and 396.8–406.3 mbsf (Core 180-1118A-21R).

Deformation consists of dm-sized slump folds commonly found throughout 50-cm-long deformed intervals (intervals 180-1118A-14R-1, 55–90 cm; and 14R-2, 0–40 and 80–115 cm; and 14R-3, 5–70 cm). Individual folds are usually truncated both on top and bottom by flat-lying sliding planes with sense of motion compatible with the asymmetry of the folds (intervals 180-1118A-14R-2, 94–96 cm; 14R-3, 10–28 cm; and 21R-1, 47–48 cm). Slump folds show nearly horizontal axes (intervals 180-1118A-14R-2, 0–12 and 108–115 cm). The close association of folding and minor faulting is well documented at interval 180-1118A-14R-1, 60–70 cm, where steep and closely spaced reverse microfaults dissect a slightly overturned fold limb, both fault and fold displaying similar verging. This local compressional faulting indicates that sediments were already sufficiently lithified to deform in a relatively brittle manner, yet still plastic enough to also record folding. Slump fold limbs are also locally intensely disrupted by low-angle (20°–40°) extensional faulting (interval 180-1118A-14R-2, 110–115 cm).

F42. Structural features at Site 1118, p. 96.
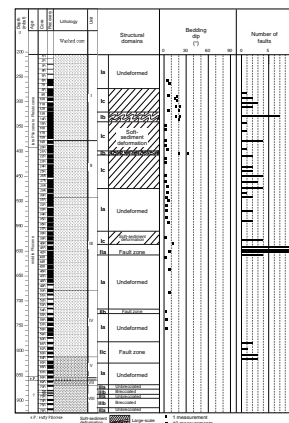
F43. Bedding dips in Domains I and II, p. 97.
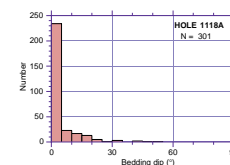
Subdomain Ic

The structures of Subdomain Ic also result from soft-sediment deformations, but differ from the structures described above with respect to their scale, their vertical distribution, and their frequency. Nearly each core of Subdomain Ic contains one thin discrete deformed zone a few centimeters thick separating much thicker intervals with no deformation and horizontal bedding (Table T6). Deformation consists of centimeter-scale slump folding and normal microfaulting (Fig. F44) that are assumed to have occurred at an early stage shortly after deposition of the sediments. The more demonstrative examples are vertical, locally reverse, faults that flatten downward into horizontal clay-rich intervals (interval 180-1118A-25R-3, 50–55 cm), and normal faults filled with disturbed sediments (interval 180-1118A-25R-2, 50–62 cm). The microscale deformations regularly distributed throughout Subdomain Ic may reflect instability caused by rift-related earthquakes.

Domain II

The lower part of the sedimentary sequence comprises three fault zones (Subdomains IIa, IIb, and IIc).

Subdomain IIa

The first evidence for brittle faulting is found in Subdomain IIa at 583.7–608.4 mbsf (Sections 180-1118A-40R-4, to 42R-8), where slickensided fault planes dip generally at moderate to low angles (<60°) and show dip-slip motion (Fig. F45A). The fragmentation of clayey material regarded as scaly fabrics is related to either shallow-angle faulting (intervals 180-1118A-42R-2, 66–70 cm; 42R-3, 3–7 cm; and 42R-8, 7–11 cm), or more rarely to nearly vertical dip-slip faulting (interval 180-1118A-41R-4, 120–145 cm).

Evidence for multistaged brittle deformation is provided in interval 180-1118A-40R-4, 50–98 cm, where a well-laminated upward-fining sequence is cut by two steep (70°) normal faults facing to the east (core reference frame) with flat-lying beds in the hanging wall. They are labeled Fe in Figure F46A. On the contrary, the footwall is much more intricate and has shallow (25°–30°), west-dipping normal faults (Fw) whose footwall has bedding steepening progressively upward. These two opposite-facing extensional fault patterns may involve early shallow structures (Fw) with progressively rotated hanging walls as faulting propagated forward (Fig. F46B). As a response to the possible locking of this earlier shallow fault system, steeper faults (Fe) might have developed later with opposite vergence, probably facilitated by the favorable dipping attitude of the previously rotated strata.

In addition to this two-staged brittle faulting, earlier soft-sediment deformation is also documented in interval 180-1118A-40R-4, 50–98 cm. It is expressed in the dominantly clayey hanging-wall sequences of the fault (Fe) by a nearly vertical fault cutting through horizontal sandy layers with a normal offset (~1 cm) that fades away rapidly upward and downward. This fault is, therefore, likely to form an early compaction-induced structure, and finally, the structure observed in Core 180-1118A-41R is assumed to have recorded at least three stages of extensional synsedimentary faulting.

Table T6. Deformed intervals and corresponding structures, **p. 182.**

F44. Normal microfault zone in Subdomain Ic, **p. 98.**
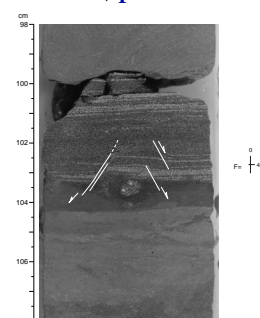
F45. Slickenside plunge vs. fault dip for Domain II, **p. 99.**
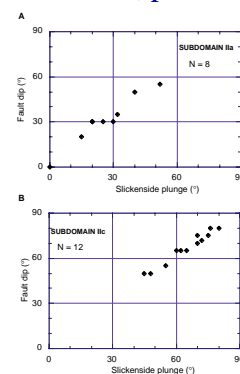
F46. Extensional faulting in Subdomain IIa, **p. 100.**
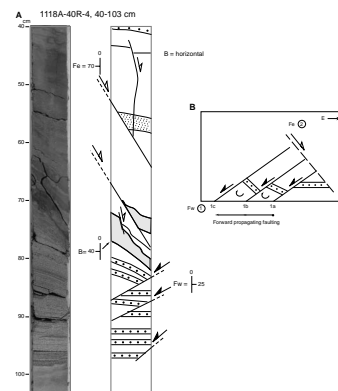
Subdomain IIb

Subdomain IIb represents a narrow normal fault zone at 714.4–715.8 mbsf (Section 180-1118A-54R-1) that includes steep (70°–85°) conjugate fault surfaces with dip-slip slickensides.

Faulting is well developed in Subdomain IIc at 784.5–813 mbsf (Sections 180-1118A-61R-3 through 64R-2), where steep conjugate fault planes dipping 50°–80° show exclusively dip-slip sense of motion (Fig. F45B). Curved secondary faults are locally observed in the hanging wall of the faults, as in intervals 180-1118A-63R-1, 40–50 and 100–110 cm.

Domain III: Dolerite

The dolerite was first encountered within Section 180-1118A-70R-3 (871 mbsf) below a conglomeratic unit composed of a carbonate matrix containing well-rounded basaltic clasts and fragments from a lagoonal environment (refer to "Lithostratigraphic Unit VII," p. 19). Two subunits are defined within the dolerite (Fig. F47).

An unbrecciated dolerite (Subdomain IIIa) exists within interval 180-1118A-70R-3, 82–140 cm (872.07–872.65 mbsf), and Sections 74R-1 and 2 (897.5–900.4 mbsf), 75R-3 (908.6–909.7 mbsf), and 76R-1 (917.0–918.3 mbsf). In this part of the sequence the rocks are mainly undeformed and a granular magmatic texture is preserved (see "Igneous and Metamorphic Petrology," p. 25). In some samples conjugate fractures or veins filled with calcite and zeolite (Fig. F48) crosscut the dolerite. These fractures and veins are oriented north-south and dip 35°–70° to the east or to the west (core reference frame). No motion is visible along the planes.

A massively brecciated dolerite (Subdomain IIIb) is found in Sections 180-1118A-71R-1 to 73R-2 (878.4–889.4 mbsf), and 74R-3 to 75R-2 (900.4–908.6 mbsf). These two zones show a progressive increase in brecciation from the fractured dolerite to the brecciated dolerite. Perpendicular veinlets invade the rock from main veins fragmenting the dolerite as fluid circulation proceeded (Fig. F49). Figure F50 shows a network of veins in the dolerite. Veining resulted in the fragmentation of the dolerite into angular domains, which are visible on the lower right part of the sample where an angular dolerite fragment in dark brown matrix has been separated from the massive dolerite. The ultimate stage of the brecciation shows a dark brown clay-sized, iron oxide–rich matrix containing angular dolerite clasts (Fig. F51). In some samples the breccia consists of individual pebbles without matrix (Fig. F52).

In the upper part of Subdomain IIIb (Sections 180-1118A-71R-1 and 72R-1 and interval 180-1118A-73R-1, 0–15 cm) the pebbles of the breccia differ from the pebbles of Sections 74R-3 to 75R-2 because they show fault planes bearing slickensides. These structures represent a deformation stage developed in the upper part of the brecciated Domain III. Thus, it is difficult to determine if the shearing occurs prior, after, or contemporaneous to the brecciation of the dolerite.

The brecciated zones localized fluid circulation, which was responsible for the alteration (weathering) of the rocks in subaerial conditions. This breccia could have been reworked later on because some fragments of the Subdomain IIIb are well rounded (see "Lithostratigraphy," p. 4).

F47. Structural interpretation of dolerite, p. 101.
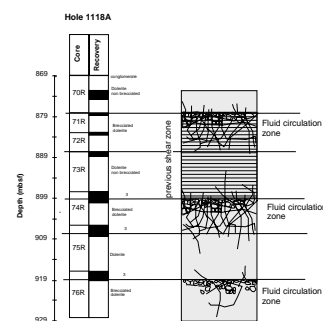
F48. Dolerite showing a calcite-zeolite vein, p. 102.
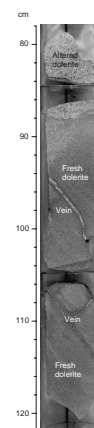
F49. Fluid infiltration through the dolerite, p. 103.
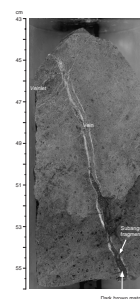
F50. Evolution of brecciation into dolerite, p. 104.
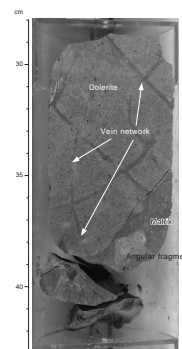
BIOSTRATIGRAPHY

Calcareous Nannofossils

Abundance and Preservation

Samples 180-1118A-1R-CC to 32R-CC contain few to abundant (mostly common), moderately to well-preserved nannofossils. In Samples 180-1118A-33R-CC through 36R-CC, nannofossils are common, but poorly preserved. From Samples 180-1118A-37R-CC through 59R-CC, nannofossils are mostly common and preservation is moderate, with the exception of Sample 180-1118A-52R-CC, in which nannofossils are rare and preservation is poor. Nannofossils are few to common in abundance from Samples 180-1118A-60R-CC through 68R-3, 109–110 cm, and preservation is moderate. Samples 180-1118A-68R-CC to 70R-CC are barren. Sample 180-1118A-71R-CC and Cores 72R to 76R contain no sediment.

Zonation

The nannofossils zonation for Hole 1118A is given in Figure **F53;** nannofossils present are listed in Table **T7.**

The last occurrence (LO) of *Discoaster brouweri* marks the top of Zone NN18. Although this species occurs consistently from Samples 180-1118A-1R-CC through 6R-CC, the numbers present are relatively less than the numbers of *D. brouweri* in Sample 180-1118A-9R-CC and below (we found no specimens of *D. brouweri* in Samples 180-1118A-7R-CC and 8R-CC). We therefore assign Samples 180-1118A-1R-CC through 8R-CC to Zone NN18/Subzone NN19A undifferentiated (*Gephyrocapsa oceanica* is absent), and Samples 180-1118A-9R-CC through 14R-CC to Zone NN18 (Fig. **F53**). The LO of *D. pentaradiatus* in Sample 180-1118A-15R-CC marks the top of Zone NN17. The top of Subzone NN16B is indicated by the LO of *D. surculus* in Sample 180-1118A-19R-CC. The LO of *D. tamalis* in Sample 180-1118A-37R-CC marks the top of Subzone NN16A. Samples 180-1118A-37R-CC to 68R-3, 109–110 cm, are in Subzone NN16A.

Planktonic Foraminifers

Abundance and Preservation

The abundance of planktonic foraminifers at this site was greatly affected by the input of detrital sand. From Samples 180-1118A-1R-CC through 24R-CC specimens were common to abundant and their preservation was good, except for Samples 180-1118A-12R-CC, 15R-CC, and 21R-CC, which had rare to few well-preserved planktonic specimens. From Sample 180-1118A-25R-CC through 30R-CC planktonic specimens were common to abundant and moderately well preserved, except for Sample 180-1118A-28R-CC in which the specimens were few with moderate preservation. From Samples 180-1118A-31R-CC through 36R-CC specimens were rare to few and moderately well preserved. Samples 180-1118A-37R-CC through 51R-CC had common to abundant planktonic specimens, which had moderate to good preservation, except for Samples 180-1118A-38R-CC, 41R-CC, 43R-CC, 45R-CC, and 51R-CC in which the specimens were rare or few with variable preservation. From Samples 180-1118A-53R-CC through 63R-CC planktonic

F51. Brecciated dolerite at Site 1118, **p. 105.**
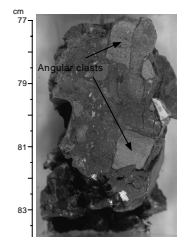
F52. Dolerite clasts without matrix, **p. 106.**
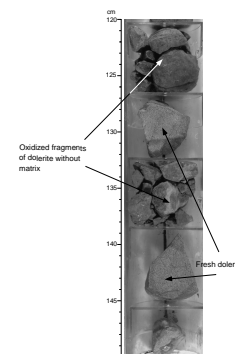
F53. Biostratigraphic units and ages, Hole 1118A, **p. 107.**
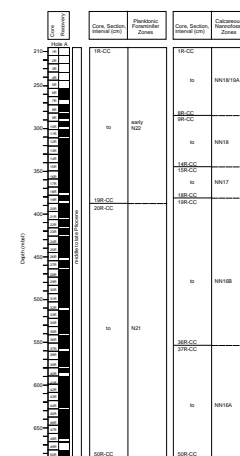
Table T7. Stratigraphic distribution of calcareous nannofossils, **p. 183.**

specimens were common and with moderate to good preservation, except for Samples 56R-CC and 58R-CC in which the specimens were few, with moderate to good preservation. Samples 180-1118A-64R-CC through 66R-CC had rare to few specimens, which were moderately well to poorly preserved. The final samples above the limestone, Samples 180-1118A-67R-CC and 68R-1, 0–1 cm, had common to abundant planktonic specimens that were moderately well preserved. In Sample 180-1118A-68R-3, 109–110 cm, the abundant planktonic specimens were poorly preserved.

Zonation

The planktonic foraminiferal zonal stratigraphy for this site is presented in Figure F53 and the species distribution is shown in Table T8. Coring began at 205 mbsf in Zone N22 of late Pliocene age. Samples 180-1118A-1R-CC through 19R-CC are assigned to early Zone N22 and on the co-occurrence in most of the samples of *Globorotalia tosaensis,* *Globigerinoides fistulosus,* and *Globorotalia truncatulinoides,* which first appears in Sample 180-1118A-19R-CC (384.2 mbsf). Samples 180-1118A-20R-CC through 51R-CC contain *G. tosaensis,* indicative of Zone N21. The LO of *Dentoglobigerina altispira* (LAD 3.09 Ma) is in Sample 180-1118A-42R-CC (608.2 mbsf). Samples 180-1118A-52R-1, 27–30 cm, through 68R-1, 0–1 cm, were assigned to Zone N20, based on the presence of *Globorotalia crassaformis* in the absence of *G. tosaensis.* Sample 180-1118A-68R-3, 109–110 cm, taken 5 cm above limestone, was assigned to Zone N20 because of the presence of only dextral *Pulleniatina.* The limestone in Core 180-1118A-68R contained common planktonic foraminifers in Sample 180-1118A-68R-4, 46–48 cm, including *Globorotalia tumida,* suggesting continued deposition in Zone N20 or at least in the latest Miocene or early Pliocene.

Benthic Foraminifers

This site was drilled in 2304 m water depth, but the upper 205 m were not cored. The paleobathymetry is indicated in Figure F54. Benthic foraminiferal assemblages suggest a middle bathyal (500–2000 m) paleodepth from Samples 180-1118A-1R-CC through 18R-CC (375.4 mbsf) with such characteristic species as *Cibicidoides rugosus, Laticarinina pauperata, Quinqueloculina venusta, Sphaeroidina bulloides,* and *Uvigerina bradyana* represented in the samples. From Samples 180-1118A-19R-CC through 68R-3, 109–110 cm (396.8–853.2 mbsf), the assemblage suggests upper bathyal depths (150–500 m). Representative species include *Martinottiella communis, Rectobolivina columellaris* striate var., *Rotalia* sp., *Siphonina tubulosa/australis,* and *Uvigerina schwageri.* Benthic foraminifers were rare in many of these samples, which contained ash and various turbidite layers. Core 180-1118A-68R below Section 3, 117 cm, contains limestone with calcareous algae, corals, smaller benthic rotaliine and milioline foraminifers, and rare larger pre-middle Miocene orbitoid and miliolid species, as well as common planktonic foraminifers. As mentioned above, in Sample 180-1118A-68R-4, 46–48 cm, *Globorotalia tumida* was among the planktonic species embedded in the limestone. The overlying upper bathyal foraminiferal assemblages (sample taken 5 cm above the limestone) also contain abundant planktonic foraminifers, including the relatively deep dwelling *Globorotalia tumida,* suggesting these limestones represent shallow-reef material, redeposited in upper bathyal depths.

Table T8. Stratigraphic distribution of planktonic foraminifers, p. 185.

F54. Age-depth relationship at Site 1118, p. 109.
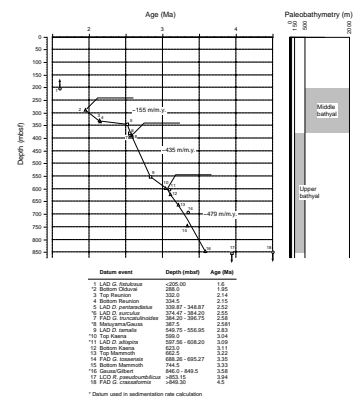
Sediment Accumulation Rate

We estimated the sedimentation rate based on nannofossil and foraminifer datum events and magnetic chron and subchron boundaries at Site 1118 (Fig. **F54**). The biostratigraphic data are indefinite above ~340 mbsf, and we have used only the paleomagnetic data to draw the sedimentation curve there.

PALEOMAGNETISM

The investigation of magnetic properties at Site 1118 included (1) the measurement of bulk susceptibility of whole core sections, (2) point susceptibility and remanent magnetization of archive half core sections, and (3) susceptibility and its anisotropy and remanent magnetization of discrete samples.

Magnetic Susceptibility

Magnetic susceptibility measurements were made on whole core sections as part of the multisensor track (MST) analysis (see **"Magnetic Susceptibility,"** p. 44, in "Physical Properties"), and on half core sections as part of the archive multisensor track (AMST) analysis. MST and AMST susceptibilities (uncorrected for volume) ranged dominantly between values on the order of 10^{-4} and 10^{-3} SI; however, near the bottom of the hole values as low as 10^{-6} SI and as high as 10^{-2} SI occurred (Fig. **F55A**). In general, susceptibility data from the MST and AMST analyses agreed; differences in magnitude can be attributed to volume differences for the uncorrected data.

The trends of susceptibility and remanent intensity data after AF demagnetization at 20 mT are broadly similar (Fig. **F55B**). Increasing susceptibility values up the recovered section suggest that the contribution of remanence-carrying ferromagnetic minerals to the susceptibility also increases upward. The very high values (10^{-2}–10^{-1} SI) below ~860 mbsf indicate that ferromagnetic minerals dominate the susceptibility near the bottom of the hole, probably related to the occurrence of volcanics (see **"Lithostratigraphy,"** p. 4, and **"Igneous and Metamorphic Petrology,"** p. 25).

Results of the measurement of the susceptibility and its anisotropy (AMS) on 119 discrete samples are shown in Figure **F56A** and **F56B**. The mean magnetic susceptibility, the degree of anisotropy (P_j) and the shape parameter (T) for the susceptibility ellipsoid (Jelinek, 1981), and the inclinations of the maximum (K_{max}) and minimum (K_{min}) axes of the susceptibility ellipsoid are shown vs. depth in Figure **F56A**. Stereonet plots in Figure **F56B** show the orientations of the principal axes of the susceptibility ellipsoids after correction for bedding tilt and for core orientation using the declinations of the stable remanent magnetization.

Mean susceptibilities from discrete samples generally agreed with long core susceptibilities. Between ~380 and 840 mbsf, P_j values were dominantly >1.05, with high values up to ~1.8 found between ~580 and 620 mbsf. These high P_j values are probably related to faulting observed in this interval (structural Subdomain Ic; see **"Subdomain Ic,"** p. 29). The wide range of P_j values between ~380 and 680 mbsf was associated with lithostratigraphic Units II and III (see **"Lithostratigraphic Unit II,"** p. 7, and **"Lithostratigraphic Unit III,"** p. 10). The high scatter in P_j values between ~260 and 300 mbsf and low values

F55. Susceptibility data, Site 1118, **p. 110.**
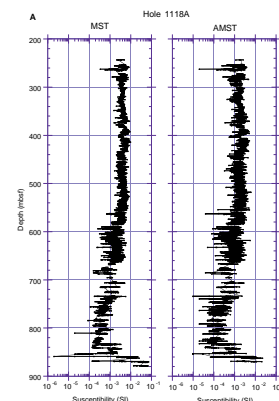
F56. AMS data: downhole plots and stereonets, **p. 112.**
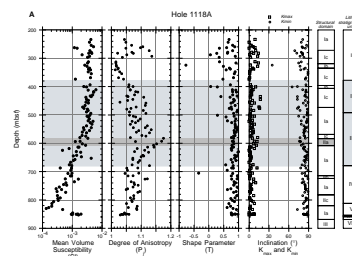
between ~300 and 380 mbsf are difficult to explain; there is no apparent correlation with the lithology (see "Lithostratigraphy," p. 4).

The T values throughout the hole were dominantly positive and >0.5, which indicates the predominance of oblate fabrics. The relatively high scatter between ~260 and 340 mbsf may be related to soft-sediment deformation observed in this interval (see "Subdomain Ic," p. 29).

Inclinations of K_{max} and K_{min} axes were strongly clustered at ~0° and 90°, respectively (Fig. F56A). Scattering of K_{max} axes toward relatively steeper values and of K_{min} axes toward relatively shallower values between ~260 and 340 mbsf correlates with the scatter in T values observed for this interval and may be related to soft-sediment deformation (see "Subdomain Ic," p. 29). After correction for core orientation, based on the polarity of the stable remanence and assuming a geocentric axial dipole field, K_{max} axes for samples from lithostratigraphic Unit III (see "Lithostratigraphic Unit III," p. 10) are preferentially aligned east-west to east-southeast to west-northwest with K_{min} axes clustered about vertical, and horizontally aligned K_{int} axes grouped about south-southwest (Fig. F56B). These data suggest an east-west to east-southeast–west-northwest paleocurrent direction. Orientations of the principal axes associated with the other lithostratigraphic units (see "Lithostratigraphy," p. 4) may reflect paleocurrent information, but the data are not as clear as those from lithostratigraphic Unit III. Therefore, interpretation of paleocurrent information based on AMS results from the other lithostratigraphic units is not attempted in this report.

In summary, compaction effects are evident from the AMS data throughout the recovered section from Hole 1118A. An east-west to east-southeast to west-southwest paleocurrent direction is inferred for lithostratigraphic Unit III; the other lithostratigraphic units may contain paleocurrent information, but the data are equivocal without additional study.

Remanent Magnetization

Measurements of remanent magnetization were made on all but the most disturbed sections from archive half cores and on discrete samples from working half core sections. Results are shown in Figures F57 and F58.

A total of 121 discrete samples were subjected to AF demagnetization experiments to assess the stability of the natural remanent magnetization (NRM). The AF demagnetization results indicate that the NRMs of the samples generally consist of two magnetic components. A soft component, probably drilling-induced, with a shallow to steep downward direction was generally removed by demagnetization levels up to 15 mT. After removal of the soft component, most samples yielded a stable component that decayed linearly toward the origin of vector plots between 15 and 25 mT (Fig. F57A, F57B, F57C, F57D); this component is referred to as the characteristic remanent magnetization (ChRM). A few samples showed erratic behavior during AF demagnetization, which indicated a large contribution of a probable drilling-induced component (Fig. F57E, F57F); the ChRM from the samples was not isolated.

In Hole 1118A, intensity of remanent magnetization of long cores after AF demagnetization at 20 mT ranged from values on the order of 10^{-4} A·m^{-1} up to values on the order of 10^{-2} A·m^{-1}, with values generally increasing up the hole (Fig. F58A).

F57. Demagnetization behavior of discrete samples, p. 114.
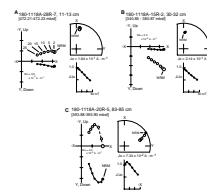
F58. Intensity, inclination, and declination, p. 116.
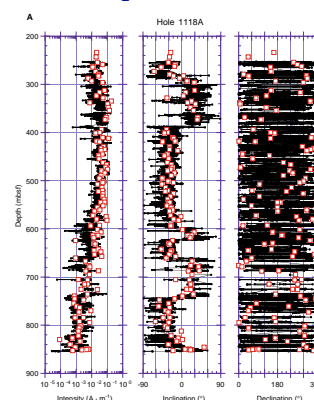
The polarity of the remanent magnetization after AF demagnetization at 20 mT for Site 1118 was determined from the inclinations. Declinations were highly scattered, which precluded their use for magnetostratigraphic interpretation. Directions were corroborated by discrete sample analysis.

Magnetostratigraphy

Figure F58A shows downcore variations of intensity, inclination, and declination from long core and discrete sample measurements. Magnetostratigraphic interpretation based on the inclinations is shown in Figure F58B.

Chron Boundaries

The polarity change at ~387.5 mbsf represents the Matuyama/Gauss boundary (2.58 Ma; Berggren et al., 1995) and is consistent with the paleontologic data (see "Biostratigraphy," p. 31).

The Gauss/Gilbert boundary (3.58 Ma; Berggren et al., 1995) is at ~846–849.5 mbsf. Using an estimated sedimentation rate of ~435 m/m.y. for the time period between 2.58 and 3.04 Ma, and a rate of ~485 m/m.y. for the time period between 3.04 and 3.58 Ma, the Gauss Chron should span ~462 m of section, which is consistent with the observed span of 458.5 to 462 m.

Subchrons

The onset of the Olduvai Subchron (C2n; 1.77–1.95 Ma; Berggren et al., 1995) is at ~288 mbsf; the termination of the Olduvai was not recovered from this site.

The termination and beginning of the Kaena Subchron (C2An.1r; 3.04–3.11 Ma; Berggren et al., 1995) are at 599 and 623 mbsf, respectively. Using an estimated sedimentation rate of ~319 m/m.y. based on the paleontologic datums at ~550 and 608 mbsf (see Fig. F54), the Kaena should span ~22 m of section, which is consistent with the observed span of ~24 m.

The Mammoth Subchron (C2An.2r; 3.22–3.33 Ma; Berggren et al., 1995) spans the interval between ~662.5 and 744.5 mbsf. Using an estimated sedimentation rate of ~485 m/m.y. (see "Sediment Accumulation Rate," p. 33), the Mammoth should span ~53 m of section, which is not consistent with the observed span of ~82 m. The termination of the Mammoth is consistent with the paleontologic data; however, there is a discrepancy between the stratigraphic positions of the first occurrence of *G. tosaensis* (3.35 Ma) and the beginning of the Mammoth (see "Biostratigraphy," p. 31).

Excursions

Evidence for the Reunion Subchron (C2r.1n; 2.14–2.15 Ma; Berggren et al., 1995) is between ~332 and 334.5 mbsf. Using an estimated sedimentation rate of ~155 m/m.y., the Reunion should span ~1.6 m of section, which is reasonably consistent with the observed span of ~2.5 m.

INORGANIC GEOCHEMISTRY

Twenty-six interstitial water (IW) samples were collected at Site 1118. Samples were taken every other core between 258 and 526 mbsf and every third core until Core 180-1118A-67R, at 842 mbsf just above the sandstone/limestone boundary. No samples are available between the mudline and ~200 mbsf because this interval was drilled but not cored. All whole-round samples yielded sufficient IW to allow shipboard determination of the same full suite of constituents as analyzed at Sites 1109 and 1115. Data from this site complement those obtained at the latter two, and the resultant north-south IW chemistry transect provides a basis for evaluating sediment diagenesis in the Woodlark Rise on a more regional basis.

Results

The IW was analyzed for salinity, pH, alkalinity, major cations (Na^+, K^+, Ca^{2+}, and Mg^{2+}) and anions (Cl^- and SO_4^{2-}), Li^+, Sr^{2+}, SiO_2, and NH_4^+. Results of shipboard inorganic chemical analyses are presented in Table T9. Profiles of inorganic constituents are presented in Figures F59 and F60. Large changes in the concentrations of many of the dissolved constituents were observed below 400 mbsf.

pH, Alkalinity, Sulfate, and Ammonium

The pH remains in a narrow range (8.1–8.6) throughout the entire sedimentary column. The samples from 427 to 635 mbsf, however, define a broad subtle maximum, whereas lower values are found below 650 mbsf. The titration alkalinity profile displays a large decrease from a maximum of 13 mM in the first sample collected to 396 mbsf (Fig. F59A). The highest alkalinity value here is nearly identical to the maximum of 13.4 mM observed at Site 1109, but substantially greater than that at Site 1115. Below 400 mbsf, alkalinity remains mostly <2 mM until 635 mbsf. A few samples near the bottom of lithostratigraphic Unit IV define a submaximum that occurs at 783 mbsf. Overall, the alkalinity profile is more similar to what was observed at Site 1109 than at Site 1115. Dissolved SO_4^{2-} is essentially absent from the pore water with only a few very small excursions at depth until 635 mbsf. An unexpected increase in the concentration of SO_4^{2-} was observed below 700 mbsf. A concentration of 13 mM, or nearly half the seawater concentration, is at 811 mbsf. No such increase was observed at the bottoms of Sites 1109 and 1115. Dissolved NH_4^+ concentrations are higher here than seen in the two other deep sedimentary profiles. The highest value of NH_4^+ (2822 µM) coincides with the highest alkalinity value and is in the first sample collected (Fig. F59A). The sharp decrease in NH_4^+ downhole to a minimum of 1375 µM at 526 mbsf and subsequent increase to a broad submaximum further downhole is also reminiscent of what was observed at Site 1109 (see Fig. F70A, p. 162, in the "Inorganic Geochemistry" section of the "Site 1109" chapter). Unlike the latter, however, the deep NH_4^+ submaximum here is characterized by substantially lower concentrations than observed at Site 1109. Additionally, the maintenance of relatively elevated concentrations of NH_4^+ near the bottom of the hole is surprising in light of the elevated SO_4^{2-} concentrations.

Table T9. Interstitial water geochemistry, Site 1118, p. 187.

F59. Interstitial water constituents, Site 1118, p. 118.
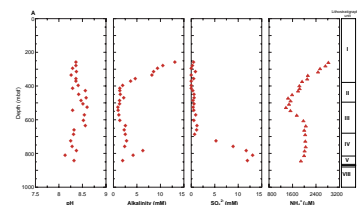
F60. Dissolved SiO_2 in sediments, p. 121.
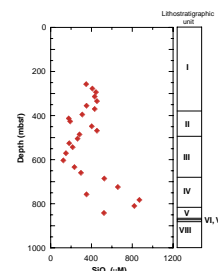
Salinity, Sodium, Chloride, Potassium, and Lithium

Salinity fluctuates only slightly between 32 and 34 (Table T9). Lower values were observed in the upper section of the sampled sediments (258–413 mbsf). A salinity of 34 at 427 mbsf is followed by a general decrease downhole and a return to this same value in the bottom three samples. The latter samples correspond to the samples defining the deep-seated SO_4^{2-} maximum. As noted at Site 1115, the salinity variations do not correlate with Na^+ or Cl^-; however, the range of variations of the latter two is much narrower here than observed at both Sites 1109 and 1115 (see "Inorganic Geochemistry," p. 54, in the "Site 1109" chapter and "Inorganic Geochemistry," p. 38, in the "Site 1115" chapter). The sharp drop in Cl^- noted in the brackish water–derived lagoonal sediments immediately above the dolerite at Site 1109 is notably absent here. Dissolved Na^+ and Cl^- display a rough inverse correlation throughout the sedimentary column, although the Na^+ minimum is present at a shallower depth than the Cl^- maximum.

The K^+ profile (Fig. F59B) displays a sigmoidal shape that is more similar to that observed at Site 1109 than at Site 1115. Yet, substantial differences exist in the K^+ profiles of all three sites. Concentrations of K^+ are slightly elevated relative to seawater near 300 mbsf, but decrease to a minimum of 4.1 mM by 543 mbsf. This minimum is lower than a comparable minimum of 6 mM near 300 mbsf at Site 1109 (see "Inorganic Geochemistry," p. 54, in the "Site 1109" chapter). The return below this depth to near-seawater concentrations of K^+ at 725 mbsf also resembles such a feature at Site 1109, although it is at much shallower depths at the latter.

Dissolved Li^+ (Fig. F59B) exhibits a nearly steady increase in concentration downhole with concentrations near 150 µM in the volcaniclastic sand-rich sediments at the bottom of the hole. These values are greater than observed at other Leg 180 sites. Furthermore, the Li^+ profile here displays none of the variations observed at Sites 1109 and 1115.

Calcium, Magnesium, and Strontium

Dissolved Ca^{2+} exhibits the narrowest range of concentrations (2.6–26 mM) of the three northern sites. This constituent is most depleted relative to seawater at 258 mbsf, below which it increases to a well-defined maximum near 500 mbsf. Although Ca^{2+} concentrations decrease to about a 10% enrichment over seawater by 725 mbsf, significant increases are observed in the underlying volcaniclastic sand-rich sediments of lithostratigraphic Unit V (see "Lithostratigraphic Unit V," p. 16). The Mg^{2+} profile remains in a narrow concentration range of 35–38 mM from 258 to 604 mbsf. Decreases in concentration that are below this depth contrast sharply with those observed at Sites 1109 and 1115. The minimum of 24 mM in the deepest IW sample is ~45% of the seawater value. This is a much greater concentration than observed at the other northern sites where Mg^{2+} concentrations were as low as 11 and 2 mM, respectively.

The Sr^{2+} profile at Site 1118 fluctuates in the range 53–83 µM between 257 and 544 mbsf (Table T9; Fig. F59C), below which a smooth and substantial increase in concentration is found to the bottom of the hole. The maximum Sr^{2+} concentration of 631 µM is in lithostratigraphic Unit V within volcaniclastic sands and coincides with the most elevated Li^+ concentrations. Excluding the upper 250 mbsf of

the hole, which was not sampled, the Sr^{2+} profile seems most similar to that observed at Site 1109, although the maximum concentration is only about one third of that at the latter site. Additionally, the Sr^{2+} maximum is not as sharply defined as the increase noted in the aragonitic shell-rich sediments of lithostratigraphic Unit VII at Site 1109 and the subsequent decrease toward the underlying dolerite. The latter feature is absent here (see "Lithostratigraphic Unit VII," p. 19).

Silica

The dissolved SiO_2 profile (Fig. F60) displays more complexity than those of other pore-water constituents at this site, as it did at Sites 1109 and 1115 (see "Inorganic Geochemistry," p. 54, in the "Site 1109" chapter and "Inorganic Geochemistry," p. 38, in the "Site 1115" chapter). Because the upper 250 mbsf of the profile are missing here, it is impossible to know at what depth in the sediments dissolved SiO_2 exhibits its primary transitions from low concentrations to the range of 400–500 µM, which is usually observed in the upper several hundred meters. Additionally, the return to concentrations of SiO_2 <200 µM, observed at depth at Sites 1109 and 1115, does not occur here. Rather, the highest SiO_2 concentrations (822–871 µM) are present in the samples near the boundary between lithostratigraphic Units IV and V (see Fig. F60). Comparing the profiles from the three northern margin sites, it appears that the profile here is most similar to that of Site 1109. A major difference is a substantial downhole shift of the SiO_2 concentration maximum that was observed in the deeper of the two high-porosity intervals at Site 1109 (see Fig. F71, p. 165, in the "Site 1109" chapter).

Discussion

Although many of the data needed to interpret the changes in the chemistry of interstitial fluids at Site 1118 were not processed as fully as those from other sites because of time constraints, certain similarities in some of the IW constituent profiles from Sites 1109, 1115, and 1118 suggest that the same diagenetic reactions mediate the pore-water composition at Site 1118. Furthermore, the IW chemistry appears most similar between Sites 1109 and 1115. Among the similarities can be included the behavior of pH, alkalinity, SO_4^{2-}, and NH_4^+ in the upper section of these sites. Although the upper 200 m of Site 1118 was not cored, it appears that the chemistry of the biologically influenced constituents follows similar trends in the upper 500 m at Site 1109 and the upper 700 m at Site 1118. This is not entirely surprising because the sediments of the thick onlap sequence at Site 1118 represent an expanded version of part of the section cored at Site 1109. It is also thought that within these sediments volcanic matter alteration reactions and clay-mineral diagenesis occur. The variations in the Ca^{2+}, K^+, and, to a lesser extent, Mg^{2+} profiles are consistent with this inference. Differences in the profiles of these same constituents are greater deepest in the sediments at each site. This probably arises as a result of the substantially different lithologies encountered deep in the sediments at each site.

Thus, concentrations of IW constituents in the upper portions of all holes primarily reflect the oxidation of organic matter mediated by microbial activity and the concomitant early diagenesis of biogenic car-

bonates. Specific reactions believed to occur include the dissolution of aragonite and its recrystallization into low-magnesian calcite. The dominant lithologies and mineralogies at the three sites support this inference (see "Lithostratigraphy," p. 4; "Lithostratigraphy," p. 7, in the "Site 1109" chapter; and "Lithostratigraphy," p. 5, in the "Site 1115" chapter).

Deeper downhole, volcanic alteration and authigenesis become more important. These processes are common to each site and include alteration of volcanic ash layers as well as volcaniclastic sands disseminated in carbonates, precipitation of authigenic clay minerals (e.g., chlorite and smectite), as well as conversions of pre-existing detrital clays (e.g., illite and/or illite/smectite interlayering).

Some of the marked differences between the three sites result primarily from variations in the thickness of selected lithologies and/or the presence of different lithologies at one site relative to the other. Paramount among these are the existence of a lagoonal/brackish water to freshwater transitional sediment sequence overlying dolerite at the bottom of Site 1109, a connectivity between the forearc sediment sequence and the synrift sediments at Site 1115, and the absence of the transitional lagoonal/brackish water to freshwater sequence at Site 1118. The occurrence of a marked limestone/coarse sandstone neritic sediment sequence at Site 1118 likely imposes important constraints on changes in the pore-water chemistry at this site.

Profiles of dissolved K^+, Li^+, Ca^{2+}, Sr^{2+}, and SiO_2 (Figs. F59A, F59B, F60) demonstrate the importance of the presence of abundant volcaniclastic sands and of a high porosity on the pore-water chemistry. Because rates and stratigraphic occurrences of silica diagenesis in sediments are mediated strongly by temperature (Torres et al., 1995, and references therein), it is interesting to speculate that the more elevated temperature gradient at Site 1118 compared to Sites 1109 and 1115 (see "Temperature Data," p. 51) should have contributed to the existence of lower concentrations of dissolved SiO_2. The presence of abundant and only slightly altered to relatively unaltered volcanic matter deep in the coarse-grained sediments of lithostratigraphic Unit V imparts, however, an important additional constraint. This is manifested by substantially more elevated dissolved SiO_2 than might have been expected simply based on depth and temperature. The highest dissolved Li^+ concentration in the pore water from northern sites is also observed here and is consistent with a higher temperature alteration of volcanic matter. Additionally, the elevated Sr^{2+} concentrations, in the absence of a biogenic carbonate source (e.g., aragonitic gastropod shells observed at Sites 1109 and 1115), also support the inference of a volcanic source.

Summary

The chemical composition of the IW is influenced by a series of sedimentary diagenesis reactions. The alteration of volcanic matter (whether as ash layers or dispersed throughout the sediments), carbonate recrystallization reactions mediated by the microbially driven oxidation of organic matter, and silicification reactions all contribute to the observed profiles of pore-water constituents.

ORGANIC GEOCHEMISTRY

At Site 1118, the shipboard organic geochemistry program consisted of determinations of TOC, inorganic carbon, total carbon, total nitrogen, and total sulfur in sediments, in addition to the routine hydrocarbon gas safety monitoring procedure. The analytical techniques used are outlined in "Organic Geochemistry," p. 25, in the "Explanatory Notes" chapter.

Volatile Hydrocarbons

Headspace methane concentrations for Site 1118 display a typical profile for deep-sea sediments (Fig. F61; Table T10). Methane concentrations were found to be low (≤3.30 ppmv) between 214 and 243 mbsf. Below this depth, the C_1 concentration increased rapidly to ~40,000 ppmv by 304 mbsf. Methane concentrations remained between 16,000 and 98,000 ppmv until 660 mbsf where they decreased slowly to ≤9 ppmv by 734 mbsf. Methane remained below this concentration to the bottom of the hole. Ethane was the only other hydrocarbon detected. This was found at concentrations ≤55 ppmv between 264 and 686 mbsf, which coincided with the broad methane maximum (Fig. F61; Table T10). The C_1/C_2 ratio decreased from ~5000 at ~300 mbsf to ~1600 at ~600 mbsf. The broad interval of elevated methane and ethane concentrations between ~300 and ~700 mbsf coincides with the absence of sulfate in the sedimentary interstitial water (Fig. F59A) and indicates that the methane and ethane at this site are most likely of biogenic origin.

CaCO₃, Sulfur, Organic Carbon, and Nitrogen

Sedimentary $CaCO_3$ concentrations at Site 1118 are shown in Table T11 and Figure F62. Between 200 and ~600 mbsf, $CaCO_3$ contents are generally <20 wt%. The peak concentration (72.5 wt%) found at 279 mbsf represents a layer rich in foraminifers (see "Lithostratigraphic Unit I," p. 4). Between ~600 and ~850 mbsf, corresponding to the lower half of lithostratigraphic Unit III through Unit V (Fig. F1), $CaCO_3$ concentrations are more variable and range between 0 and 36 wt%. The data scatter is caused by the presence of thin ash layers throughout these units, which are characterized by low $CaCO_3$ levels. The peak in $CaCO_3$ between 854 and 869 mbsf represents lithostratigraphic Unit VII, a layer of reworked shallow-water carbonate deposits (Fig. F1).

Organic carbon and sulfur concentrations in sediments at Site 1118 were low, averaging 0.28 and 0.19 wt%, respectively (Table T11; Fig. F62). The peaks in both organic carbon (0.73 wt%) and sulfur (1.18 wt%) at 256 mbsf correspond to an interval of bioturbated volcaniclastic siltstone and claystone that is probably partially pyritized (see "Lithostratigraphic Unit I," p. 4). Organic carbon and sulfur display a trend of generally increasing concentrations downhole between 300 and 800 mbsf. The data between ~500 and ~800 mbsf, however, display considerable scatter, thought to be caused by the presence of thin ash layers that have exceptionally low organic carbon and sulfur concentrations. The available C/N ratios show that the organic carbon has a mixed marine and terrigenous source with one exception (650 mbsf), which shows a marine origin for the organic material (Table T11).

F61. C_1, C_2, and C_1/C_2 hydrocarbon contents, p. 122.
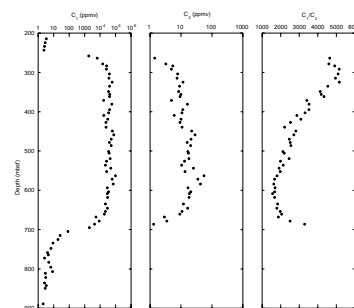
Table T10. Headspace gas in sediments, Site 1118, p. 188.

Table T11. Calcium carbonate, carbon, nitrogen, and sulfur contents, p. 189.

F62. $CaCO_3$, organic carbon, and sulfur contents, p. 123.
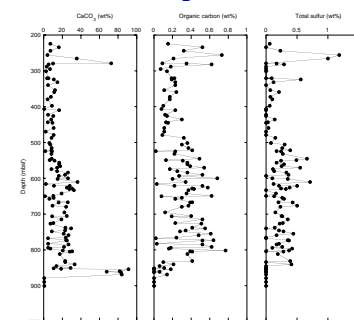
MICROBIOLOGY

Eight samples for direct microscopic examination were obtained from the lower portion of Hole 1118A, the lowest of which represent the deepest samples obtained to date from deep-sea sediments for enumeration of in situ bacterial populations.

Bacteria were present in all samples examined from 505 to 842 mbsf (Table **T12;** Fig. **F63**). The size of the bacterial population at Site 1118 lies within the 95% prediction limits of Parkes' general model for bacterial depth distributions in deep-sea sediments (Parkes et al., 1994; Fig. **F63**). Bacterial numbers appear to decrease more rapidly than predicted in the indurated material below ~750 mbsf, although porosity remains fairly high (40%–50%). However, significant numbers of bacteria were present in the deepest sample analyzed (842 mbsf) at 3.2×10^5 cells/cm^3. Dividing and divided cells follow a similar trend to total bacterial numbers and were present in all samples.

Microbial activity is responsible for many geochemical changes downhole. Depletion of IW sulfate by ~240 mbsf (Fig. **F59A**) and the subsequent rapid increase in methane concentrations (Fig. **F61**) are caused by the competitive advantage of sulfate-reducing bacteria over methanogenic bacteria in obtaining organic substrates. Conversely, below ~700 mbsf, the situation is reversed: an increase in pore-water sulfate concentration is accompanied by a rapid decrease in methane concentration (Fig. **F61**). Downhole ammonia profiles (Fig. **F59A**) also demonstrate that bacterial degradation of organic matter is continuing deep within the sediments. C_1/C_2 ratios remain high (>1000) throughout the hole, which is indicative of a biogenic source (Fig. **F61**).

Site 1118 data reinforce the findings from Site 1115 by demonstrating the presence of bacterial populations in indurated sedimentary strata at depths >800 mbsf. Below 842 mbsf, the degree of induration of the rocks is so great that the microbiological sampling methods (hammering a sterile plastic syringe into the core) were ineffective. Bacteria are present in all samples down to this point. Thus, although we have defined a limit for current sampling techniques, the limit of the biosphere in deep sediments remains undefined.

PHYSICAL PROPERTIES

Introduction

Physical properties evaluation at Site 1118 included nondestructive measurements of bulk density, bulk magnetic susceptibility, natural gamma ray, and *P*-wave velocity on unsplit cores using the MST. Discrete measurements of longitudinal and transverse *P*-wave velocities and index properties were collected on split cores. Because of the semi-indurated to well-lithified nature of the recovered sediment, thermal conductivity was measured solely from discrete rock samples. Neither undrained shear strength nor unconfined compressive strength were measured at Site 1118 because the level of sediment consolidation was too high.

Density and Porosity

Bulk densities at Site 1118 were derived from both gamma-ray attenuation porosity evaluator (GRAPE) measurements conducted on unsplit

Table T12. Bacterial populations and dividing and divided cells, **p. 191.**

F63. Bacterial populations and dividing and divided cells, Site 1118, **p. 124.**
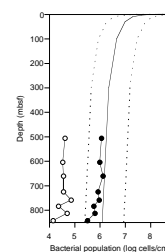
cores and discrete mass and volume measurements (Table **T13;** also in **ASCII format**). A full compilation of GRAPE data in ASCII format is also presented with the MST measurement data set on the accompanying LDEO CD-ROM. Composite profiles of these independently derived bulk densities indicate a similar trend in the two data sets with the discrete measurements defining an upper boundary of the GRAPE densities (Fig. **F64**). As observed at earlier Leg 180 sites (e.g., **"Site 1115"** chapter), GRAPE underestimation of bulk density is most likely related to small core diameters, a ramification of the RCB-coring method. Because of the high magnitude of scatter in the GRAPE data, our discussion will focus on the discrete bulk density profile.

Bulk densities at Site 1118 remain approximately constant for most of the borehole (Fig. **F64**). From the onset of significant core recovery at ~250 mbsf and extending to a depth of ~410 mbsf, bulk densities are characterized by minor scatter and average ~1.8 g·cm^{-3}. Between ~410 and 440 mbsf, the bulk densities exhibit a marked offset, averaging 1.9 g·cm^{-3}. This is observed within the claystones, siltstones, and sandstones of lithostratigraphic Unit II. Below 440 mbsf, the bulk densities remain fairly constant, ranging between 1.8 and 2.0 g·cm^{-3} until 670 mbsf. At 670 mbsf, bulk density decreases to less than 1.8 g·cm^{-3}, which corresponds to the transition from lithostratigraphic Unit III to Unit IV. Following this decrease, the densities within lithostratigraphic Unit IV increase slightly with depth, reaching a value of 1.9 g·cm^{-3} at 812 mbsf. Within the top of Unit V, from 812 to 833 mbsf, bulk densities average 1.9 g·cm^{-3}. In the lower interval of Unit V, however, the bulk densities increase significantly from 1.9 g·cm^{-3} at 833 mbsf to >2.0 g·cm^{-3} at 845 mbsf. From 845 to 862 mbsf, spanning the packstones of Unit VI and the paraconglomerates of Unit VII, densities further increase to 2.4 g·cm^{-3}. High bulk densities (2.8–2.9 g·cm^{-3}) at the base of the borehole correlate to the dolerite of lithostratigraphic Unit VIII. Bulk density outliers within the sedimentary units of the succession (i.e., 433, 503, and 767 mbsf) cannot be explained geologically and, instead, are likely a result of experimental or instrument-related error.

The profile of Site 1118 grain densities indicates a linear decrease in density with depth (Fig. **F65A**). Exceptions are found at ~440 mbsf, where a slight offset to lower grain densities is observed, and between 620 and 640 mbsf and 833 and 862 mbsf, where densities locally increase from ~2.6 to >2.7 g·cm^{-3}. A minor increase in the magnitude of scatter is seen in lithostratigraphic Unit III, which may be related to the degree of sandstone and siltstone interbedding within these sediments. As with the bulk density outliers, the peak grain density values at 433, 503, and 767 mbsf most likely reflect experimental or instrument-related error. High grain densities of 2.9 g·cm^{-3} at the base of the succession are derived from the dolerite of lithostratigraphic Unit VIII.

Porosity-depth relationships are often a function of loading history and lithostratigraphic variations. At Site 1118, a combination of these factors may be responsible for the relatively high porosities observed throughout the depth profile (Fig. **F65B**). From the onset of coring at 205 mbsf, porosities within the sedimentary succession decrease gradually with depth, but exhibit a lower boundary of only 40%. For homogeneous sediments that are not overpressured, porosity loss typically follows an exponential relationship (e.g., Terzaghi, 1925; Athy, 1930). The porosities in the upper depths (<380 mbsf) of Site 1118 thus fall within an expected range. In contrast, the porosities observed at greater depths (i.e., 380–670 mbsf) decrease only slightly and are

Table T13. Index properties measured, Site 1118, **p. 192.**

F64. Site 1118 bulk density, **p. 125.**
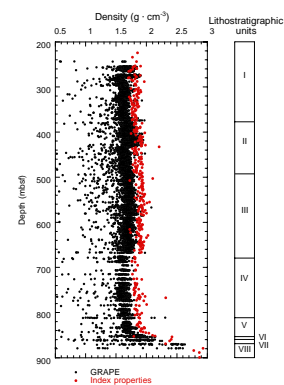
F65. Site 1118 grain density and porosity, **p. 126.**
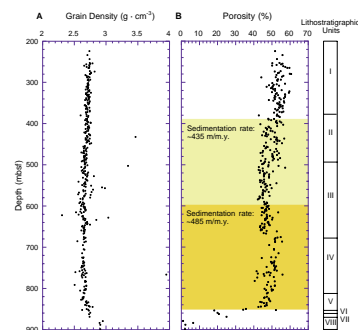
unusually high. Such a profile may reflect underconsolidation over this depth range, possibly induced by high sedimentation rates (435 and 485 m/m.y; highlighted zones in Fig. **F65B**). A sharp increase to porosities >50% is observed beginning at ~670 mbsf, after which the porosities gradually decrease but remain >40% to a depth of 850 mbsf. This abrupt increase corresponds to a thick, moderately calcareous sand unit (see **"Downhole Measurements,"** p. 45) and the transition into coarse, volcaniclastic sands (see **"Lithostratigraphic Unit IV,"** p. 13). The higher porosities in the 670–850 mbsf interval may, therefore, be a function of both lithostratigraphic change and a high sedimentation rate (485 m/m.y.). At the base of the borehole, porosities decrease from ~35% at 850 mbsf to <5% at 899 mbsf, reflecting the transition from packstones and paraconglomerates (lithostratigraphic Units VI and VII, respectively) to dolerite conglomerate (lithostratigraphic Unit VIII).

Compressional Wave Velocity

Compressional wave, or *P*-wave, velocity was measured on split cores using the PWS3 contact probe system. All cores were sufficiently indurated for ~10-cm³ sample cubes to be prepared, thereby allowing for velocity measurement in the transverse (x and y) and longitudinal (z) directions. The velocity data are presented in Figure **F66** and Table **T14** (also in **ASCII format**).

Both transverse and longitudinal velocities show a generally linear relationship with depth with some smaller scale variations (Fig. **F66**). Superposed logging velocities on the longitudinal (z) velocity show reasonable agreement. In addition, the logging velocities provide information about the uncored interval. The logging data indicate a slight increase in velocities upsection between 210 and 260 mbsf and show a trend above ~210 mbsf that differs from that defined for ~260 to ~800 mbsf within the cored interval (see **"Downhole Measurements,"** p. 45).

Between 260 and ~450 mbsf, velocities range between ~1650 and 2000 m·s⁻¹. A slight but abrupt decrease in both transverse and longitudinal velocities is found at ~660–670 mbsf, corresponding with the transition from lithostratigraphic Units III to IV. Lithostratigraphic Unit IV is a silty claystone/clayey siltstone interbedded with coarse-grained volcaniclastic sands and is consistent with the logging data interpretation that defined a relatively thick sand layer between 693 and 736 mbsf (see **"Log Unit L8,"** p. 47). Velocities increase rapidly across the transition defined by lithostratigraphic Units V and VI; lithostratigraphic Unit V is characterized by variably interbedded, poorly sorted mixed sandy and silty claystones, siltstones, and cemented sandstones with coarse-grained sandstones rich in bioclasts toward the base of the unit. Lithostratigraphic Unit VI is a shallow-water limestone (see **"Lithostratigraphic Unit VI,"** p. 18). Velocities continue to increase through lithostratigraphic Unit VII, exceeding 5000 m·s⁻¹ in the dolerite at the base of the borehole. In general, neither the linear increase of velocity with depth nor the observed minor variations (e.g., at ~540 and ~660–670 mbsf) appear to be related to variations in carbonate content (see **"CaCO3, Sulfur, Organic Carbon, and Nitrogen,"** p. 40).

Although there is a considerable amount of scatter within the anisotropy data (Fig. **F67**), transverse and longitudinal velocities typically vary by less than ± 10%. From 220 to 280 mbsf, anisotropy is positive, which indicates that the transverse velocities are greater than longitudinal velocities. In contrast, longitudinal velocities generally exceed the

F66. Site 1118 *P*-wave velocities, **p. 127.**
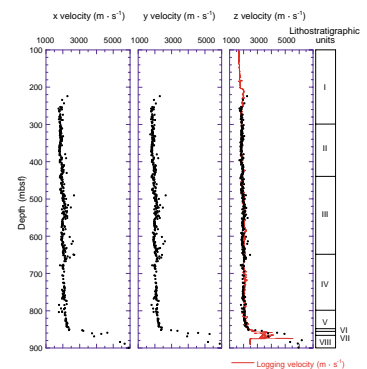
Table T14. Longitudinal and transverse velocities, Site 1118, **p. 199.**

F67. Site 1118 longitudinal vs. transverse velocities and anisotropy vs. depth, **p. 128.**
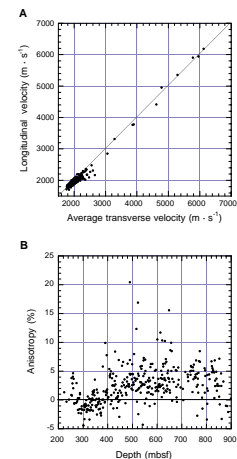
transverse velocities between 280 and 380 mbsf. From 380 to 900 mbsf, the anisotropies are consistently skewed by ~5% toward higher transverse velocities. There is no obvious explanation for the positive-negative change in anisotropy at ~280 mbsf.

Thermal Conductivity

Thermal conductivity data were obtained as a series of two to four repeat measurements per interval (i.e., discrete samples) and are reported in Table **T15** (also in **ASCII format**). Thermal conductivity data with depth are presented as mean averages of the repeat measurements shown in Figure **F68**.

Above 280 mbsf, thermal conductivities exhibit some scatter with values ranging from 1.00 to ~1.30 W·m^{-1}·°C^{-1} (Fig. **F68**). Between 280 and 520 mbsf, thermal conductivity values increase slightly from ~1.00 W·m^{-1}·°C^{-1} to ~1.25 W·m^{-1}·°C^{-1}. Within lithostratigraphic Unit III, values range between 1.15 and 1.20 W·m^{-1}·°C^{-1} and remain fairly constant with depth. At 680 mbsf, the thermal conductivities are characterized by an offset, whereby the values decrease from ~1.80 to <1.00 W·m^{-1}·°C^{-1}. From 680 to 850 mbsf, spanning the claystones and siltstones of Units IV and V (see **"Lithostratigraphic Unit IV,"** p. 13, and **"Lithostratigraphic Unit V,"** p. 16), conductivities increase to 1.40 W·m^{-1}·°C^{-1}. The lowermost rocks recovered from Site 1118 constituting packstones, grainstones, and dolerite, are thermally more conductive with values ranging between ~1.50 and 2.00 W·m^{-1}·°C^{-1}.

Magnetic Susceptibility

At Site 1118, estimates of magnetic susceptibility readings were routinely obtained as part of the MST measurement. The quality of magnetic susceptibility data is often poor in RCB-cored boreholes such as Site 1118, commonly because of a combination of reduced core diameter and core fracturing. The full magnetic susceptibility measurement data set can be found as part of the MST compilation in ASCII format on the accompanying LDEO CD-ROM.

The magnetic susceptibility of the recovered section is displayed in Figure **F69A** and is compared with the remanent magnetic intensity (Fig. **F69B**). A general correlation exists for the first-order variation in magnetic susceptibility and remanent magnetic intensity. This correlation implies that, in general, the mineralogy controlling the magnetic susceptibility is the same as that controlling the remanent magnetic intensity. At the grain-size scale and, thus, the distribution of sandstones and siltstones, there is no consistent relationship among magnetic susceptibility, remanent magnetic intensity, and grain size (see **"Lithostratigraphy,"** p. 4). The compressed scale of Figure **F69** allows only the general trends in the magnetic susceptibility to be identified. In particular, there exists a first-order difference between the high-amplitude susceptibility observed within the upper part of the section (240–580 mbsf) and the low-amplitude susceptibility within the lower part of the section (580–840 mbsf). The transition is found within lithostratigraphic Unit III. Second-order trends are represented by the relatively high amplitude susceptibility variations present at the base of lithostratigraphic Unit V and the transition between the packstones and grainstones of lithostratigraphic Unit VI and the paraconglomerates of lithostratigraphic Unit VII (~860 mbsf). Numerous local maxima
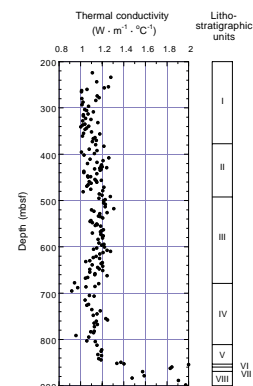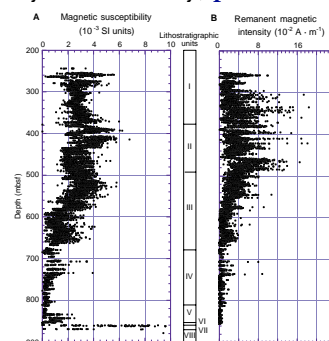
were observed, the more prominent at 390, 410, 520, and 640 mbsf. With the exception of lithostratigraphic Units VI and VII, there is no clear relationship between lithology and magnetic susceptibility. Further, sedimentation rates determined from biostratigraphy (see "Sediment Accumulation Rate," p. 33) exceed 400 m/m.y. for the stratigraphic succession spanning the first-order change in susceptibility. Therefore, we conclude that no obvious relationship exists between sedimentation rate and the variations in magnetic susceptibility.

Natural Gamma Ray

Natural gamma ray (NGR) emissions were recorded on cores from Site 1118 as part of the continuous MST measurements. The corresponding emission count is plotted in Figure F70B with magnetic susceptibility (Fig. F70A) for comparison. Superposed on the NGR count is the total gamma-ray (HSGR) logging data. The agreement between the MST gamma-ray data and the logging gamma-ray data provides confidence in using the logging curves in regions of poor core recovery. A full compilation of NGR values is presented with the MST measurement data set in ASCII format on the accompanying LDEO CD-ROM.

Apart from a relative low NGR count between 240 and 285 mbsf and 860 and 880 mbsf, NGR is rather uniform down the borehole with values generally ranging between 15 and 30 c/s. Between 240 and 530 mbsf, there exist a number of small undulations in the NGR count. Local maxima are found at 310, 350, 400, 475, and 850 mbsf. Below ~530 mbsf, the NGR count remains essentially constant down to a depth of ~840 mbsf (Fig. F70B). No obvious relationship exists with the majority of the succession, although it might be reasonable to interpret the high-frequency variation in NGR count observed in both the MST and logging data to be a function of the continuous sequence of alternating sands and silty clays of lithostratigraphic Units I, II, III, and IV (see "Lithostratigraphy," p. 4). It is interesting to note that lithostratigraphic Unit IV, characterized by coarse-grained volcaniclastic sands, has no obvious response in the NGR count. The shallow-water packstones and grainstones of lithostratigraphic Unit VI (see "Lithostratigraphic Unit VI," p. 18) correspond to a local maximum in the NGR count. Toward the base of the borehole, the NGR counts drop to nearly zero within the dolerite conglomerates of Unit VIII.

DOWNHOLE MEASUREMENTS

Operations

Three logging strings were run in Hole 1118A: one triple combo string that logged from a total depth of 891 mbsf to above mudline; one FMS-sonic string that logged a first pass from total depth (891 mbsf) to 92 m above total depth and a second pass from total depth to the bottom of the pipe at 98 mbsf; and a VSP run (Table T16). The VSP data and operations are described in "Vertical Seismic Profile and Depth Conversion," p. 52, and this section concentrates on the other runs.

For the first run, the pipe was raised to 99 mbsf, and the triple combo with the dual induction tool (DIT) (see Table T7, p. 74; Fig. F15, p. 66; both in the "Explanatory Notes" chapter) was lowered downhole. Natural gamma ray (HNGS) was monitored during the descent in the pipe to locate the mudline where the string was stopped for 3 min to provide a

F70. Site 1118 magnetic susceptibility and NGR, p. 131.
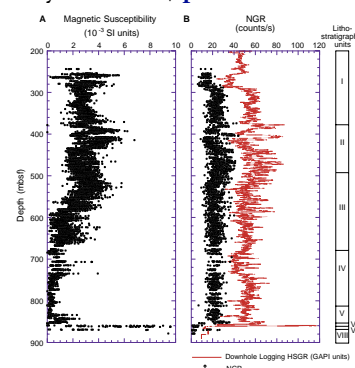
Table T16. Summary of logging operations, Site 1118, p. 211.

depth reference for the temperature-logging tool (TLT) temperature log. Upon reaching open hole, HNGS and DIT data were logged during the descent to total depth (Table T16). An upward log was then recorded at 300 m/hr. The tool string was stopped at the mudline for a few minutes both to run calibrations and to provide a depth reference for the TLT data, and logging continued up to 67 m above seafloor. After this pass the tool was lowered again to record the evolution of temperature at three stations (415, 625, and 835 mbsf) where the tool was stopped for 10 min at each station. The tool string was then pulled out of the hole.

For the second run, the bottom of the pipe remained at 99 mbsf and the FMS-sonic string (see Table T7, p. 74; Fig. F15, p. 66; both in the "Explanatory Notes" chapter) was lowered downhole. The string reached near total depth (Table T16), and a first pass was recorded up at 300 m/hr for 92 m to better cover the bottom part of the hole. The tool was lowered again to total depth for a second pass. The imaging log ended at the bottom of the pipe at 98 mbsf (Table T16) where the pads were closed, but natural gamma ray continued to be recorded up to 67 mbsf.

Depth Shifts

The mudline wireline depth (Table T16), which defines the depth shift from meters below rig floor to meters below seafloor applied to the logs (Fig. F71A, F71B), was located by its associated NGR decay for the triple combo run (Fig. F72). The depth shift for the second FMS-sonic pass was derived by correlating the NGR with that of the triple combo run within the 283–303 and 373–387 mbsf intervals that were chosen for their large characteristic variations (Figs. F73, F74). The depth shift for the first FMS-sonic pass was derived by correlating the NGR with that of the second FMS pass within the 855–865 mbsf interval. Note that differential cable stretching results in a depth mismatch up to 0.75 m between the FMS and the triple combo passes at the bottom of the log as shown in that interval (Fig. F75).

Lithologic Analysis

Ten logging units are defined (Fig. F76), based mainly on natural gamma ray, the relationship between the neutron (APLC) and density porosity (DPHI), the photoelectric effect (PEFL) (see "Downhole Measurements," p. 34, in the "Explanatory Notes" chapter), and the results of core analysis (see "Lithostratigraphy," p. 4).

Log Unit L1 (100–204 mbsf)

The neutron porosity is larger than the density porosity, which indicates the dominance of clay. Coarse-grained beds are rare, although several thin silty streaks occur. A thin layer at 186 mbsf may be calcite rich as indicated by a spike in PEFL.

Log Unit L2 (204–255.5 mbsf)

This unit is predominantly silty at the bottom, but grades upward into a formation that is primarily clay, again as indicated by the relationship between the density and neutron porosities. The unit is distinguished from log Unit L1 by its lower porosity and higher gamma-ray

F71. Hole 1118A composite log, p. 132.
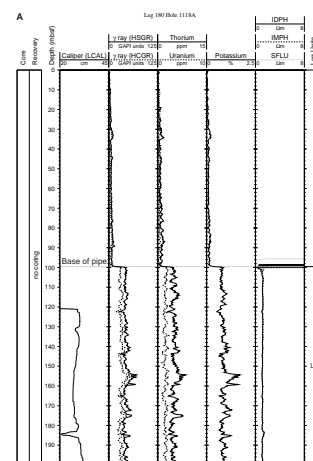
F72. Total gamma ray from triple combo at mudline, p. 142.
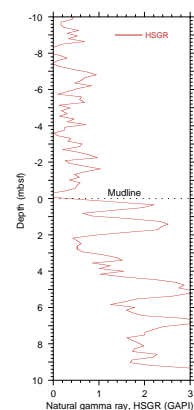
F73. Total gamma ray in 283–303 mbsf interval, p. 143.
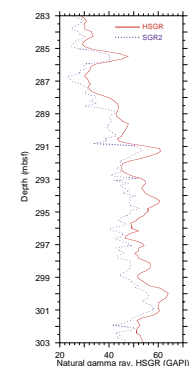
values. Near the top, several short (2–5 m) fining upward sequences can be seen, each with a silty base marked by a low in porosity.

Log Unit L3 (255.5–292 mbsf)

This unit is similar to Unit L1, showing a high clay content and some thin silty beds, but no clean sand beds. However, it displays lower natural gamma ray.

Log Unit L4 (292–347 mbsf)

There is generally more convergence between the density and neutron porosities here along with a 20 GAPI gamma ray increase, suggesting that the background sedimentation in this unit is silty. Thin intervals of greater convergence of the porosity curves are inferred to be sandy.

Log Unit L5 (347–402 mbsf)

The porosity curves diverge again, showing that this unit is primarily clay with some thin sandy beds and some silty intervals a few meters thick. One interval from 374 to 389 mbsf shows elevated natural gamma-ray magnitudes associated with Th and K increases. The slight convergence of porosities over the interval suggests that it contains a significant amount of fine-grained volcaniclastic material.

Log Unit L6 (402–438 mbsf)

The top 9 m of this unit are a massive radioactive sand like those observed in Holes 1109D and 1115C. Density and neutron porosities converge well, and the Th/K value is ~6. Below this sand, this unit displays higher PEFL and resistivity and lower gamma ray than Unit L5, suggesting higher carbonate content. This lower interval is also clay rich, and no thin clean beds are visible.

Log Unit L7 (438–682 mbsf)

The background sedimentation appears to be silty with several thin (<1 m) sandy beds. An interesting change occurs at ~604 mbsf: above this, all sandy beds are radioactive, whereas below this depth, sandy beds are associated with a decrease in natural gamma-ray magnitude. There also appears to be a change in the average Th/K value from ~5 above to ~3 below, suggesting less volcanic input.

Log Unit L8 (682–857 mbsf)

Just 8 m below the top of this unit is a massive sand almost 40 m thick; it is characterized by low PEFL, convergence of porosities, and relatively low natural gamma-ray magnitude. Below and in the 8 m above this, several similar but thinner intervals are visible alternating with sequences of clay and silt where the porosities diverge. The bottom 7 m of the unit shows a decrease in porosity and an increase in gamma-ray magnitude, which is associated with an increase in Th and K content; this is likely another volcaniclastic sand. This sand is probably calcareous as well, particularly where the PEFL reaches 4 barns/e⁻.

F74. Total gamma ray in 373–388 mbsf interval, **p. 144.**
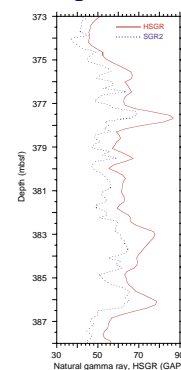
F75. Total gamma ray in 855–865 mbsf interval, **p. 145.**
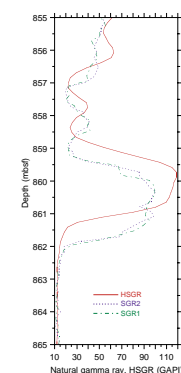
F76. Hole 1118A log units and correlations, **p. 146.**
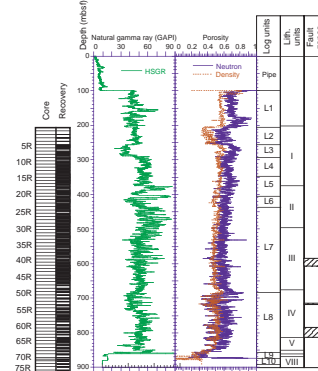
Log Unit L9 (857–873 mbsf)

This unit is dominated by calcium carbonate, as shown by the PEFL of 5 barns/e⁻ and low natural gamma-ray magnitude. Two interesting features stand out: a radioactive sand and a calcareous conglomerate. From 860 to 861.5 mbsf, there is a highly radioactive sandy bed with good density-neutron convergence and a decrease in PEFL. The Th/K ratio shoots up to 10, and a mild increase in uranium is seen. This suggests the presence of mafic volcanic minerals. From 868.5 to 870 mbsf, there is an increase in bulk density and a subsequent large separation of the porosity curves. PEFL remains relatively high at 4.25. From the FMS image, we infer that this bed is a conglomerate. It corresponds to a calcareous, basaltic conglomerate recovered in the core (see **"Lithostratigraphic Unit VIII,"** p. 21).

Log Unit L10 (873–890 mbsf)

The neutron and natural gamma-ray sensors did not reach this unit; however, the top 5 m is visible on the density and PEFL curves. Bulk density is high, close to 2.7 g·cm⁻³, and PEFL ranges between 4 and 5 barns/e⁻. The FMS log shows that the entire unit is a conglomerate; the large, boulder-sized clasts are likely to be the dolerite that was recovered in core at this depth (see **"Lithostratigraphic Unit VIII,"** p. 21). A calcareous matrix may be boosting the PEFL.

Borehole Geometry, Magnetic Field, and FMS Dynamics

The accelerometer data of the FMS show that the hole deviation first increases with depth up to 3.5° at 810 mbsf and then decreases (Fig. **F77**). The hole azimuth varies from 150° at the top to 188° at 810 mbsf (Fig. **F78**). Tool acceleration magnitudes (Fig. **F79**) deviate by 0.2 m·s⁻² from the average, which is about twice the amount of a good quality run (such as the lower run in Hole 1109D, see **"Downhole Measurements,"** p. 69, in the "Site 1109" chapter). This indicates irregular tool movements and lower quality raw images, as was observed during logging.

The FMS caliper data reveal a significant hole ellipticity except in the 550–680 mbsf interval, which is totally included in Unit L7 (Fig. **F80**).

This data also revealed two intervals where the smallest diameter is below the drill-bit size (25 cm [9 ⅞ in]). The 204–255.5 mbsf interval corresponds exactly to Unit L2, and the 682–875 interval corresponds to Units L8 and L9. In these intervals, it can be noted that the largest diameter recorded by the FMS caliper is smaller than those recorded by the hostile environment lithodensity sonde (HLDS) 7 hr before. This suggests that the hole was slowly closing during logging operations.

Washouts spaced out at ~10-m intervals are probably caused by the circulation that is maintained when the drill bit progression halts during core retrieval.

The FMS tool rotated counterclockwise as shown by the pad 1 azimuth, except in the 330–420 mbsf interval where the largest diameter azimuth remains steadily north-south (Fig. **F80**). This interval also corresponds to a large ellipticity. This is consistent with observations in Hole 1109D and 1115C (see **"Site 1109"** and **"Site 1115"** chapters) and could be related to a north-south minimum horizontal principal stress direction or to structural orientations.

F77. Hole 1118A deviation, **p. 147.**
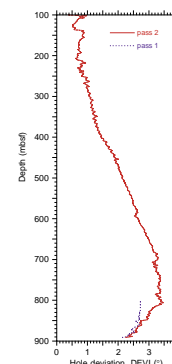
F78. Hole 1118A azimuth, **p. 148.**
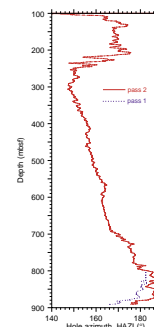
F79. FMS tool string acceleration in Hole 1118A, **p. 149.**
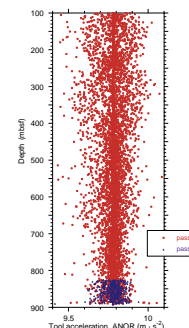
F80. Hole 1118A geometry, **p. 150.**
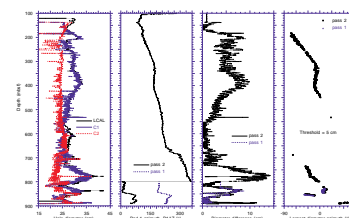
The magnetometer measurements yield a stable inclination around –30°, except at the bottom of the hole in log Units L9 and L10, where it becomes variable and reaches up to –27° (Fig. F81). The magnetic intensity shows the same stability above log Units L9 and L10 and similar variation within these units (Fig. F81).

FMS Images

One main FMS pass and one short pass were recorded at Site 1118 (Table T16). FMS processing steps for this site included speed correction, depth shifting to meters below seafloor using an estimated mud-line of 2313.7 m for each FMS log, and static and dynamic normalization using a 1-m window. The image quality is good between 138 and 190 mbsf for the main pass and 825 and 890 mbsf for the short pass. The high contrast in resistivity between the low-resistivity clays and silts in the top portion of the hole and the high-resistivity limestone and dolerite in the bottom portion resulted in poor resolution of the smaller scale resistivity variations in the statically normalized images. Comparison of the gamma-ray logs indicates a depth offset between the triple combo and the lower portion FMS images (Fig. F75); that is, the FMS depths within log Units L9 and L10 are actually ~75 cm deeper than the triple combo logs. Postcruise processed data available in the LDEO CD-ROM minimize the depth offset between the triple combo and FMS-sonic logs by applying a differential depth shift.

Log Unit L1 (100–204 mbsf)

Very thin (2–3 cm), moderately resistive, flat-lying beds characterize log Unit L1. These beds are interpreted to be dominantly clays based on both the FMS images and the conventional logs. Thin, more resistive beds are commonly interbedded within this unit. Approximately 1-m scale coarsening upward sequences are recognized as units with relatively sharp, low-resistivity bases and gradational increases in resistivity toward the tops as shown in Figure F82. The thickness of the high-resistivity layers increases up to ~10 cm toward the base of log Unit L1.

Log Unit L2 (204–255.5 mbsf)

FMS-image quality is poor within log Unit L2 because of poor pad contact with the borehole wall. The large-scale resistivity is low in the statically normalized FMS, indicating high clay content. Sedimentary layering is not well defined within this unit, but this may be an imaging artifact. A few meter-scale fining upward sequences with resistive bases are more clearly observed in this unit.

Log Unit L3 (255.5–292 mbsf)

The top of log Unit L3 is clearly imaged in the FMS data with the reappearance of thinly layered clayey beds similar to those of log Unit L1. Bed thicknesses are slightly greater, including thicker (~15 cm) resistive interbeds. At 268 mbsf, beds show a sudden increase in dip of ~15° to the west that decreases to nearly horizontal with depth and changes to a northwest dip direction at 282 mbsf. This structure appears to be a depositional feature as no fractures are observed. The base of log Unit L3 is comprised of wavy, steeply dipping foresets with variable dip directions as shown in Figure F83.

F81. Magnetic field inclination and intensity in Hole 1118A, p. 151.
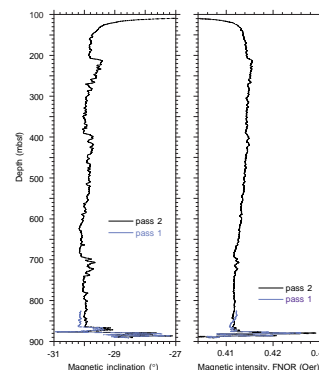
F82. Hole 1118A statically and dynamically normalized FMS images, p. 152.
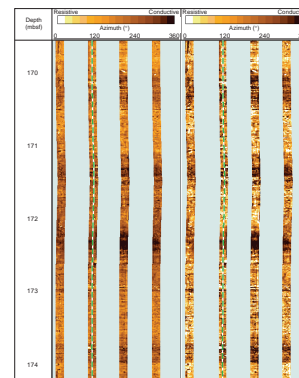
F83. Hole 1118A dynamically normalized FMS image and tadpole plot, p. 153.
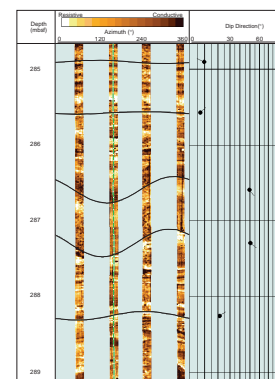
Log Unit L4 (292–347 mbsf)

The top of log Unit L4 displays similar bedding structures as log Unit L3; however, the bed boundaries are more diffuse. Bed dips throughout this unit generally range between 15° and 20° to the west, changing to a more northwestward dip direction with depth. Beds lie nearly horizontal at the base of this unit. A few 50° to 60° southward-dipping resistive fractures occur between 316 and 323 mbsf.

Log Unit L5 (347–402 mbsf)

A decrease in large-scale resistivity indicating increased clay content between 347 and 389 mbsf marks the top portion of log Unit L5. Beds are flat lying, but occasionally dip up to 10° to the southeast and southwest. Resistivity is greater in the lower portion of this unit below 389 mbsf, and sandy, resistive interbedded layers are more common; however, bedding structures remain thin and flat lying.

Log Units L6 and L7 (402–438 mbsf; 438–682 mbsf)

Thin (<5 cm), flat-lying, conductive, clayey beds with generally thicker (10 cm) resistive interbeds characterize log Units L6 and L7. Large-scale resistivity varies throughout this section, whereas bed forms are generally uniform. Log Unit L6 is composed of more conductive, clayey material, whereas log Unit L7 contains both conductive and resistive intervals. Resistivity generally increases with depth; however, below ~568 mbsf, highly conductive, interbedded clay layers appear in the form of irregular wavy beds between the more uniform, flat-lying resistive layers as shown in Figure F84.

Log Unit L8 (682–857 mbsf)

Log Unit L8 displays a grainy texture in the FMS images, which is characteristic of carbonate-rich material as observed in the nearby Sites 1109 and 1115 (see "Downhole Measurements," p. 69, in the "Site 1109" chapter and "Downhole Measurements," p. 52, in the "Site 1115" chapter). Beds are relatively thick (<20 cm or more) and flat lying throughout most of this unit, except where bedding is highly disturbed. The base of this unit is composed of a highly resistive sandy or carbonate-rich interval between 850.5 and 857 mbsf.

Log Unit L9 (857–873 mbsf)

High resistivity and a grainy texture characterize log Unit L9, which is interpreted to be composed of carbonate-rich material based on both the FMS and the conventional logs. The dynamically normalized FMS image displays 5–10 cm thick, relatively conductive and resistive layers of limestone between 857 and 860 mbsf. Between 861.7 and 870 mbsf, beds display irregular, wavy bedding with more sharply defined boundaries, which overlie a 1.5-m-thick, more resistive interval containing angular clasts. Based on the analysis of logs and core samples, three lithologic units are recognized in this interval: a sandy unit between 860.1 and 861.7 mbsf; a limestone conglomerate unit between 861.7 and 868.5; and a conglomerate containing basalt and dolerite cobbles between 868.2 and 870 mbsf (see "Lithostratigraphy," p. 4). The base of this unit between 870 and 874 mbsf is comprised of a limestone unit with wavy and disturbed bedding structures.

F84. Hole 1118A statically and dynamically normalized FMS images of log Unit L7, p. 154.
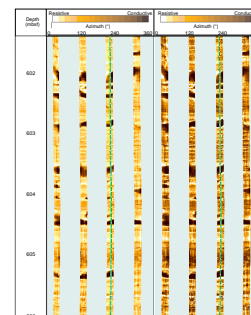
Log Unit L10 (873–890 mbsf)

Large (<40-cm diameter), resistive, rounded clasts within a more conductive, clayey matrix indicate that log Unit L10 is a conglomerate (Fig. F85). Clast sizes display a wide range in diameter, but show an overall decrease with depth to the base of the logged interval at 890 mbsf. This unit is capped by a ~45-cm-thick highly resistive layer that is interpreted to be a dolomite based on comparison with the conventional log data.

Temperature Data

TLT borehole temperature recorded during the triple combo string's first downward and upward passes are shown in Fig. F86. Because no in situ temperature data could be obtained for Hole 1118A using the Adara or DVTP tools, a second pass was conducted that was dedicated to temperature measurements after the first triple combo log was completed. The tool string was lowered to 415, 625, and 835 mbsf, and held for ~10 min at each station (Fig. F87).

A mudline temperature of 2.2°C was recorded during the first downward pass of the triple combo (Fig. F86). On the first upward logging pass, a distinct increase in temperature is observed above 700 mbsf. This increase is also visible, but less pronounced, on the second upward pass (Fig. F87), during which the tool string was brought up much more quickly (~2700 m/hr). This increase in temperature strongly suggests an influx of warm fluids at ~700 mbsf. Fluid flow up the borehole had been noted during the prelogging wiper trip (see "Operations," p. 3) and was treated by pumping mud into the hole. Interstitial water chemistry shows complex behavior in Hole 1118A, which suggests the possibility of elevated temperatures but does not definitively indicate fluid migration (see "Inorganic Geochemistry," p. 36).

The probable occurrence of fluid migration complicates estimation of in situ temperatures from open hole temperatures, because the classical extrapolation accounts only for conductive heat flow. Upward flow of warm fluid may have warmed the hole, and subsequently pumping of mud would have cooled the borehole and slowed upward fluid migration. As a result, only data from the deepest station (835 mbsf) were used to estimate equilibrium temperature, because this depth is likely to be less affected by fluid advection.

Equilibrium temperature at 835 mbsf was approximated by plotting the temperature as a function of ln $[t/(t–s)]$, where t is the total time elapsed since the drill bit penetrated that depth, and s is the total time elapsed between the initial penetration and the cessation of circulation (Fig. F88). The line was then extrapolated to infinite time (where ln $[t/(t–s)] = 0$). This method was introduced by Bullard (1947) and previously applied to open-hole temperature measurements from ODP Leg 123 (Castillo, 1992). Results suggest an approximate equilibrium temperature of 55°C at 835 mbsf. From this approximation and the mudline temperature, a gradient of 0.06°C·m^{-1} (60°C·km^{-1}) can be calculated. However, this should only be considered a very rough estimate because of the strong evidence that the thermal profile is not linear above this depth.

F85. Hole 1118A statically and dynamically normalized FMS images, log Unit L10, **p. 155.**
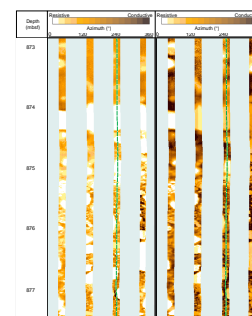
F86. Hole 1118A temperature from triple combo first pass, **p. 156.**
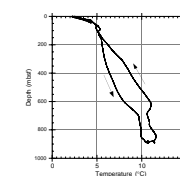
F87. Hole 1118A temperature data during TLT temperature pass, **p. 157.**
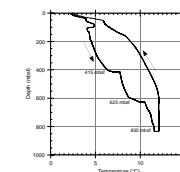
F88. Temperature vs. ln$[t/(t–s)]$ from TLT at 835 mbsf, **p. 158.**
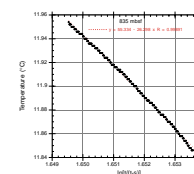
VERTICAL SEISMIC PROFILE
AND DEPTH CONVERSION

A VSP experiment was carried out during the logging run at Site 1118. The goals of the VSP experiment were to give accurate depth estimations of reflectors identified in the multichannel seismic (MCS) data, allowing correlation with lithostratigraphic units, and to provide parameters with which to improve processing of existing MCS data. A 300-in³ air gun was used to generate a source signal, which was received in the hole by the WST. The source signal was also recorded on a hydrophone close to the air gun (see "Vertical Seismic Profiling," p. 42, in the "Explanatory Notes" chapter).

As part of the preparation for recording the VSP, the end of the drill pipe was positioned at 110 mbsf. A restriction in the hole prevented the WST from being lowered past 690 mbsf. The WST was raised to 686.1 mbsf, at which point the clamping arm was engaged, pushing the instrument against the wall of the hole. A total of 20 stations were occupied. The clamping interval was 30 m, except in the case of the last station, which was 25 m above the previous station (Table T17). At each station, the air gun was triggered several times. Each good shot was stacked, with firing continuing until the stack contained seven shots. Clamping quality was excellent at all stations.

The Schlumberger MAXIS system was used for preliminary shipboard processing of the VSP. *P*-wave transit times, used to derive interval velocities and check-shot information, were picked as the first arrival in the downgoing wavefield at the WST (Table T20, p. 296, in the "Site 1109" chapter). Velocity filtering, wave shape deconvolution, a zero-phase 10- to 60-Hz bandpass filter, and corridor stacking were applied to the data (see "Vertical Seismic Profiling," p. 42, in the "Explanatory Notes" chapter). A five-level velocity filter was used to separate the upgoing and downgoing wavefields. The resulting traces were stacked into a single corridor stack. Reflection events in the migrated MCS data at this location correlate well with those of the VSP, although relative amplitudes need some adjustment postcruise to account for the automatic gain control applied to the MCS data only (Fig. F89).

Interval velocities were calculated between all stations (Table T17; Fig. F90). Fitting a straight line by linear regression gives an average interval velocity of 1934 m·s⁻¹ between 121.0 and 686.1 mbsf (Fig. F90).

To convert between seismic traveltime and depth below seafloor, we examined the velocity information available from laboratory measurements and sonic logs to develop a model of the variation of velocity with depth. In this model, the more densely sampled velocities (DTCO; see "Downhole Measurements," p. 45) measured downhole were used in preference to values determined from laboratory measurements. Laboratory measurements of velocity were used below 875 mbsf, where log sonic velocities were absent. Above 100 mbsf, neither laboratory nor logging measurements of velocities were taken. To estimate the velocity over this interval, the first arrival time of the VSP station at 121.1 mbsf was converted to two-way traveltime (TWT) (Table T18) relative to the seafloor. Using this information and the velocity profile between 100 and 121.1 mbsf, we derived an average interval velocity of 1690 m·s⁻¹ for the interval from 0 to 100 mbsf.

The resultant velocity-depth function of the borehole (Fig. F91) was passed through a 2-m Gaussian filter and resampled to 1 m before being used to convert from depth to TWT. To confirm the viability of the

Table T17. Data for each station during the VSP experiment, **p. 212.**

F89. VSP corridor stack between migrated MCS traces, **p. 159.**
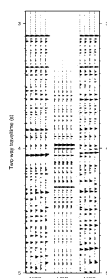
F90. Depth vs. transit time, Site 1118 VSP, **p. 160.**
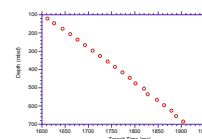
Table T18. Comparison of VSP check-shot data with depth estimates, **p. 213.**

F91. Depth-converted MCS and VSP data, **p. 161.**
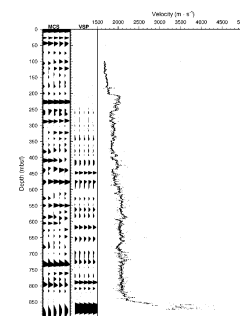
depth conversion, it was compared with VSP check-shot information. The *P*-wave transit times to the WST geophone at depth (Table T17) were corrected for the geometry of the experiment (see "Vertical Seismic Profiling," p. 42, in the "Explanatory Notes" chapter) to give a direct and absolute tie between TWT and depth. This traveltime can then be directly correlated to the MCS data. The VSP experiment covered a wide depth range, so that we can accurately tie depth to time over a significant portion of the borehole. Table T18 shows that the difference between the VSP depth and that calculated for an equivalent time from the velocity-depth function ranges from 0.05 to 15.24 m, with an average of 5.98 m. Additional work using the VSP results as a check-shot survey will allow us to reduce these errors.

Figure F92 shows the correlation between the MCS data in time, the depth-converted MCS traces, and the lithostratigraphy column (see "Lithostratigraphy," p. 4). Lines are drawn at 30-m intervals connecting the depth-converted MCS data and the lithostratigraphy column to the MCS data in time. A prominent reflector at 3.33-s two-way traveltime, or 220 mbsf, corresponds to a prominent regional reflector that was interpreted as a sandy horizon at approximately the same depth at Site 1109 (see "Downhole Measurements," p. 69, in the "Site 1109" chapter). At this site and at Site 1109, this was a zone of very low recovery. A reflector at 3.97-s TWT falls at 855 mbsf at Site 1118. It is not clear if this reflector is from the top of lithostratigraphic Unit VI, VII, or maybe even VIII. The depth-converted VSP corridor stack generally correlates well with the depth-converted MCS data. The strong reflector at 855 mbsf discussed above is clearly visible at the same depth in the VSP trace. Refinements in the depth conversion, further processing of the VSP data, and production of synthetic seismic traces will aid in the correlation between this site and other sites.
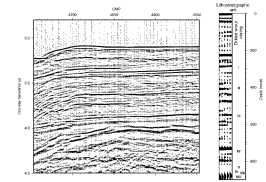
REFERENCES

Athy, L.F., 1930. Density, porosity, and compaction of sedimentary rocks. *AAPG Bull.,* 14:1–24.

Berggren, W.A., Kent, D.V., Swisher, C.C., III, and Aubry, M.-P., 1995. A revised Cenozoic geochronology and chronostratigraphy. *In* Berggren, W.A., Kent, D.V., Aubry, M.-P., and Hardenbol, J. (Eds.), *Geochronology, Time Scales and Global Stratigraphic Correlation.* Spec. Publ.—Soc. Econ. Paleontol. Mineral. (Soc. Sediment. Geol.), 54:129–212.

Bullard, E.C., 1947. The time necessary for a borehole to attain temperature equilibrium. *Mon. Not. R. Astron. Soc., Geophys. Suppl.,* 5:127–130.

Castillo, D.A., 1992. Thermal and hydrologic properties of old oceanic crust in Hole 765D, Argo Abyssal Plain, Indian Ocean. *In* Gradstein, F.M., Ludden, J.N., et al., *Proc. ODP, Sci. Results,* 123: College Station, TX (Ocean Drilling Program), 515–522.

Jelinek, V., 1981. Characterization of the magnetic fabric of rocks. *Tectonophysics*, 79:63–67.

Parkes, R.J., Cragg, B.A., Bale, S.J., Getliff, J.M., Goodman, K., Rochelle, P.A., Fry, J.C., Weightman, A.J., and Harvey, S.M., 1994. A deep bacterial biosphere in Pacific Ocean sediments. *Nature,* 371:410–413.

Terzaghi, K., 1925. *Erdbaumechanik auf bodenphysikalischer Grundlage:* Leipzig (Deuticke).

Torres, M.E., Marsaglia, K.M., Martin, J.B., and Murray, R.W., 1995. Sediment diagenesis in Western Pacific Basins. *In* Taylor, B., and Natland, J. (Eds.), *Active Margins and Marginal Basins of the Western Pacific.* Geophys. Monogr., Am. Geophys. Union, 88:241–258.

Figure F1. Lithology of Hole 1118A showing the different units recognized and their basic characteristics (for key to symbols, see Fig. F2, p. 52, in the "Explanatory Notes" chapter).
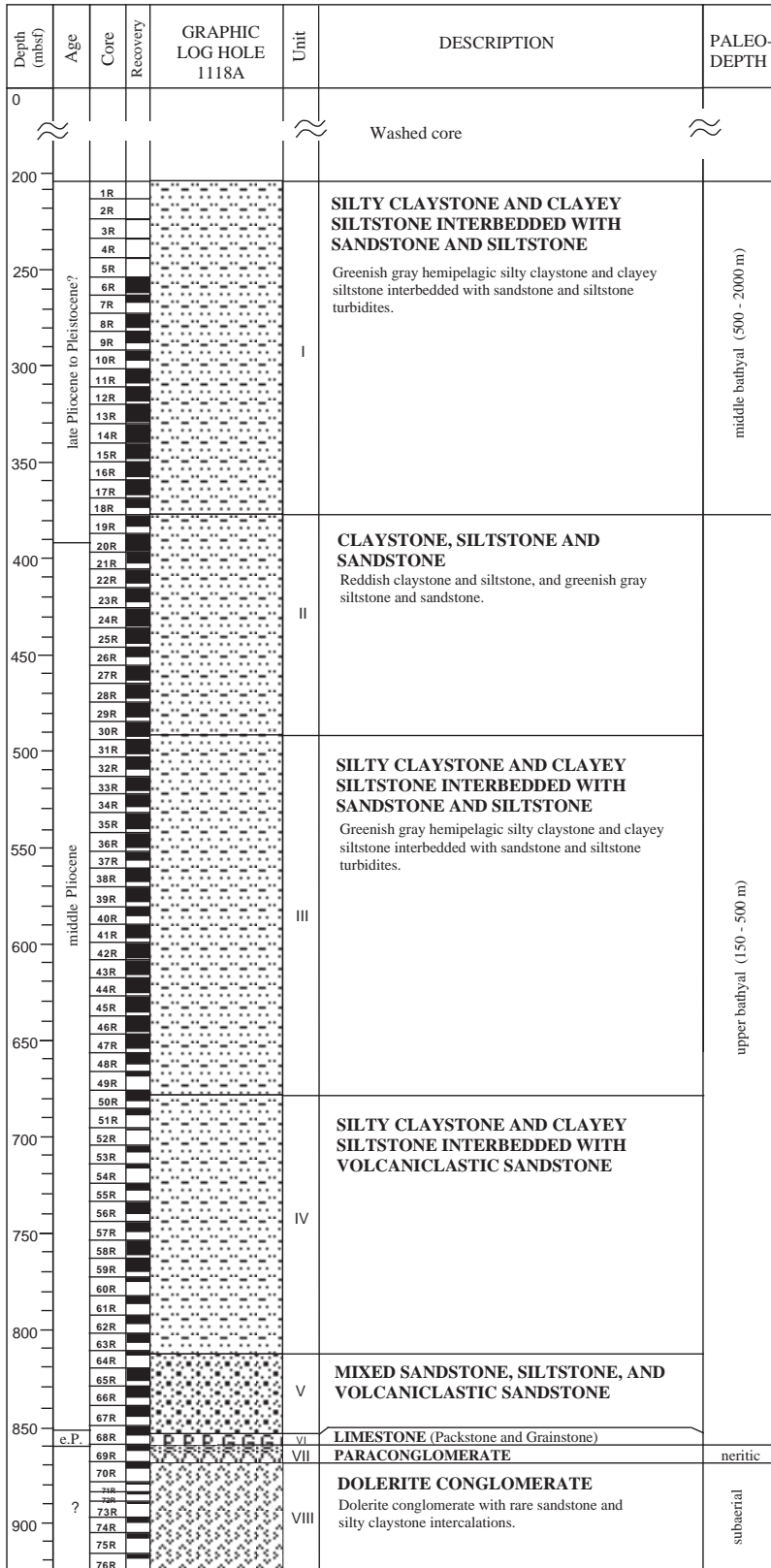
e.P.: early Pliocene

Figure F2. Grain-size trend (generalized from the barrel sheets) in all the units observed in Hole 1118A (for key to symbols, see Fig. F2, p. 52, in the "Explanatory Notes" chapter). Note that trends may be anomalous in areas of low core recovery.
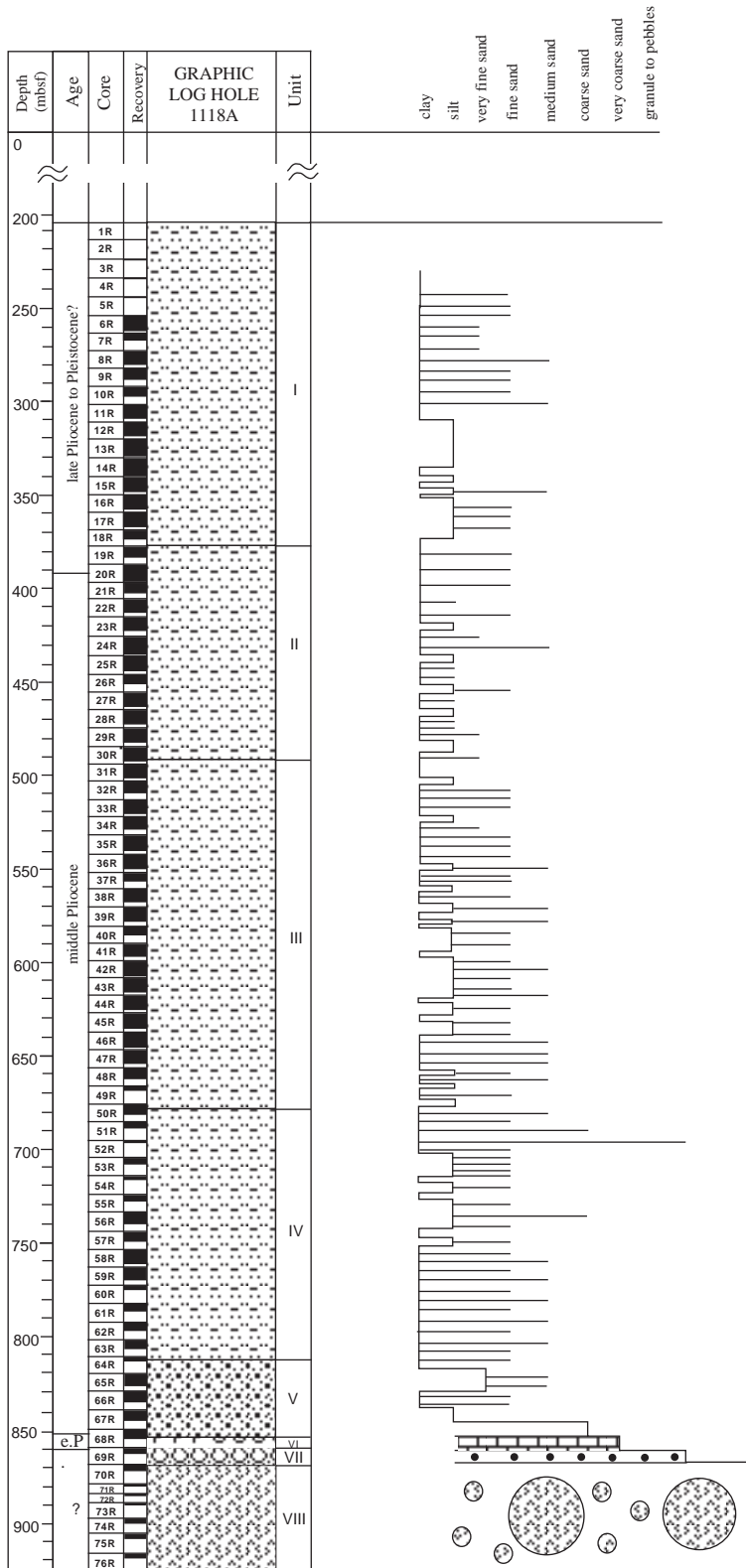
e.P.: early Pliocene

Figure F3. Strongly bioturbated silty claystone with well-developed *Zoophycos* burrows (interval 180-1118A-11R-5, 26–53 cm).
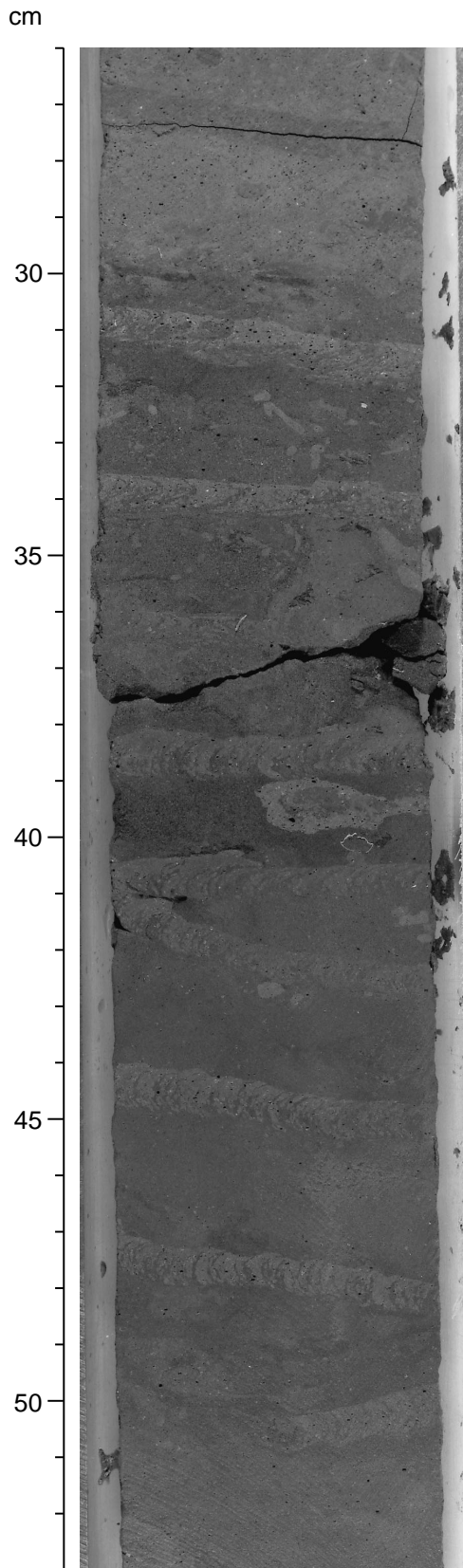
Figure F4. Contorted and deformed silty claystone and siltstone enclosed by less deformed and unde-formed sediments of similar texture and composition (interval 180-1118A-13R-5, 70–110 cm).
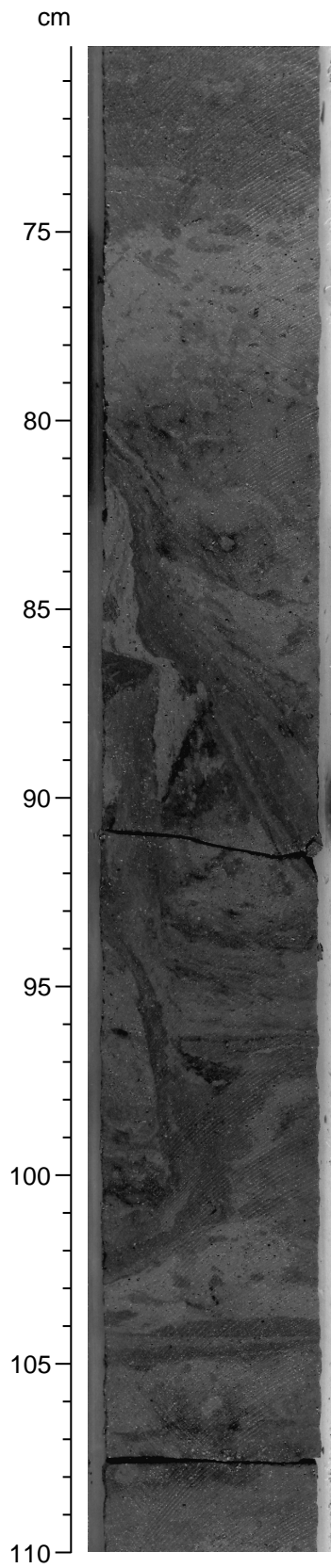
Figure F5. Laminae and thin beds of graded siltstone and clayey siltstone (interval 180-1118A-17R-2, 10–25 cm).
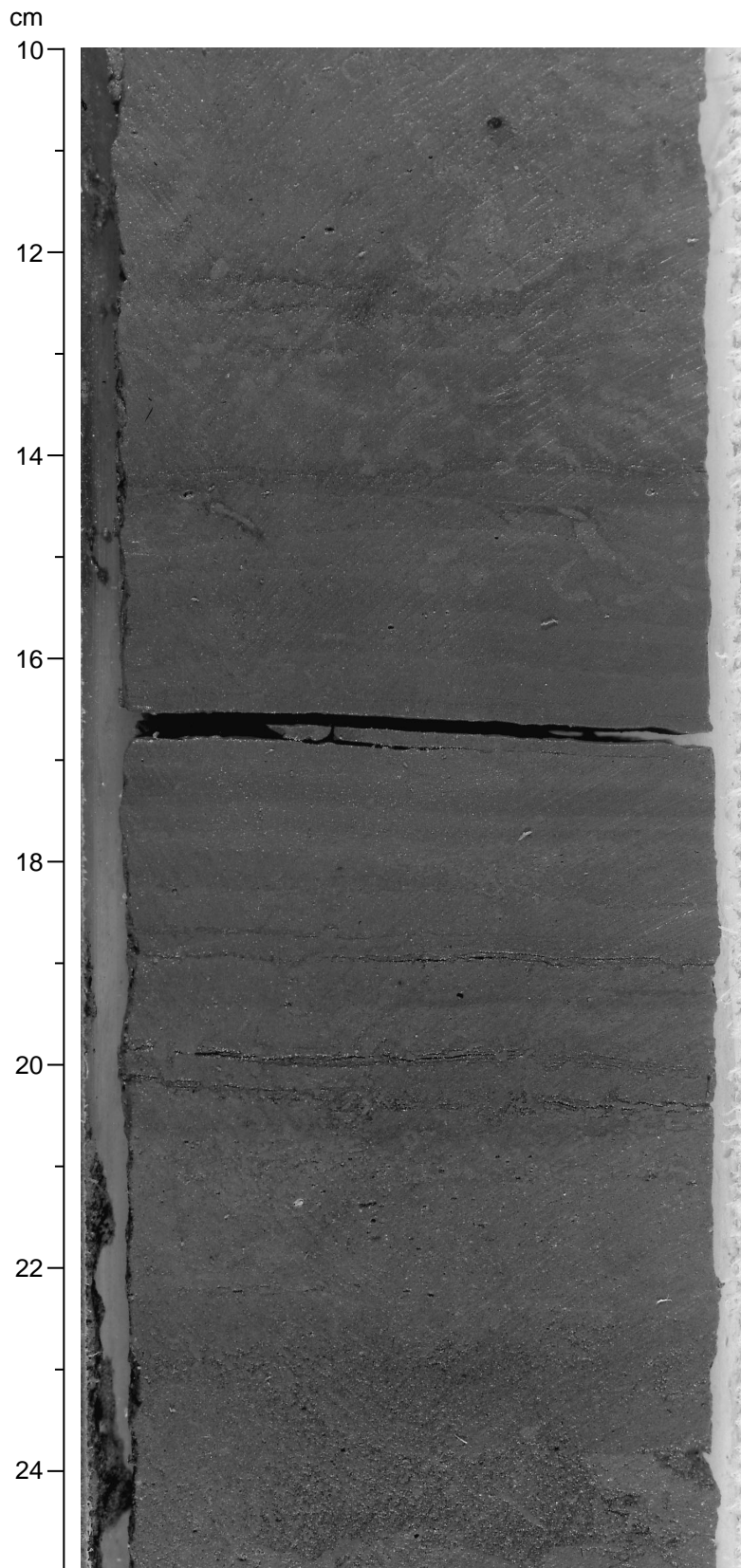
Figure F6. Laminated silty claystone and clayey siltstone, some with parallel lamination at the base (130–131 cm) (interval 180-1118A-27R-1, 120–140 cm).
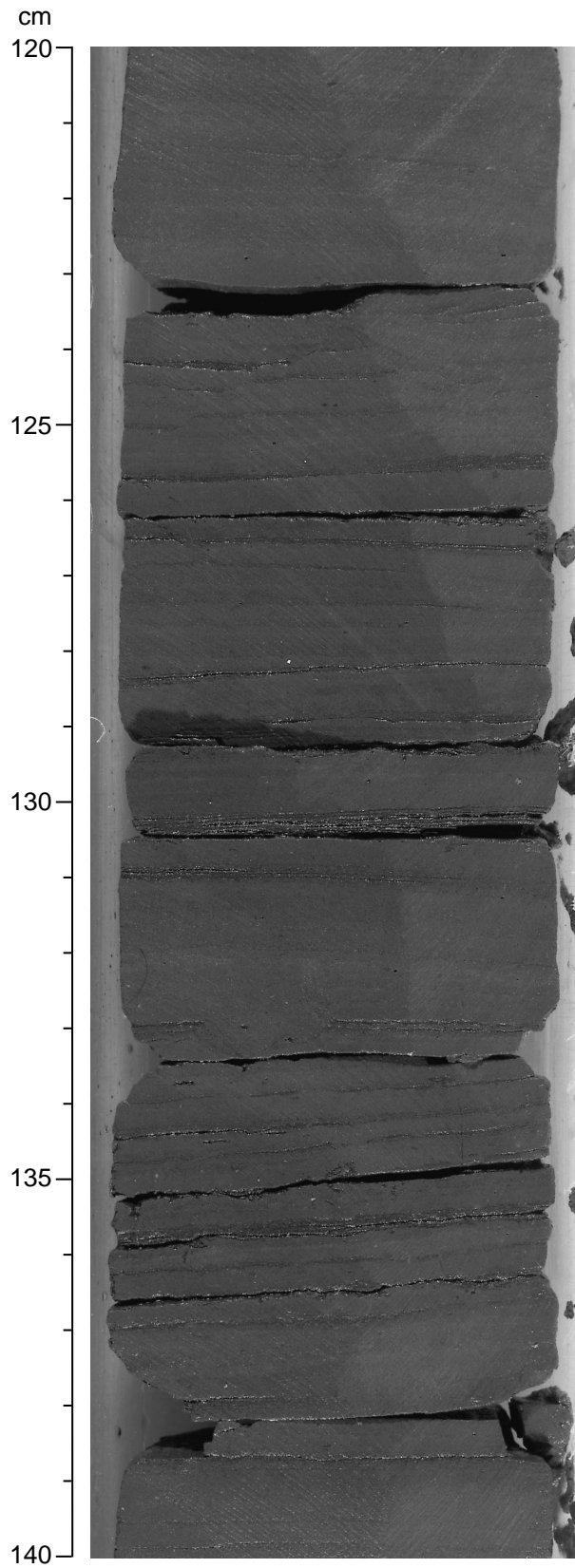
Figure F7. Thick, normal-graded (from medium-grained sand to silt) beds with flutes mark at its base (at 59 cm) (interval 180-1118A-23R-4, 30–65 cm).
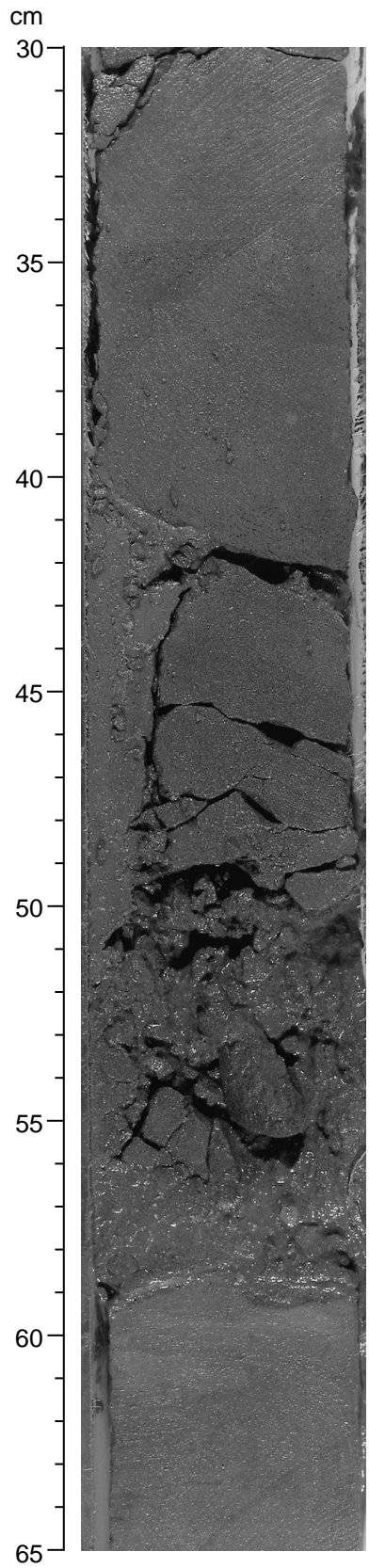
Figure F8. Digital photomicrograph (plane-polarized light) of a moderately sorted, fine-grained volcani-clastic sandstone with a silty clay matrix. Composed of angular detrital grains of biotite, hornblende, feld-spar, and quartz. Rare subrounded plagioclase-phyric basalt grains and planktonic foraminifers (Sample 180-1118A-24R-5, 105–107 cm).
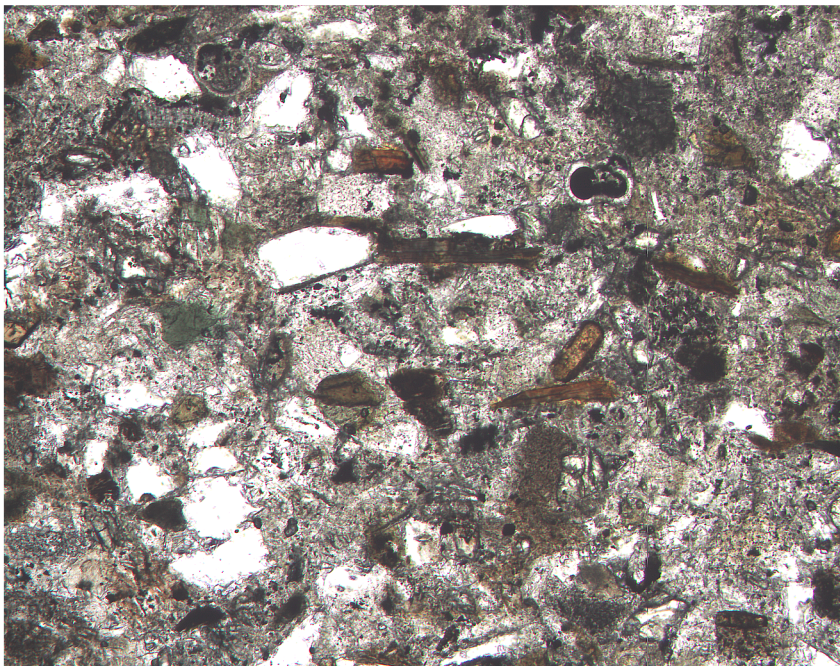
1 mm

Figure F9. Contorted and deformed fine-grained sediments (interval 180-1118A-21R-4, 125–148 cm).
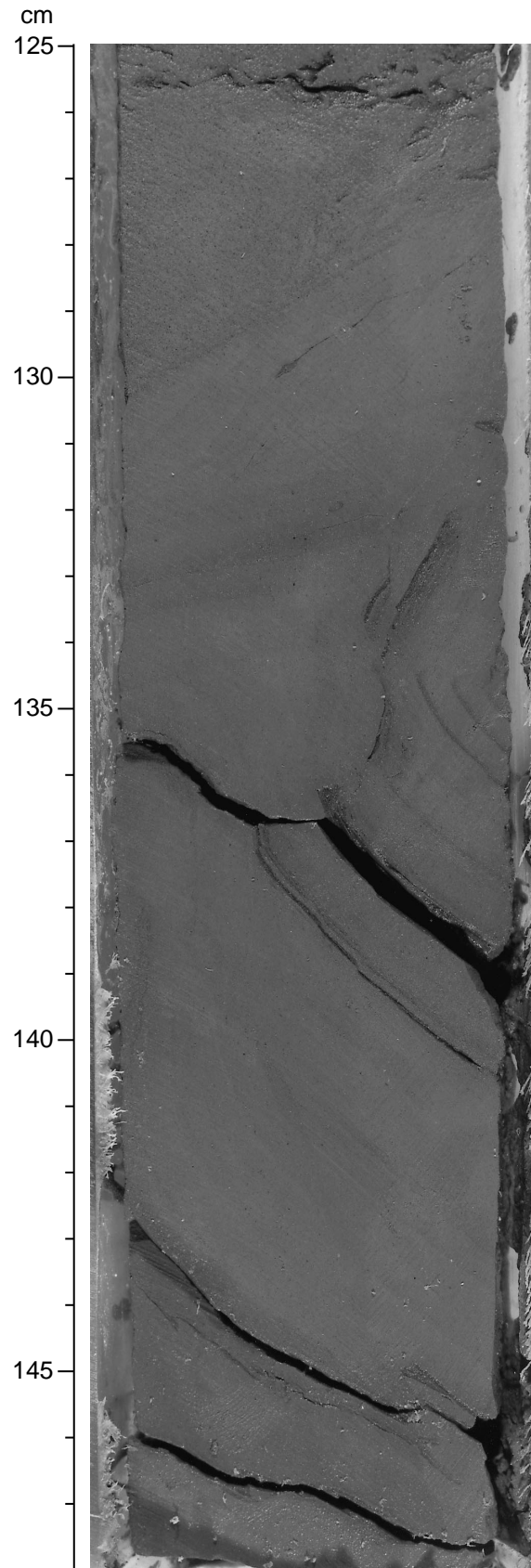
Figure F10. Siltstone/claystone couplets (interval 180-1118A-42R-8, 22–44 cm).
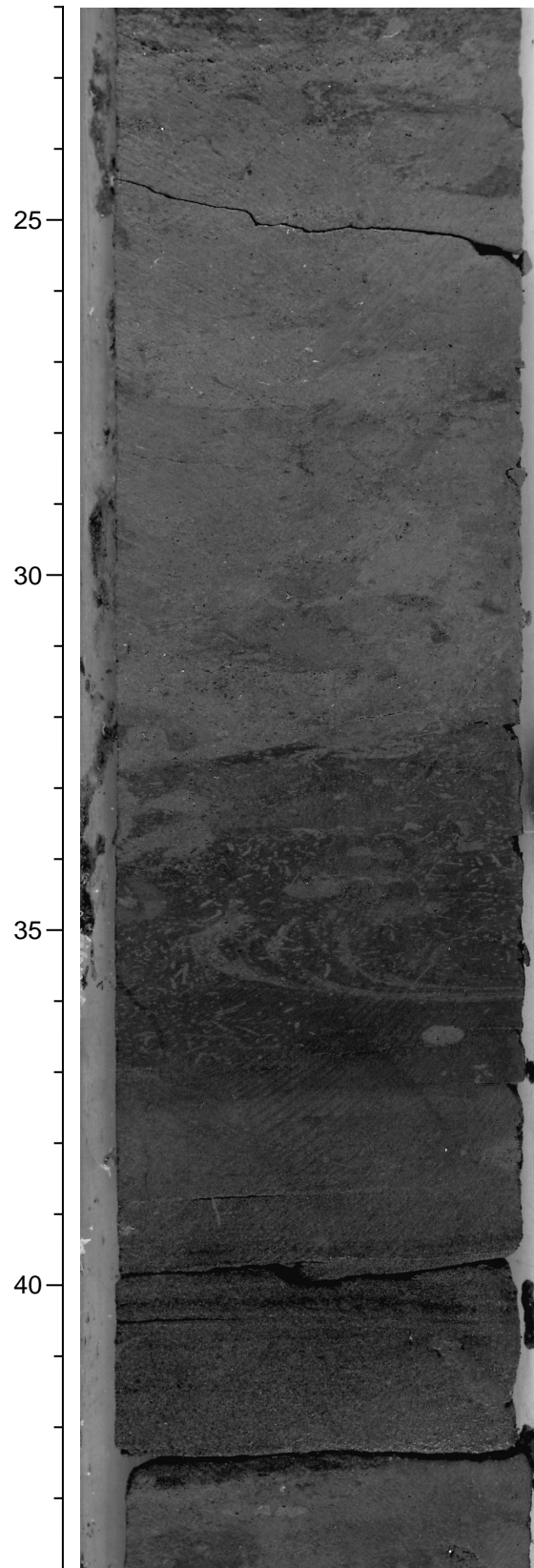
Figure F11. Sand/siltstone graded bed (77–97 cm). Note the parallel-laminated lower part of the bed (interval 180-1118A-38R-2, 65–100 cm).
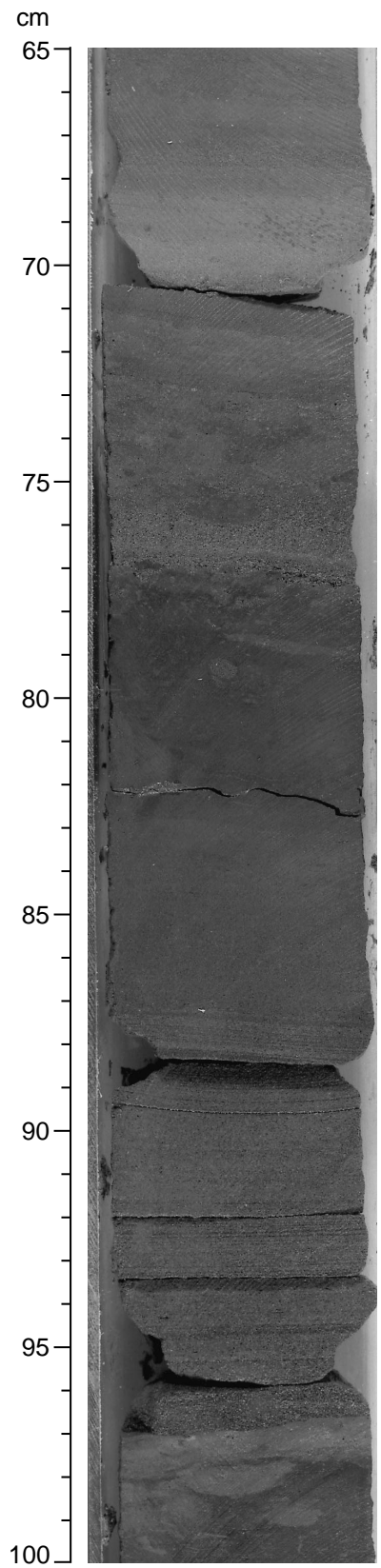
Figure F12. Climbing-ripple lamination followed by a parallel-laminated interval that grades into massive siltstone. Note the high angle of climb of individual ripple sets (interval 180-1118A-39R-3, 121–134 cm).
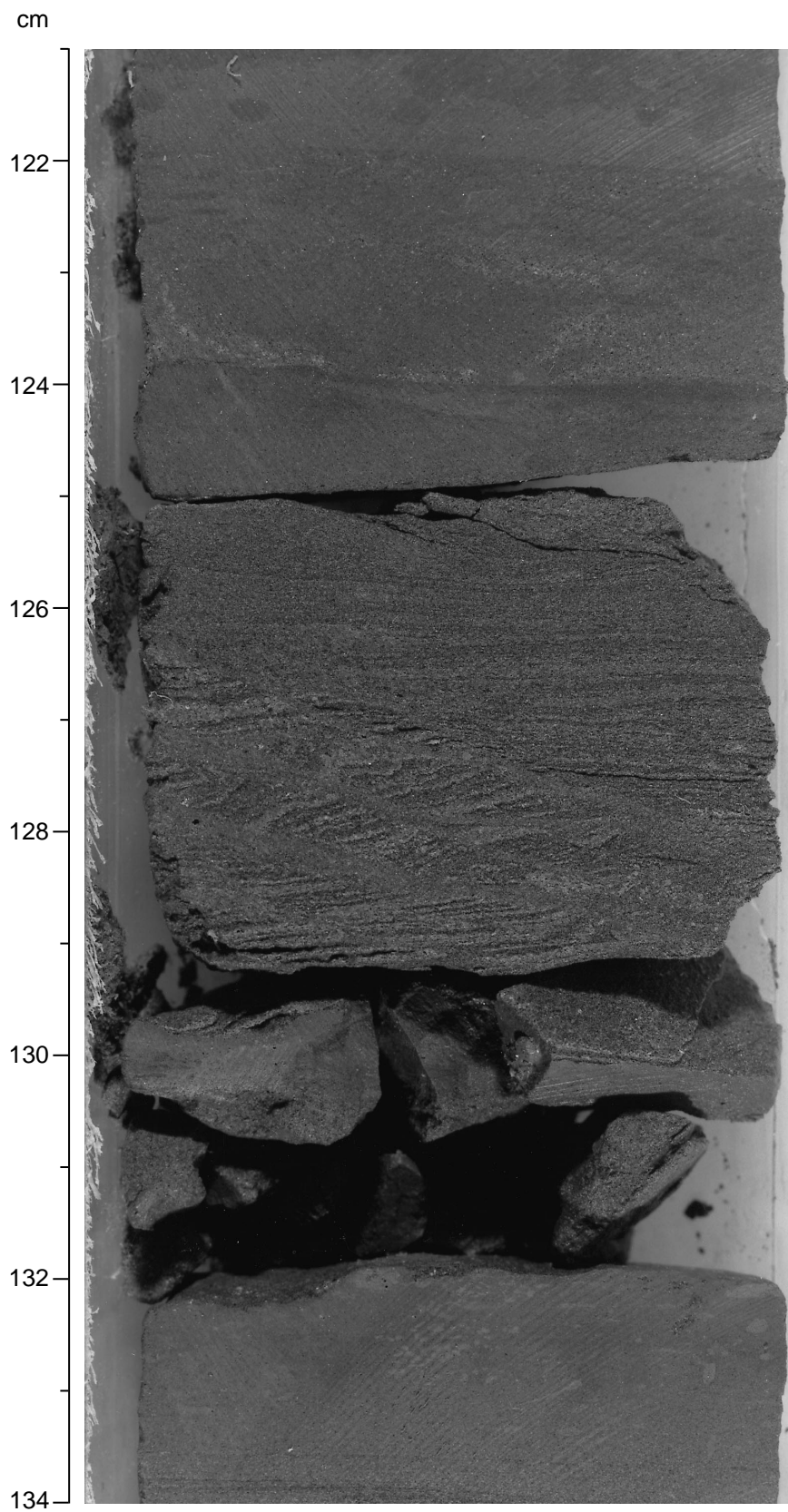
Figure F13. Water-escape structure comprising coarse-grained sandstone within a poorly sorted clayey silt-stone (interval 180-1118A-40R-1, 80–125 cm).
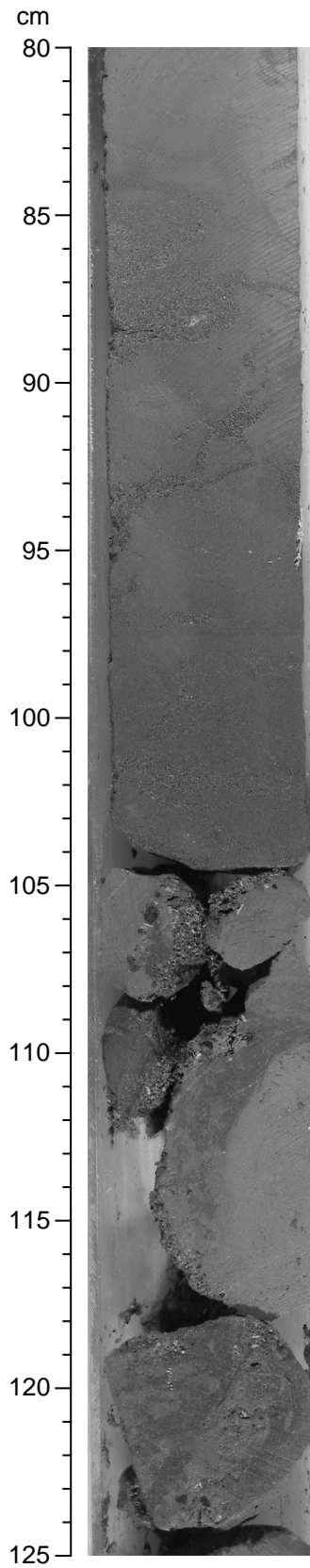
Figure F14. Digital photomicrograph (plane-polarized light) of a moderately sorted, fine-grained volcani-clastic sandstone with a silty clay matrix. This comprises common rounded plagioclase phyric basalt clasts and detrital grains of amphibole, biotite, quartz, and feldspar. Common planktonic foraminifers (Sample 180-1118A-35R-1, 140–143 cm).
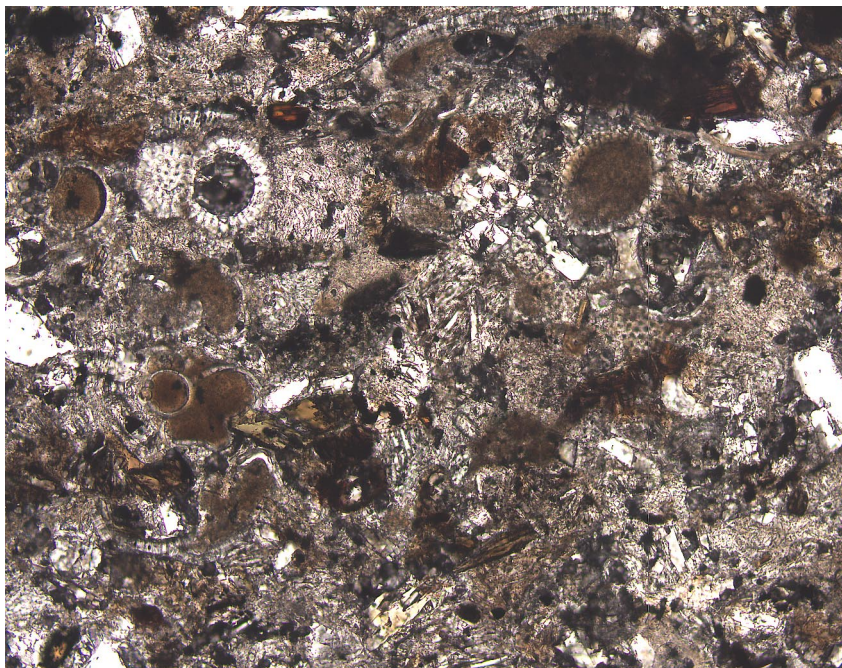
1 mm

Figure F15. Digital photomicrograph (plane-polarized light) of a crystal vitric tuff with abundant angular, fresh pipe-vesicle glass shards in a glassy matrix (Sample 180-1118A-38R-3, 128–130 cm).
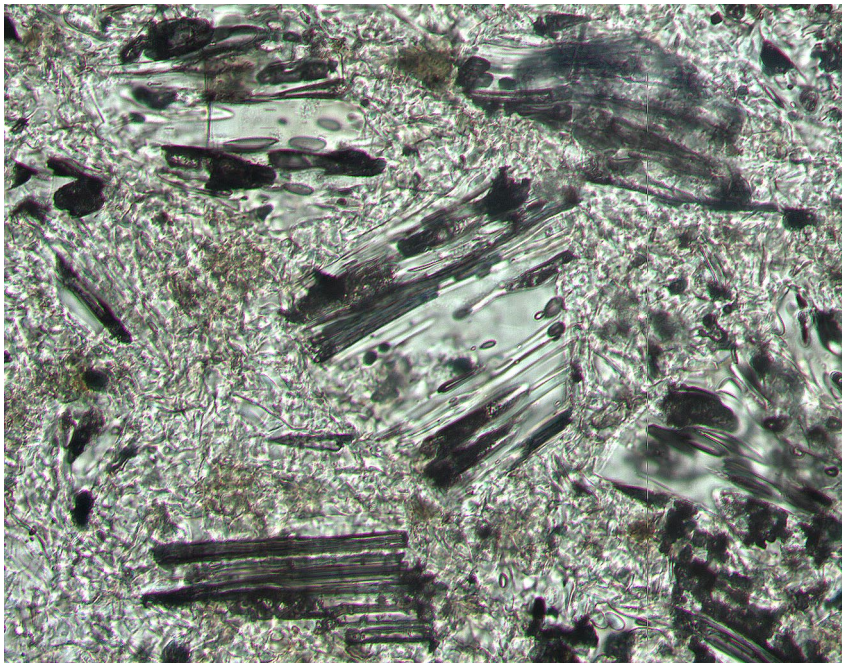
0.5 mm

Figure F16. Deformed laminated sandstone bed. The laminations in the lower part are flat but cut by faults, whereas the upper part of the bed shows an increasing angle of tilt with the upper part folded (interval 180-1118A-40R-4, 40–103 cm).
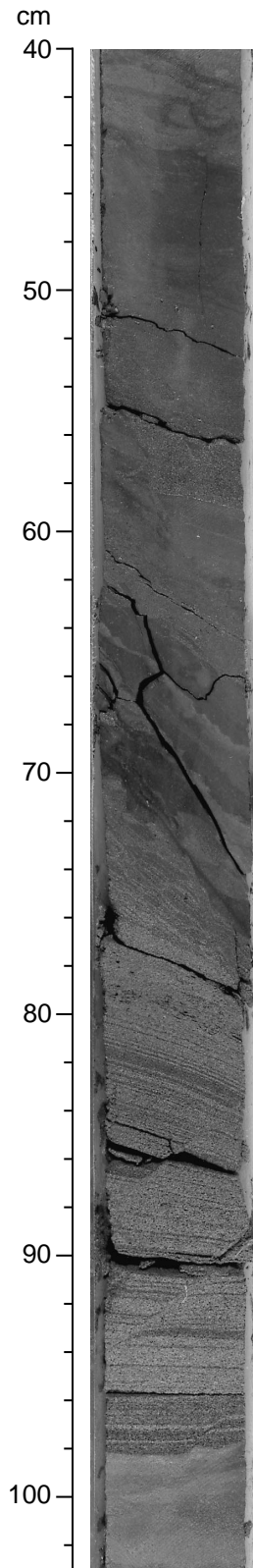
Figure F17. Bioturbated silty claystone and clayey siltstone (interval 180-1118A-54R-1, 98–125 cm).
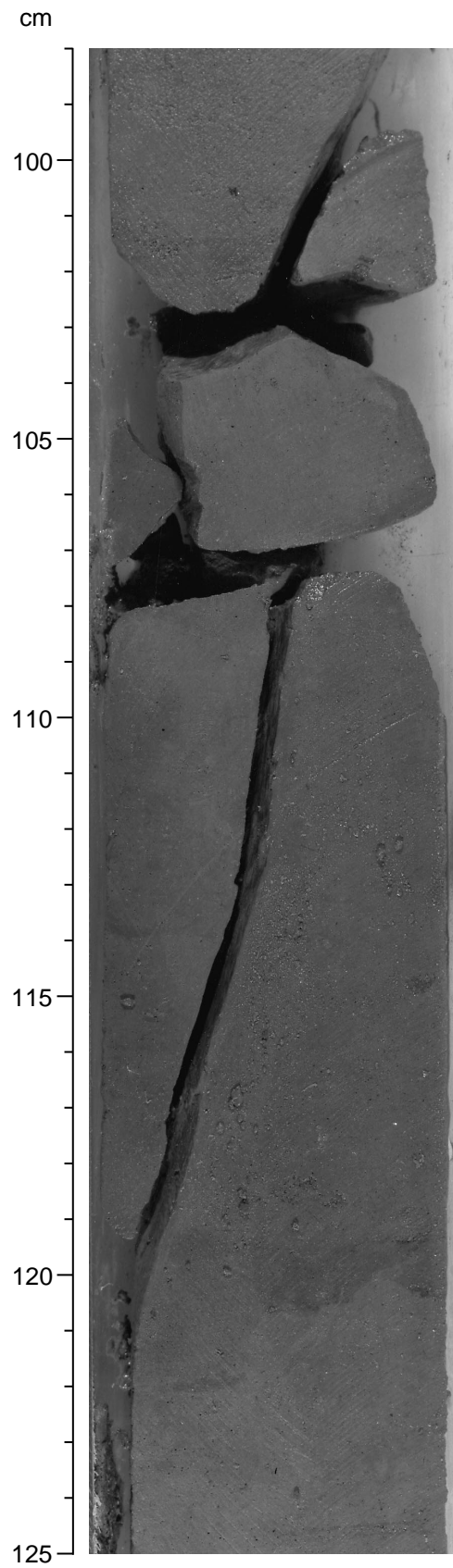
Figure F18. Normal-graded volcaniclastic sandstone that is overlain sharply by parallel-laminated fine-grained volcaniclastic sand (interval 180-1118A-56R-1, 106–113 cm).
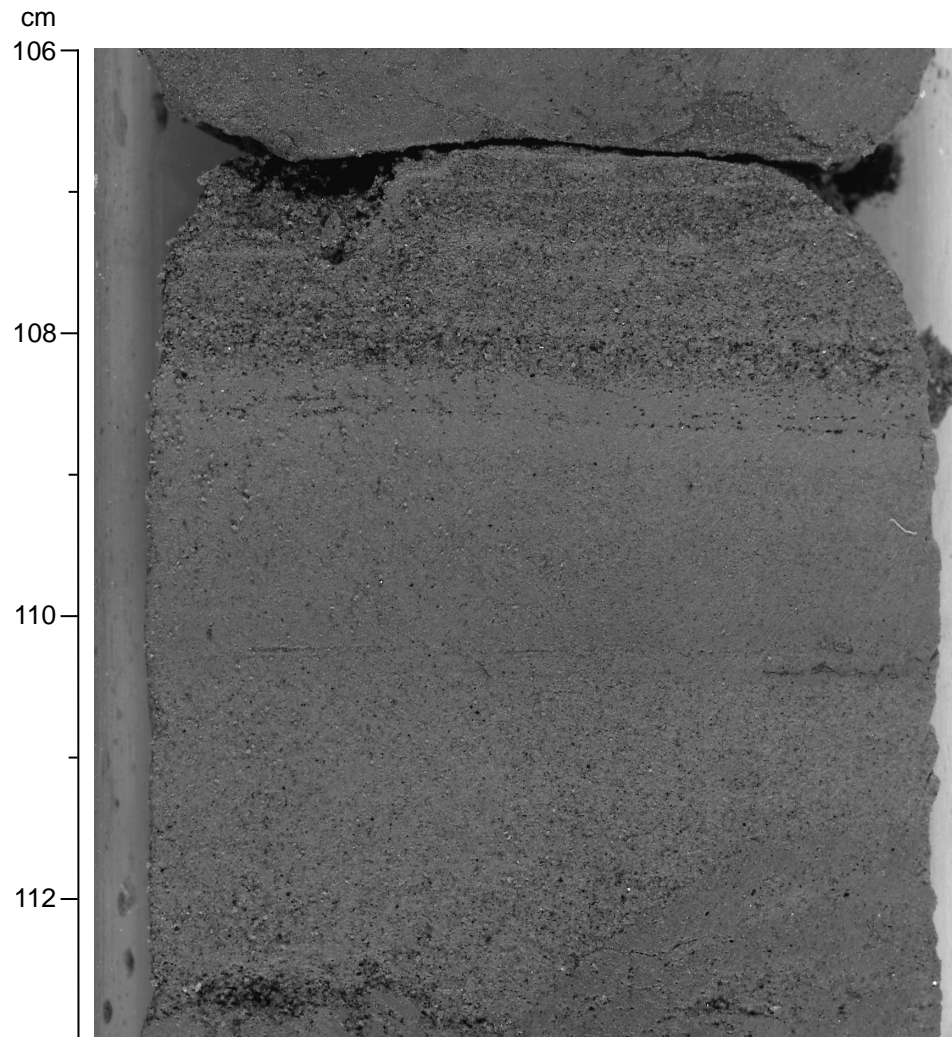
Figure F19. Interbedded normally graded volcaniclastic sandstone with volcanic ash laminae each of which has sharp basal contacts and exhibits normal grading (interval 180-1118A-61R-1, 39–60 cm).
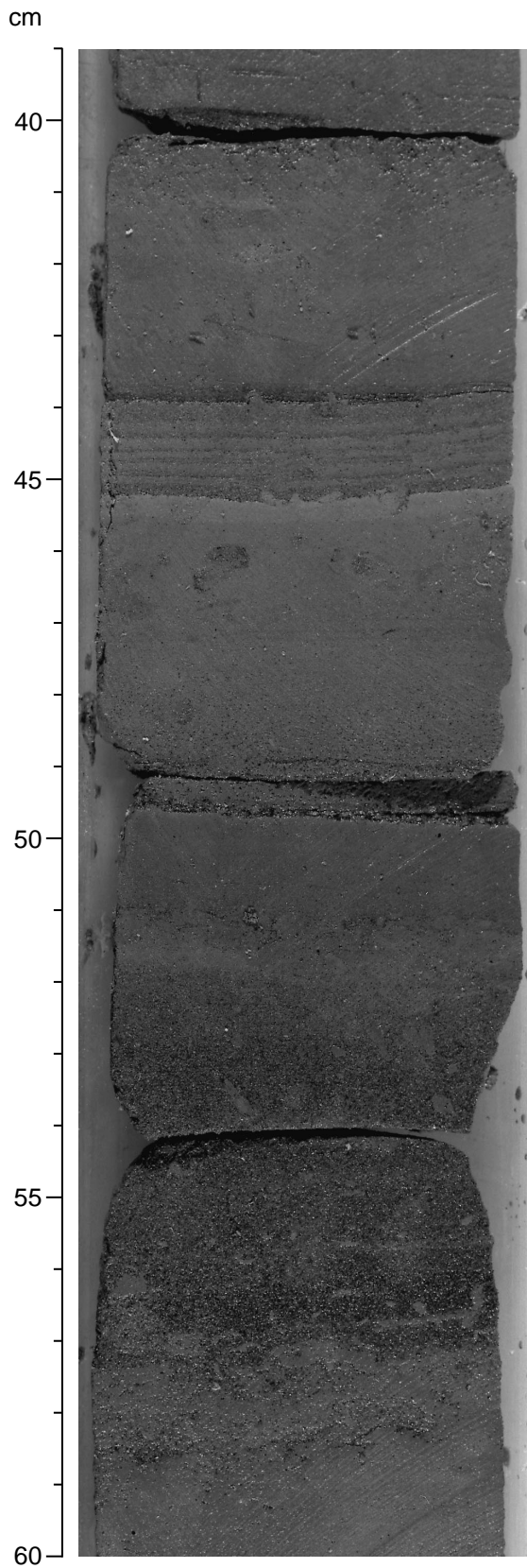
Figure F20. Digital photomicrograph (plane-polarized light) of a crystal vitric tuff composed of abundant angular vesicular glass shards, common angular fresh crystals of biotite, hornblende, plagioclase, and quartz in a fine glassy matrix (Sample 180-1118A-58R-3, 38–40 cm).
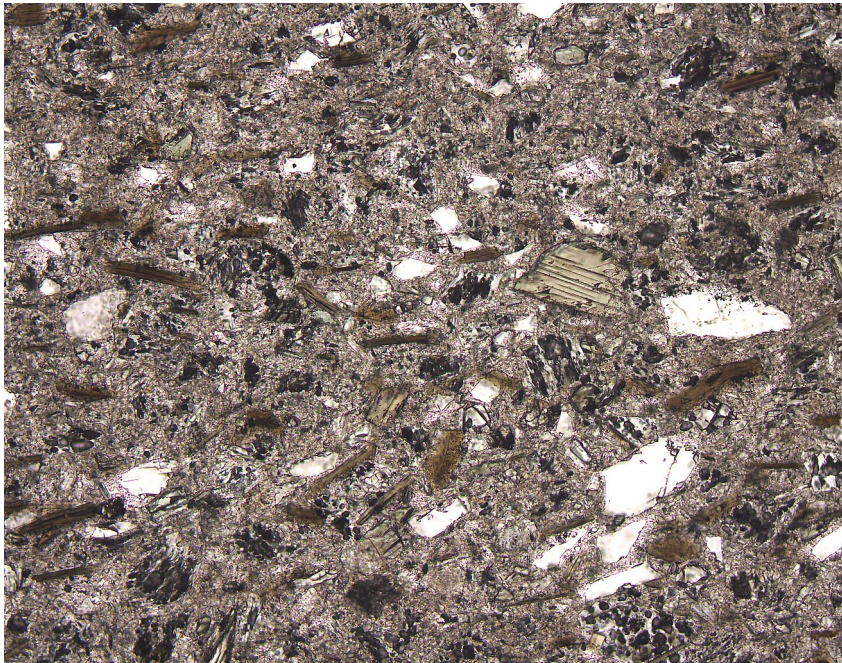
1 mm

Figure F21. Digital photomicrograph (plane-polarized light) of a subrounded fragment of hornblende and plagioclase-phyric basalt with a glassy matrix (center) within a medium-grained volcaniclastic sandstone. Surrounding grains include fresh crystals of hornblende, plagioclase, quartz, and glass shards. Planktonic foraminifers rarely occur (Sample 180-1118A-67R-4, 73–74 cm).
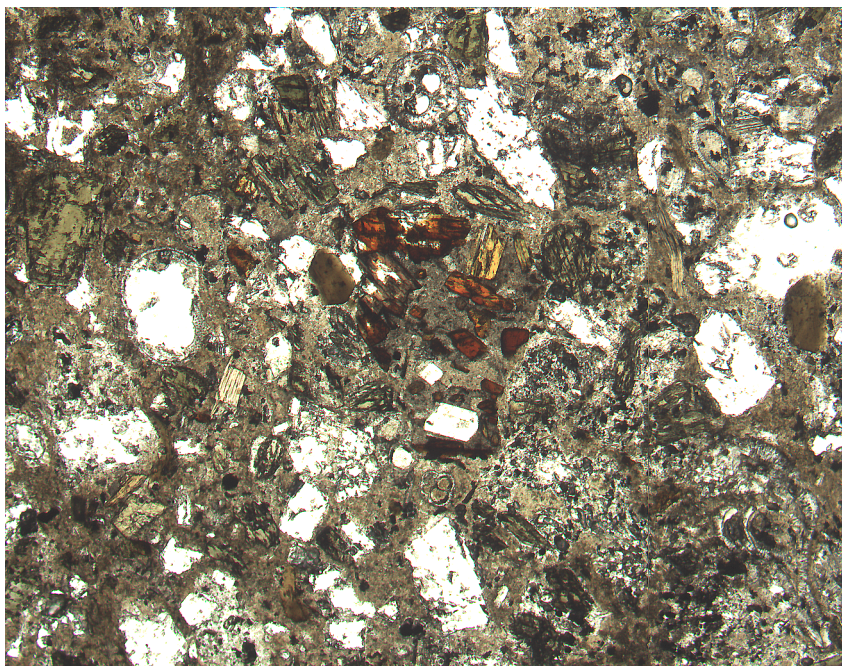
2 mm

Figure F22. Strongly bioturbated silty claystone and clayey siltstone (interval 180-1118A-67R-1, 100–125 cm).
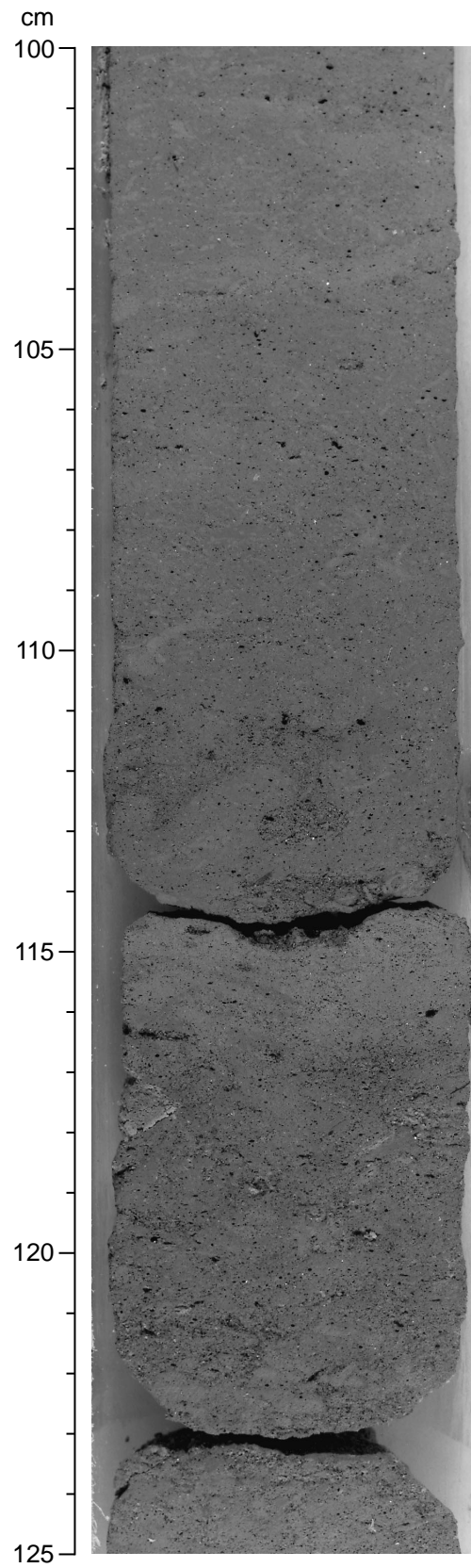
Figure F23. Normally graded mixed sandstone with detrital mineral grains and rare shell fragments (interval 180-1118A-66R-3, 0–32 cm).
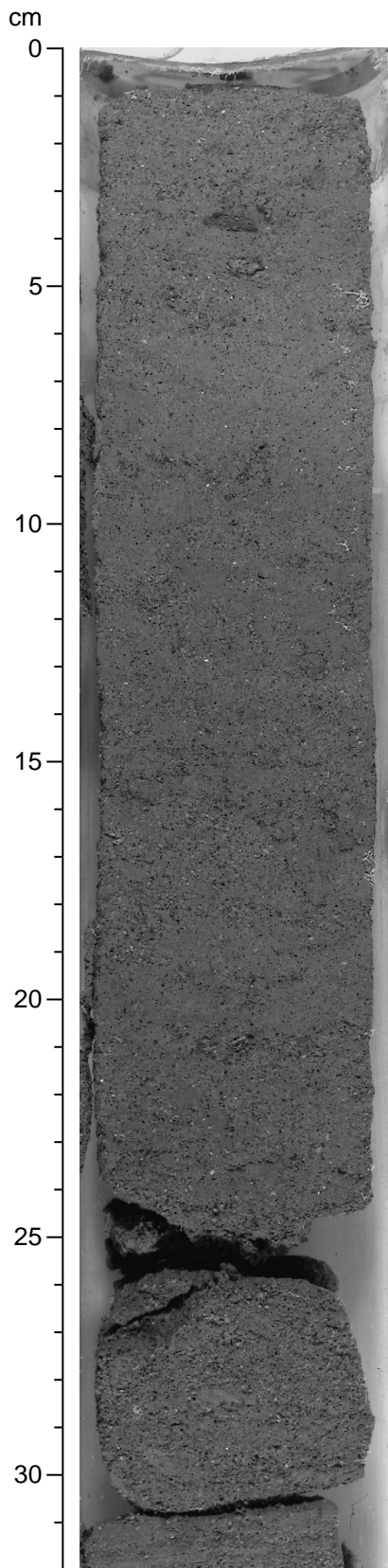
Figure F24. Mixed bioclastic sandstone sharply overlain by a parallel-laminated bed of coarse-grained sand-stone (interval 180-1118A-68R-2, 70–90 cm).
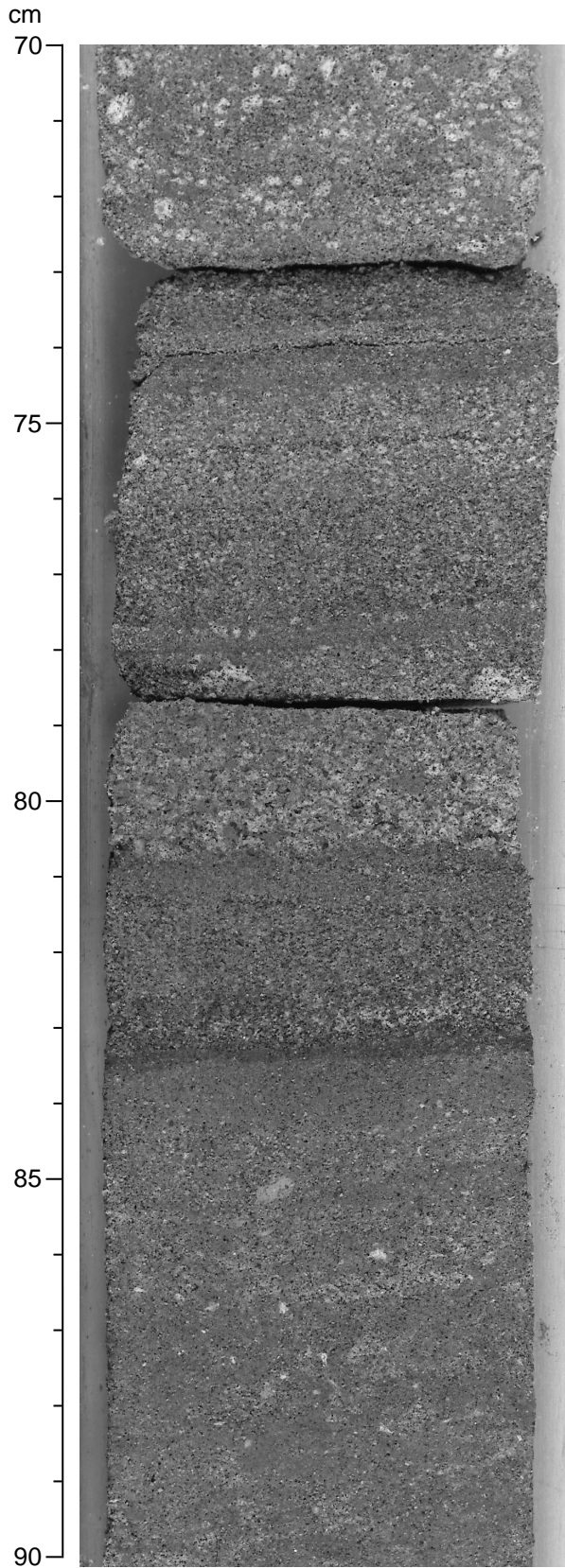
Figure F25. Packstone and grainstone sharply overlain by mixed sandstone with well-rounded claystone clasts, probably marking a scour contact (interval 180-1118A-68R-3, 101–127 cm).
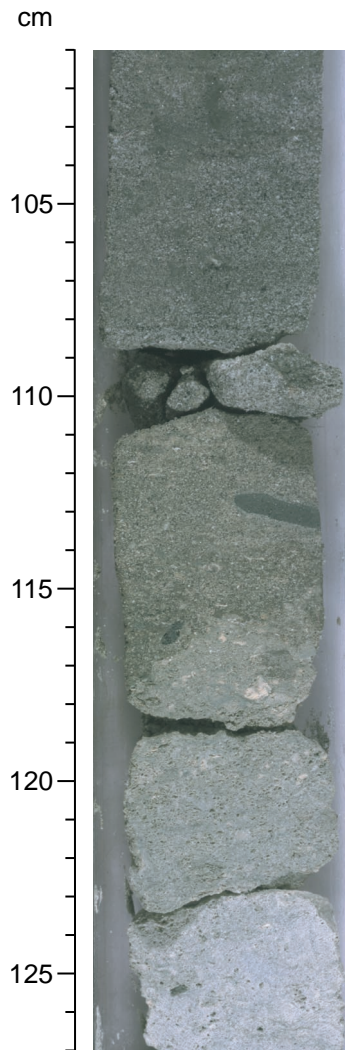
Figure F26. Paraconglomerate with well-rounded large pebbles of igneous rocks. These pebbles are set in a matrix of shell fragments and coarse-grained sand (interval 180-1118A-69R-3, 33–65 cm).
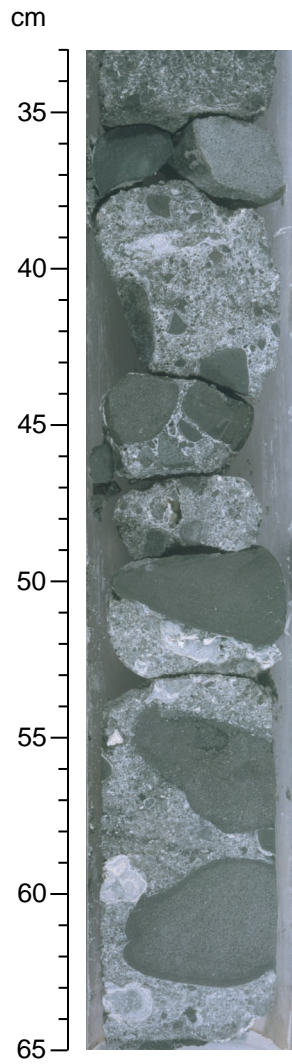
Figure F27. Digital photomicrograph (plane-polarized light) of a large rounded, weakly chloritized plagioclase and clinopyroxene-phyric basalt fragment (center) within a poorly sorted, mixed paraconglomerate. Common biogenic detritus includes benthic and planktonic foraminifers, algae, and shell fragments in a sparry calcite cement. Rare fresh angular plagioclase grains (Sample 180-1118A-69R-1, 35–37 cm).
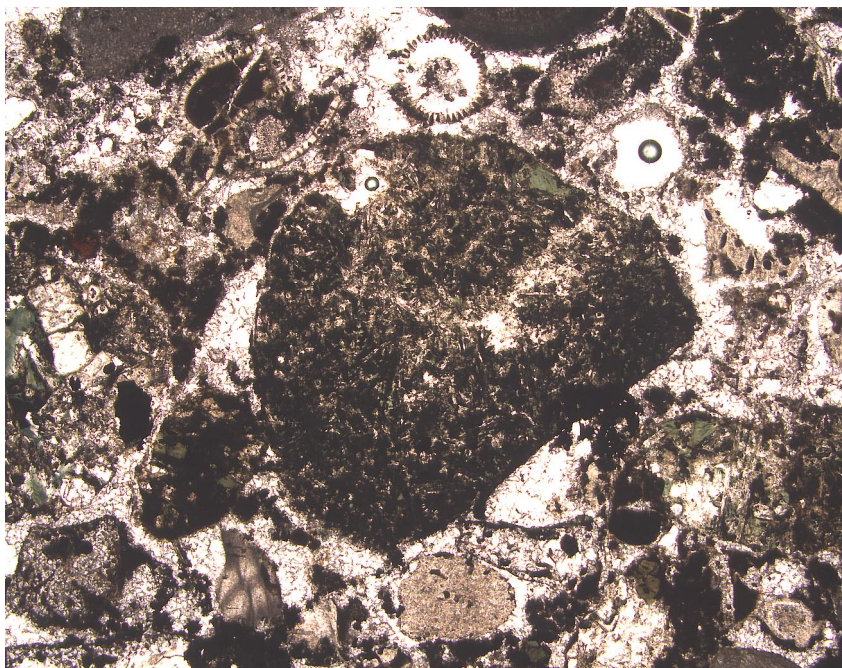
2 mm

Figure F28. Calcareous sandstone with abundant fragments of basalt, rhodoliths, and algal and coral fragments (interval 180-1118A-70R-1, 45–57 cm).
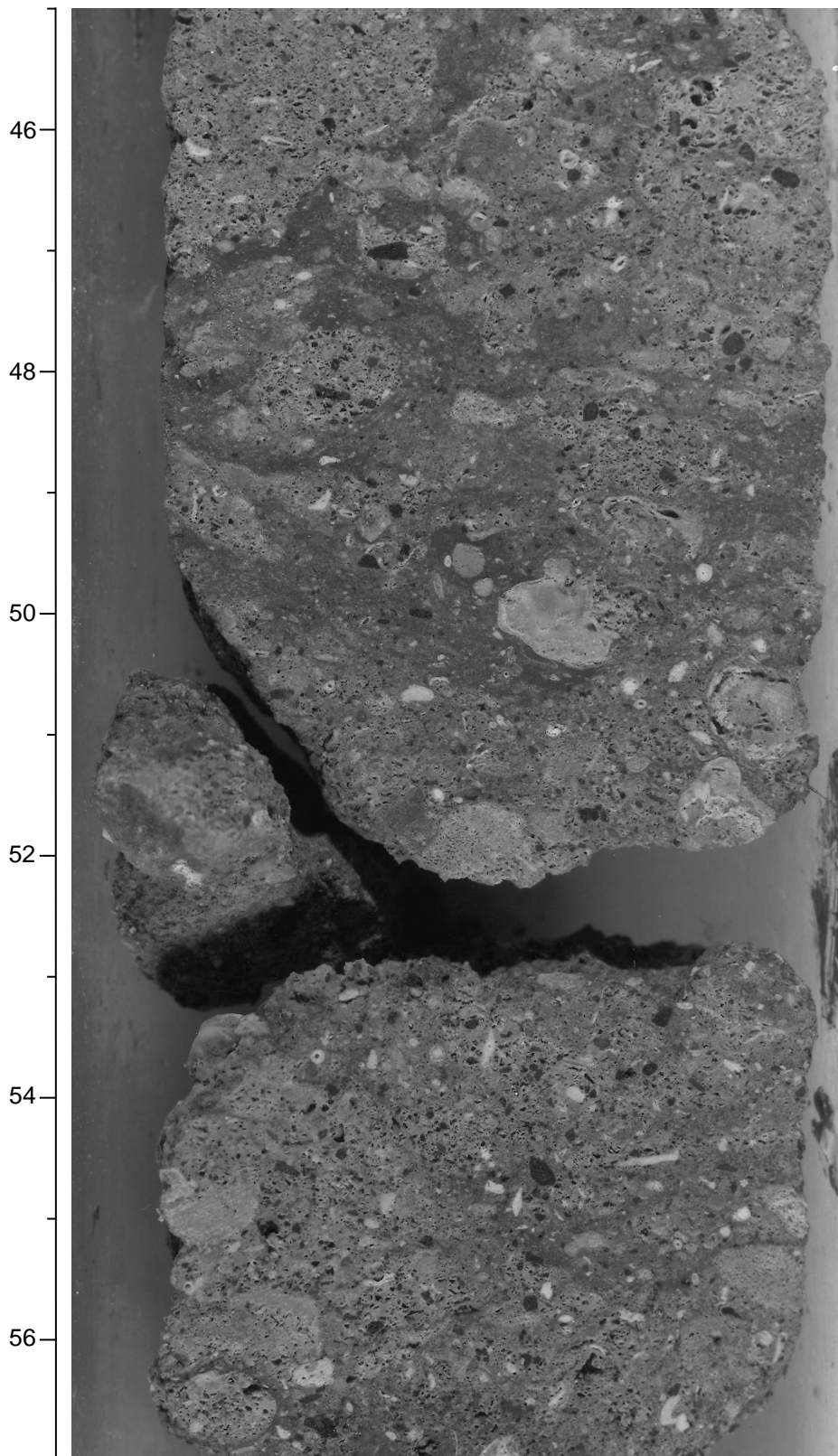
Figure F29. Grainstone comprised of abundant fragments of benthic and planktonic foraminifers, coralline algae, shells, and coral fragments in a micritic cement. Rare chloritized basalt grains and angular fresh plagioclase grains (Sample 180-1118A-70R-1, 0–1 cm).
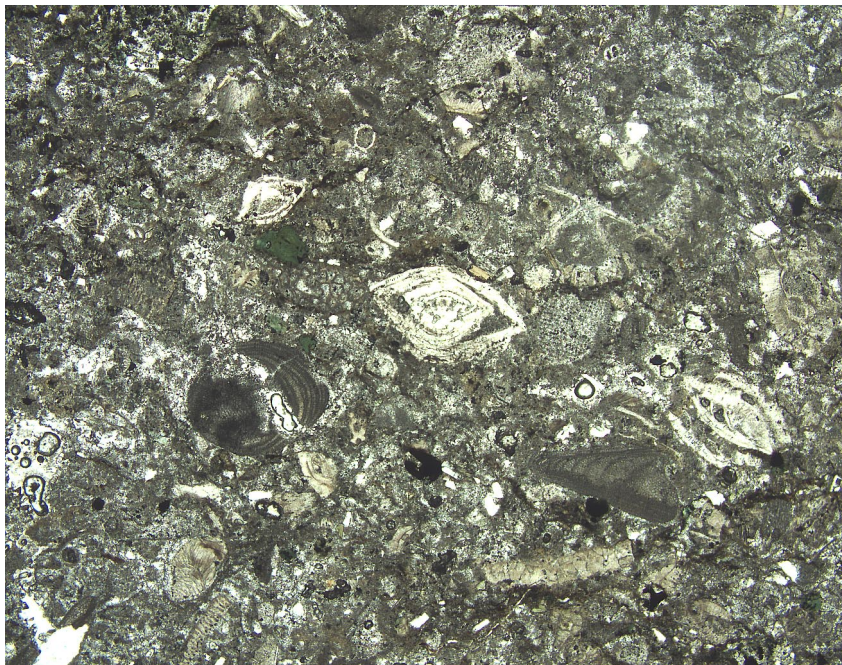
4 mm

Figure F30. Massive dolerite/basalt sharply overlain by bioclastic carbonate followed by pieces of sandy carbonate, algal limestone (75–80 cm), then sandy paraconglomerate. The FMS interpretation suggests that the sharp planar contact between the dolerite/basalt and grainstone above may be an artifact of drilling (interval 180-1118A-70R-1, 66–97 cm).
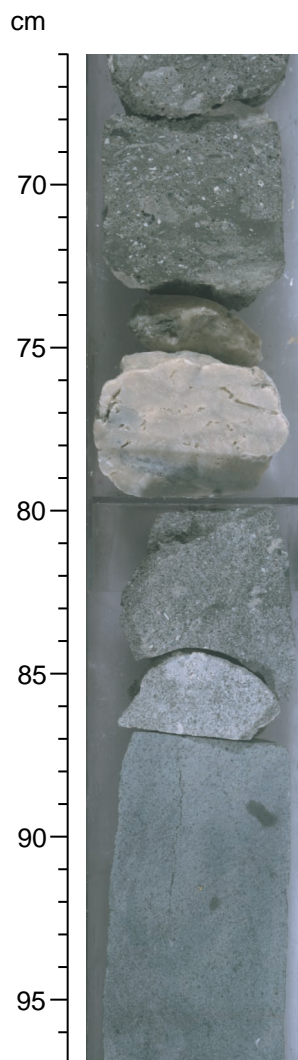
Figure F31. Digital photomicrograph (plane-polarized light) of a well-rounded plagioclase- and clinopyroxene-phyric basalt fragment within a chloritized silty matrix. Rare surrounding subangular grains are plagioclase and clinopyroxene (Sample 180-1118A-71R-1, Piece 1, 13–15 cm).
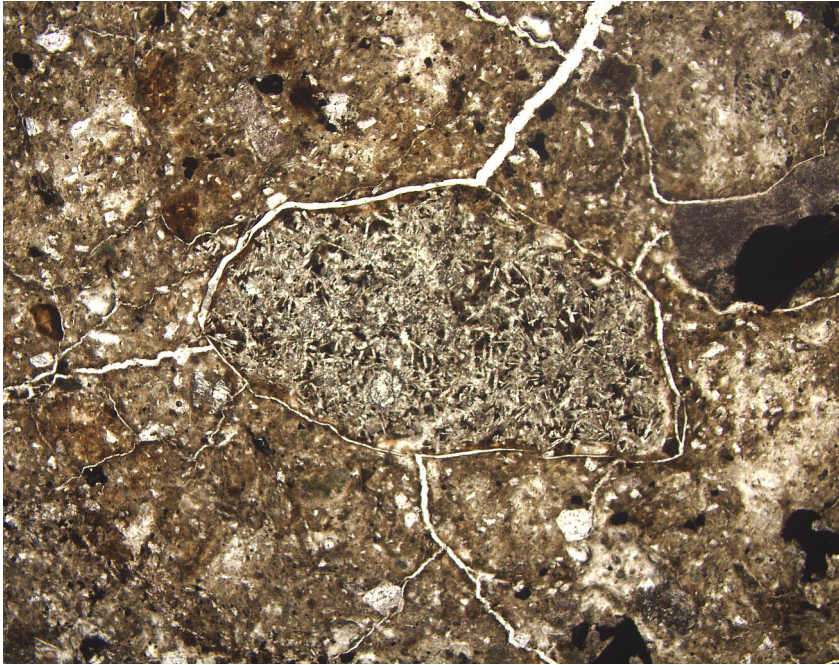
4 mm

Figure F32. Polymict breccia of angular-subangular clasts of basalt/dolerite within a matrix of altered coarse-grained to granule-sized sandstone derived from basalt and dolerite. Unit VIII (interval 180-1118A-72R-1, 77–84 cm).
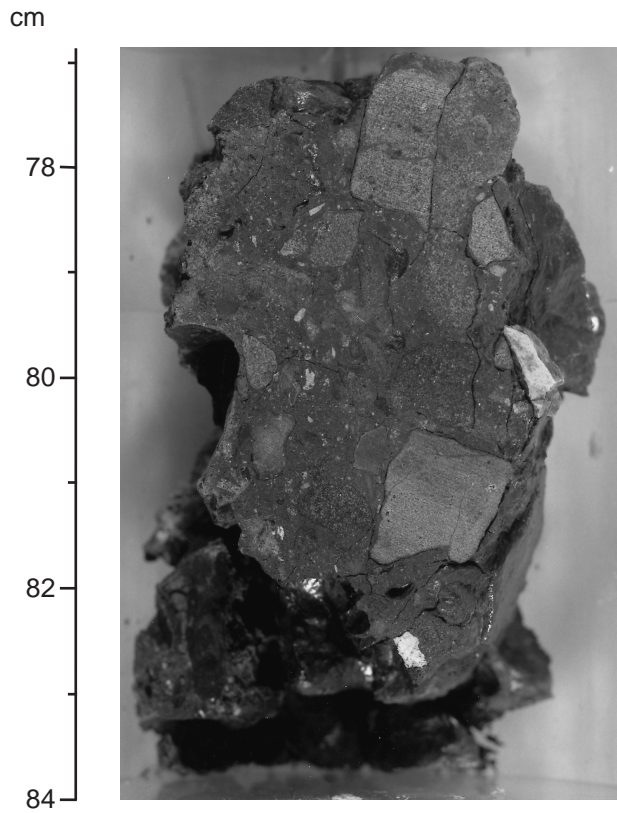
Figure F33. Number of volcanogenic ash layers (black) and total volcanogenic ash thickness (shaded) per core in centimeters at Site 1118. Note that the variation may not be representative of the actual recovery within intervals of low recovery.
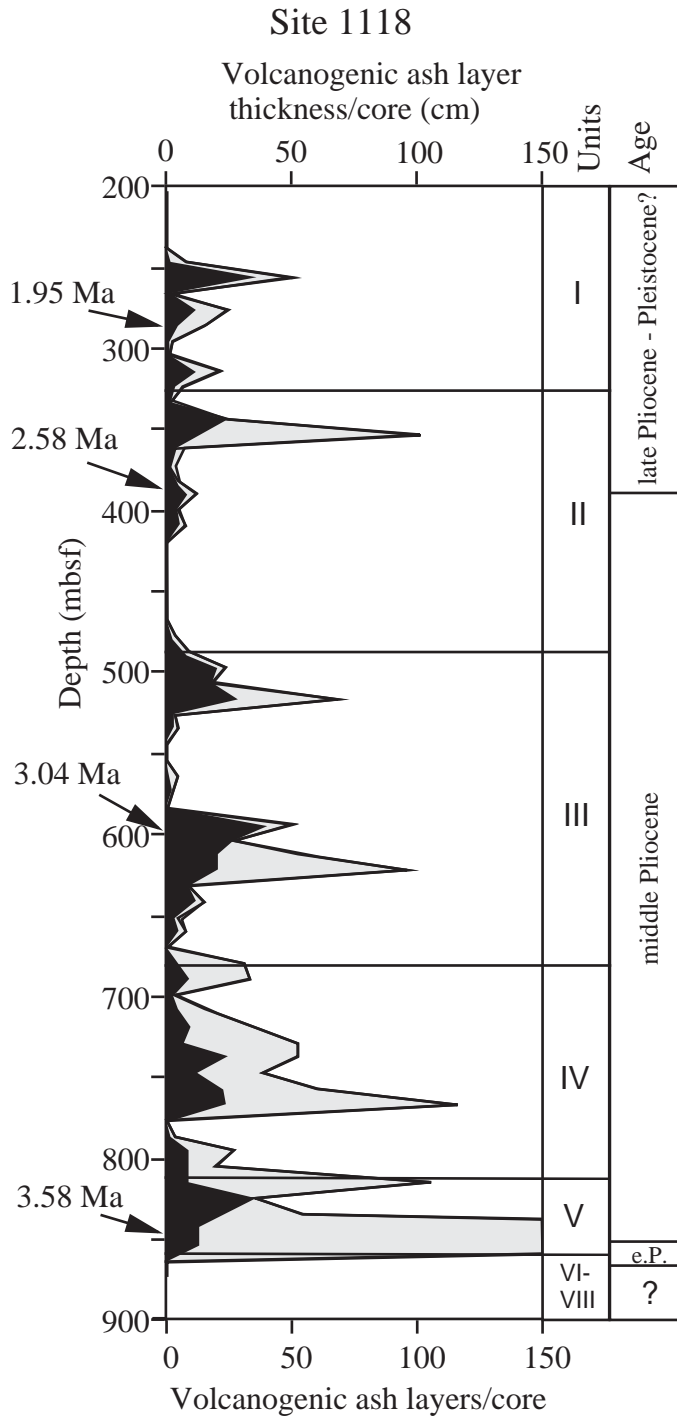
e.P. = early Pliocene

Figure F34. Diagram illustrating the recovery and rock types from Sections 180-1118A-70R-3 to 76R-2. Abbreviations show the locations of samples for the following: TSB = thin-section billets, XRD = X-ray diffraction; XRF = X-ray fluorescence. (Numbers are those of the samples reported in Tables T4, p. 180, and T5, p. 181.)

Hole 1118A Recovery, Analyses Log

TSB (dolerite)
XRD

TSB (dolerite)
XRD
XRF 2

TSB (dolerite)

TSB (dolerite)
XRD

TSB (dolerite, basalt, pegmatite)
XRD
XRF 3,4

TSB (dolerite, pegmatite)
XRF 5,6,7
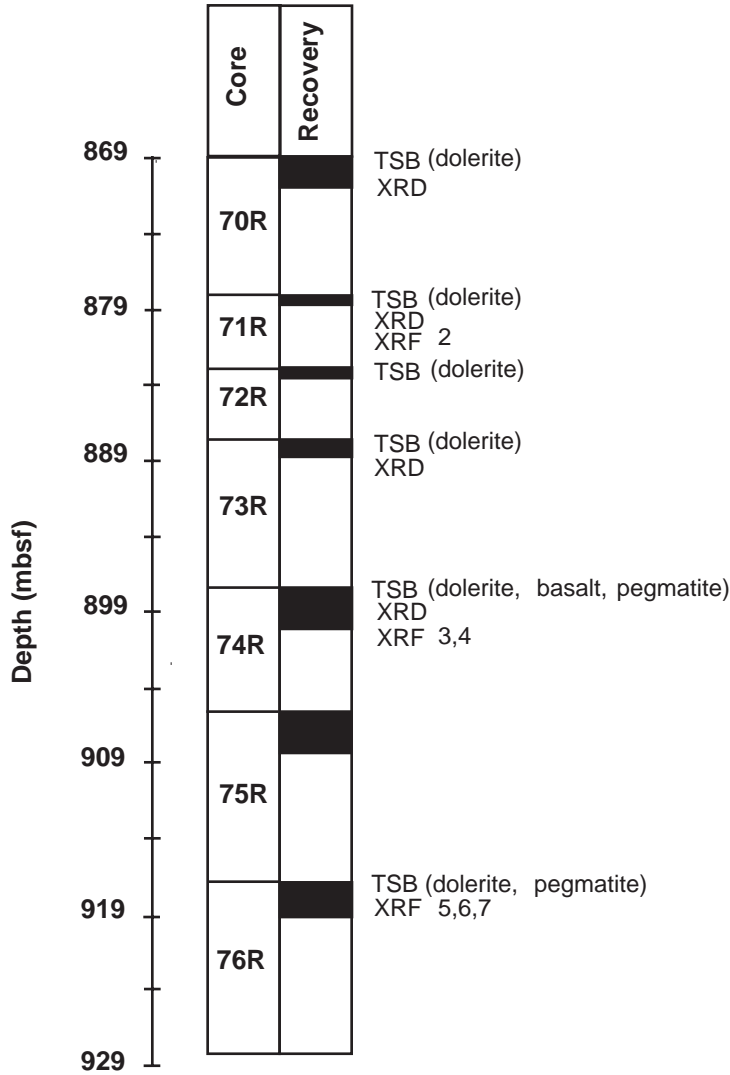
Figure F35. Fresh and cohesive section of granular dolerite crosscut by a fracture (interval 180-1118A-73R-1, 25–55 cm).
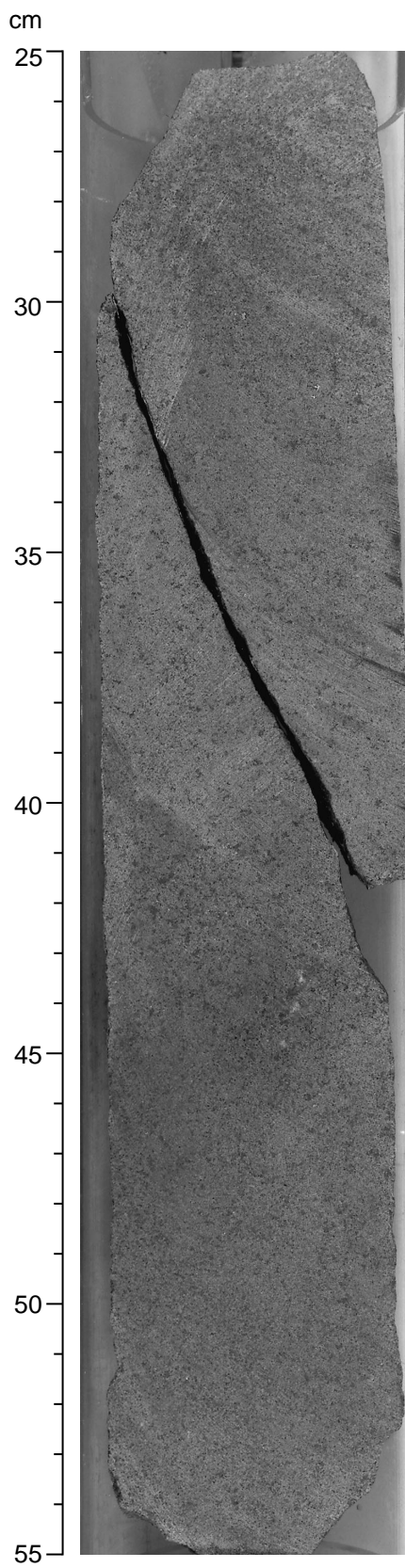
Figure F36. Brecciated and altered dolerite originally forming conglomerate matrix (interval 180-1118A-76R-1, 46–53.5 cm).
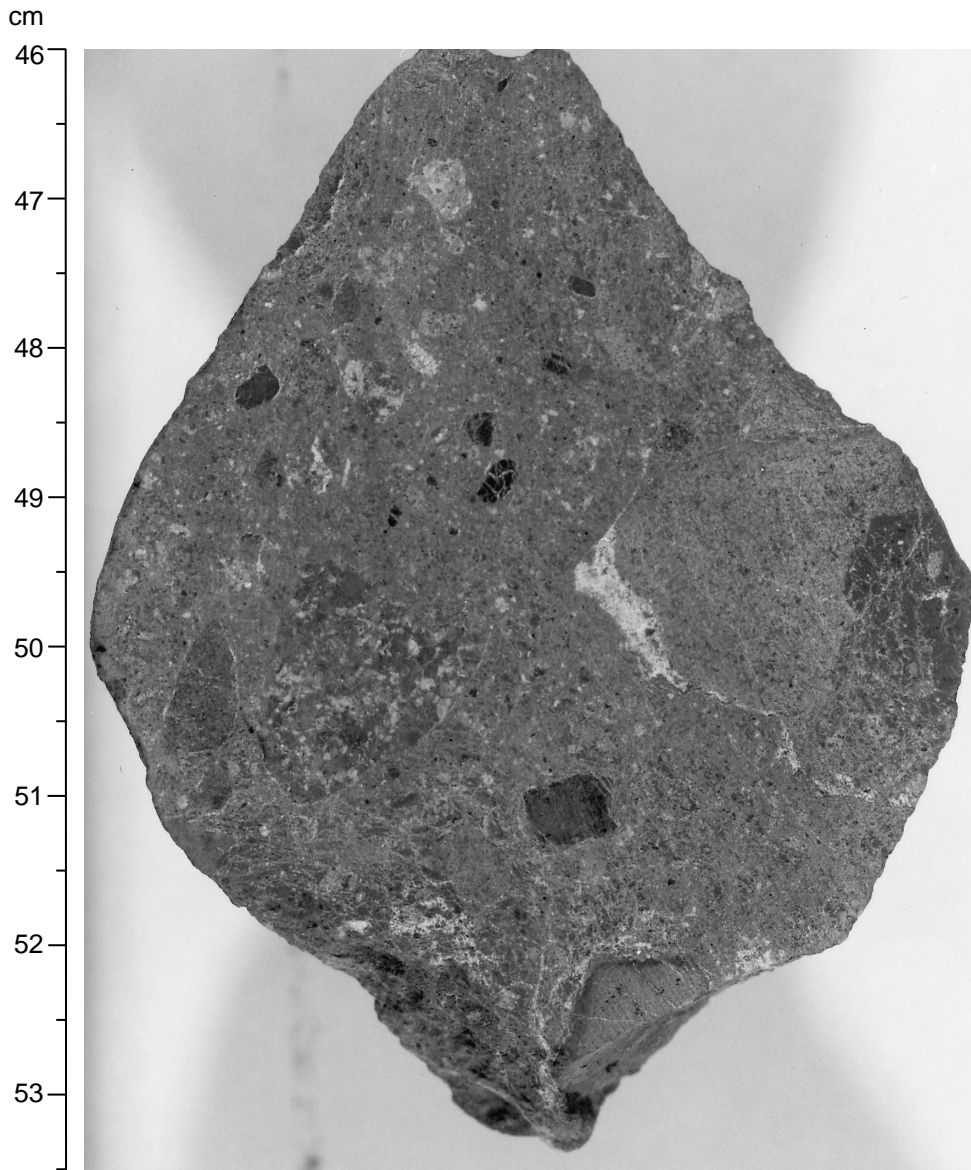
Figure F37. Digital photomicrograph of a vein filled with calcite (Calc) and zeolite (Zeo) crosscutting a granular dolerite. Oxidation of the dolerite moves from the veins into the dolerite. Fragments of the granular dolerite (Do) are found within the vein (Sample 180-1118A-76R-1, 90–93 cm). Mag = magnetite; Plg = plagioclase; and Chl = chlorite.
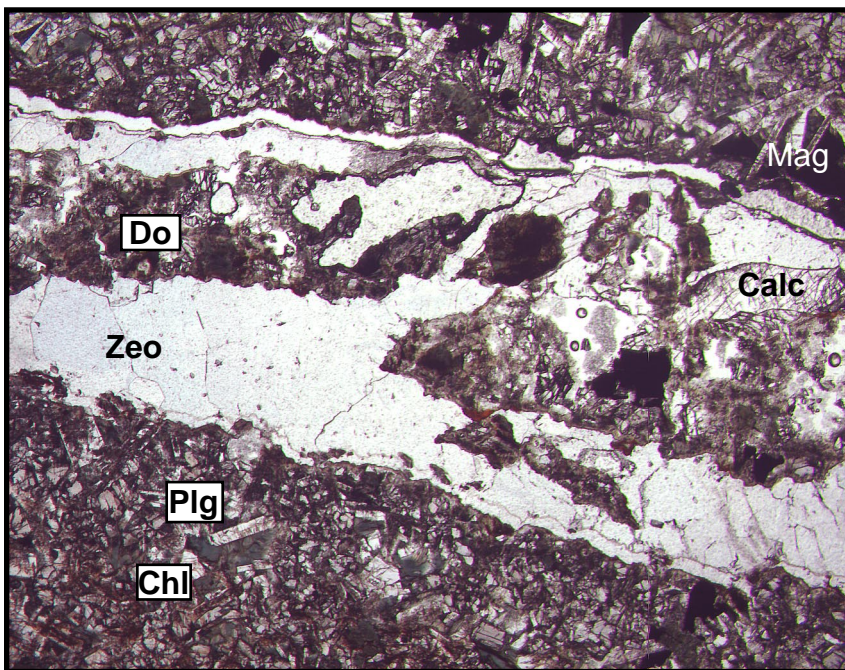
4 mm

Figure F38. Digital microphotograph (plane-polarized light) of a granular dolerite with altered plagioclase, extensive areas of chlorite formation, and large iron oxides (Sample 180-1118A-73R-1, 25–27 cm). Mag = magnetite; Chl = chlorite; Cpx = clinopyroxene; and Sau = saussurite-altered plagioclase.
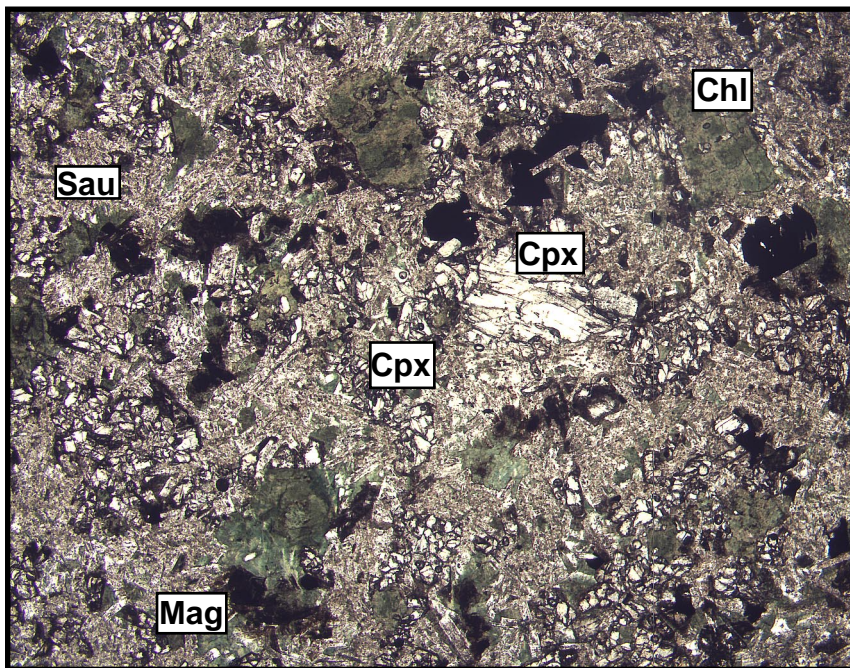
4 mm

Figure F39. Digital photomicrograph of dendritic magnetite (Mag) in the pegmatitic dolerite (Sample 180-1118A-74R-2, Piece 5C, 140–142 cm). Plg = plagioclase; Cpx = clinopyroxene; and Chl = chlorite.
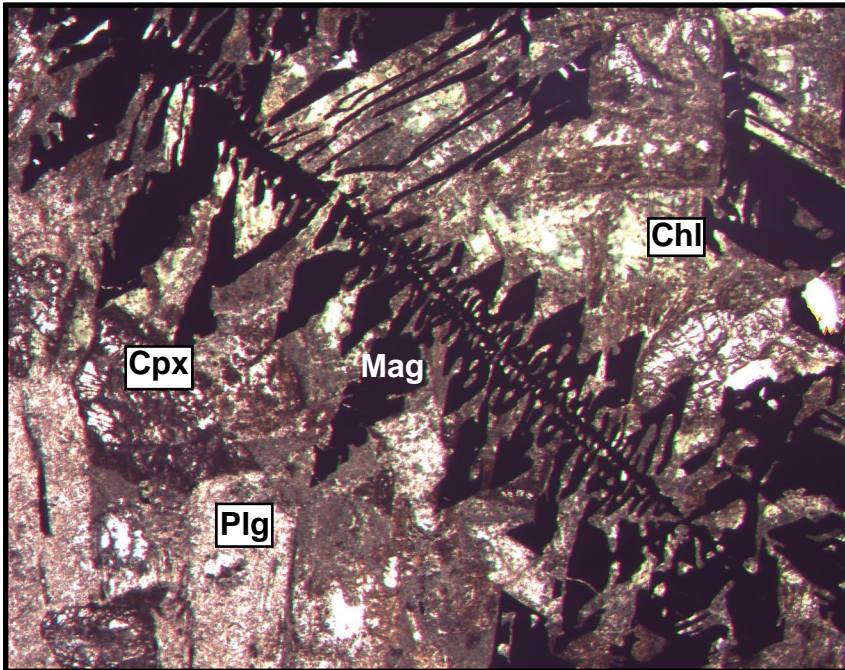
4 mm

Figure F40. Digital photomicrograph (plane-polarized light) of microphenocrysts of plagioclase (Plg) and clinopyroxene (Cpx) in a variolitic groundmass (Sample 180-1118A-74R-1, Piece 16, 124–126 cm).
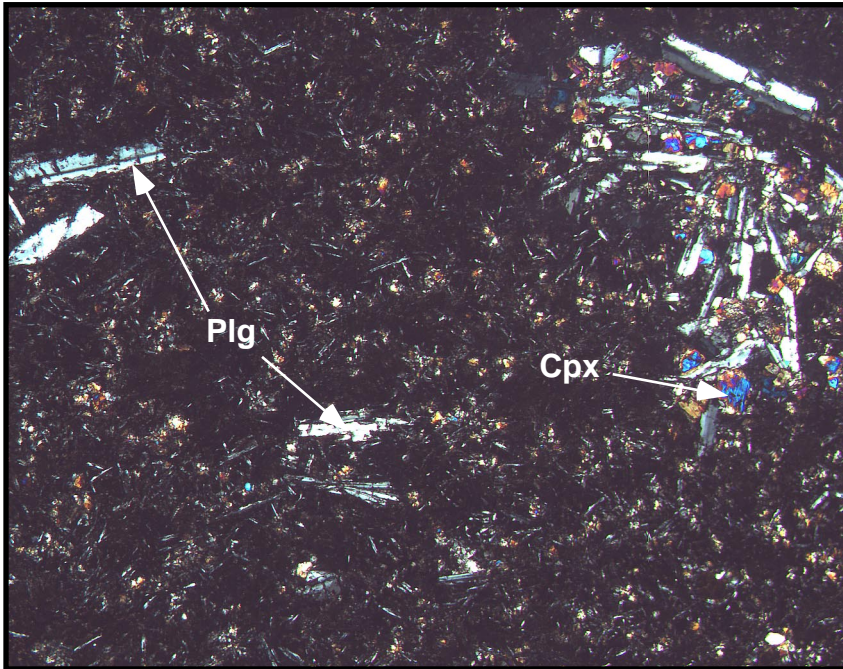
2 mm

Figure F41. Selected major and trace elements from Site 1118 plotted against the differentiation index FeO*/MgO.
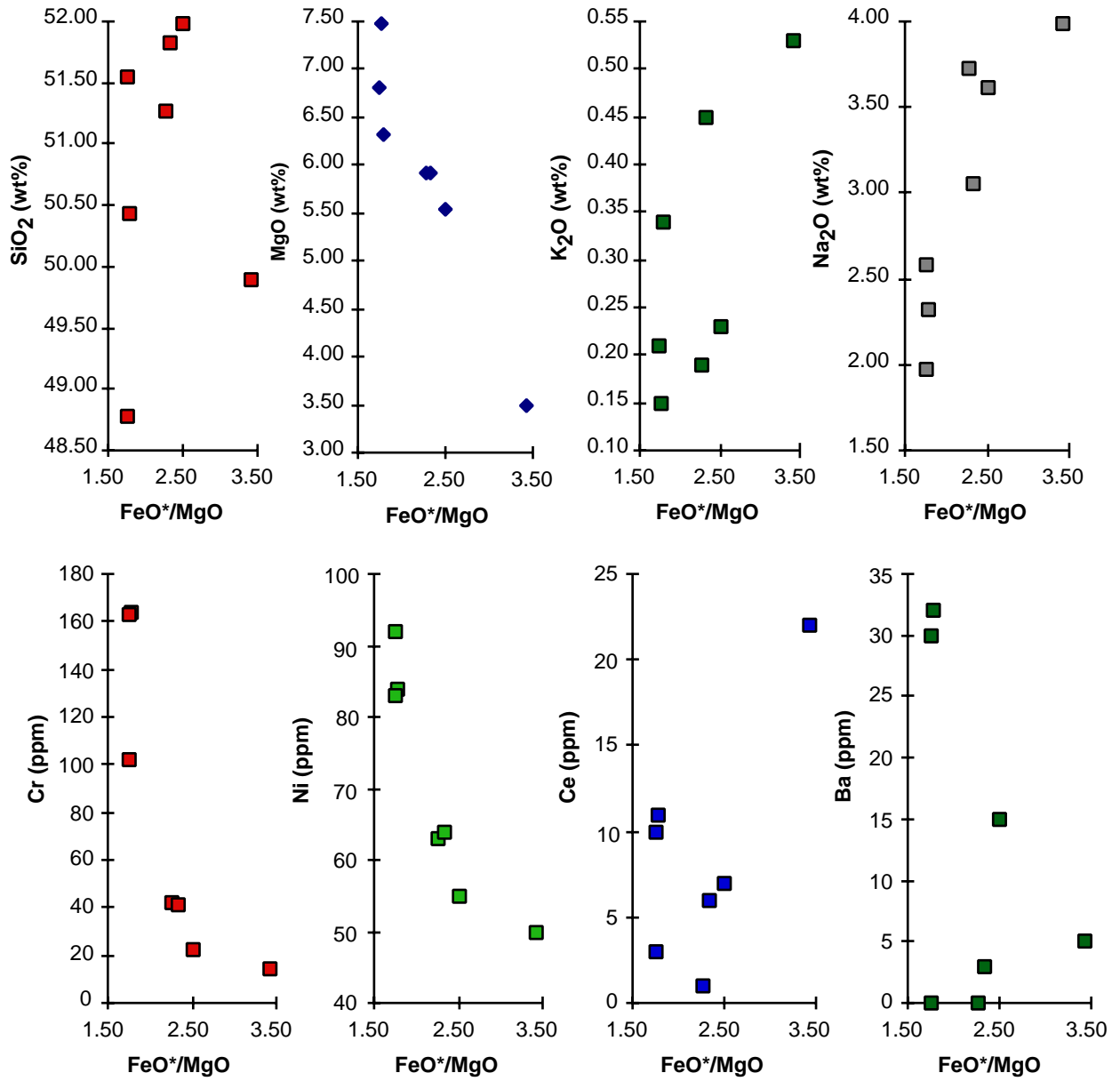
Figure F42. Summary of the main structural features observed at Site 1118 (for key to symbols, see Fig. F2, p. 52, in the "Explanatory Notes" chapter).
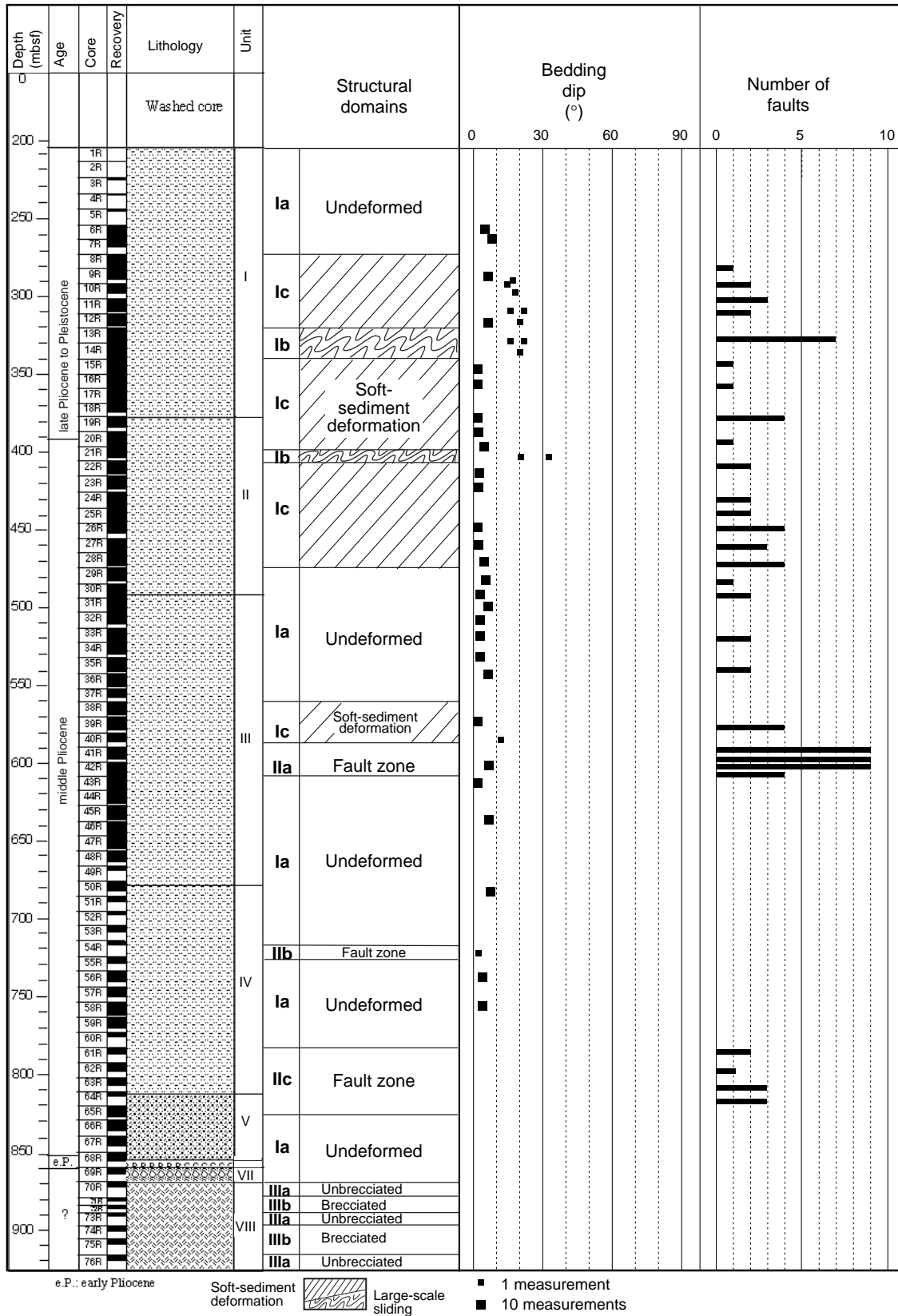
Figure F43. Bedding dips measured in Domains I and II. N = number of measurements.
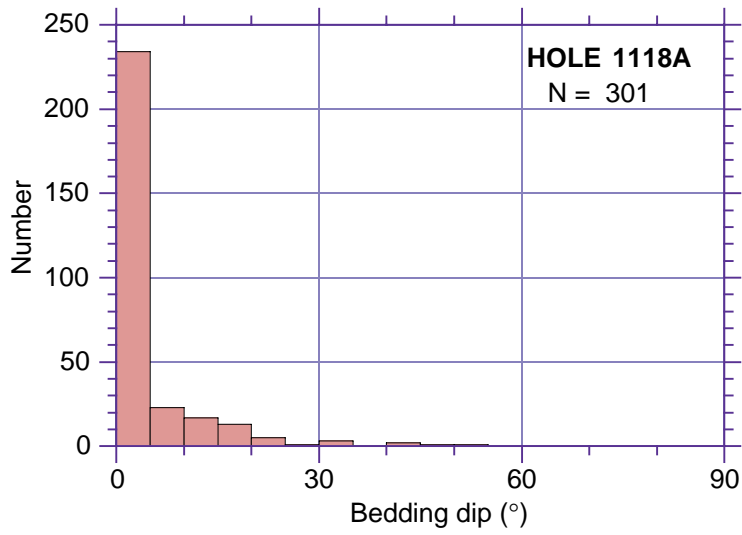
Figure F44. Discrete normal microfault zone in Subdomain Ic (interval 180-1118A-39R-3, 98–108 cm [573.75 mbsf]). F = fault orientation and dip (in core reference frame).
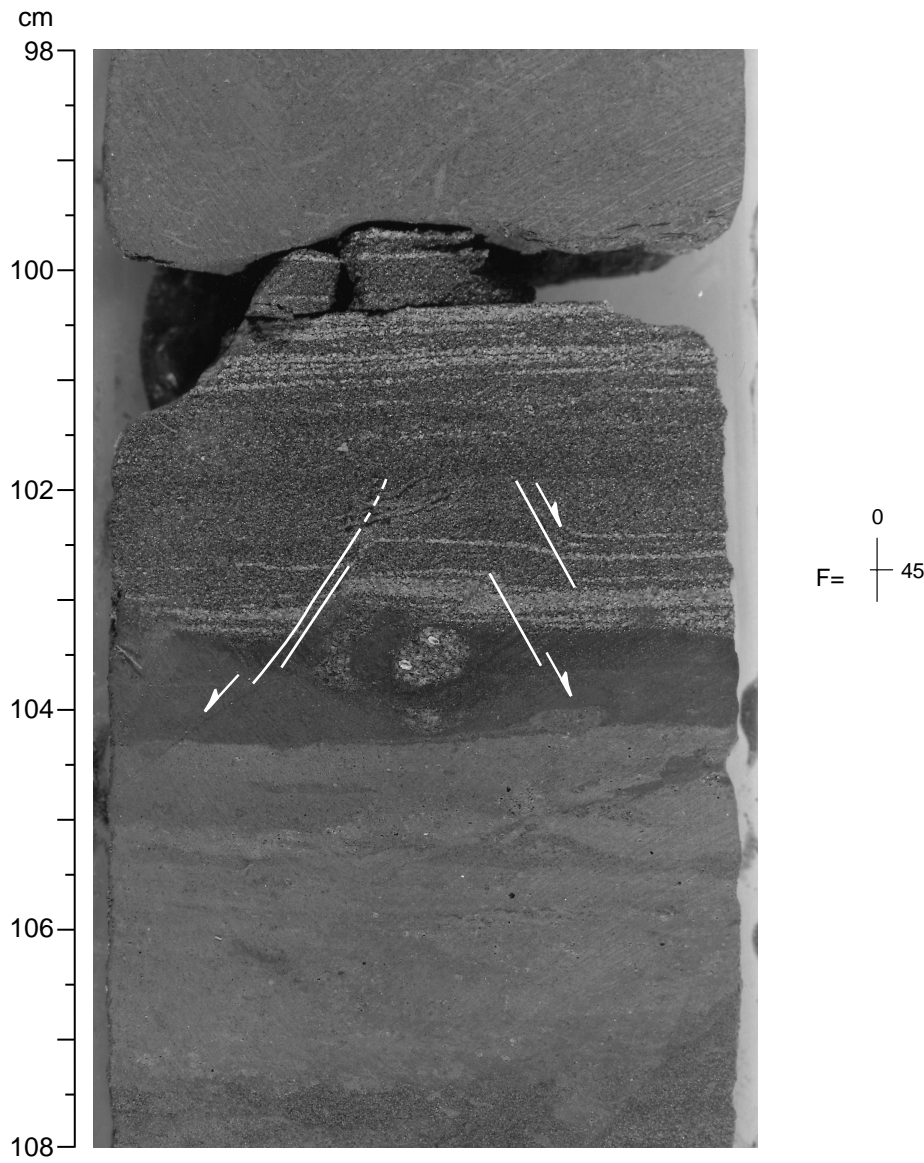
Figure F45. Slickenside plunge vs. fault dip diagram for Domain II. **A.** Subdomain IIa. **B.** Subdomain IIc. N = number of measurements.
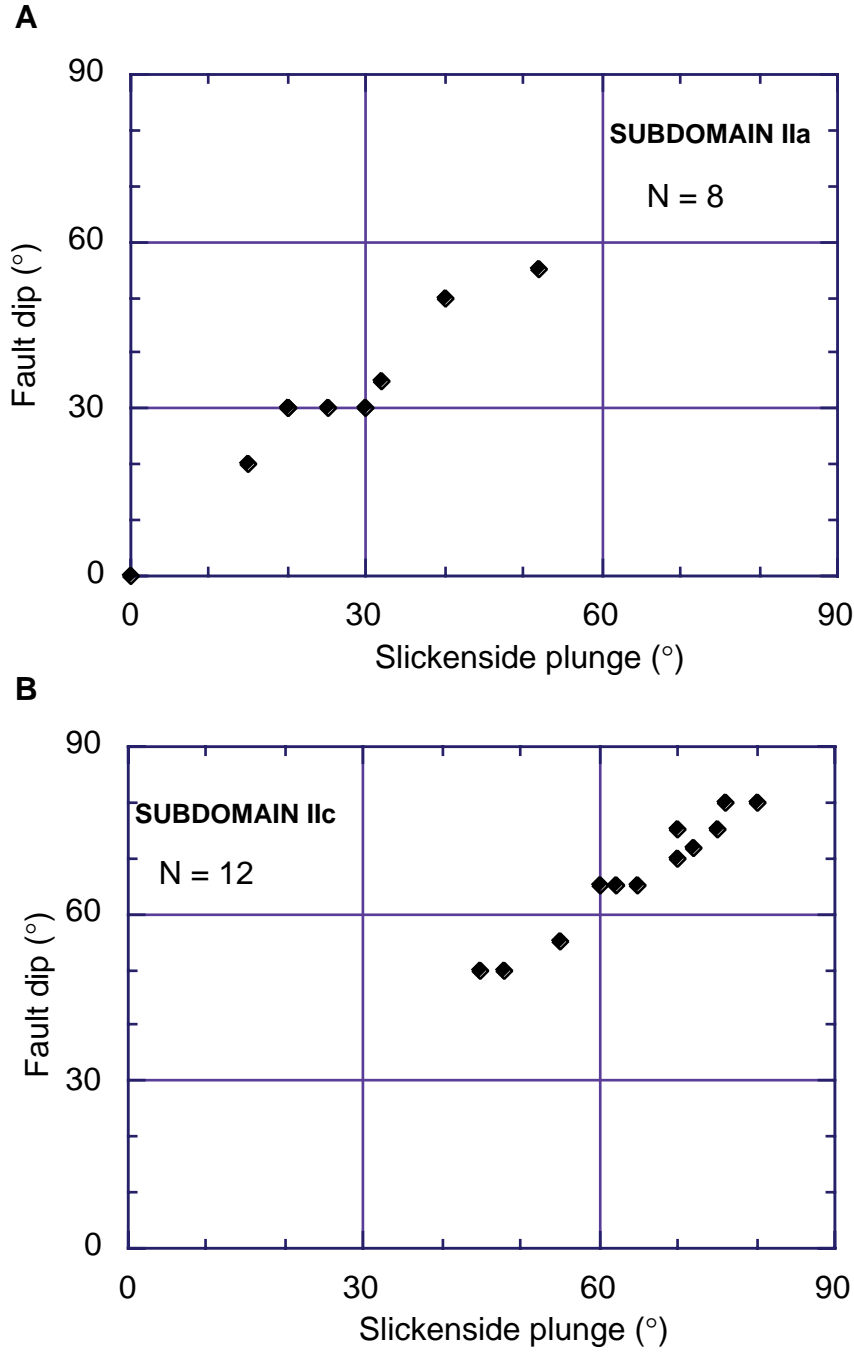
Figure F46. Polyphased extensional faulting in Subdomain IIa (interval 180-1118A-40R-4, 40–103 cm [583.76 mbsf]). **A.** Core observations: B = bedding orientation and dip; F = fault orientation and dip. **B.** Sketch showing (1) the successive strata rotations in the hanging wall of the west-dipping fault network, and (2) the timing relationships between faults Fe and Fw. (Orientation in core reference frame) Fe = fault facing to the east; Fw = fault facing to the west.
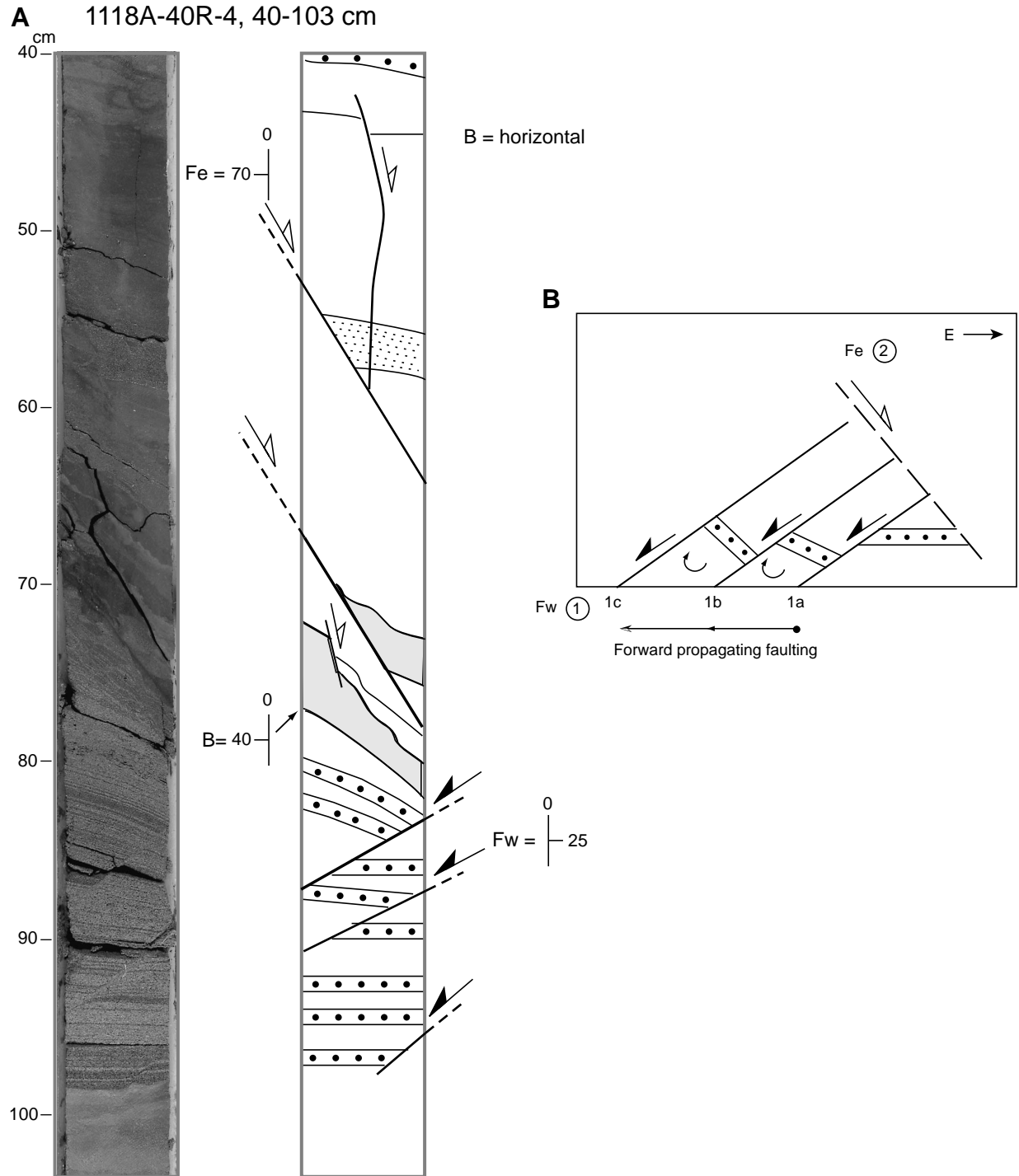
Figure F47. Recovery of the dolerite from Hole 1118A and structural interpretation for the development of the breccia.
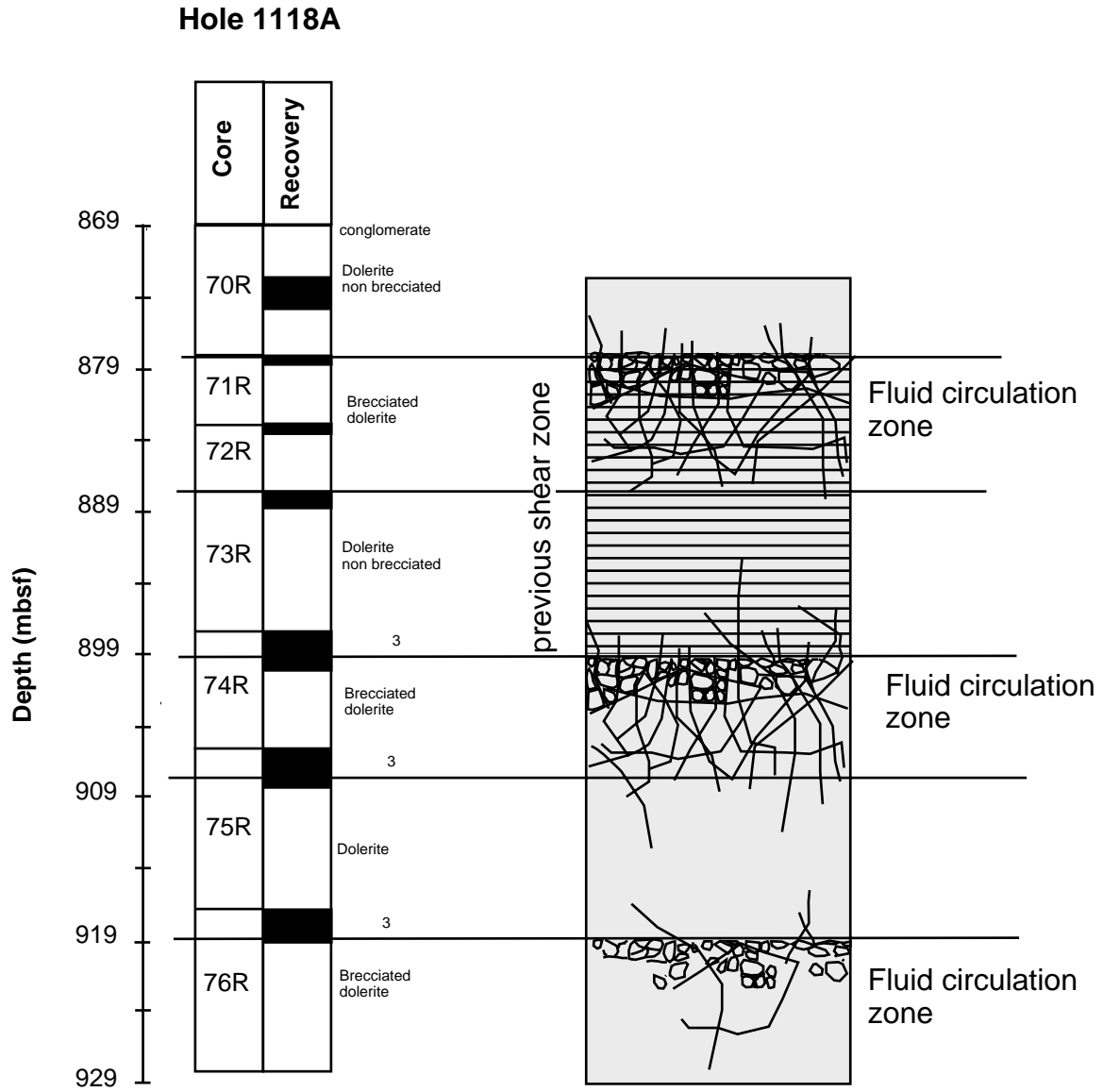
Figure F48. Split core of the dolerite showing a north-south (in core reference frame) calcite-zeolite vein cutting the rock. The upper part of the sample shows an altered zone related to the fluid circulation along the vein (Sample 180-1118A-76R-1, 78–122 cm).
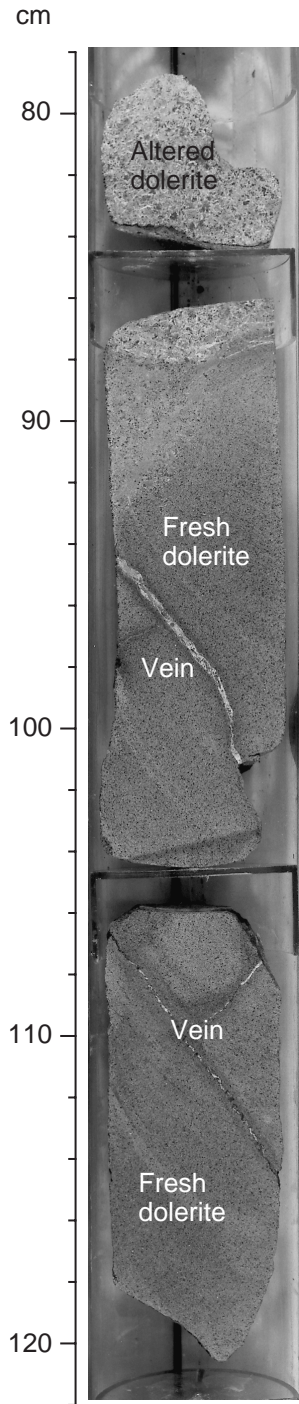
Figure F49. Close up of the fluid infiltration through the dolerite from the open fracture (Sample 180-1118A-75R-2, 43–56 cm).
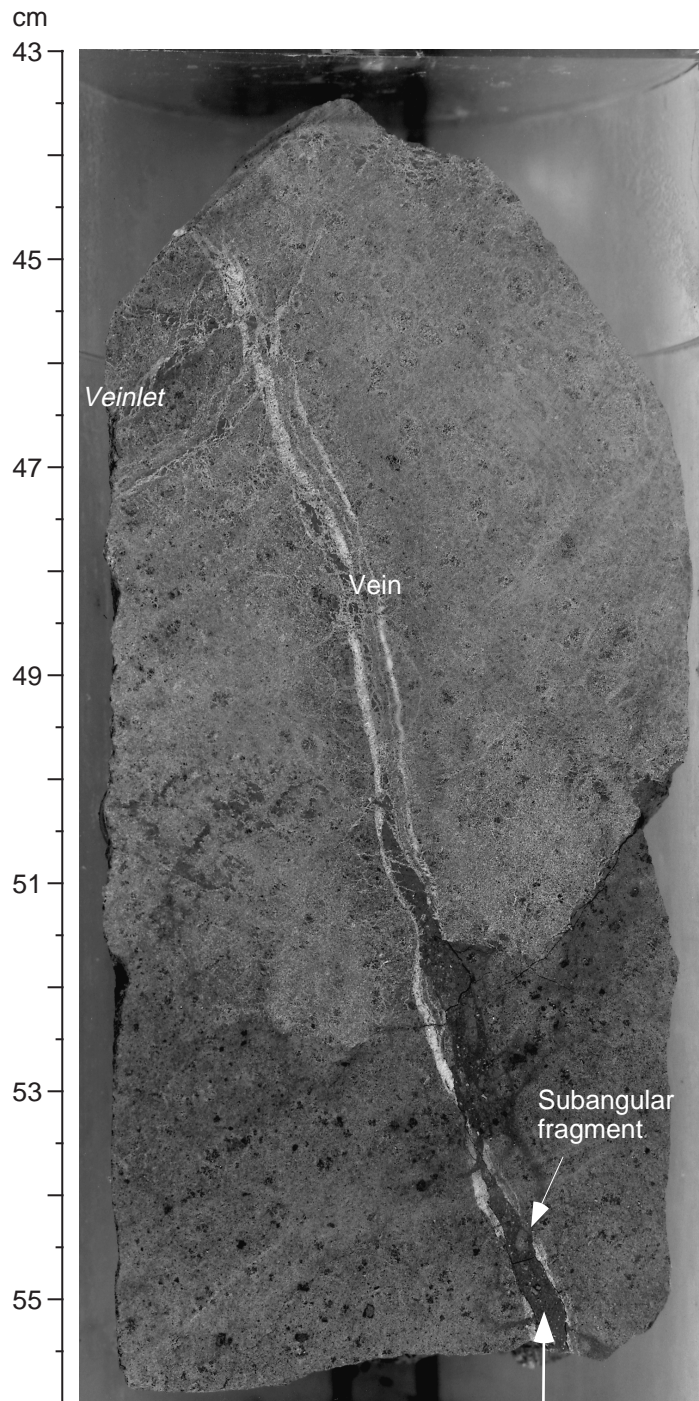
Dark brown matrix

Figure F50. Close up showing the evolution of the brecciation into the dolerite. The network of veins fragmented the rock and induced the weathering of the dolerite into a carbonate-clay-rich matrix in which an angular fragment of dolerite is visible (Sample 180-1118A-75R-2, 28–43 cm).
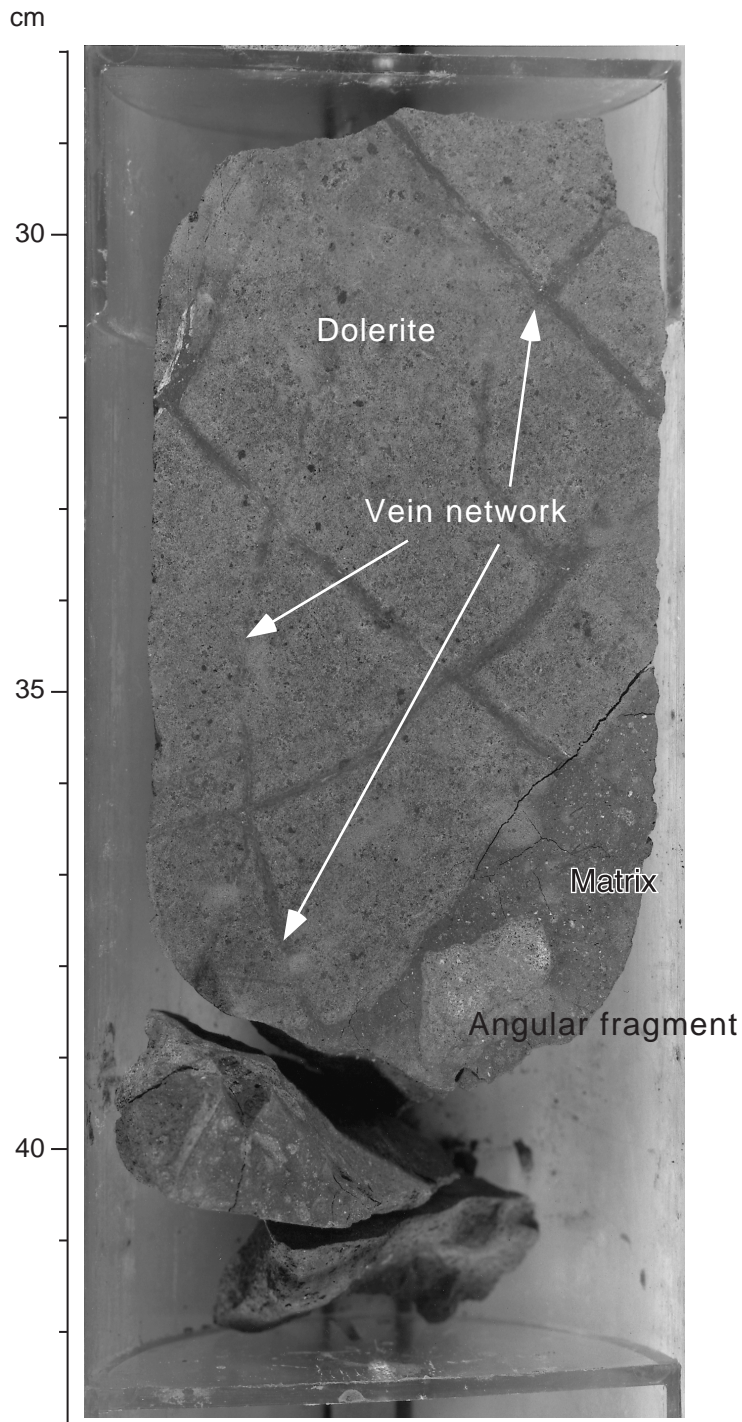
Figure F51. Highly brecciated dolerite consisting of angular clasts of dolerite within a dark brown matrix (Sample 180-1118A-72R-1, 77–84 cm).
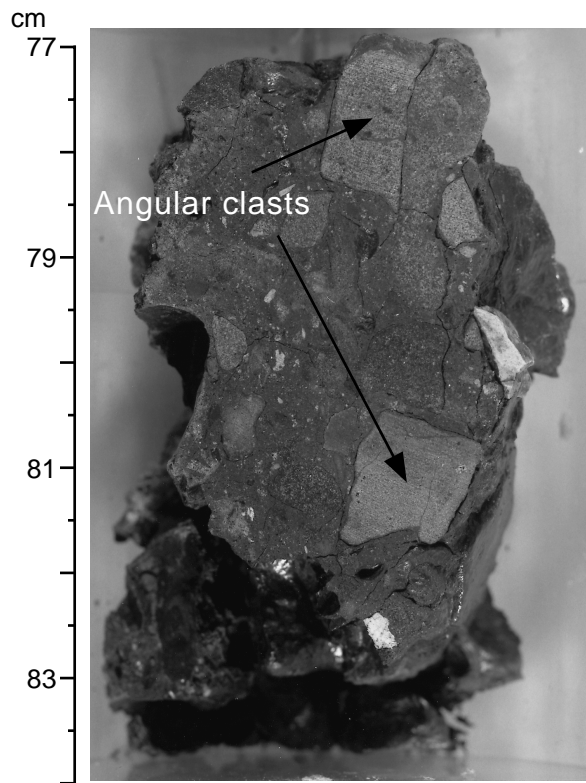
Figure F52. Subrounded to angular fragments of dolerite without matrix associated with relatively fresh dolerite block (Sample 180-1118A-73R-1, 120–150 cm).
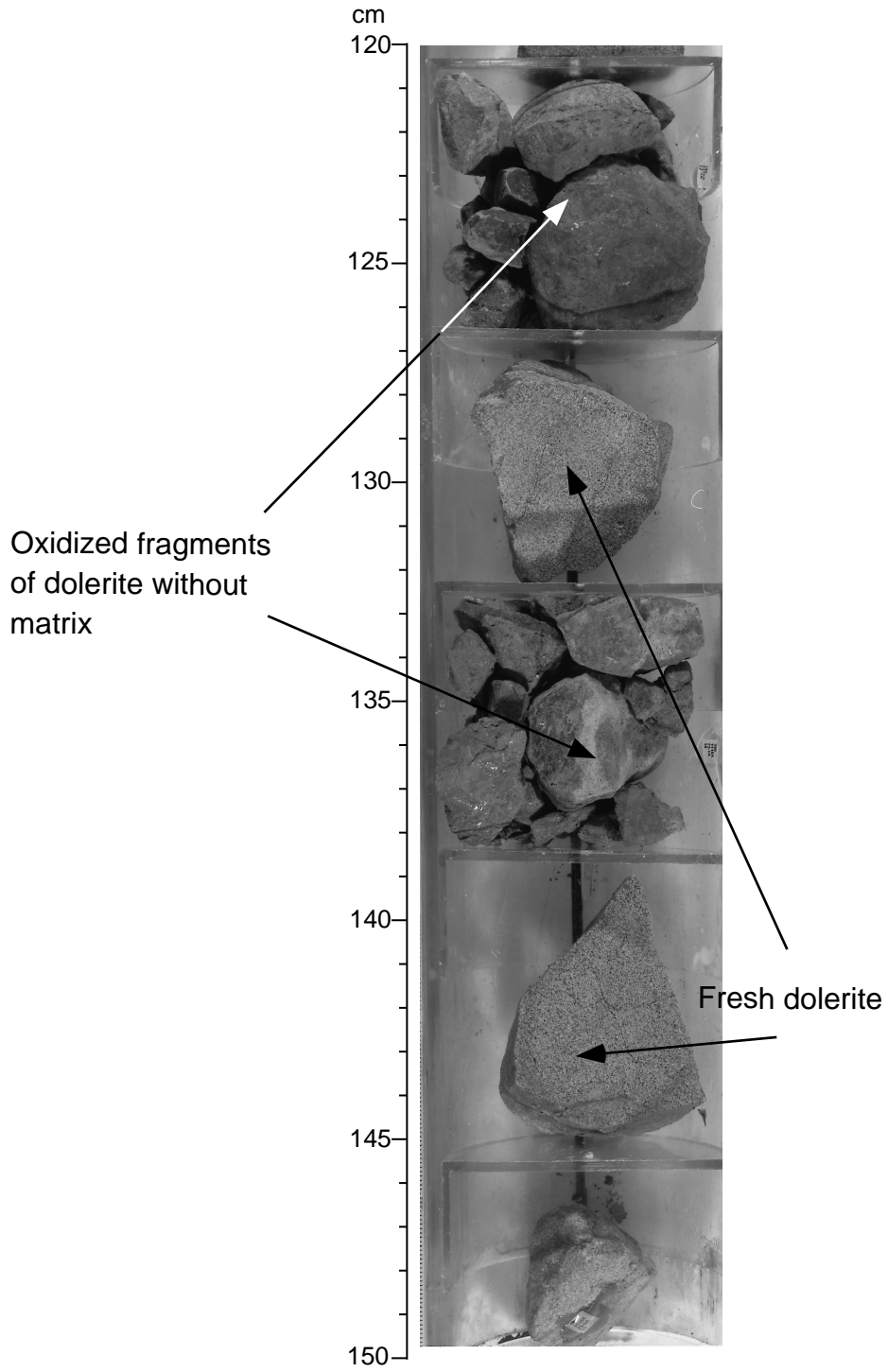
Figure F53. Biostratigraphic units and ages for Hole 1118A. Dashed lines indicate the true zonal boundary may lie above or below the indicated level. (Continued on next page.)
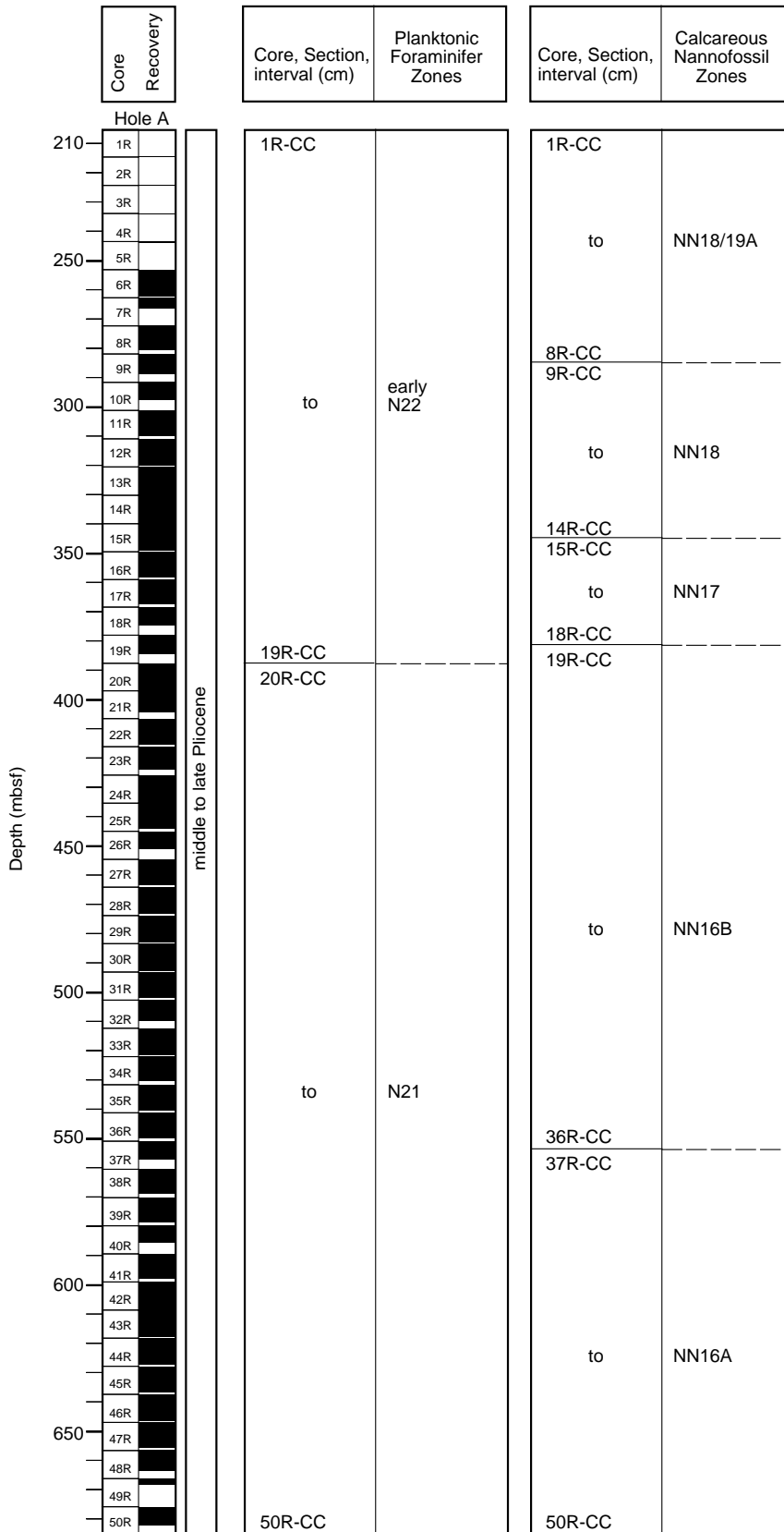
Figure 53 (continued.)
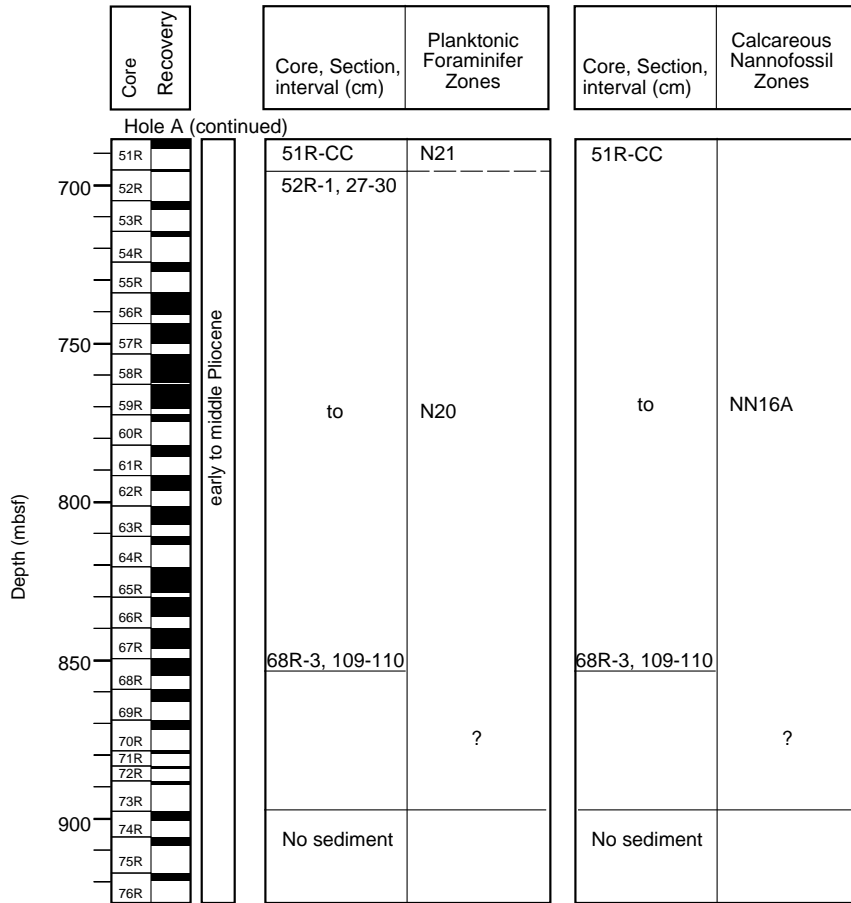
Figure F54. Age-depth relationship at Site 1118 based on nannofossil (square) and planktonic foraminiferal (circle) datum events and magnetic chron and subchron boundaries (triangle), and paleobathymetry (right column) based on benthic foraminifers. Sediment accumulation rates are estimated in m/m.y. The numbers plotted near the symbols correspond to numbers in the left column of the datum table.

	Datum event	Depth (mbsf)	Age (Ma)
1	LAD *G. fistulosus*	<205.00	1.6
*2	Bottom Olduvai	288.0	1.95
3	Top Reunion	332.0	2.14
4	Bottom Reunion	334.5	2.15
5	LAD *D. pentaradiatus*	339.87 - 348.87	2.52
*6	LAD *D. surculus*	374.47 - 384.20	2.55
7	FAD *G. truncatulinoides*	384.20 - 396.75	2.58
*8	Matuyama/Gauss	387.5	2.581
9	LAD *D. tamalis*	549.75 - 556.95	2.83
*10	Top Kaena	599.0	3.04
*11	LAD *D. altispira*	597.56 - 608.20	3.09
12	Bottom Kaena	623.0	3.11
13	Top Mammoth	662.5	3.22
14	FAD *G. tosaensis*	688.26 - 695.27	3.35
15	Bottom Mammoth	744.5	3.33
*16	Gauss/Gilbert	846.0 - 849.5	3.58
17	LCO *R. pseudoumbilicus*	>853.15	3.94
18	FAD *G. crassaformis*	>849.30	4.5

* Datum used in sedimentation rate calculation

Figure F55. Susceptibility data (uncorrected for volume) for Site 1118. **A.** Comparison of susceptibilities from MST and AMST measurements.
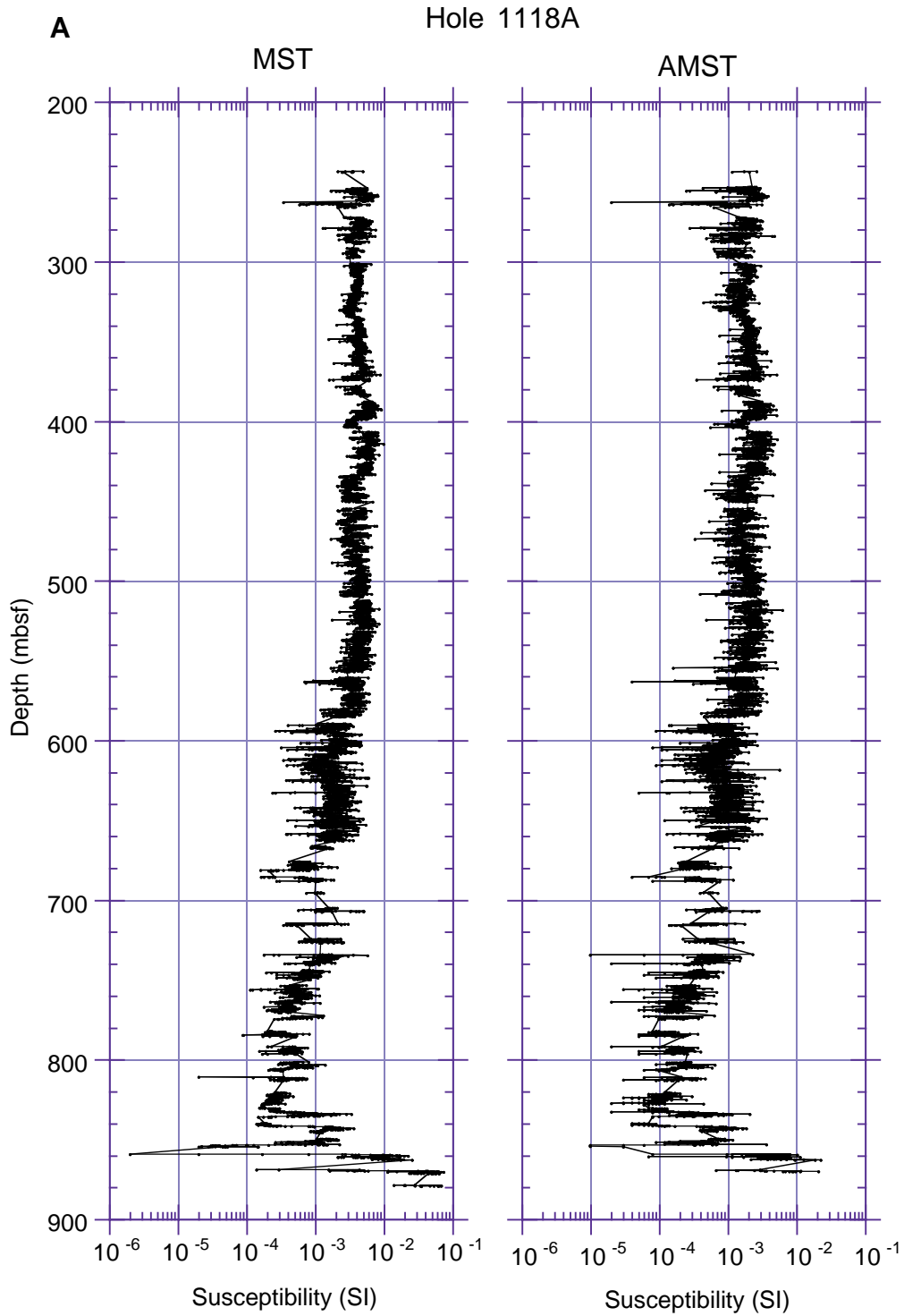
Figure F55 (continued). B. Comparison of MST susceptibilities with remanent intensity after AF demagnetization at 20 mT.

B   Hole 1118A
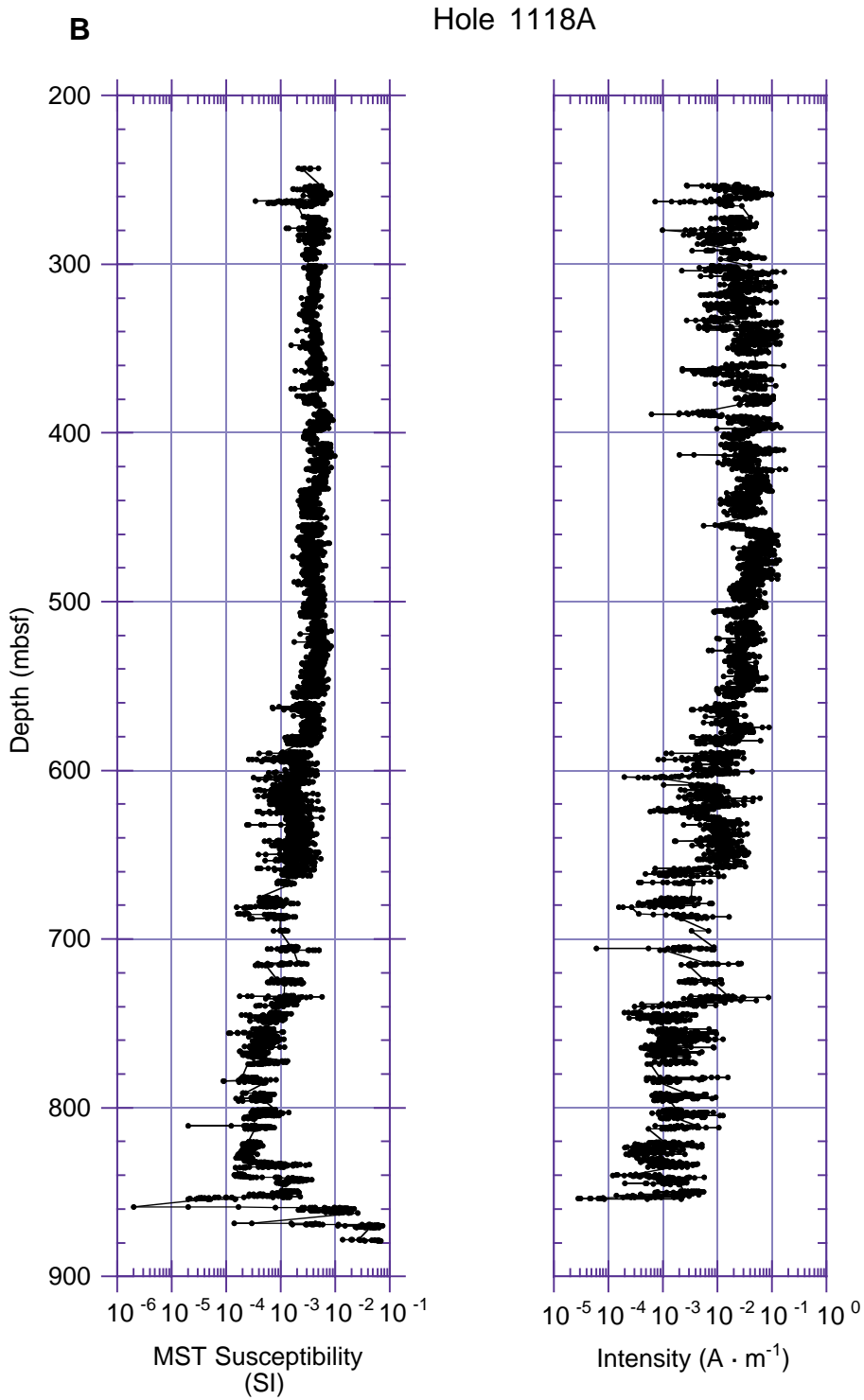
Figure F56. Susceptibility and its anisotropy (AMS) data for discrete samples from Site 1118. **A.** Downhole plots of the variation of AMS parameters. Degree of anisotropy (P_j) and the shape parameter (T) calculated according to Jelinek (1981). Lighter shading: interval in which the scatter in P_j values may be related to lithology (for lithostratigraphic units, see "Lithostratigraphy," p. 4). Darker shading: interval in which the scatter in AMS parameters may be related to structure (for structural domains, see "Structural Geology," p. 28). (Continued on next page.)
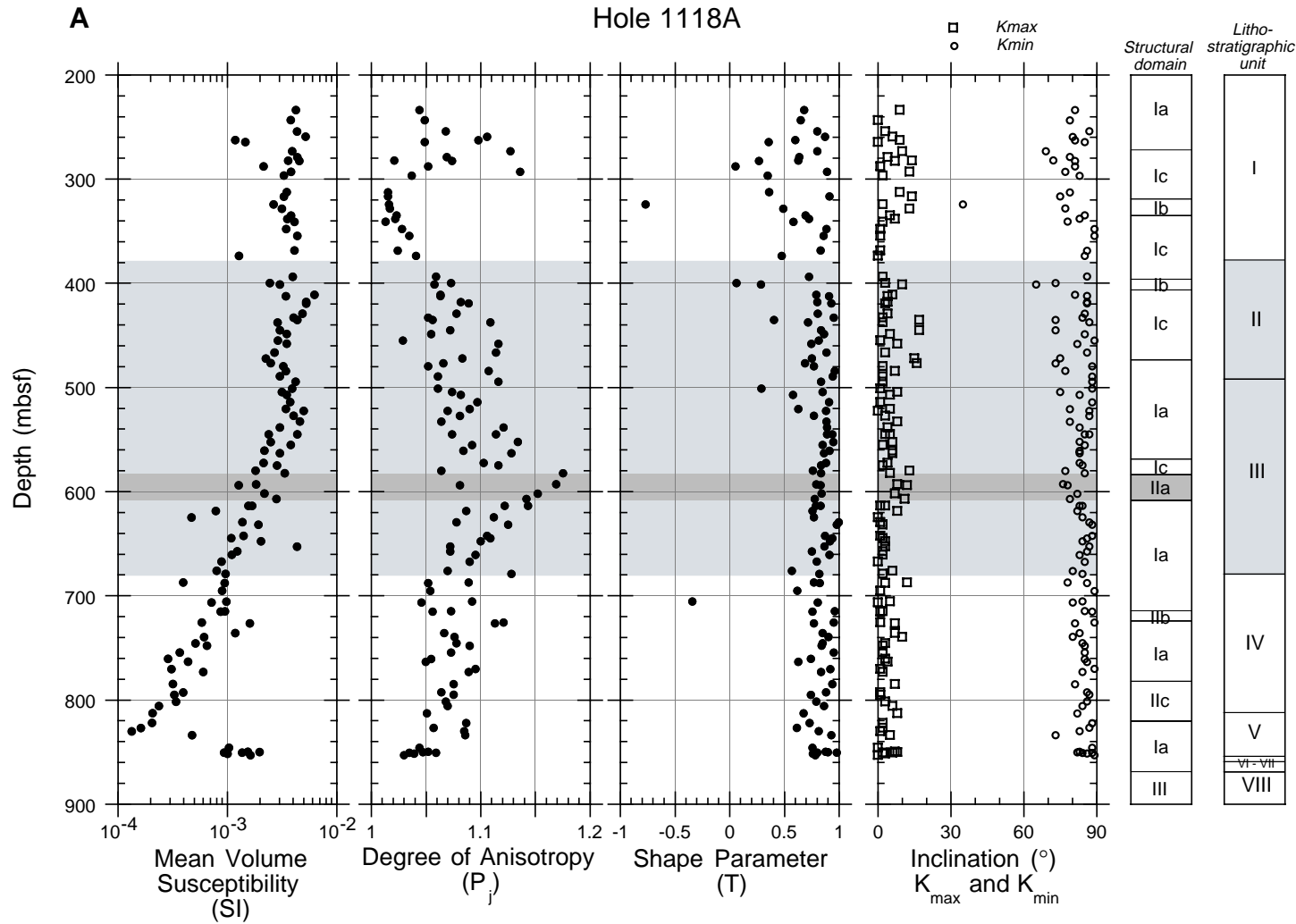
Figure F56 (continued.) B. Stereonet plots of K_{max}, K_{int}, and K_{min} axes for lithostratigraphic Units I through V (for description of lithostratigraphic units, see "Lithostratigraphy," p. 4). K_{max}, K_{int}, and K_{min} are the maximum, intermediate, and minimum axes, respectively, of the susceptibility ellipsoid.

B Hole 1118A

Directions of Magnetic Susceptibility Axes
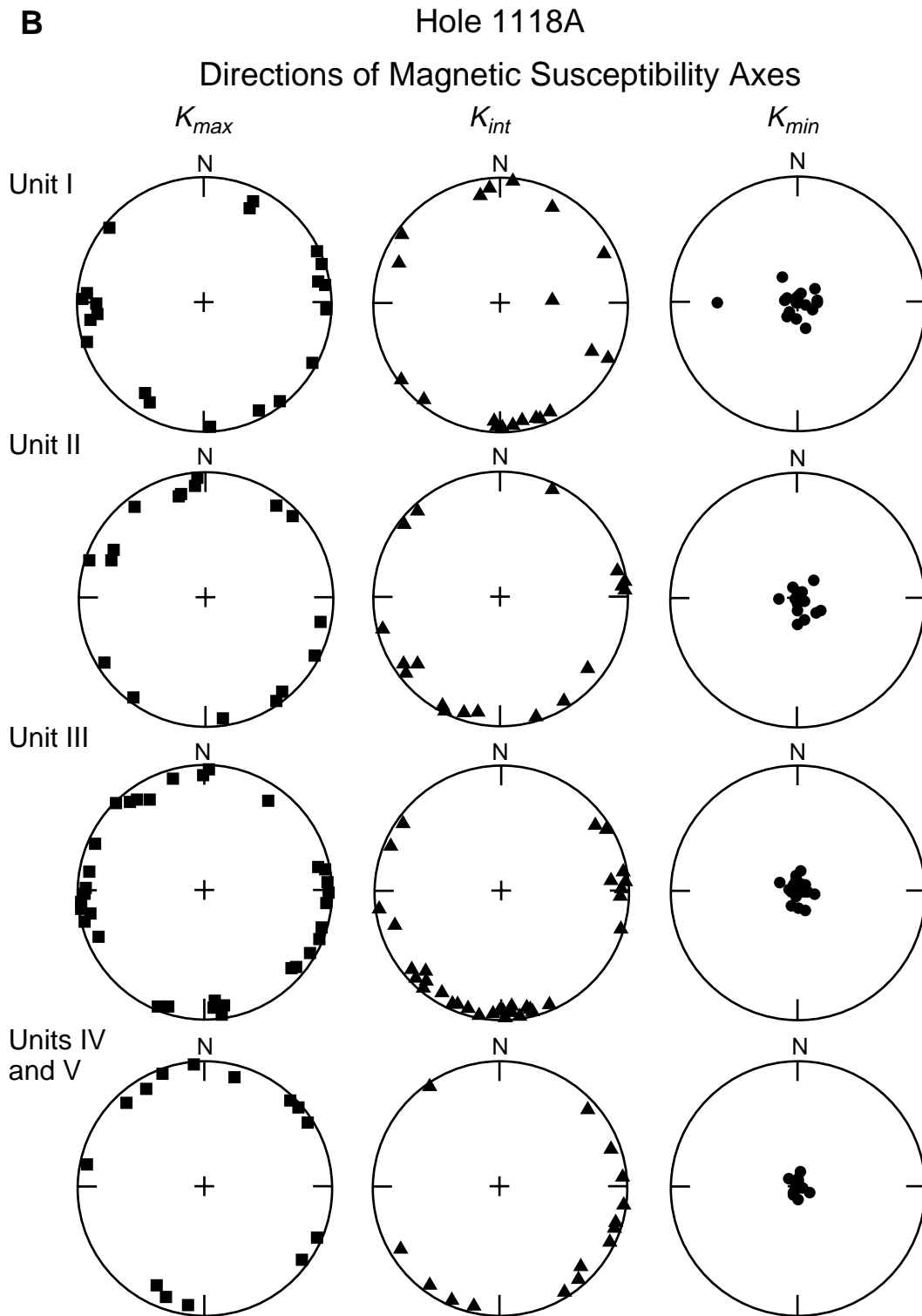
Figure F57. Demagnetization behavior of discrete samples from working halves of core sections. **A.** Sample 180-1118A-28R-7, 11–13 cm (472.21–472.23 mbsf). **B.** Sample 180-1118A-15R-2, 30–32 cm (340.85–340.87 mbsf). **C.** Sample 180-1118A-20R-5, 83–85 cm (393.88–393.90 mbsf). NRM = natural gamma ray; Div. = division; Jo = NRM intensity. (Continued on next page.)

A 180-1118A-28R-7, 11-13 cm
[472.21-472.23 mbsf]

$Jo = 1.64 \times 10^{-1} A \cdot m^{-1}$

B 180-1118A-15R-2, 30-32 cm
[340.85 - 380.87 mbsf]

$Jo = 2.14 \times 10^{-1} A \cdot m^{-1}$

C 180-1118A-20R-5, 83-85 cm
[393.88-393.90 mbsf]

$Jo = 7.34 \times 10^{-2} A \cdot m^{-1}$
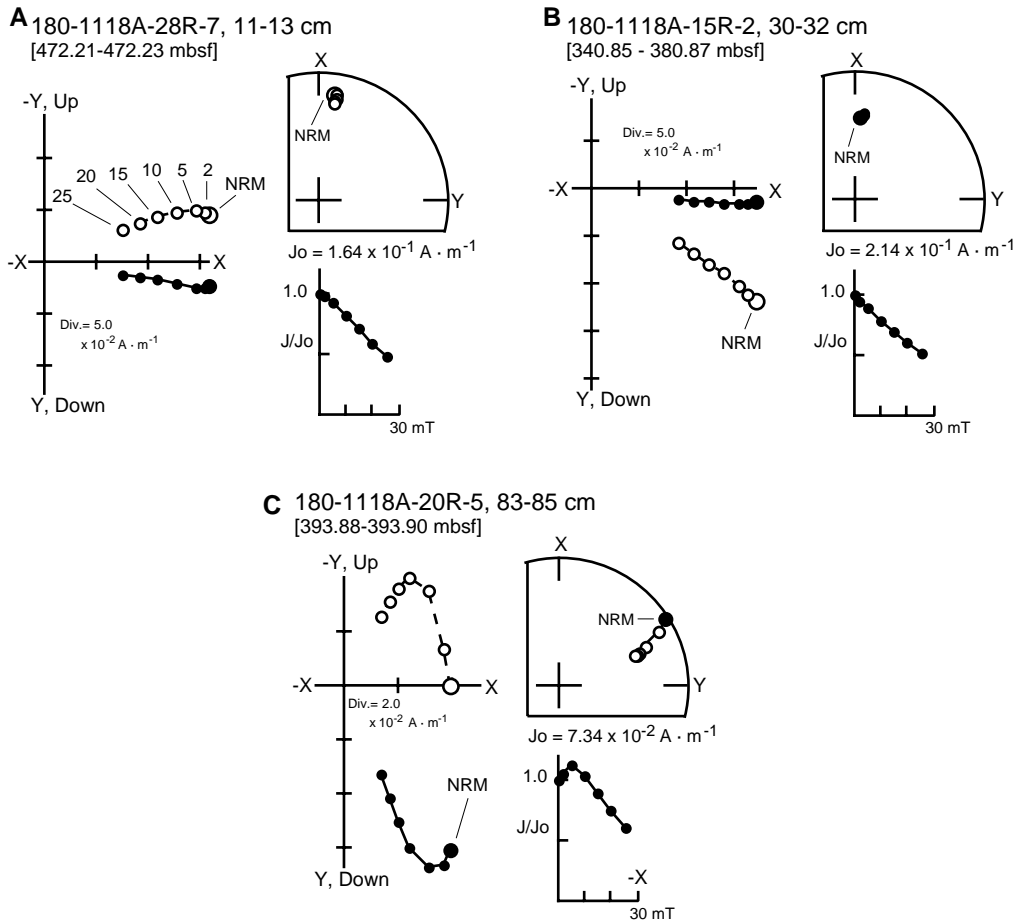
Figure F57 (continued.) D. Sample 180-1118A-42R-7, 64–66 cm (606.82–606.84 mbsf). **E.** Sample 180-1118A-62R-1, 116–118 cm (792.66–792.68 mbsf). **F.** Sample 180-1118A-48R-4, 29–31 cm (660.80–660.82 mbsf). Vector plots: horizontal component = solid circles; vertical component = open circles. Stereonet plots: lower hemisphere = solid circles; upper hemisphere = open circles.

D 180-1118A-42R-7, 64-66 cm
[606.82-606.84 mbsf]

$J_o = 5.46 \times 10^{-2}\,\mathrm{A \cdot m^{-1}}$

E 180-1118A-62R-1, 116-118 cm
[792.66-792.68 mbsf]

$J_o = 2.95 \times 10^{-3}\,\mathrm{A \cdot m^{-1}}$
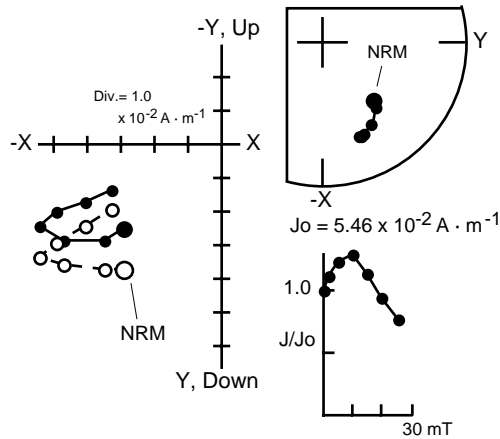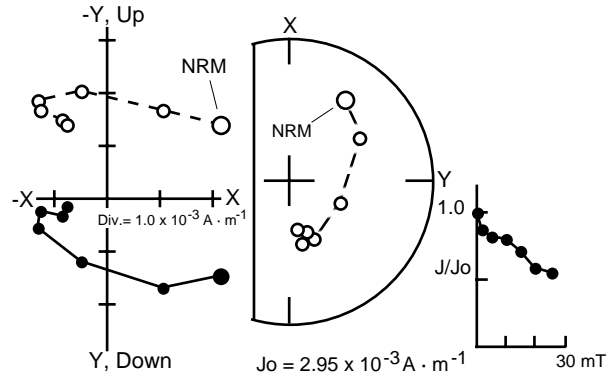
F 180-1118A-48R-4, 29-31 cm
[660.80-660.82 mbsf]

$J_o = 1.18 \times 10^{-2}\,\mathrm{A \cdot m^{-1}}$
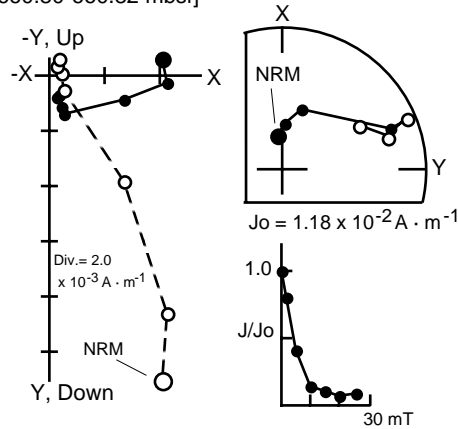
Figure F58. A. Downhole plots of intensity, inclination, and declination. Data from long cores after AF demagnetization at 20 mT shown as black dots; data from discrete samples after AF demagnetization at 25 mT shown as open squares. (Continued on next page.)

A

Hole 1118A
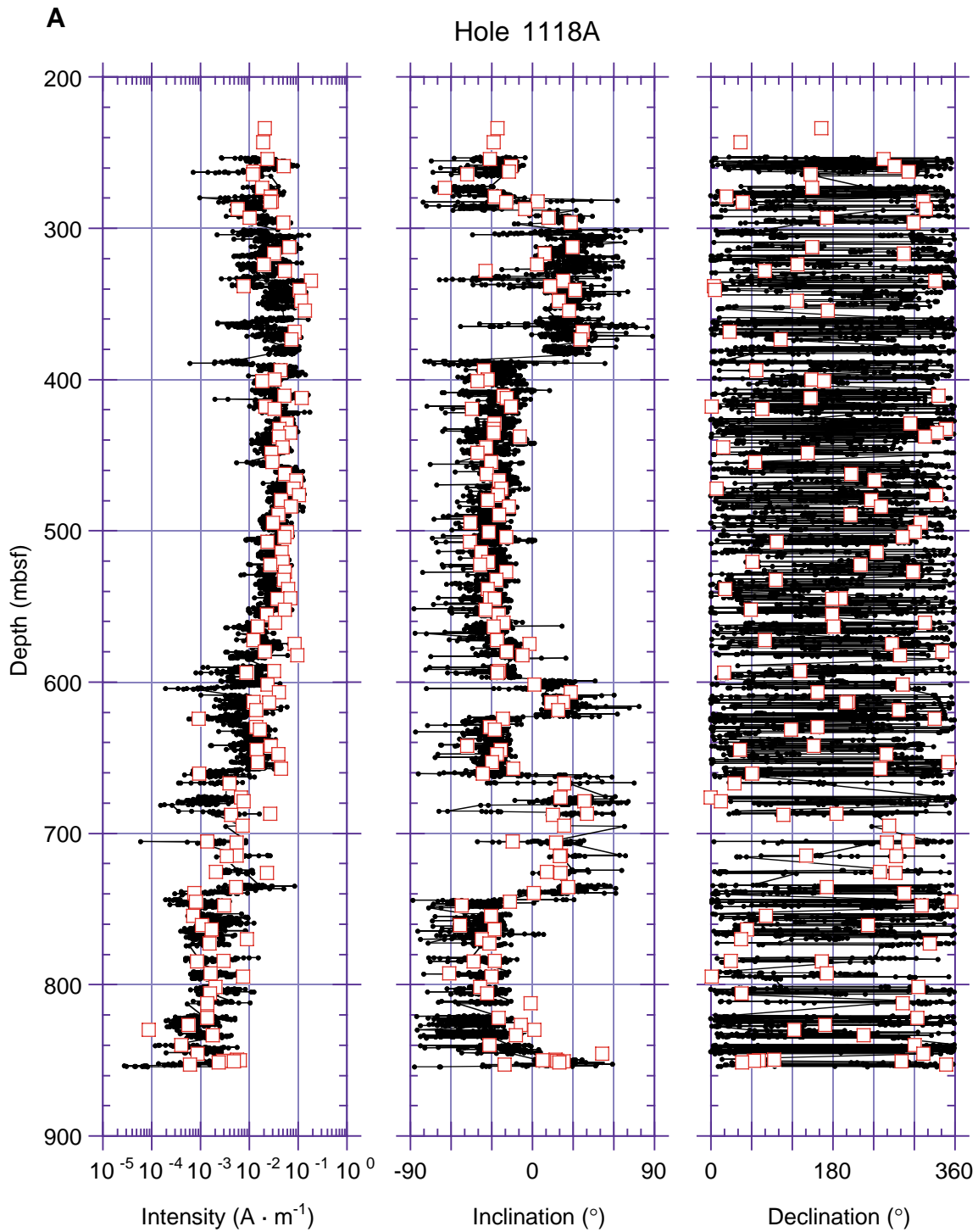
Figure 58 (continued.) B. Downhole plot of inclinations with magnetostratigraphic interpretation. Polarity: normal = black; reversed = white; undetermined = diagonal lines. Chrons: C2n = Olduvai (1.77–1.95 Ma); C2r.1n = Reunion (2.14–2.15 Ma); C2r.1r and C2r.2r = lower parts of the Matuyama (1.95–2.14 Ma and 2.15–2.58 Ma, respectively); C2An.1n = upper part of the Gauss (2.58–3.04 Ma); C2An.1r = Kaena (3.04–3.11 Ma); C2An.2n = middle part of the Gauss (3.11–3.22 Ma); C2An.2r = Mammoth (3.22–3.33 Ma); C2An.3n = lower part of the Gauss (3.33–3.58 Ma); C2Ar = upper part of the Gilbert (3.58–4.18 Ma).
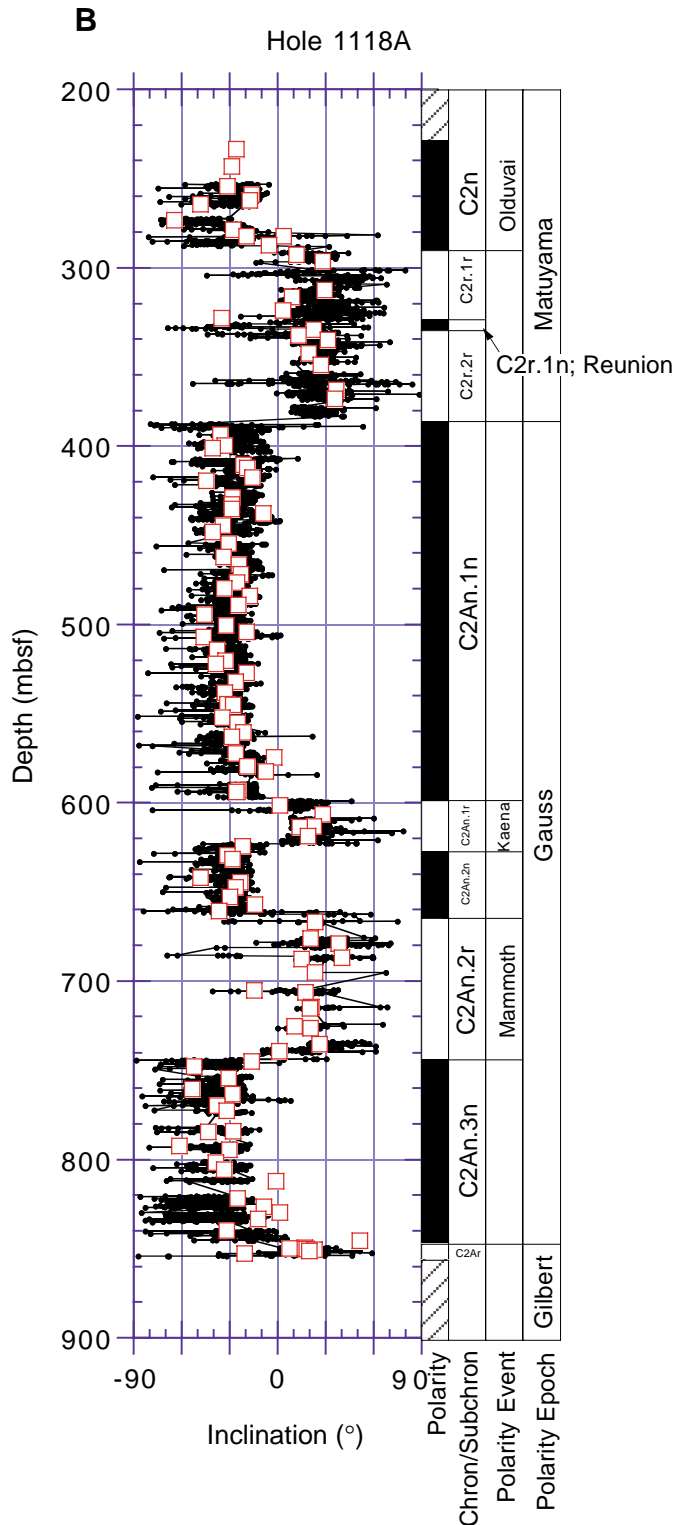
Figure F59. Depth profiles of interstitial water constituents, Site 1118. **A.** pH, alkalinity, SO_4^{2-}, and NH_4^+. (Continued on next two pages.)
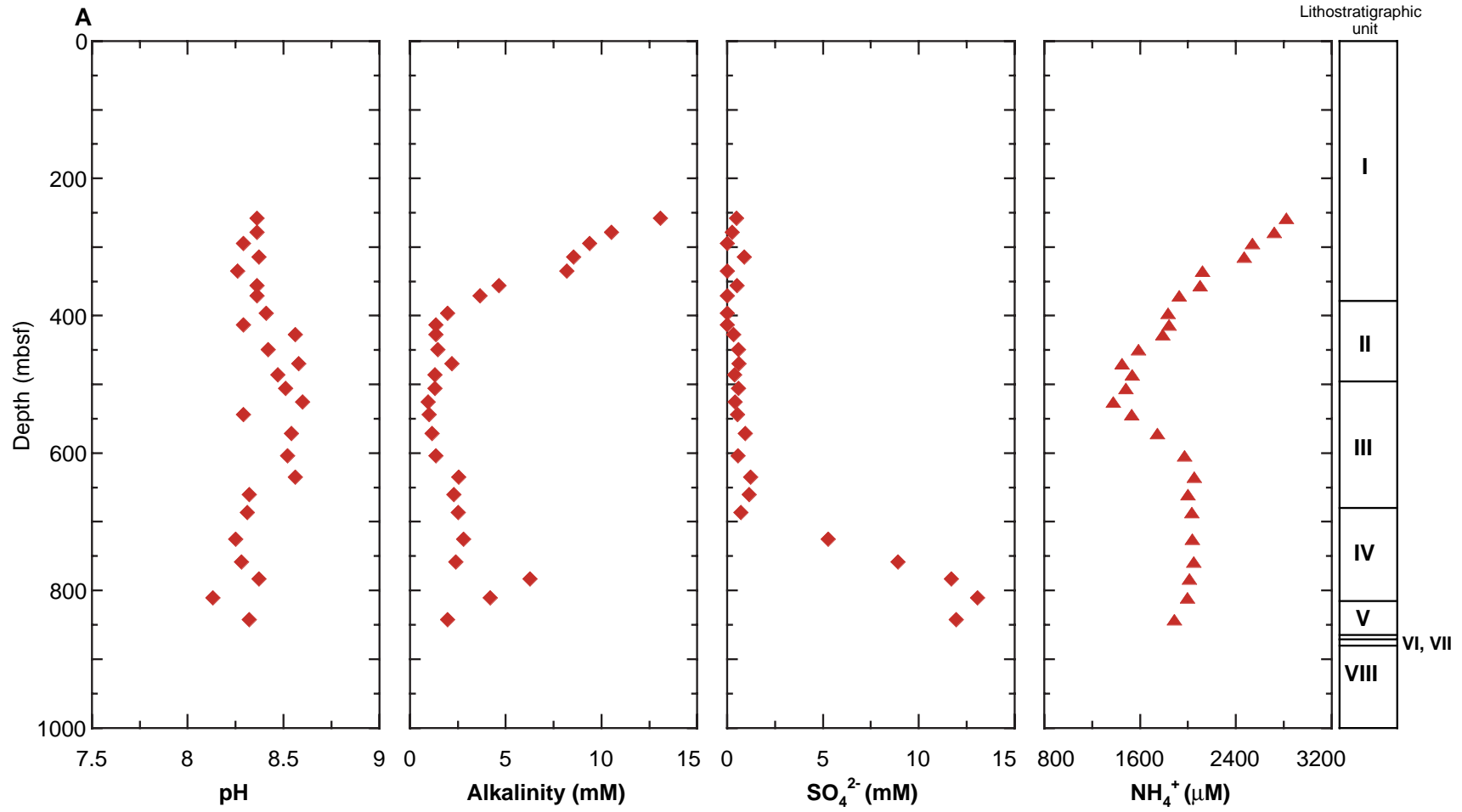
Figure F59 (continued.) B. Na+, Cl−, K+, and Li+.
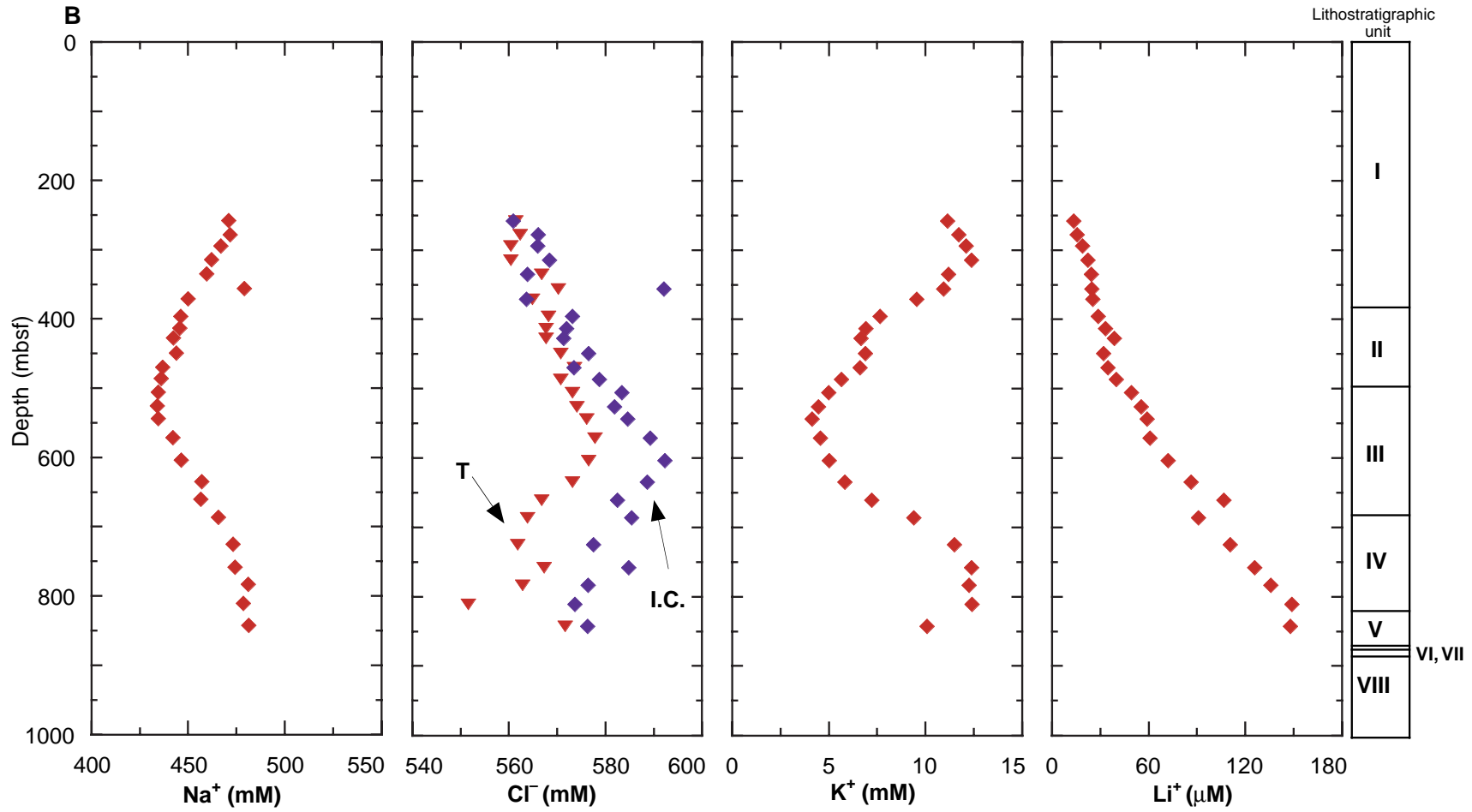
Figure F59 (continued.) C. Ca²⁺, Mg²⁺, Sr²⁺, and Ca/Mg.
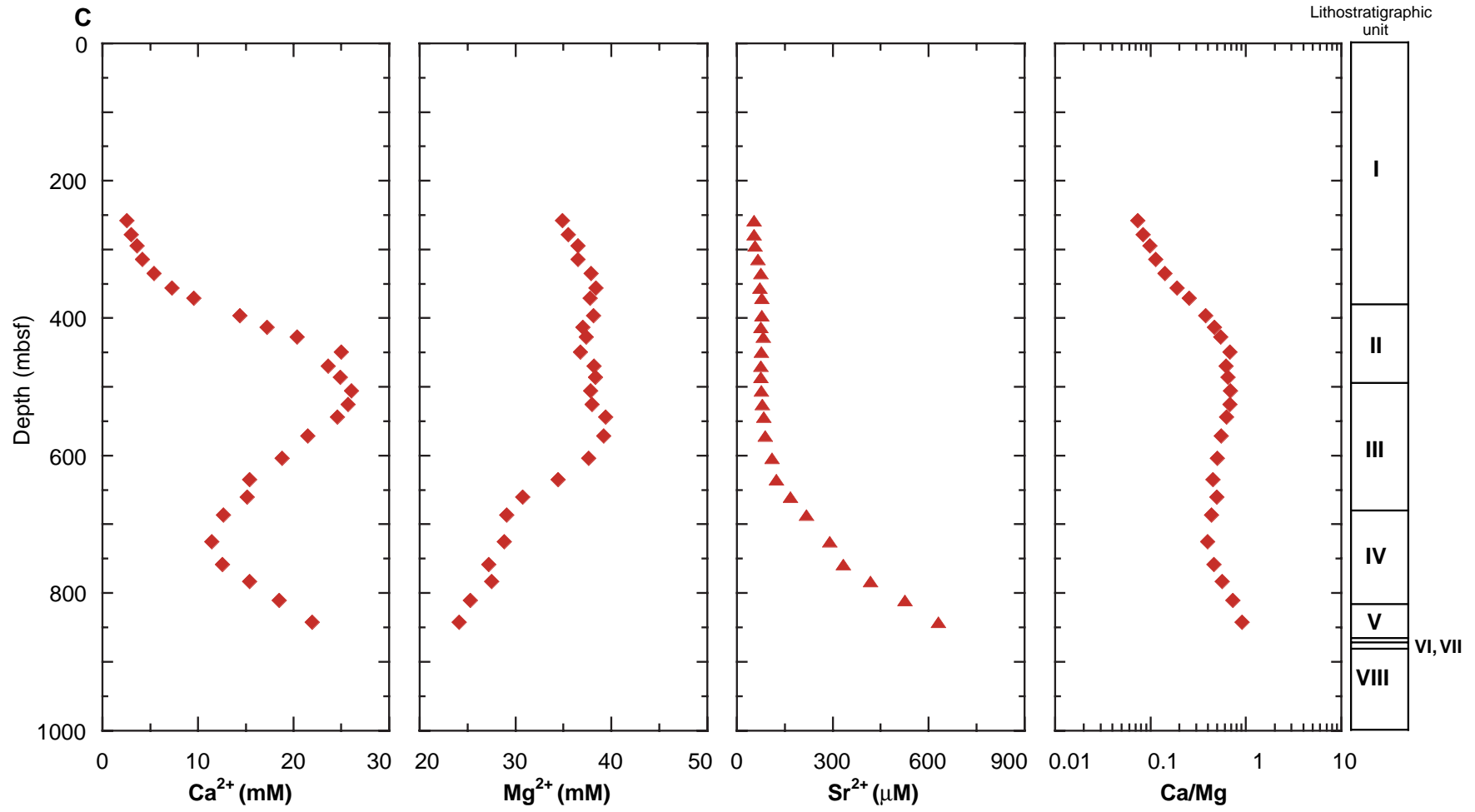
Figure F60. Dissolved SiO$_2$ in sediments, Site 1118.
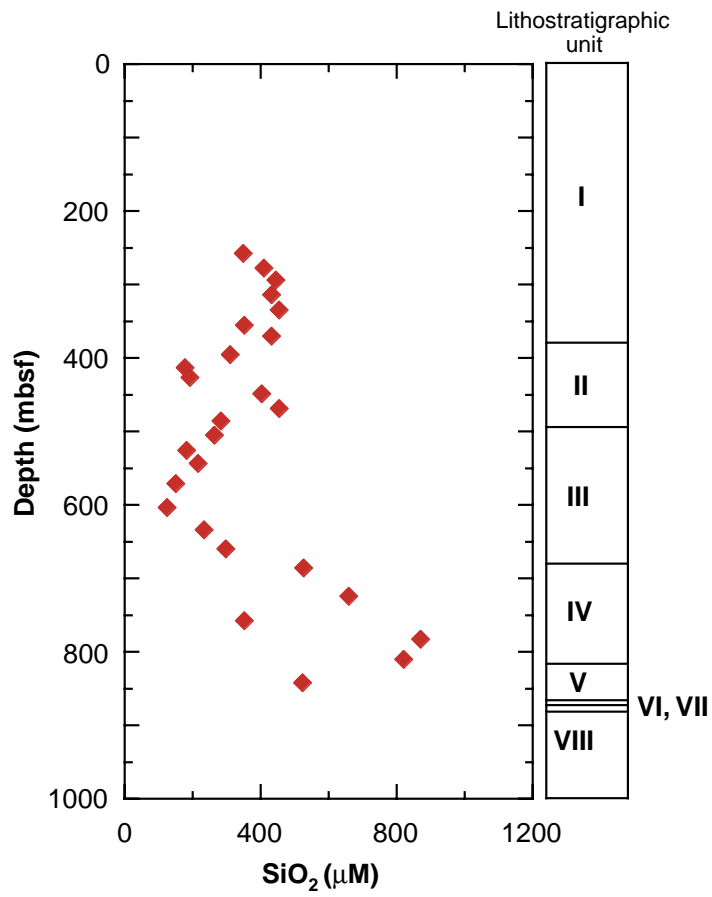
Figure F61. C_1, C_2, and C_1/C_2 hydrocarbon contents, Site 1118.
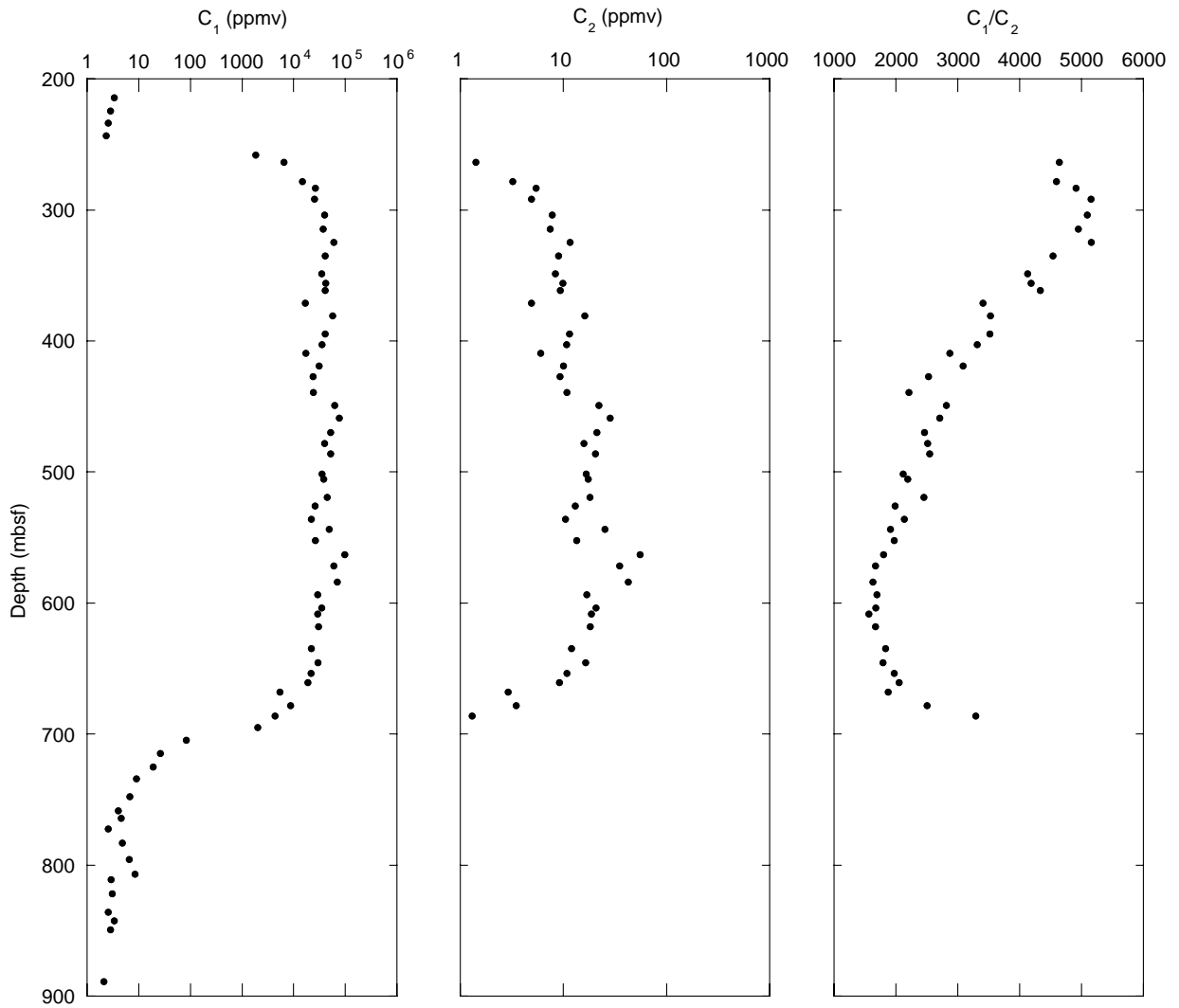
Figure F62. CaCO₃, organic carbon, and sulfur contents, Site 1118.
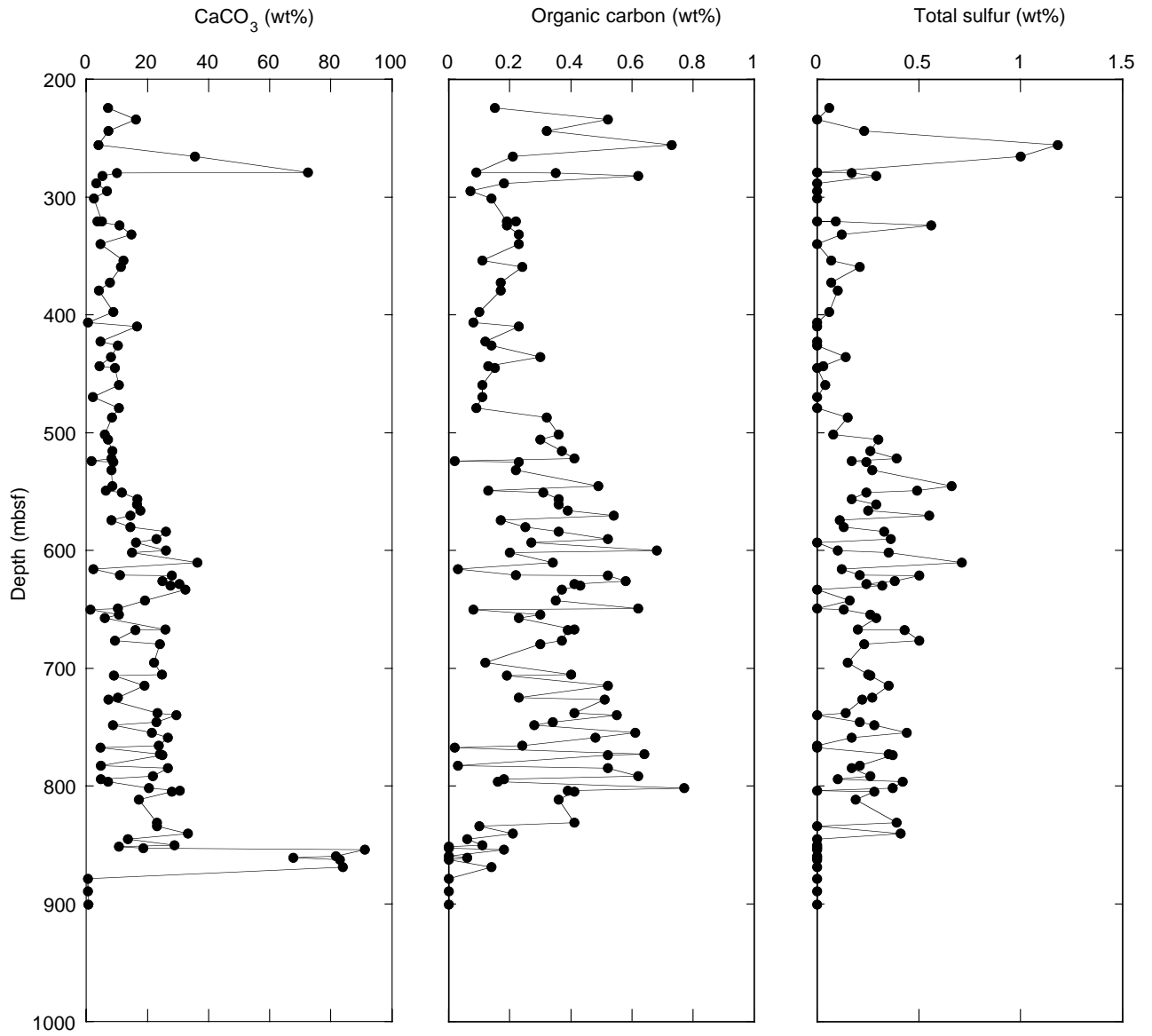
Figure F63. Depth distributions of total bacterial populations (solid circles) and dividing and divided cells (open circles) in sediment samples from Site 1118. The solid curve represents a general regression line of bacterial numbers vs. depth in deep-sea sediments (Parkes et al., 1994) with 95% upper and lower prediction limits shown by dashed curves.
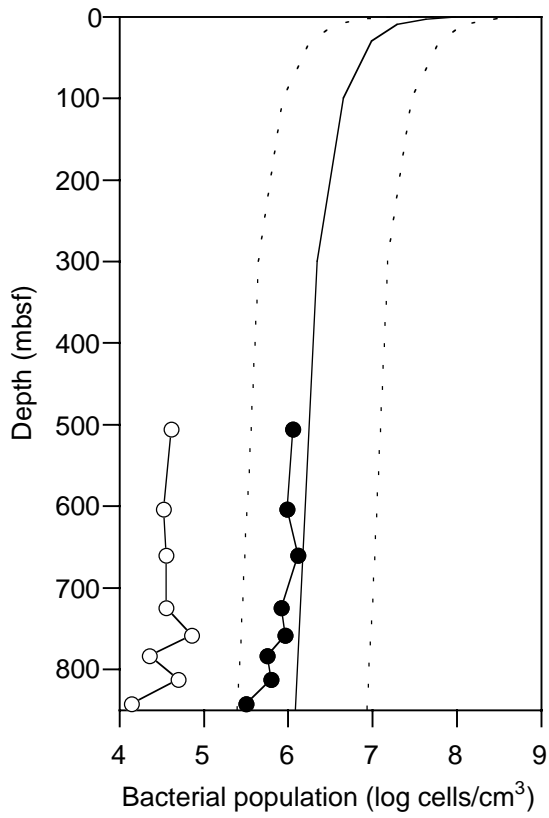
Figure F64. Bulk density derived from GRAPE and index properties measurements.
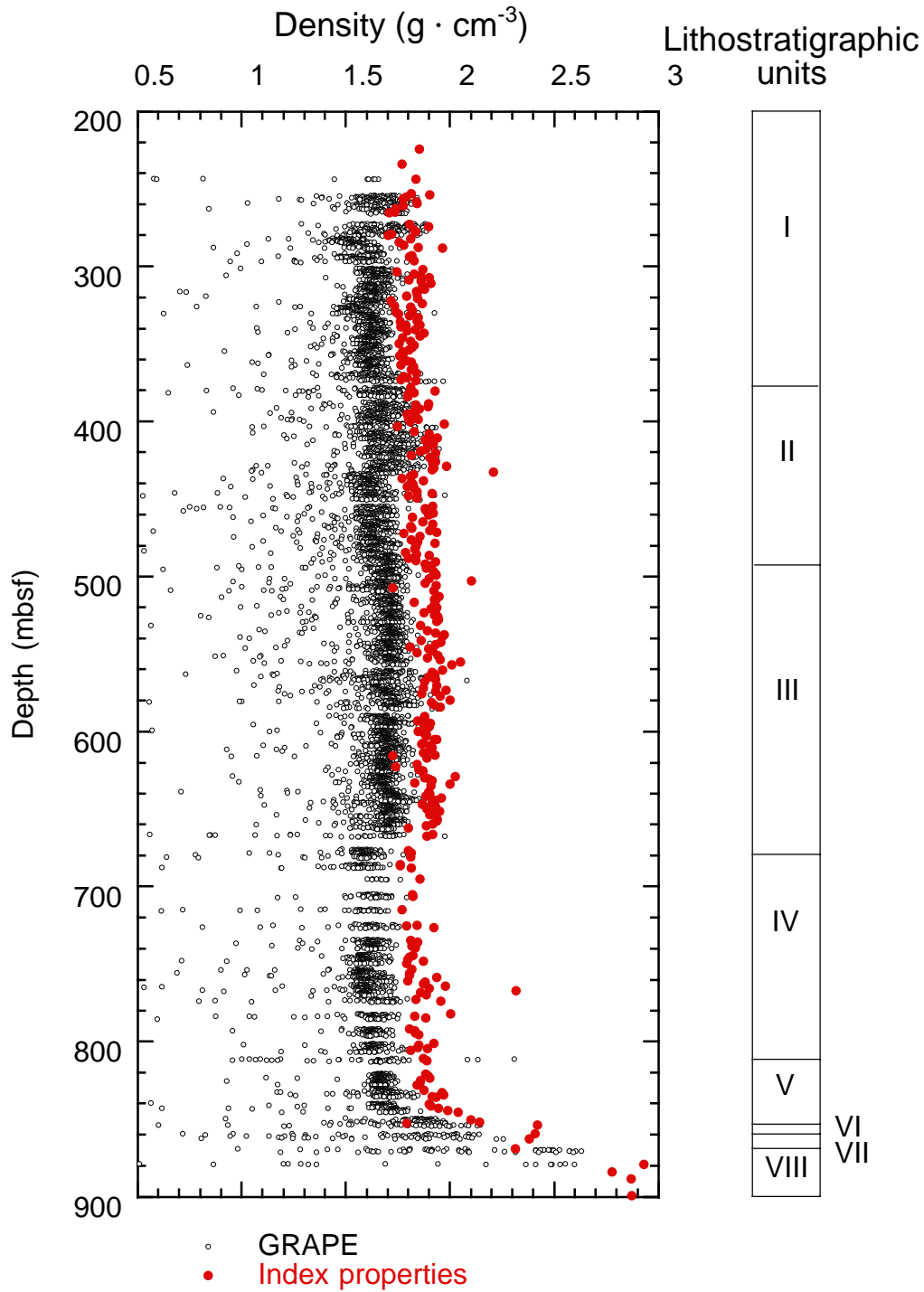
Figure F65. Site 1118 **(A)** grain density derived from MAD index properties measurements and **(B)** porosity. Highlighted intervals represent zones of high sedimentation rates.
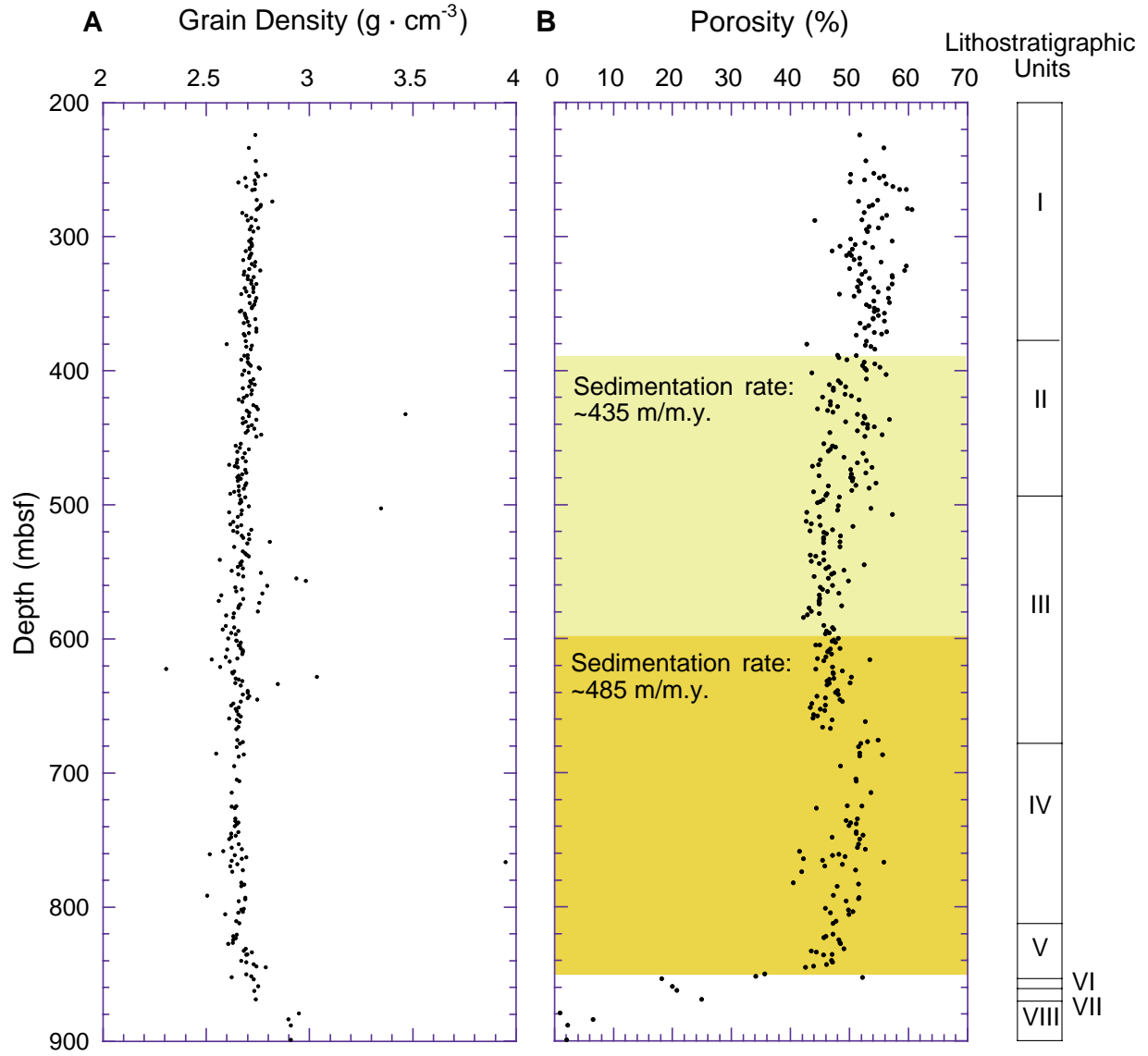
Figure F66. Site 1118 *P*-wave velocities (x, y, and z).
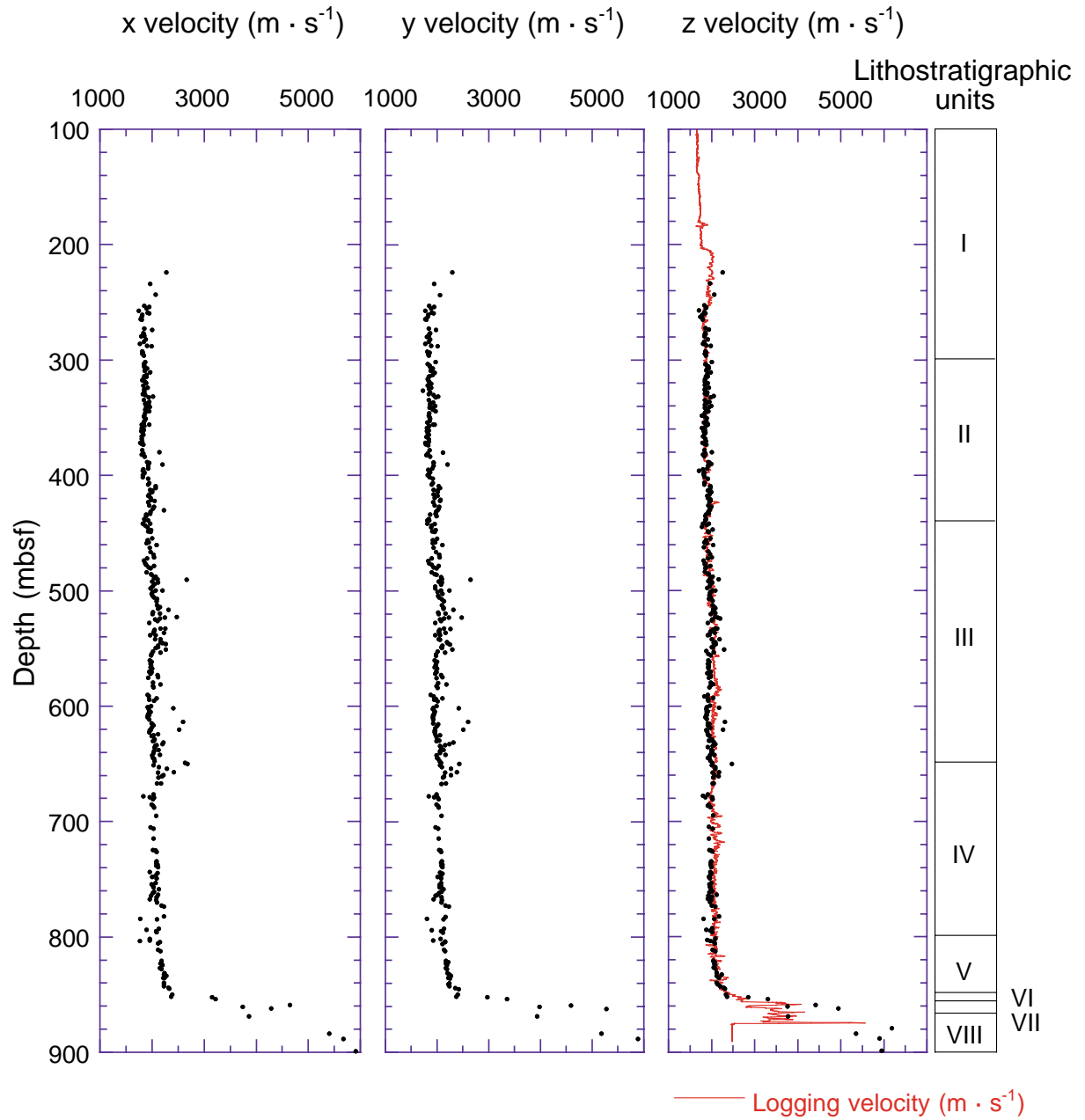
Figure F67. A. Longitudinal velocity vs. the average transverse velocity, and **B.** *P*-wave anisotropy (for method used, see "Compressional Wave (P-wave) Velocity," p. 30, in the "Explanatory Notes" chapter). A positive anisotropy indicates that the transverse velocity is greater than the longitudinal velocity.
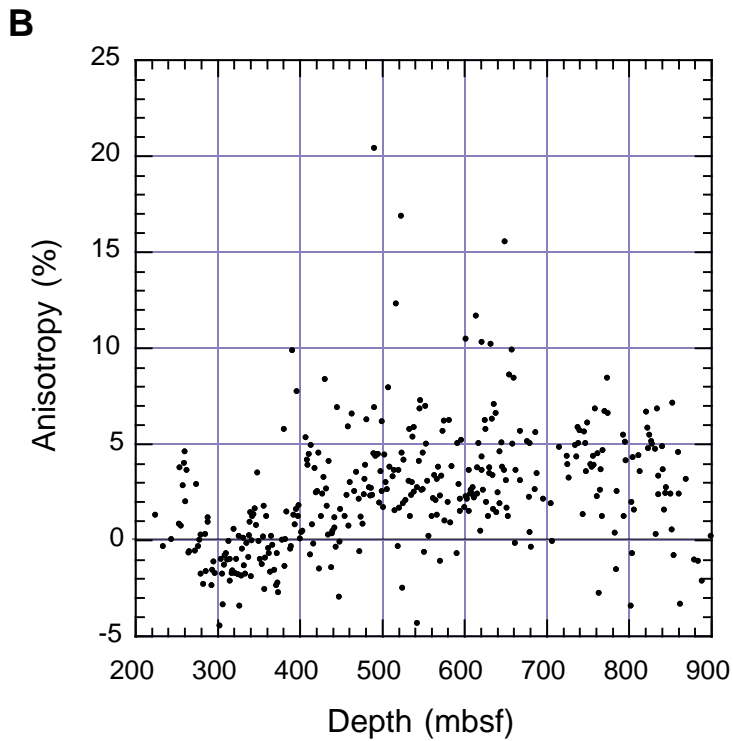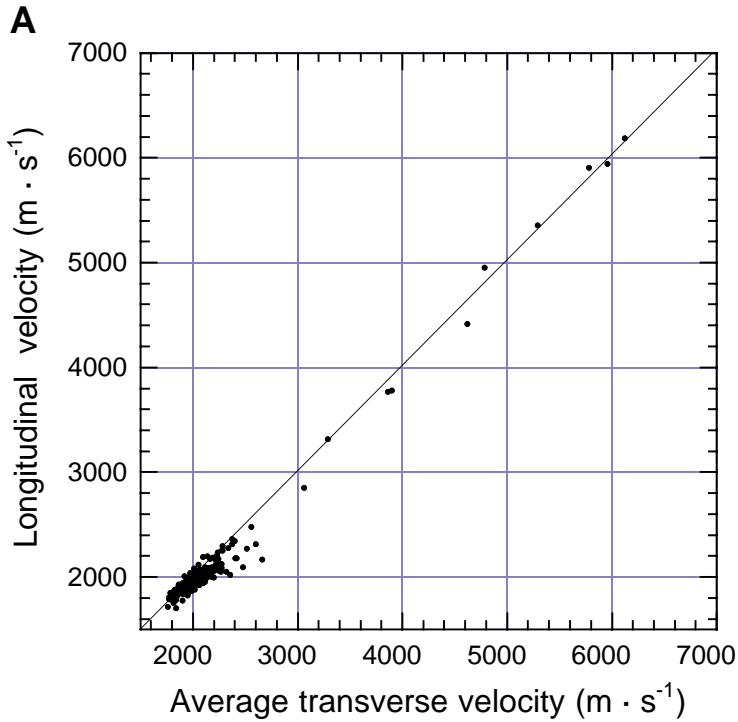
Figure F68. Site 1118 thermal conductivity. Note that only the mean averages of all repeat measurements from each interval are presented here.
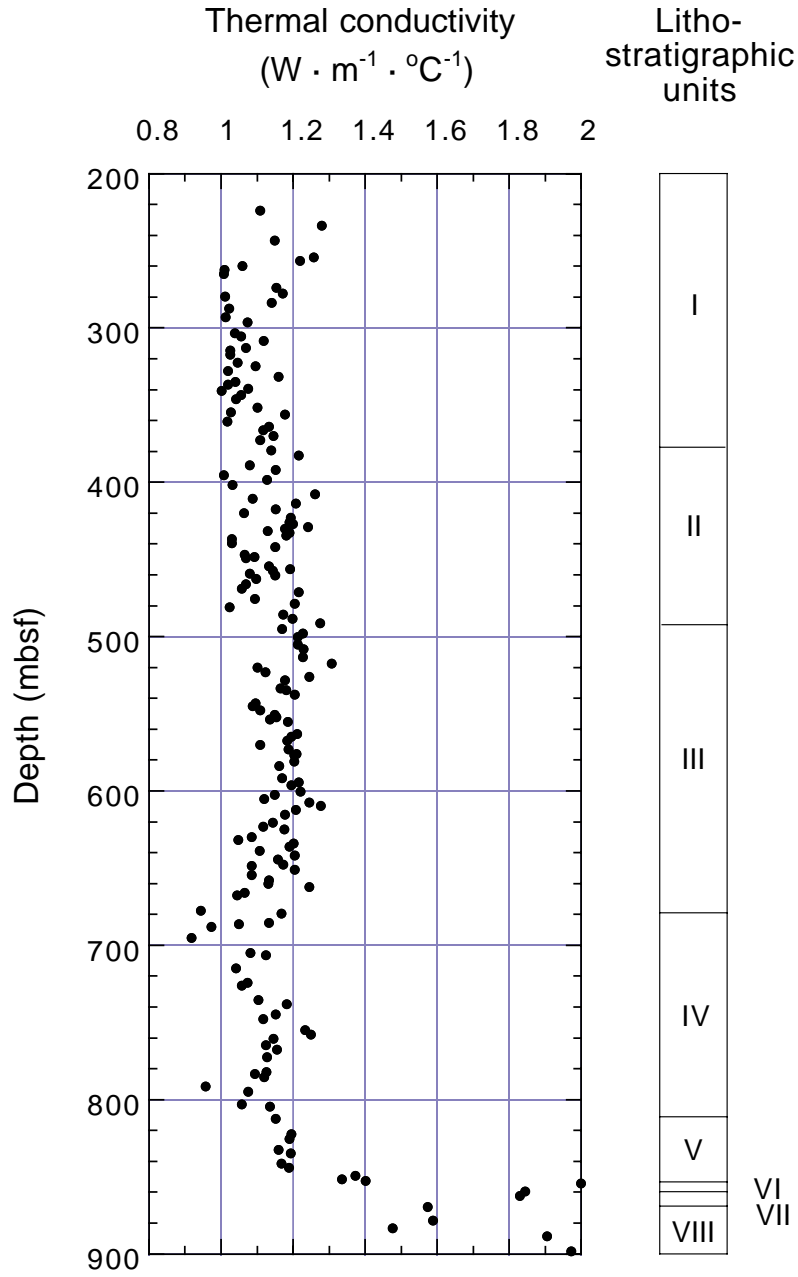
Figure F69. Site 1118 (**A**) magnetic susceptibility and (**B**) remanent magnetic intensity data.
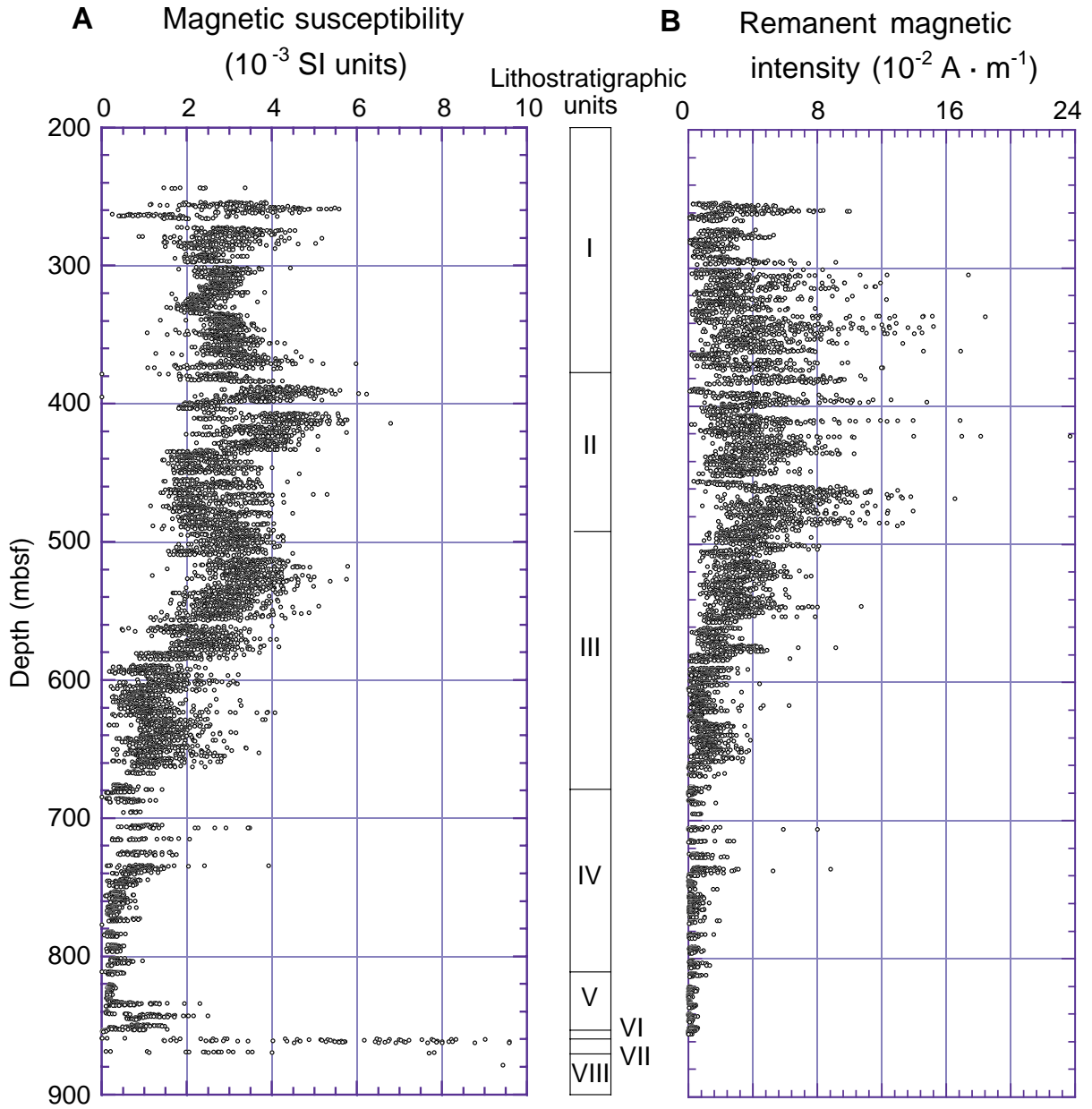
Figure F70. Site 1118 (**A**) magnetic susceptibility and (**B**) NGR results.
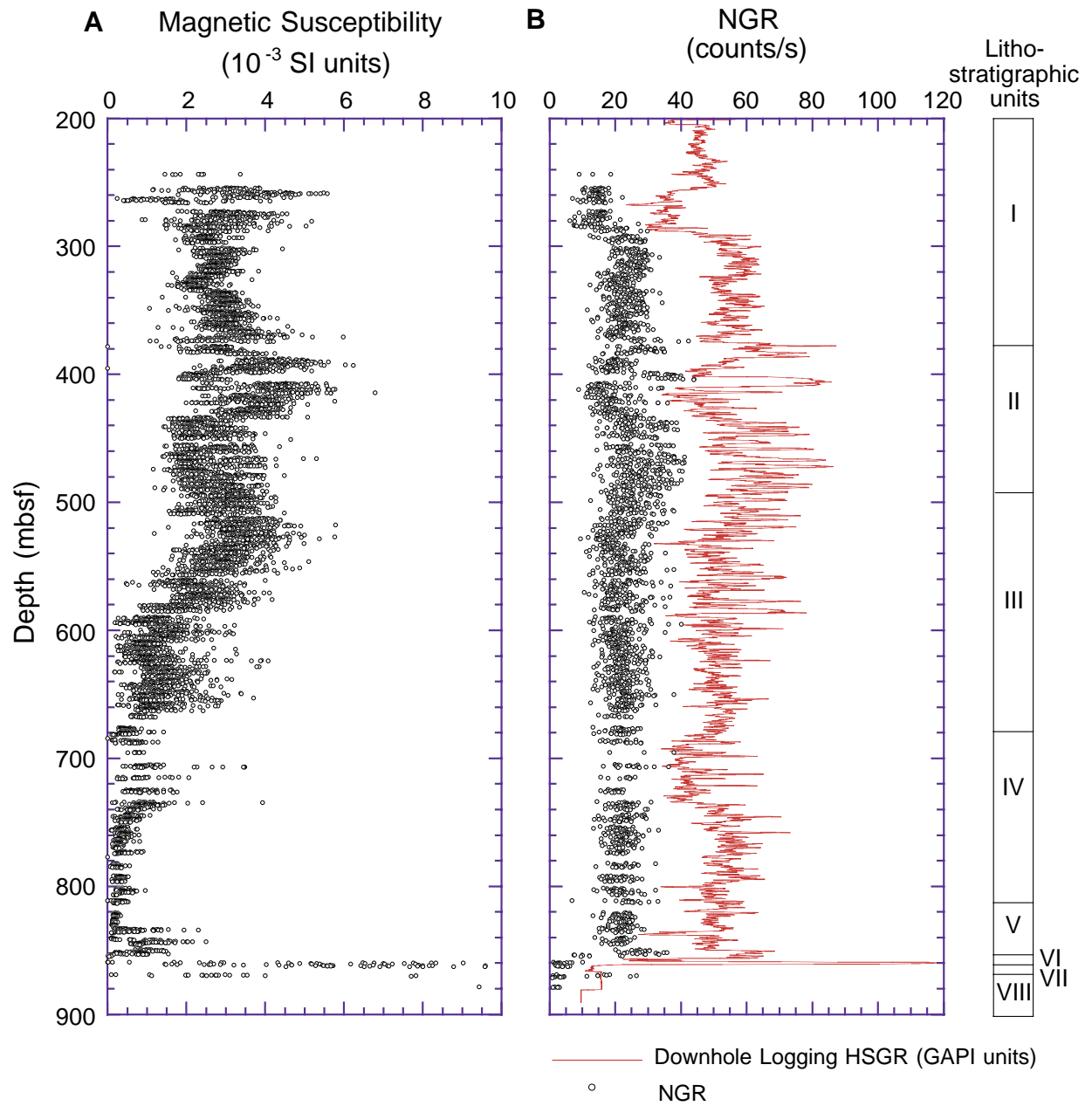
Figure F71. Hole 1118A composite log from 0 to 926 mbsf. **A.** Left to right: (1) core number and recovery intervals; (2) caliper measurements from the triple combo run (LCAL); (3) total natural gamma ray (HSGR) and total natural gamma ray minus uranium contribution (HCGR); (4) thorium and uranium content; (5) potassium content; (6) resistivity from the DIT tool, consisting of deep induction (IDPH), medium induction (IMPH), and shallow spherically focused current (SFLU); and (7) log units. Composite log from 0 to 200 mbsf. To compare other logs at equivalent depth, see Figure (Continued on next nine pages.)
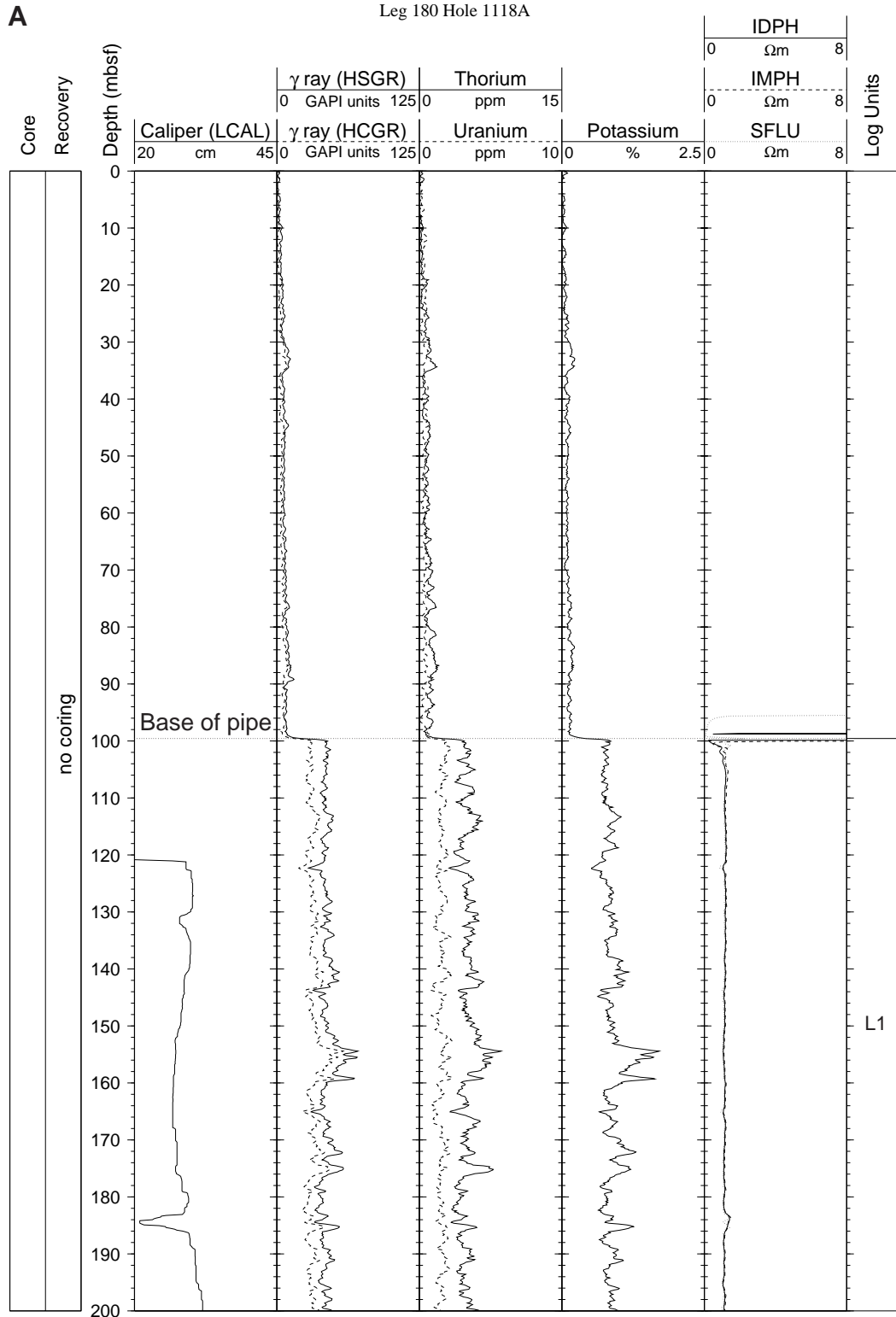
Figure F71 (continued.) Composite log from 200 to 400 mbsf. To compare other logs at equivalent depth, see Figure F71B, p. 138.

Leg 180 Hole 1118A

Figure F71 (continued.) Composite log from 400 to 600 mbsf. To compare other logs at equivalent depth, see Figure F71B, p. 139.

Figure F71 (continued.) Composite log from 600 to 800 mbsf. To compare other logs at equivalent depth, see Figure F71B, p. 140.

Figure F71 (continued.) Composite log from 800 to 926 mbsf. To compare other logs at equivalent depth, see Figure p. 141.

Leg 180 Hole 1118A
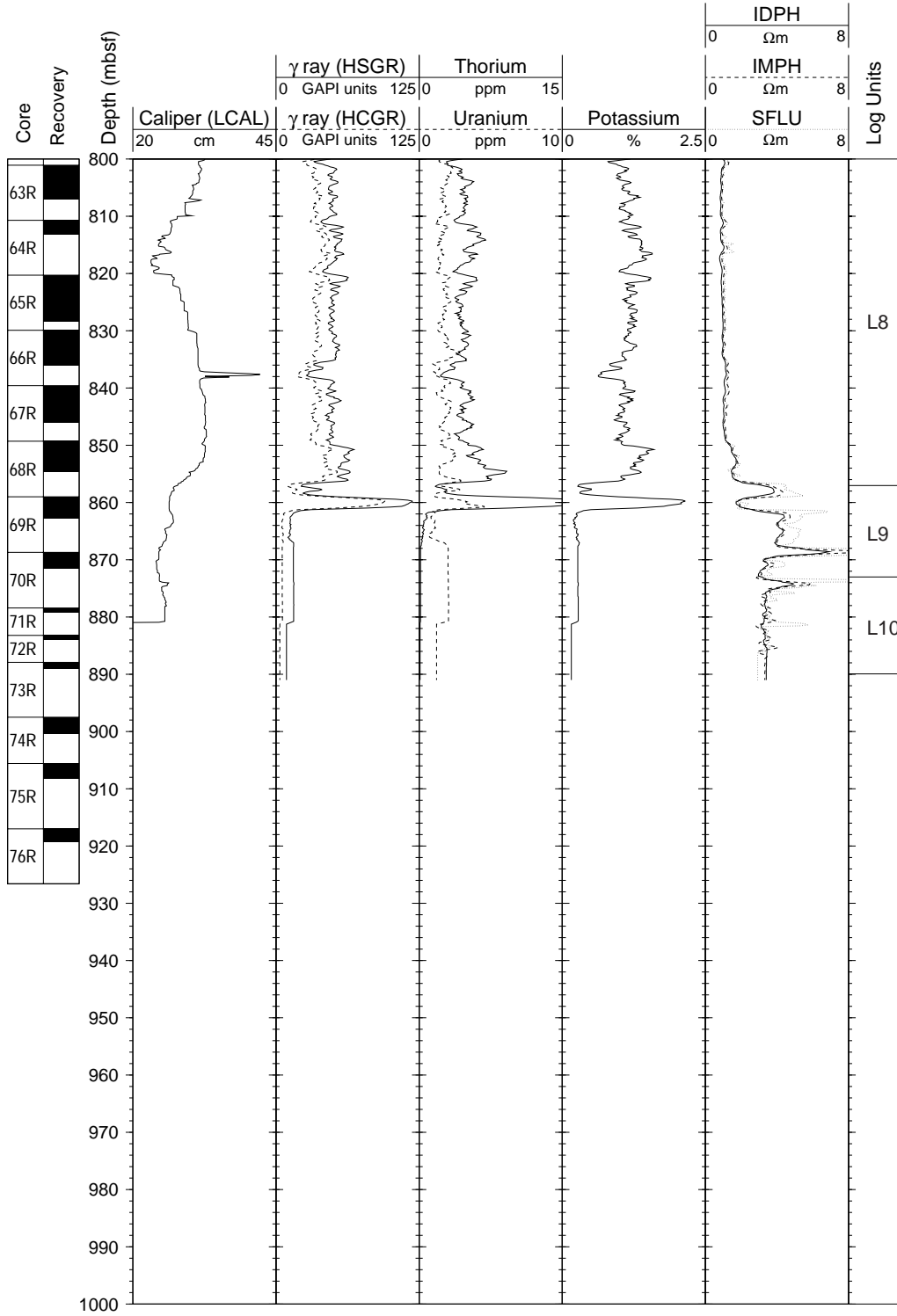
Figure F71 (continued.) B. Left to right: (1) core number and recovery intervals; (2) bulk density (RHOM) from the lithodensity sonde (HLDS) and from measurements on cores; (3) photoelectric effect (PEFL); (4) neutron porosity (APLC), density porosity (DPHI), and porosity from measurements on cores; (5) neutrons capture rate (SIGF); (6) sonic velocity from array sonic tool (DTCO) and from z-axis measurements on cores; and (7) log units. Composite log from 0 to 200 mbsf. To compare other logs at equivalent depth, see Figure F71A, p. 132.

Figure F71 (continued.) Composite log from 200 to 400 mbsf. To compare other logs at equivalent depth, see Figure F71A, p. 133.

Leg 180 Hole 1118A
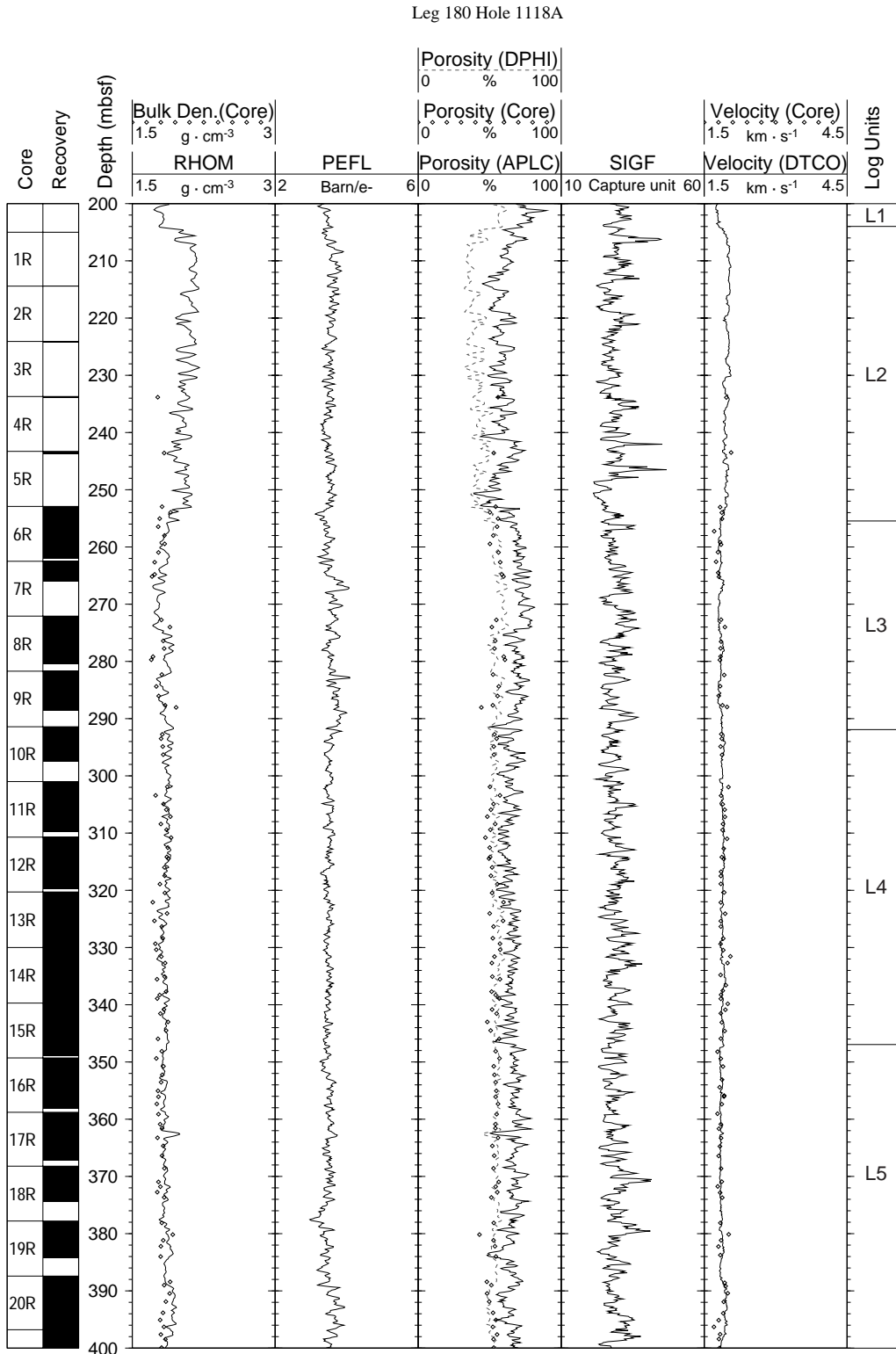
Figure F71 (continued.) Composite log from 400 to 600 mbsf. To compare other logs at equivalent depth, see Figure p. 134.

Figure F71 (continued.) Composite log from 600 to 800 mbsf. To compare other logs at equivalent depth, see Figure p. 135.
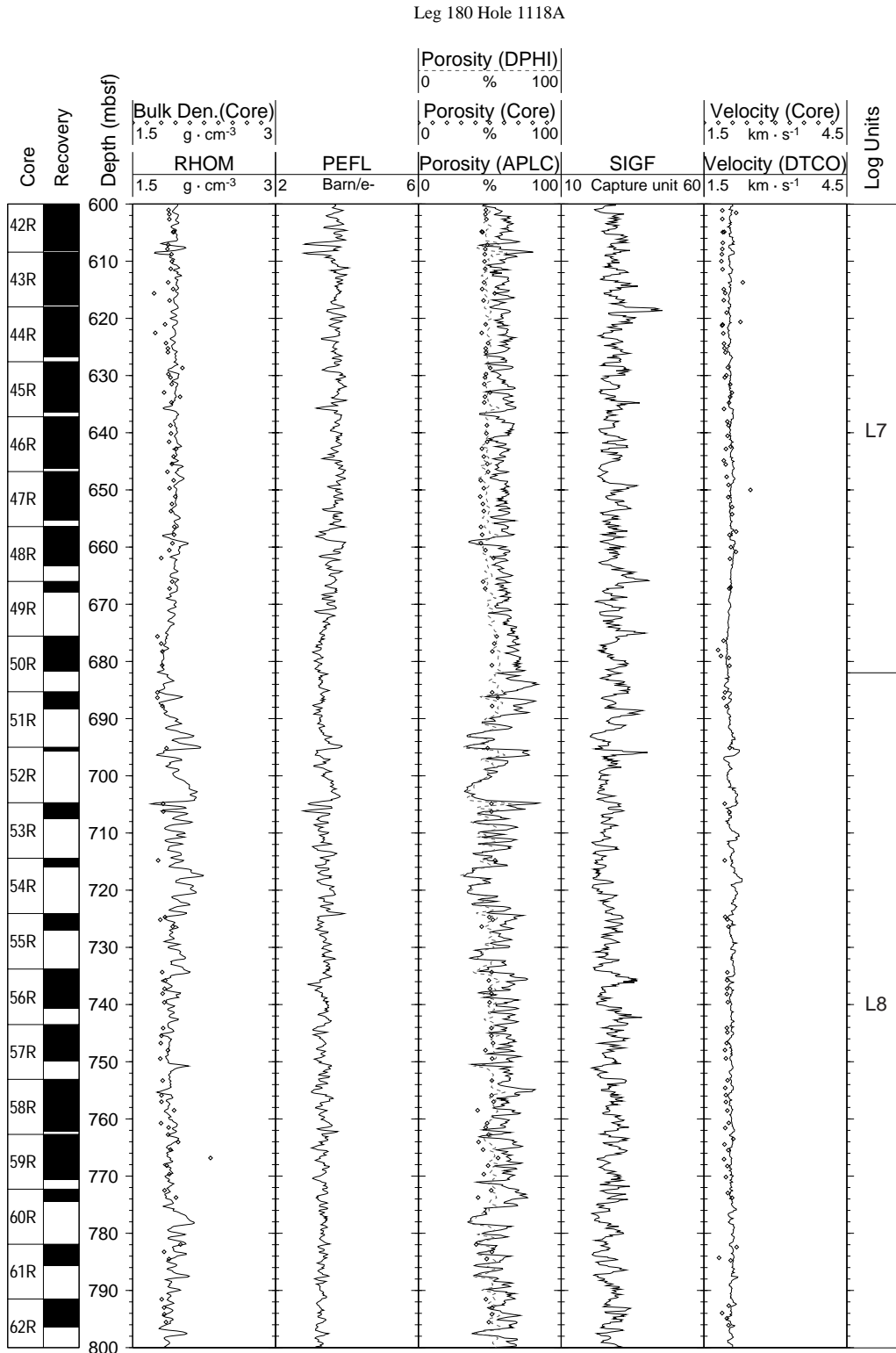
Leg 180 Hole 1118A

Figure F71 (continued.) Composite log from 800 to 926 mbsf. To compare other logs at equivalent depth, see Figure F71A, p. 136.

Leg 180 Hole 1118A
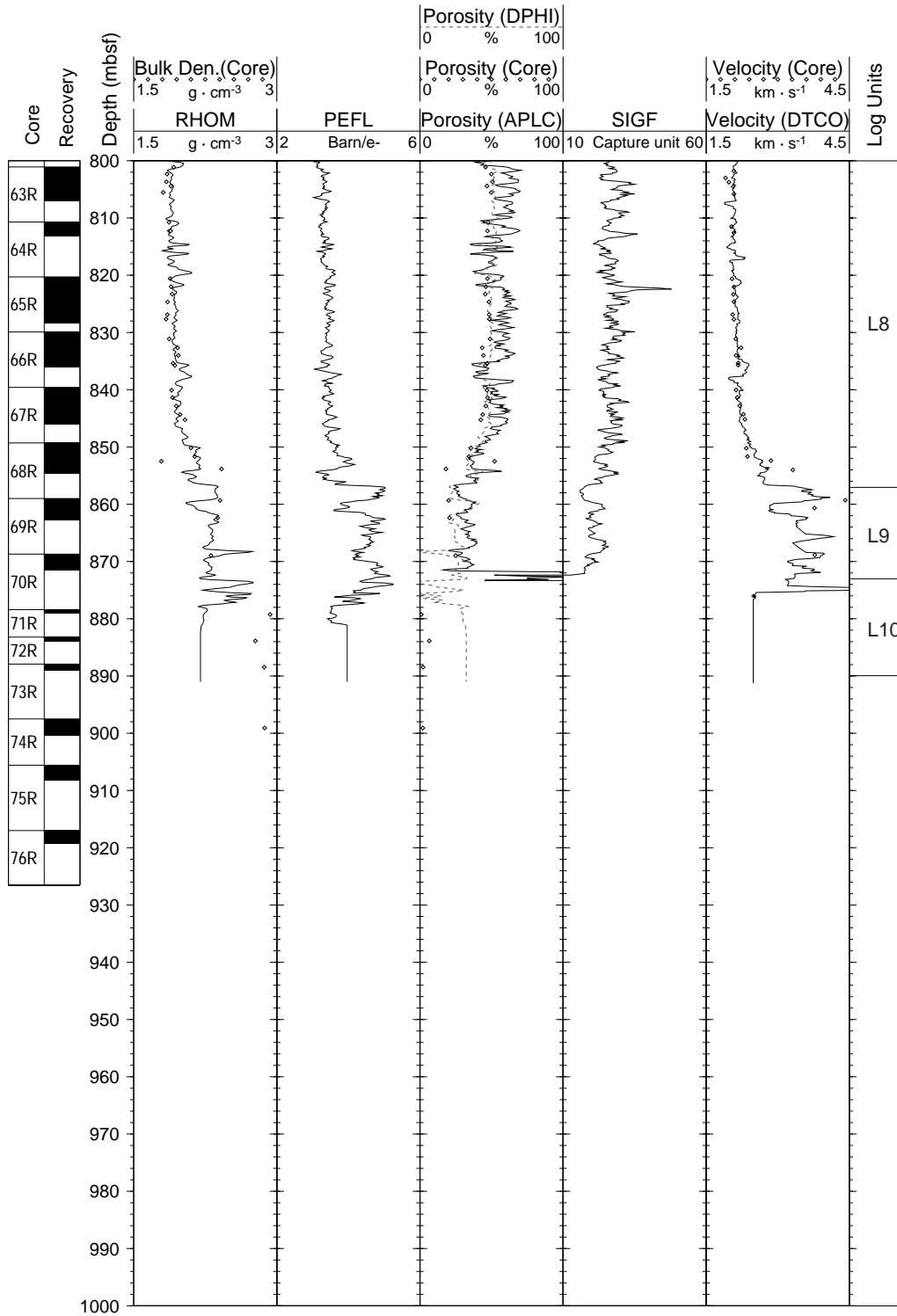
Figure F72. Hole 1118A total gamma ray (HSGR) from the triple combo at the mudline after depth shifts as in Table T16, p. 211.
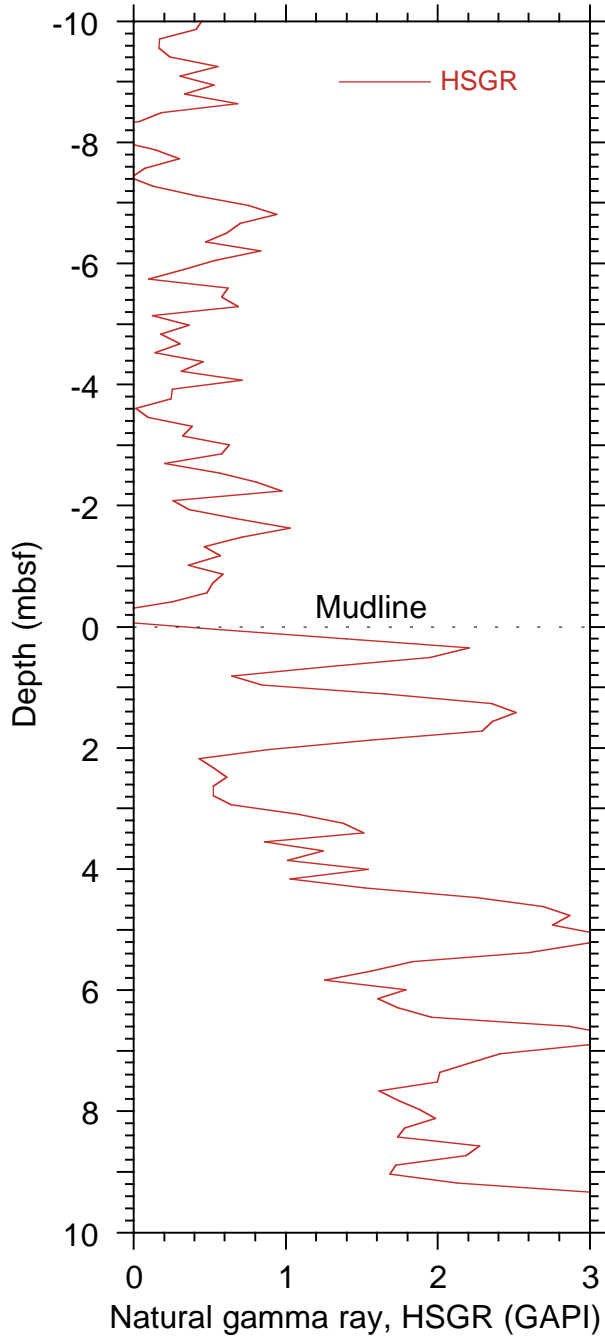
Figure F73. Hole 1118A total gamma ray in the 283–303 mbsf interval from triple combo (HSGR) and FMS-sonic pass 2 (SGR2) after depth shifts as given in Table T16, p. 211.
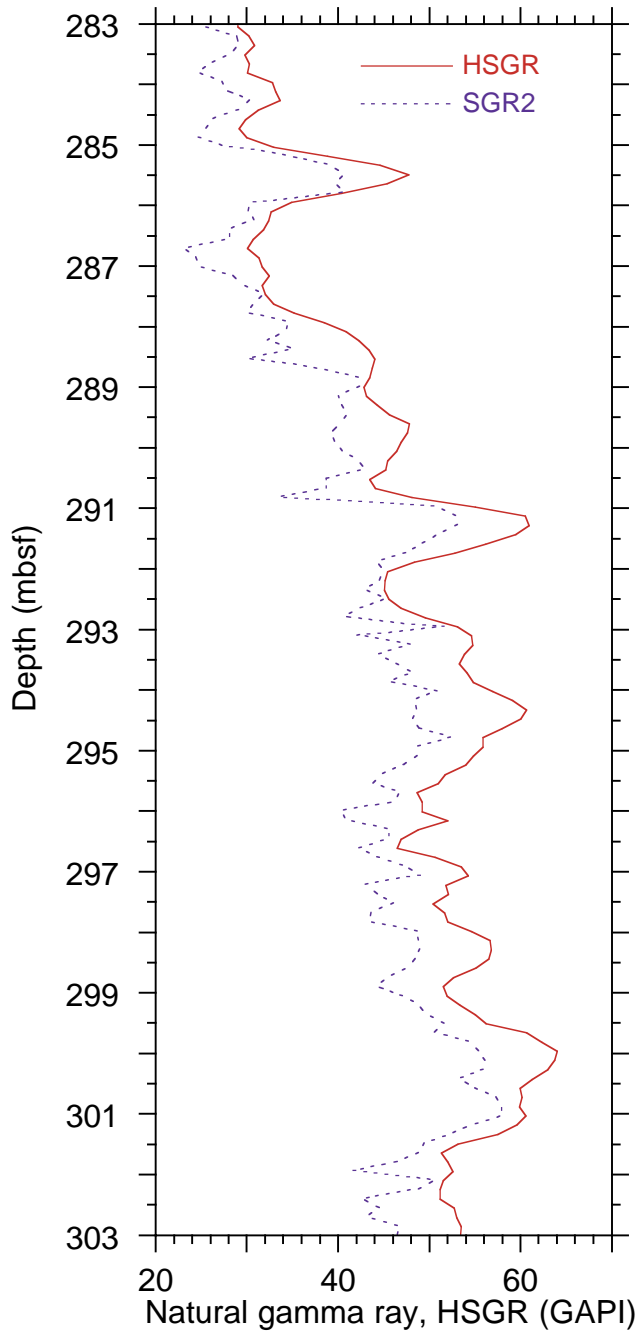
Figure F74. Hole 1118A total gamma ray in the 373–388 mbsf interval from triple combo (HSGR) and FMS-sonic pass 2 (SGR2) after depth shifts as given in Table T16, p. 211.
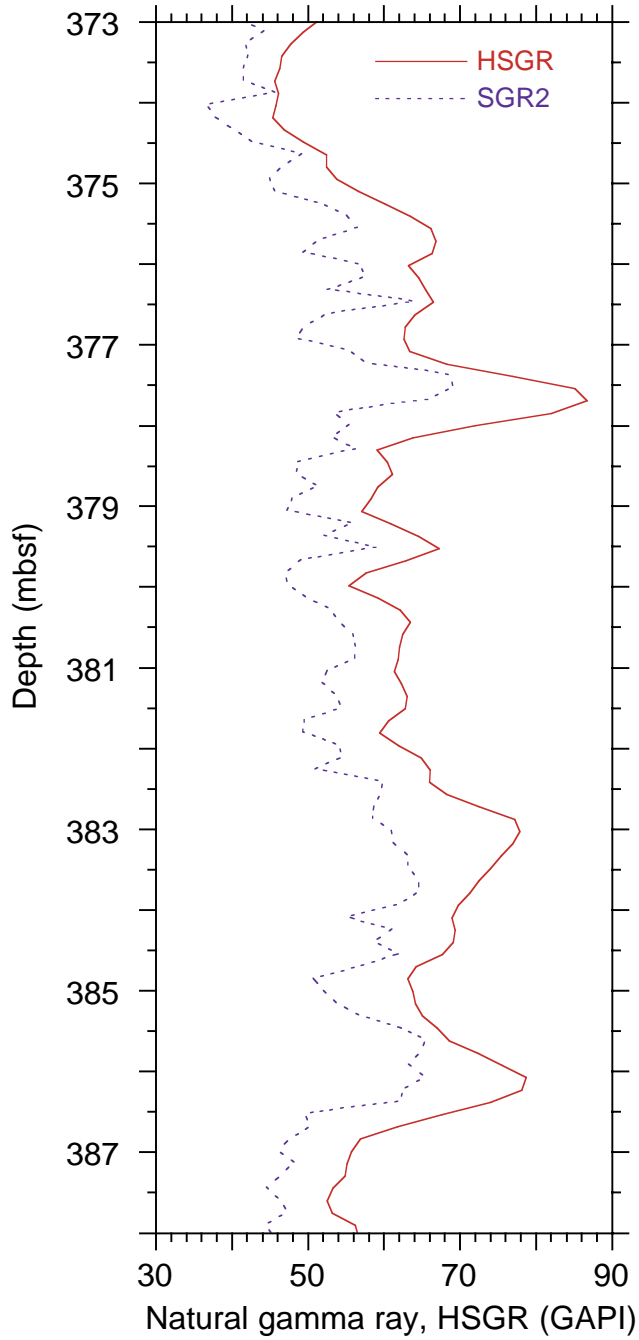
Figure F75. Hole 1118A total gamma ray in the 855–865 mbsf interval from triple combo (HSGR) and FMS-sonic string pass 2 (SGR2) and pass 1 (SGR1) after depth shifts as given in Table T16, p. 211. Note that differential cable stretching results in a 75-cm mismatch with the triple combo pass.
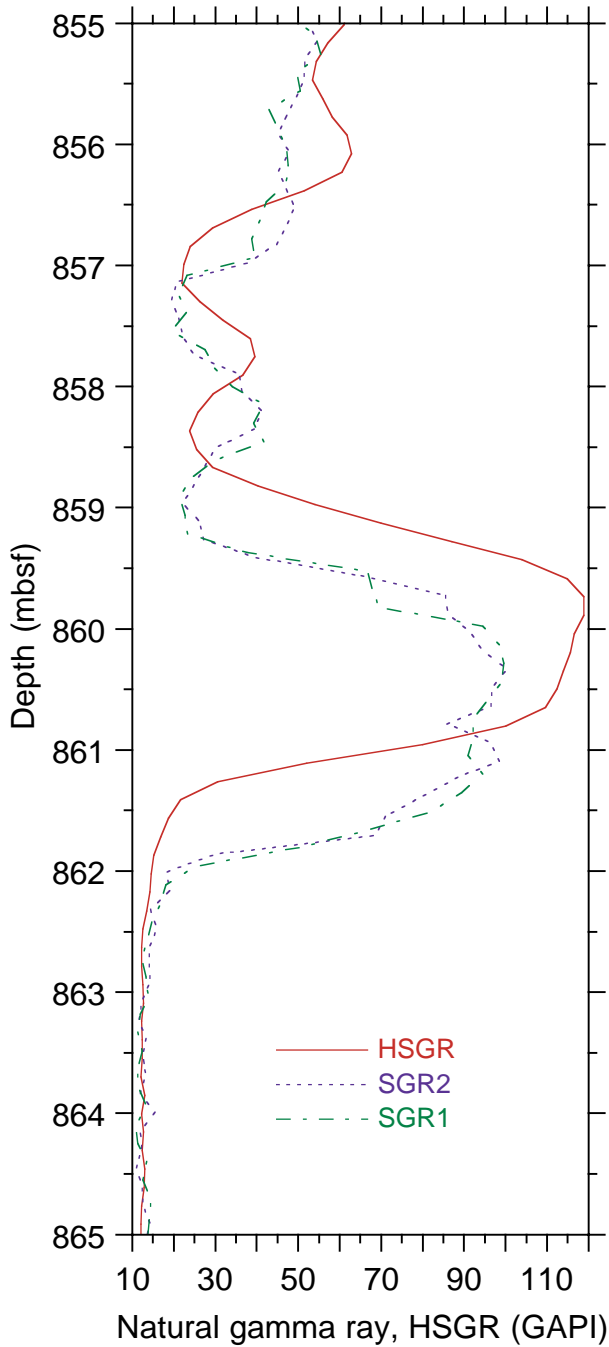
Figure F76. Lithologic units derived from logging response and core analysis in Hole 1118A. Left to right: core recovery, natural gamma ray (HSGR), density (DPHI) and neutron (APLC) porosity units defined by the logging response, lithostratigraphic units defined in "Lithostratigraphy," p. 4, and fault zones defined in "Structural Geology," p. 28. Lith. = lithostratigraphic unit.
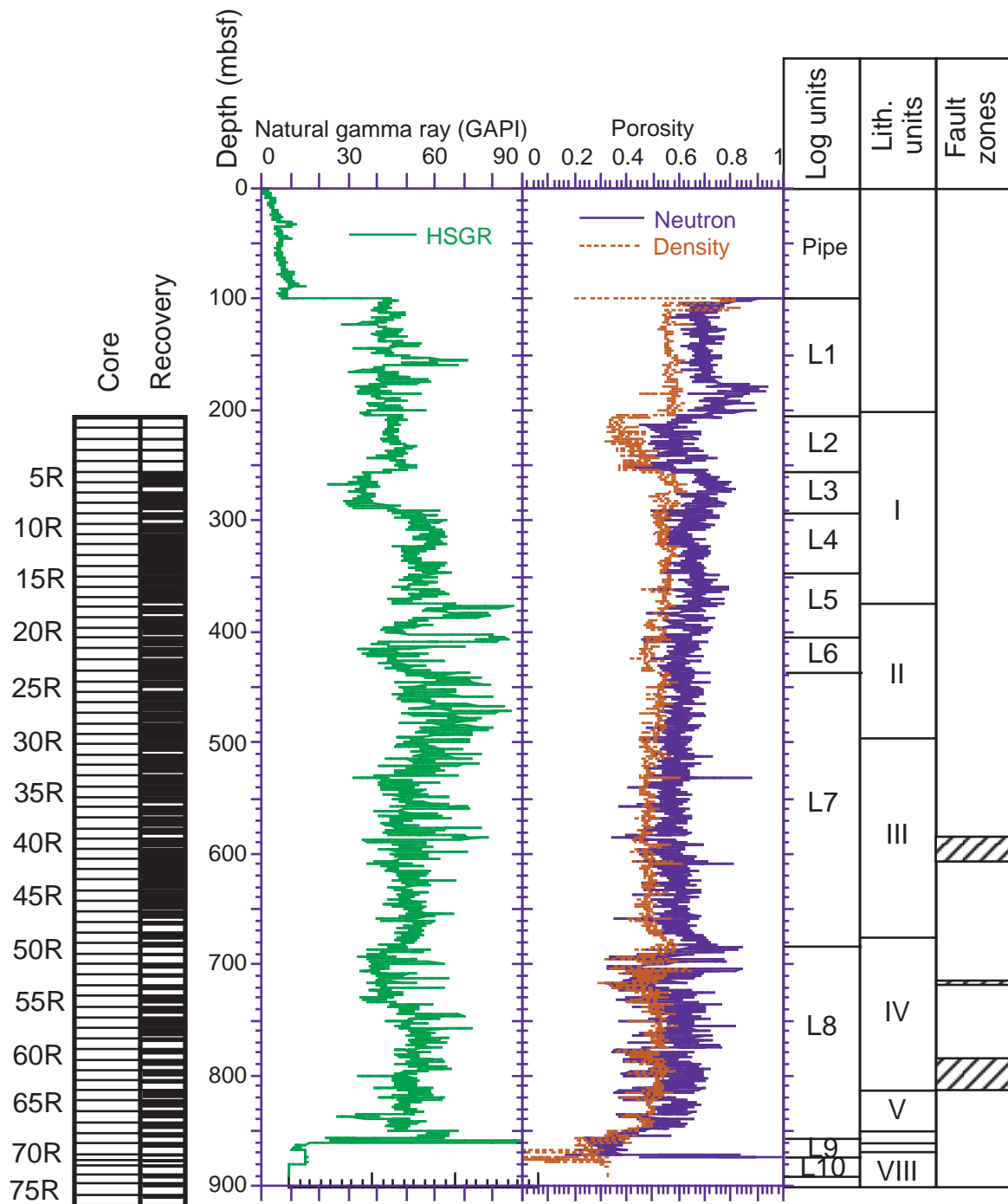
Figure F77. Hole 1118A deviation.
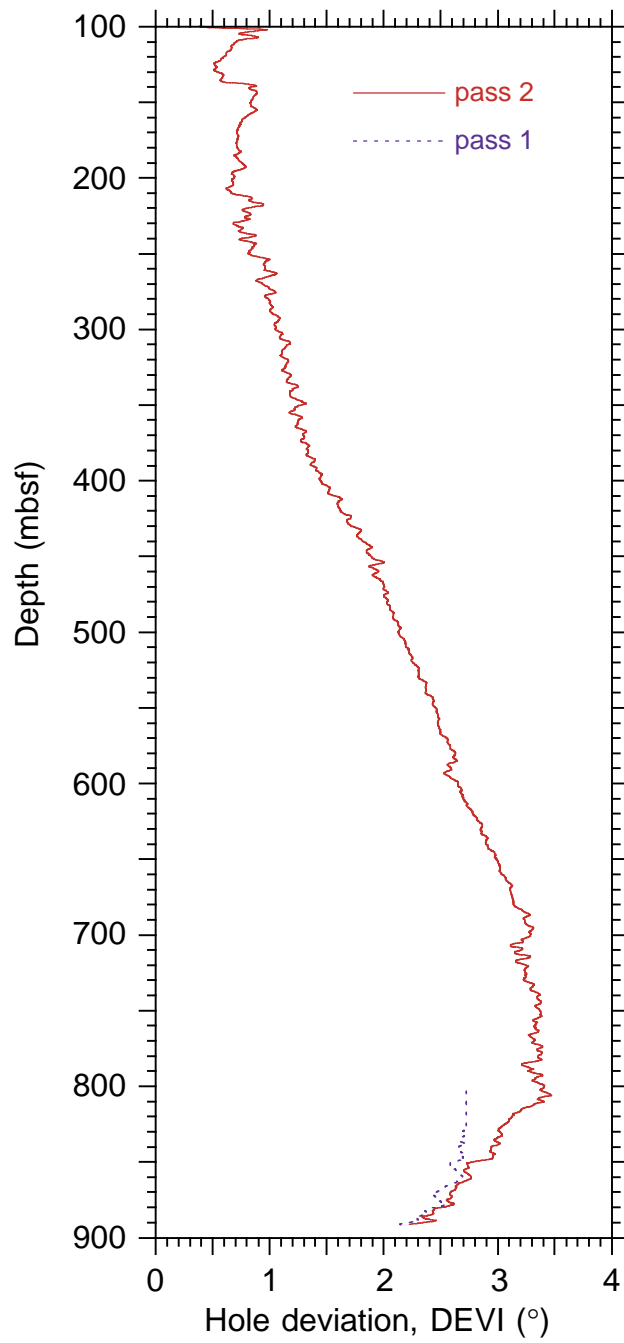
Figure F78. Hole 1118A azimuth.
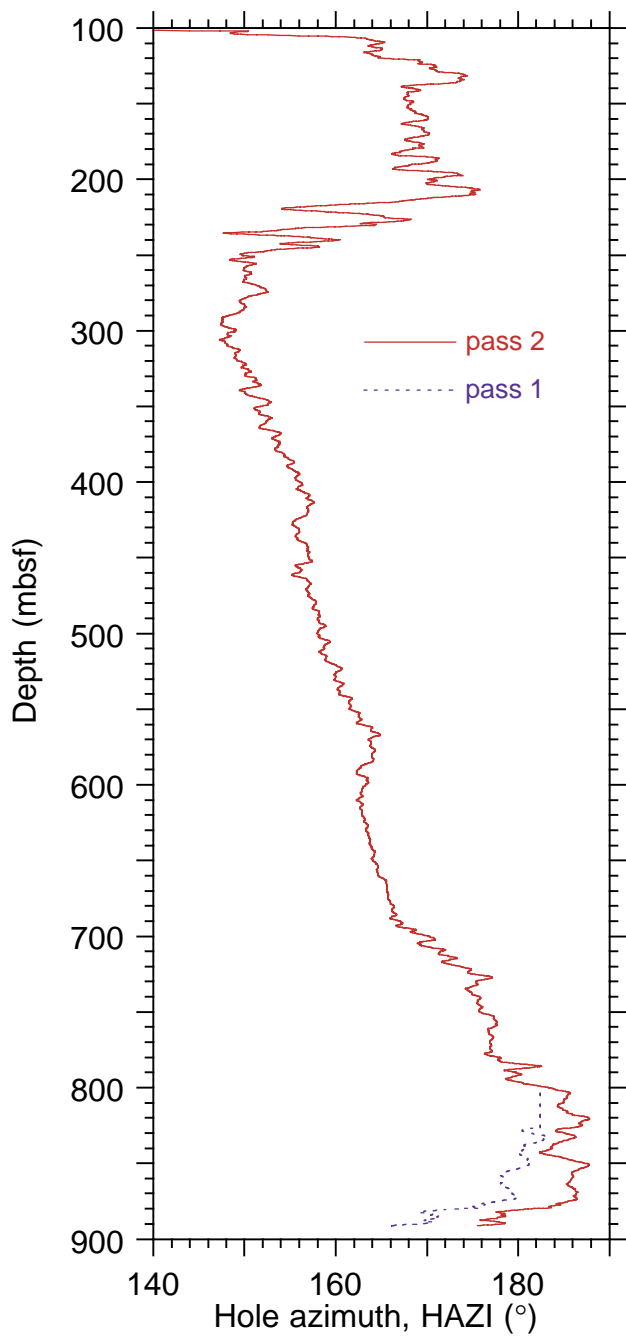
Figure F79. FMS tool string acceleration, Hole 1118A.
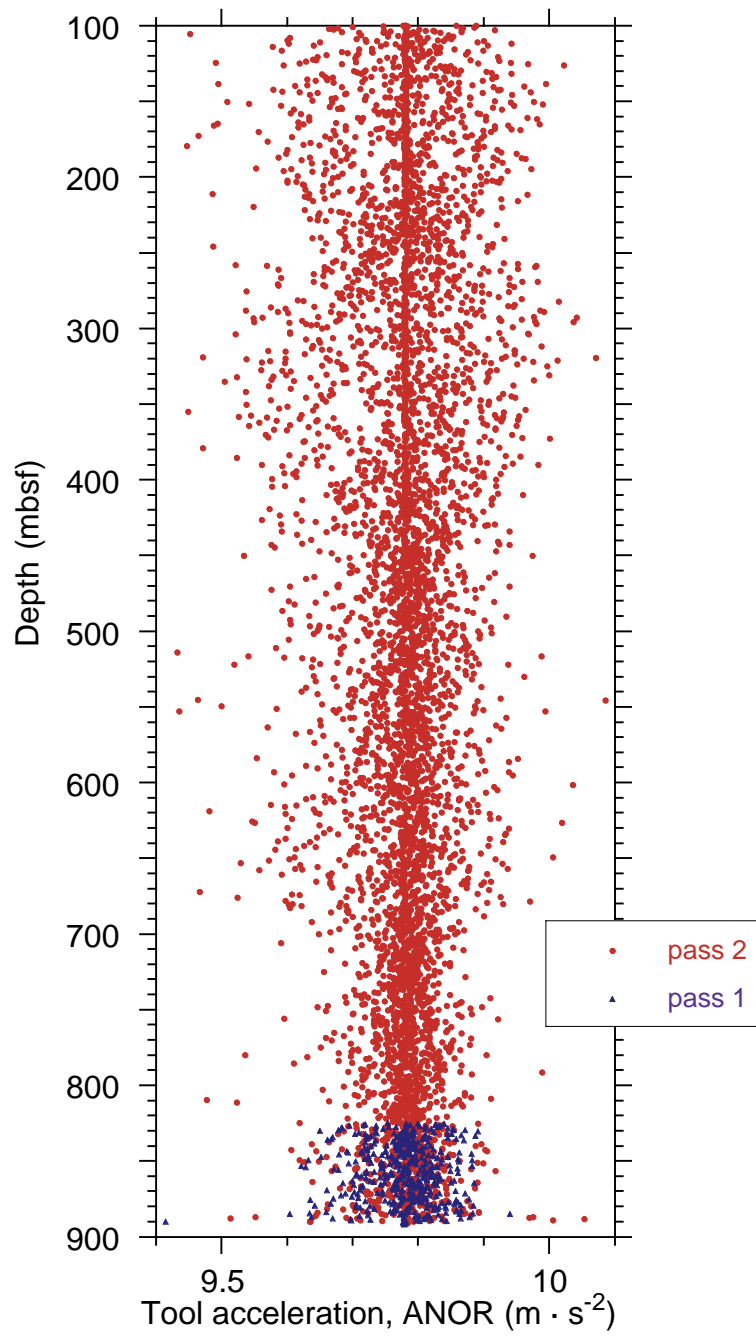
Figure F80. Hole 1118A geometry. Left to right: HLDS (LCAL) and FMS (C1 and C2) caliper data from passes 1 and 2, FMS Pad 1 azimuth (P1AZ) with respect to geographic north, absolute value of the difference between the two FMS caliper measurements (C1 and C2) for passes 1 and 2, and azimuth of the greatest diameter when the caliper difference is >5 cm.
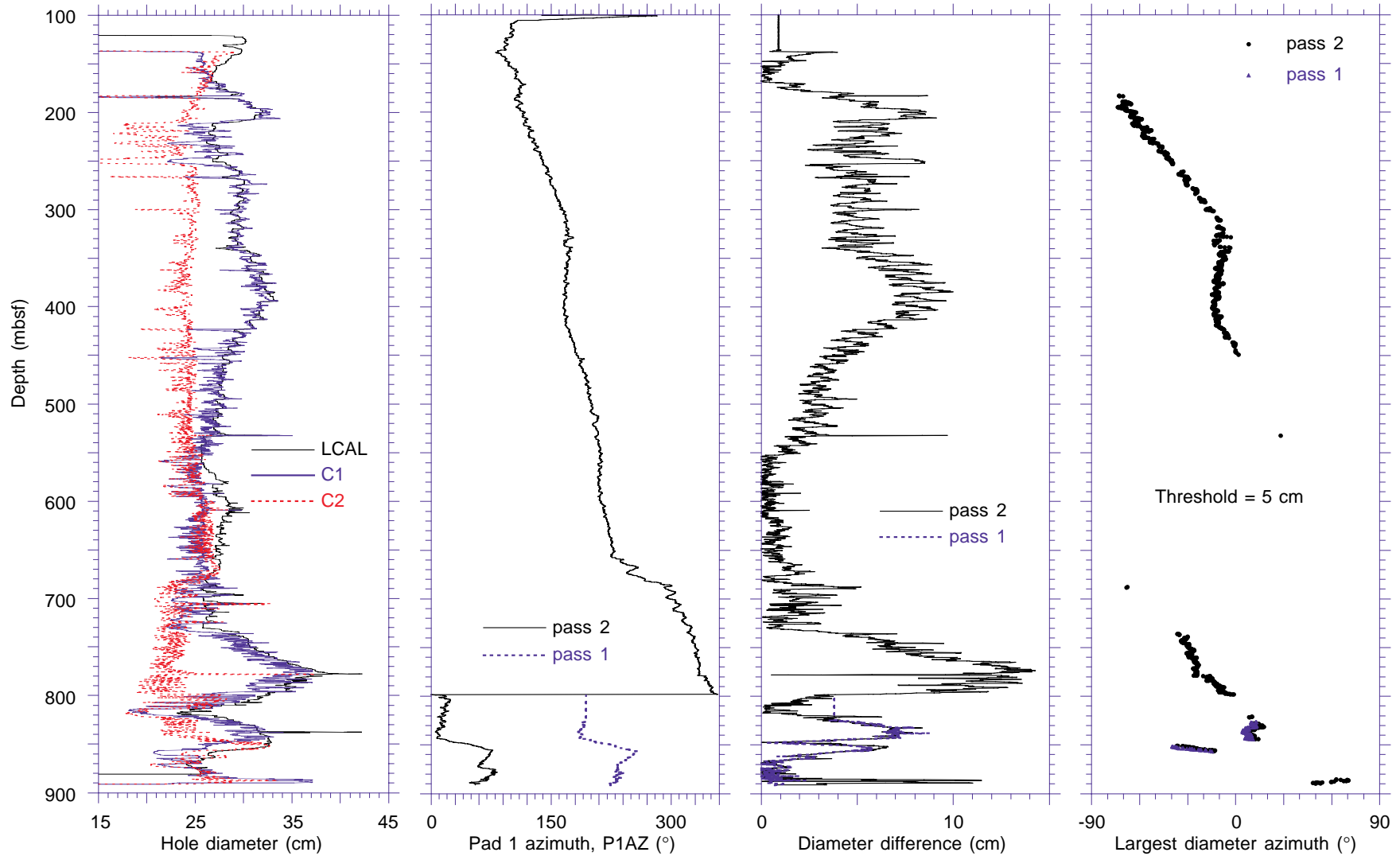
Figure F81. Magnetic field inclination (FINC) and intensity (FNOR), Hole 1118A.
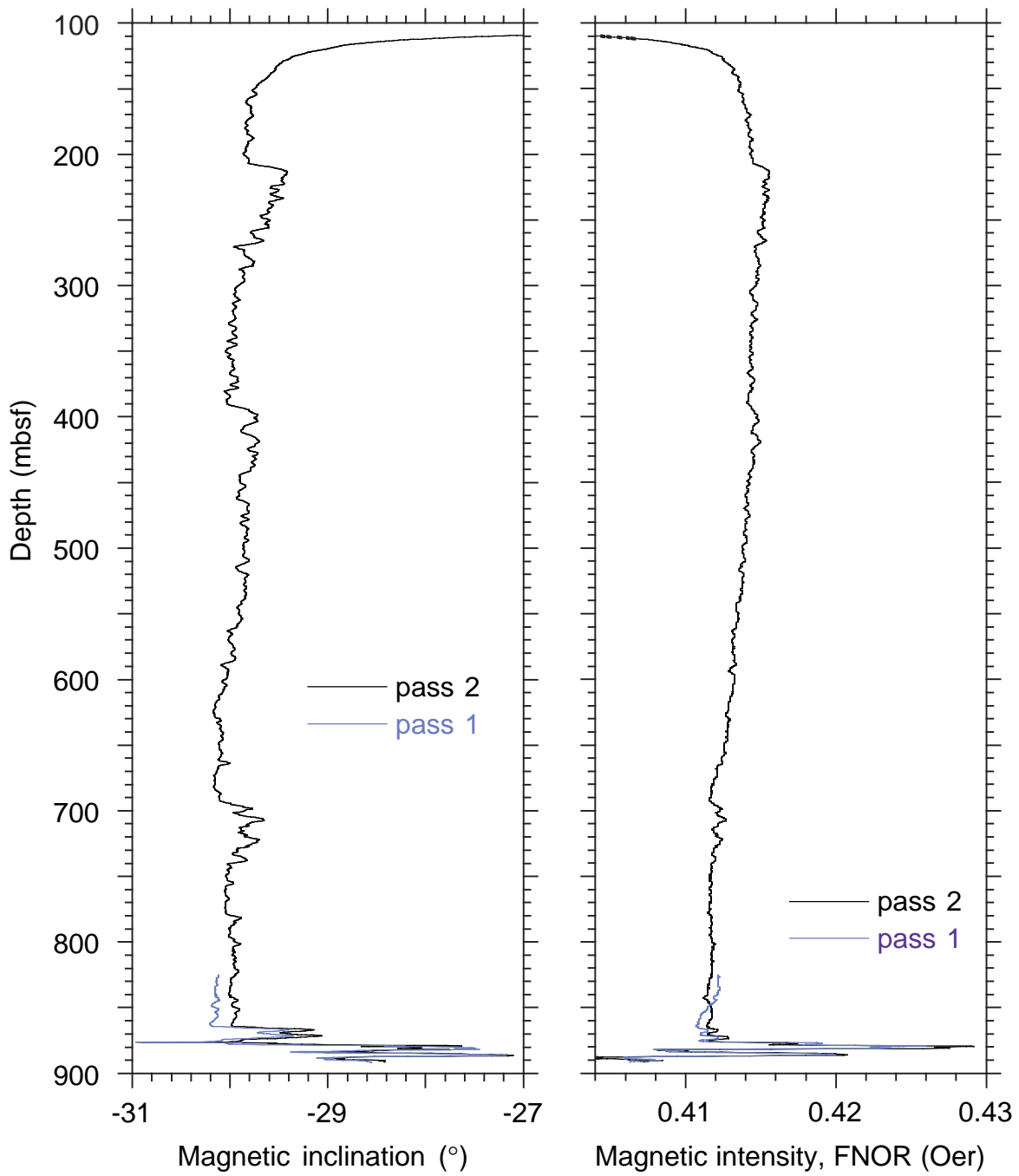
Figure F82. Hole 1118A statically (left) and dynamically (right) normalized FMS images from log Unit L1 show characteristic thin, flat-lying beds that grade between more conductive clays to more resistive sand or carbonate-rich beds. The green (dashed) lines mark the Pad 1 azimuth trace of each FMS pass. The FMS images are oriented from 0° to 360° from geographic north. Vertical scale = 1:20.
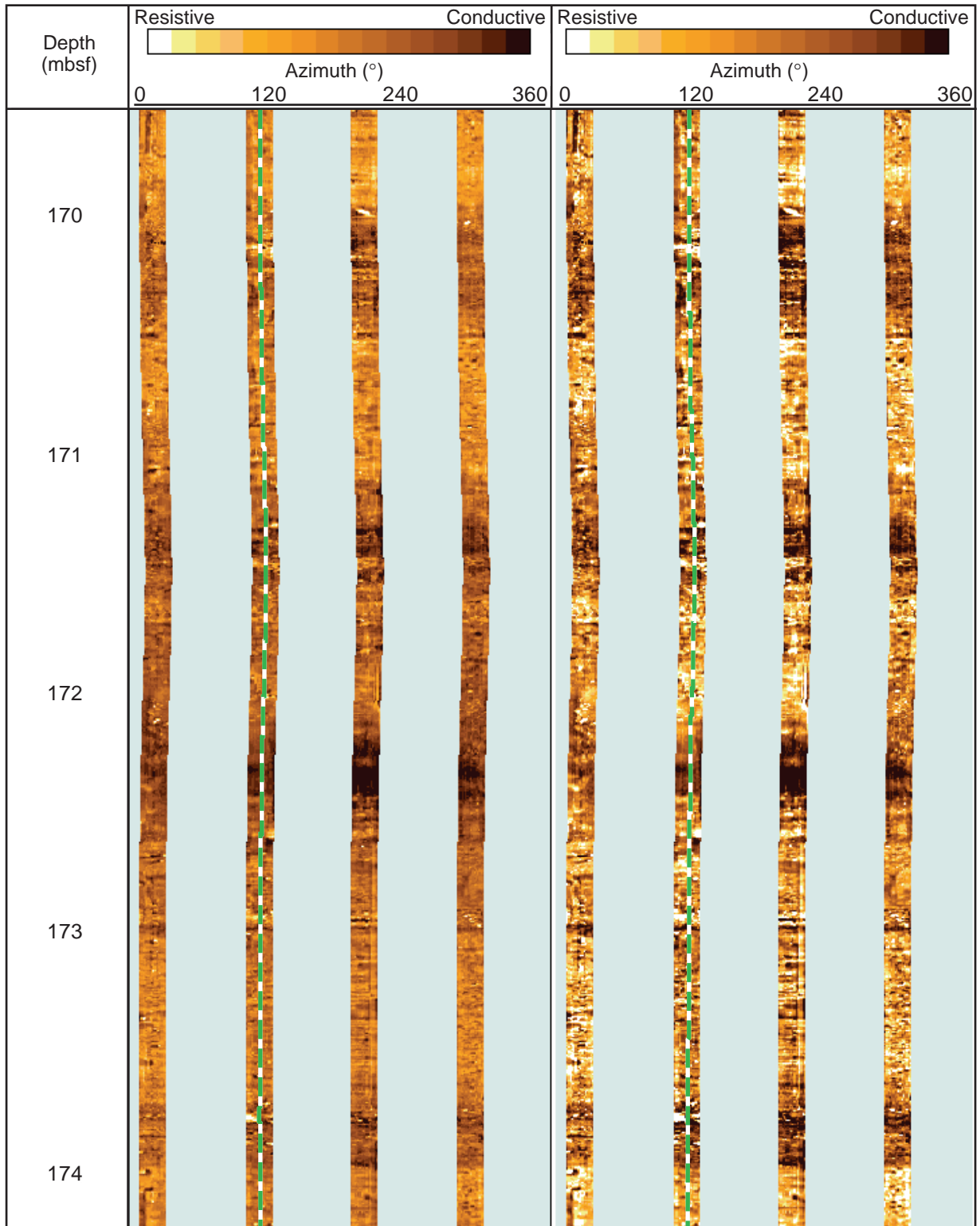
Figure F83. Hole 1118A dynamically normalized FMS image and tadpole plot displaying wavy beds and foresets at the base of log Unit L3. Tadpoles indicate the dip magnitude from 0° to 90°. Dip directions are indicated by the orientation of each tadpole tail. Vertical scale = 1:20.
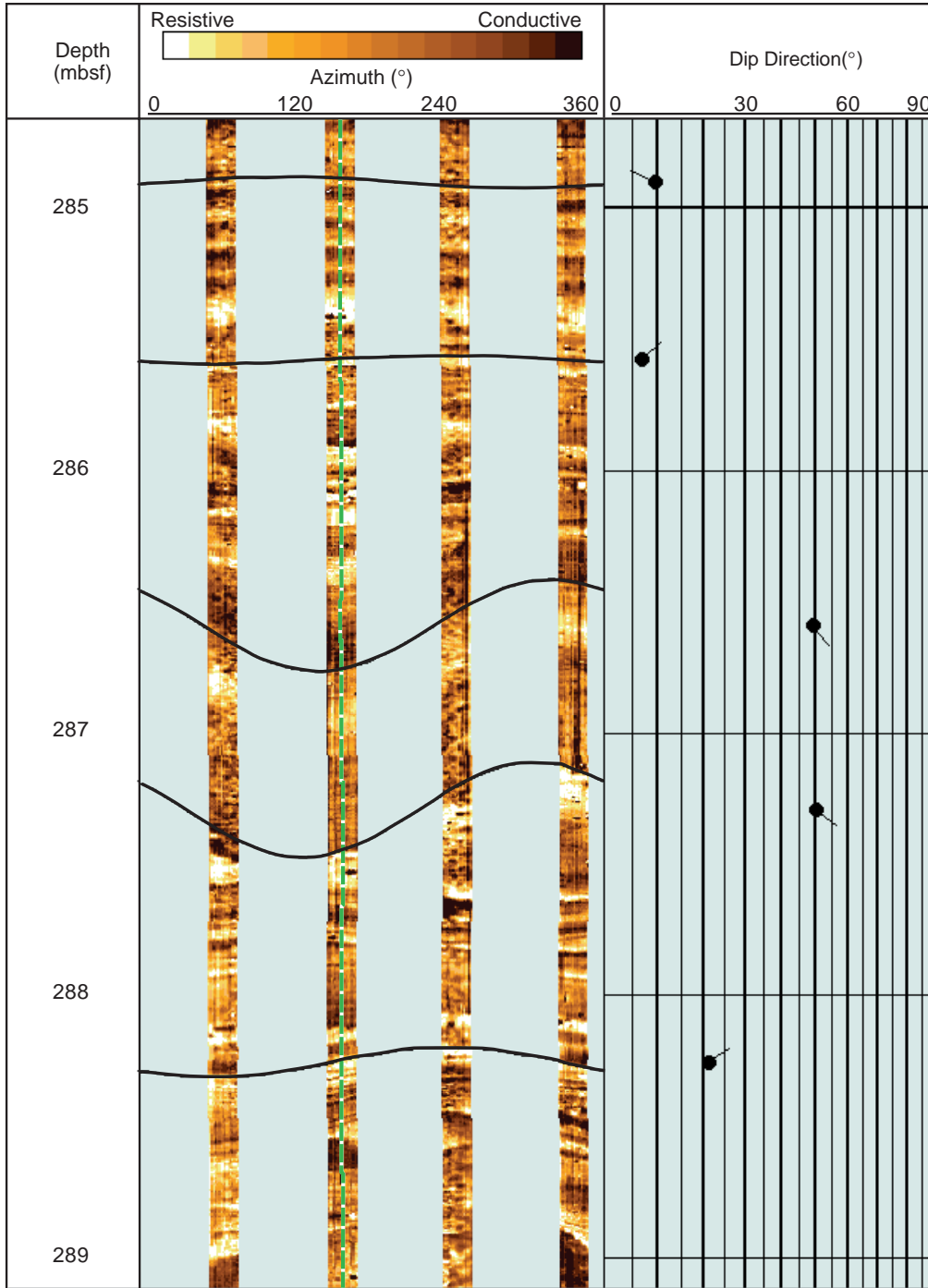
Figure F84. Hole 1118A statically (left) and dynamically (right) normalized FMS images of wavy, clayey beds that interlayer thin, resistive, more flat-lying beds of log Unit L7. Vertical scale = 1:20.
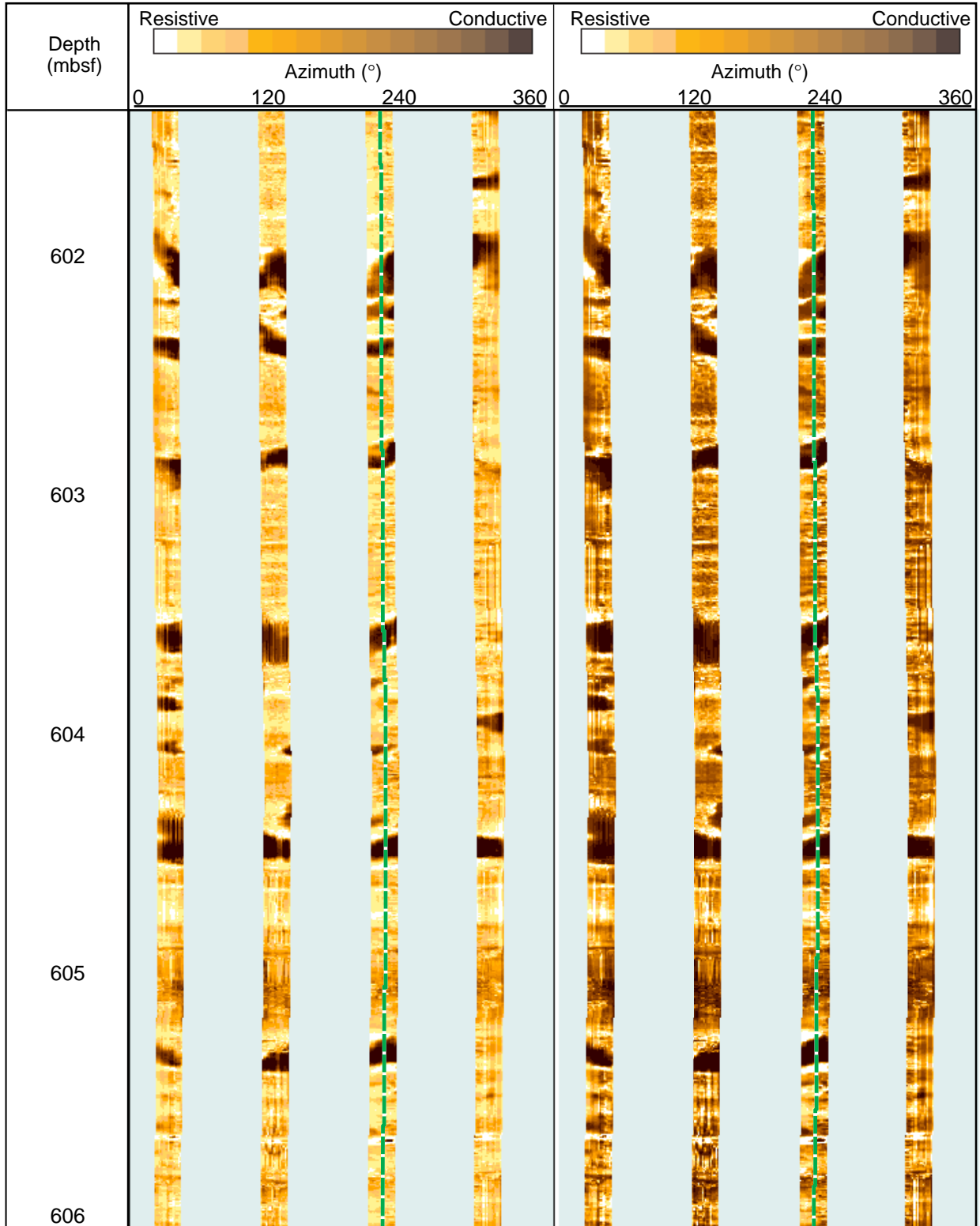
Figure F85. Hole 1118A statically (left) and dynamically (right) normalized FMS images of the boundary between the limestone base of log Unit L9 and the conglomerate of log Unit L10. An ~45-cm-thick dolomite layer lies between these units at 874 mbsf. Note: FMS depths are shifted ~75 cm below the triple combo logs within this unit.
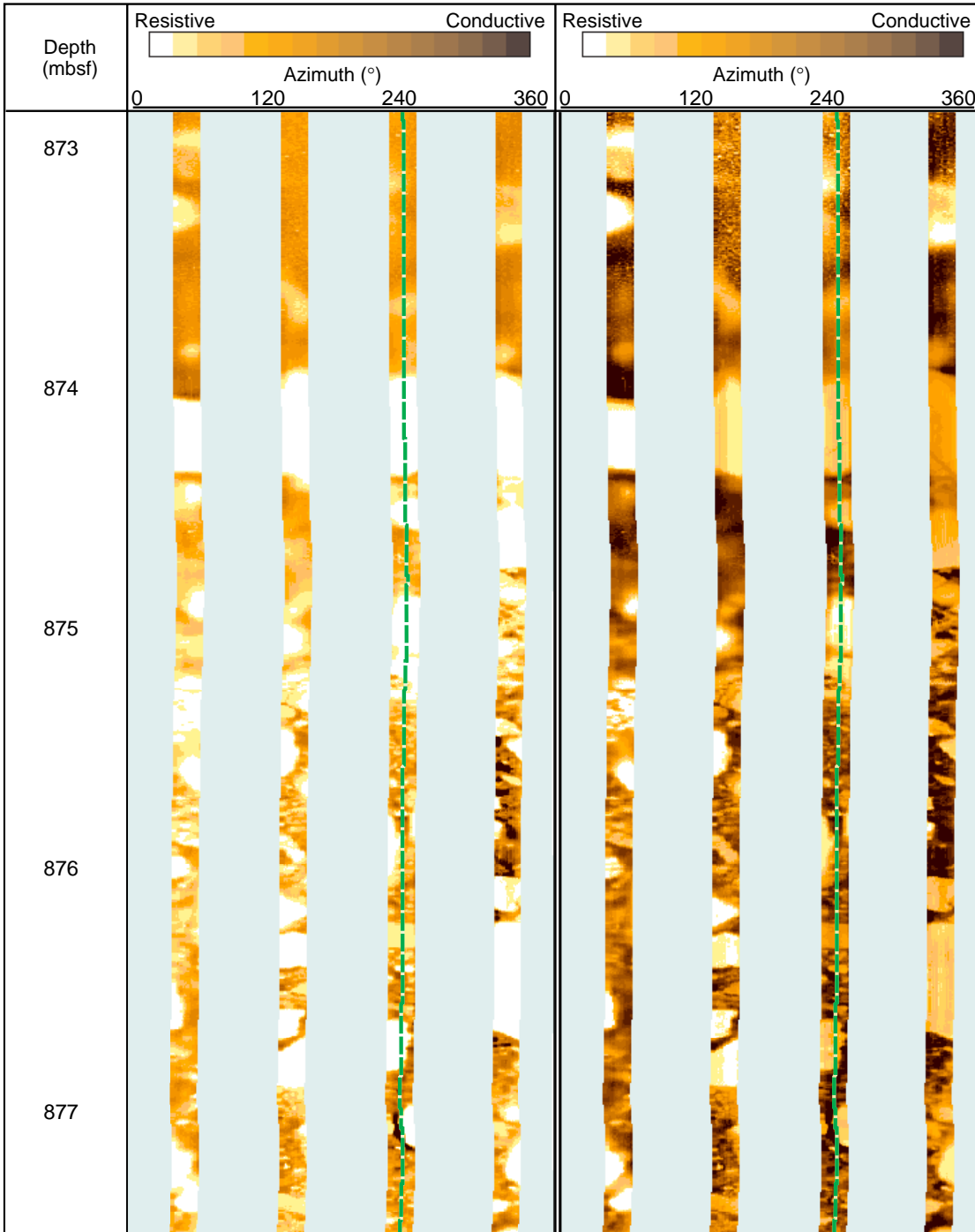
Figure F86. Hole 1118A temperature (TLT) recorded during the triple combo first pass. Data are from the slow thermistor. Arrows mark upward and downward run of the tool.
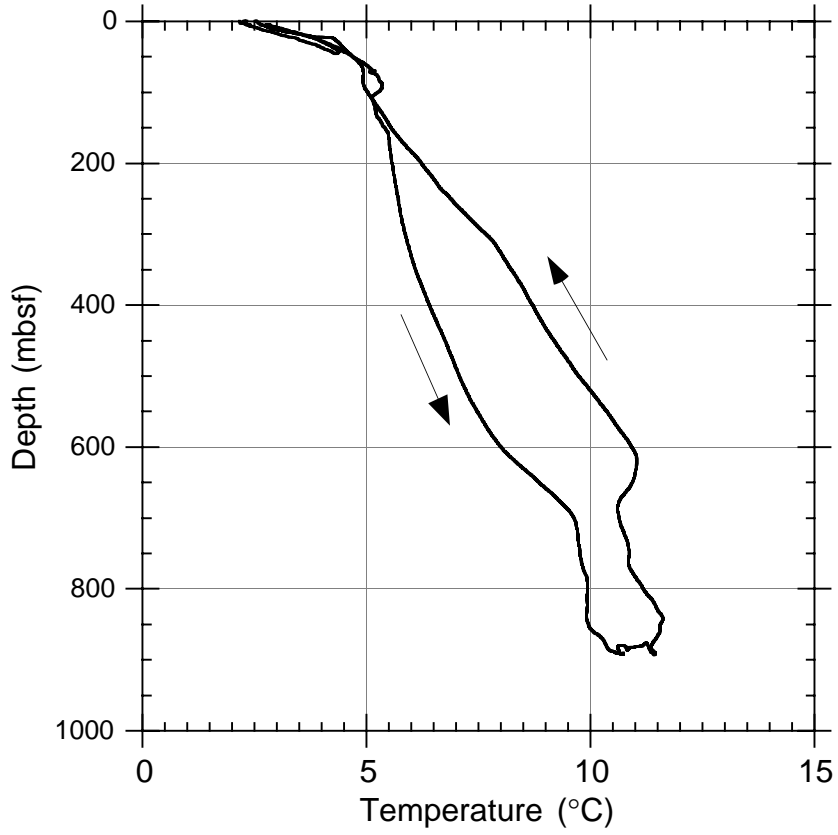
Figure F87. Hole 1118A temperature (TLT) data during dedicated temperature pass. Data are from the slow thermistor. Depth stations are marked. Arrows mark upward and downward run of the tool.
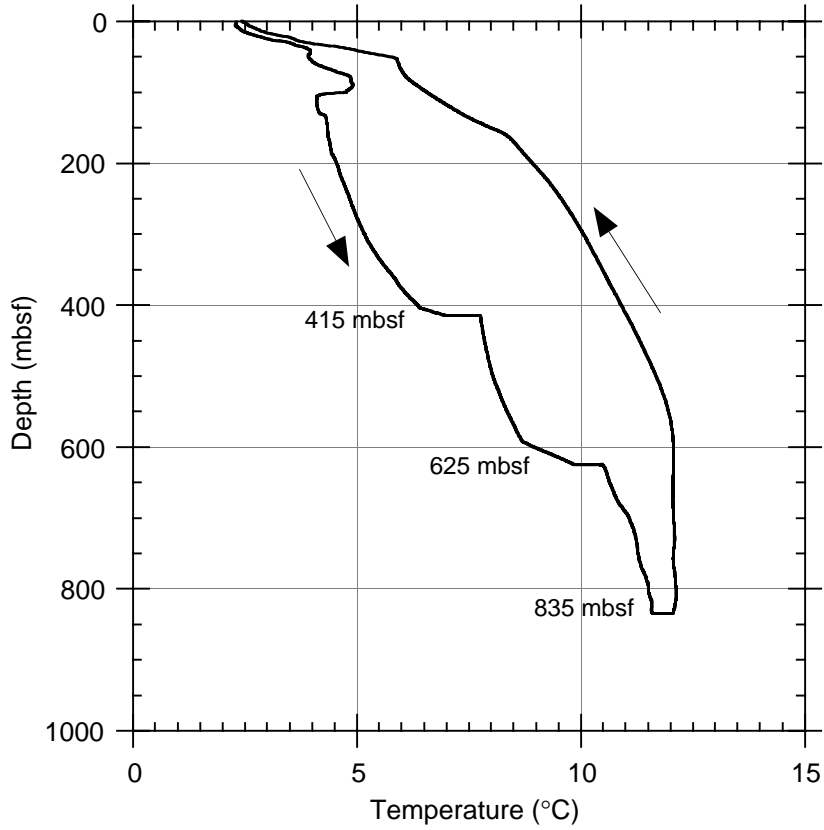
Figure F88. Temperature vs. ln[$t/(t–s)$] from the TLT at 835 mbsf in Hole 1118A. The equilibrium temperature is the y-intercept of the linear-regression line fitted to the data. t = time measured from initial drilling; s = time elapsed between initial drilling and end of circulation.
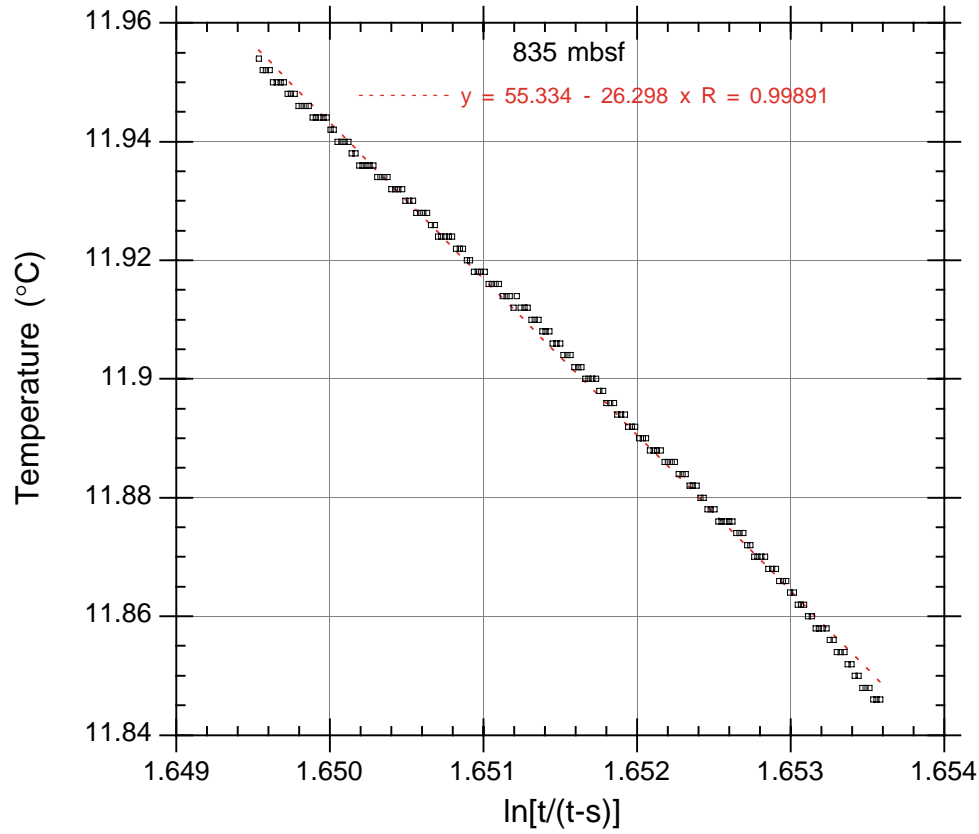
Figure F89. VSP corridor stack repeated five times and placed between five migrated MCS traces on both sides of Site 1118.
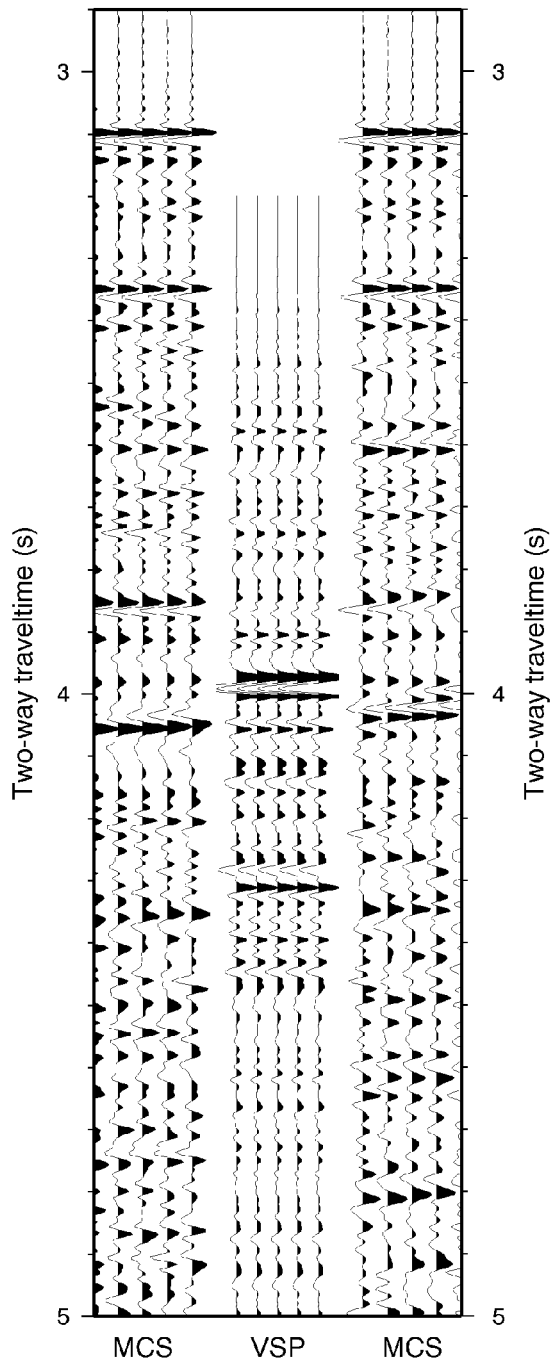
Figure F90. Depth vs. transit time for the Site 1118 VSP.
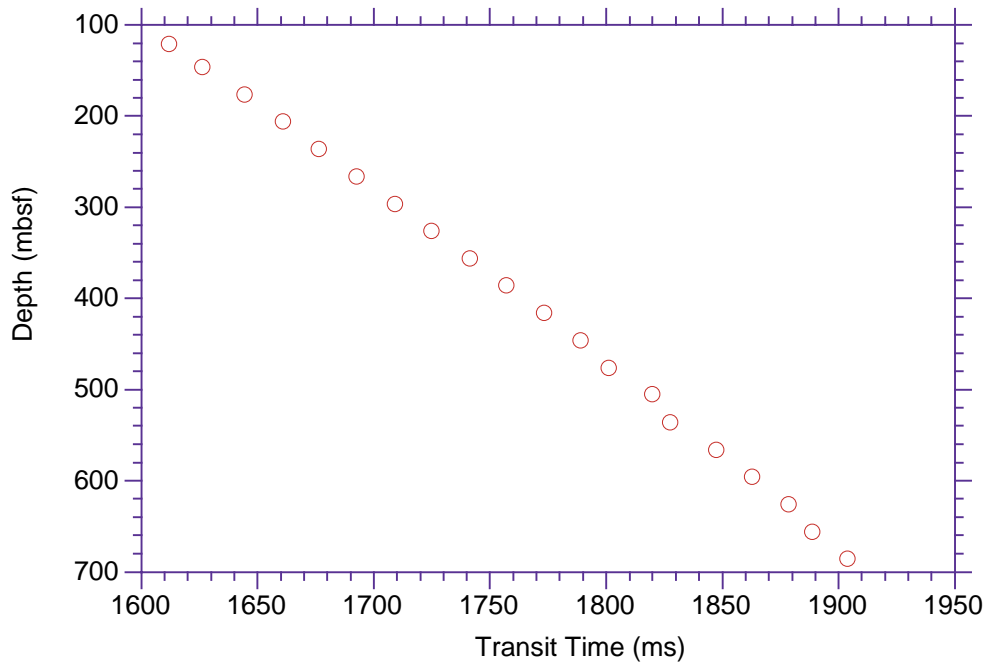
Figure F91. Depth-converted MCS data (left) and VSP data. The depth conversion was carried out using the velocity profile shown on the right.
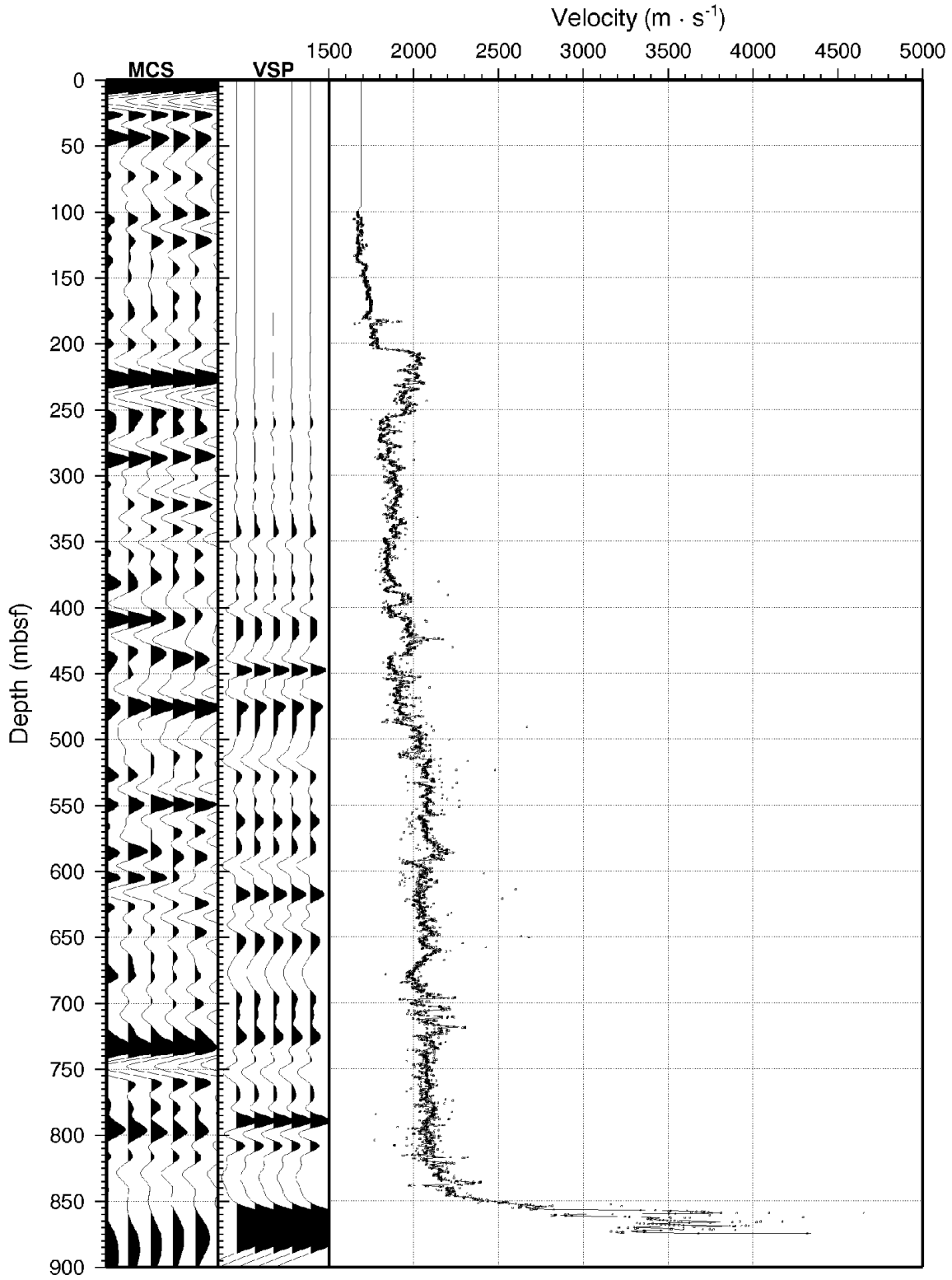
Figure F92. MCS Line EW9510–1366 cut at Site 1118. The five far right MCS traces have been depth converted and are displayed to the right with a lithostratigraphic column. Lines linking the time and depth data are spaced every 30 m. CMP = common midpoint.
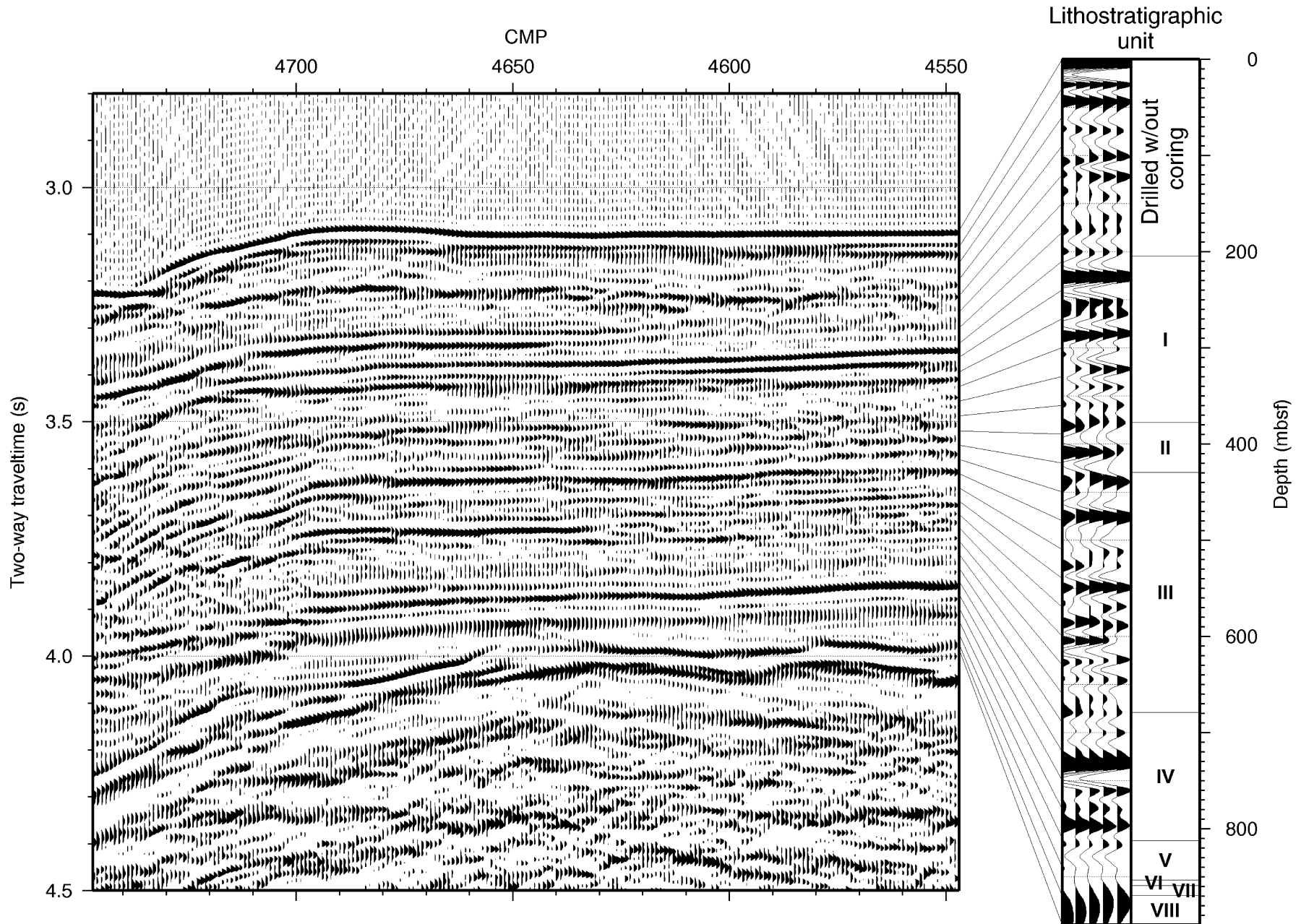
Table T1. Site 1118 coring summary. (Continued on next page.)

Hole 1118A

Latitude: 9°35.110'S
Longitude: 151°34.421'E
Seafloor (drill-pipe measurement from rig floor, mbrf): 2315.4
Distance between rig floor and sea level (m): 11.9
Water depth (drill-pipe measurement from sea level, m): 2303.6
Total depth (from rig floor, mbrf): 3242.0
Total penetration (mbsf): 926.6
Total number of cores: 76
Total length of cored section (m): 721.6
Total core recovered (m): 466.21
Core recovery (%): 65

Core	Date (1998)	Time (UTC +10 hr)	Depth (mbsf)	Length cored (m)	Length recovered (m)	Recovery (%)	Comment
180-1118A-							
		*****Drilled from 0 to 205.0 mbsf*****					Drilled without coring
1R	29 July	0405	205.0-214.4	9.4	0.02	0.2	
2R	29 July	0450	214.4-224.1	9.7	0.04	0.4	
3R	29 July	0545	224.1-233.7	9.6	0.21	2.2	
4R	29 July	0620	233.7-243.3	9.6	0.27	2.8	
5R	29 July	0705	243.3-252.9	9.6	0.40	4.2	
6R	29 July	0800	252.9-262.5	9.6	9.11	94.9	
7R	29 July	0900	262.5-272.1	9.6	3.59	37.4	
8R	29 July	0945	272.1-281.7	9.6	8.36	87.1	
9R	29 July	1045	281.7-291.4	9.7	6.91	71.2	
10R	29 July	1140	291.4-301.0	9.6	6.02	62.7	
11R	29 July	1225	301.0-310.7	9.7	8.83	91.0	
12R	29 July	1315	310.7-320.3	9.6	9.10	94.8	
13R	29 July	1405	320.3-330.0	9.7	9.55	98.5	
14R	29 July	1450	330.0-339.7	9.7	9.89	102.0	
15R	29 July	1540	339.7-349.3	9.6	9.24	96.3	
16R	29 July	1640	349.3-358.8	9.5	8.80	92.6	
17R	29 July	1740	358.8-368.2	9.4	8.40	89.4	
18R	29 July	1840	368.2-377.8	9.6	6.29	65.5	
19R	29 July	1930	377.8-387.4	9.6	6.42	66.9	
20R	29 July	2025	387.4-396.8	9.4	9.37	99.7	
21R	29 July	2120	396.8-406.3	9.5	7.38	77.7	
22R	29 July	2230	406.3-415.9	9.6	8.83	92.0	
23R	29 July	2340	415.9-425.6	9.7	7.89	81.3	
24R	30 July	0100	425.6-435.2	9.6	9.44	98.3	
25R	30 July	0220	435.2-444.8	9.6	8.57	89.3	
26R	30 July	0325	444.8-454.4	9.6	5.95	62.0	
27R	30 July	0510	454.4-463.9	9.5	8.80	92.6	
28R	30 July	0635	463.9-473.6	9.7	9.05	93.3	
29R	30 July	0800	473.6-483.2	9.6	8.96	93.3	
30R	30 July	0925	483.2-492.9	9.7	9.31	96.0	
31R	30 July	1100	492.9-502.5	9.6	8.70	90.6	
32R	30 July	1205	502.5-512.1	9.6	7.20	75.0	
33R	30 July	1320	512.1-521.8	9.7	9.04	93.2	
34R	30 July	1435	521.8-531.4	9.6	8.22	85.6	
35R	30 July	1550	531.4-541.0	9.6	8.80	91.7	
36R	30 July	1700	541.0-550.7	9.7	8.78	90.5	
37R	30 July	1810	550.7-560.3	9.6	6.28	65.4	
38R	30 July	1925	560.3-570.0	9.7	8.28	85.4	
39R	30 July	2045	570.0-579.6	9.6	8.42	87.7	
40R	30 July	2155	579.6-589.2	9.6	5.84	60.8	
41R	30 July	2310	589.2-598.8	9.6	8.39	87.4	
42R	31 July	0055	598.8-608.4	9.6	9.45	98.4	
43R	31 July	0235	608.4-618.0	9.6	9.25	96.4	
44R	31 July	0405	618.0-627.6	9.6	8.83	92.0	
45R	31 July	0555	627.6-637.2	9.6	8.81	91.8	
46R	31 July	0755	637.2-646.8	9.6	9.05	94.3	
47R	31 July	0920	646.8-656.4	9.6	8.53	88.9	
48R	31 July	1055	656.4-666.0	9.6	6.97	72.6	
49R	31 July	1240	666.0-675.6	9.6	1.95	20.3	
50R	31 July	1355	675.6-685.3	9.7	6.25	64.4	
51R	31 July	1500	685.3-695.0	9.7	2.98	30.7	
52R	31 July	1555	695.0-704.7	9.7	0.64	6.6	

Table T1 (continued).

Core	Date (1998)	Time (UTC +10 hr)	Depth (mbsf)	Length cored (m)	Length recovered (m)	Recovery (%)	Comment
53R	31 July	1715	704.7-714.4	9.7	2.82	29.1	
54R	31 July	1835	714.4-724.1	9.7	1.62	16.7	
55R	31 July	1950	724.1-733.8	9.7	3.02	31.1	
56R	31 July	2120	733.8-743.5	9.7	6.98	72.0	
57R	31 July	2300	743.5-753.1	9.6	6.38	66.5	
58R	1 Aug	0055	753.1-762.7	9.6	9.07	94.5	
59R	1 Aug	0245	762.7-772.3	9.6	7.82	81.5	
60R	1 Aug	0435	772.3-781.9	9.6	2.27	23.7	
61R	1 Aug	0600	781.9-791.5	9.6	3.72	38.8	
62R	1 Aug	0730	791.5-801.1	9.6	4.95	51.6	
63R	1 Aug	0900	801.1-810.7	9.6	5.86	61.0	
64R	1 Aug	1035	810.7-820.3	9.6	2.54	26.5	
65R	1 Aug	1220	820.3-829.9	9.6	8.13	84.7	
66R	1 Aug	1340	829.9-839.6	9.7	6.24	64.3	
67R	1 Aug	1510	839.6-849.3	9.7	6.38	65.8	
68R	1 Aug	1655	849.3-859.0	9.7	5.38	55.5	
69R	1 Aug	1930	859.0-868.7	9.7	3.81	39.3	
70R	2 Aug	0045	868.7-878.4	9.7	2.90	29.9	
71R	2 Aug	0405	878.4-883.2	4.8	0.75	15.6	
72R	2 Aug	0710	883.2-887.9	4.7	0.81	17.2	
73R	2 Aug	1025	887.9-897.5	9.6	1.19	12.4	
74R	2 Aug	1500	897.5-905.6	8.1	2.91	35.9	
75R	2 Aug	1810	905.6-917.0	11.4	2.68	23.5	
76R	2 Aug	2155	917.0-926.6	9.6	2.32	24.2	
Coring totals:				721.6	466.21	64.6	
Drilled total:				205.0			
Total:				926.6			

Note: UTC = Universal Time Coordinated.

Table T2. Site 1118 Coring summary by section. (Continued on next twelve pages.)

Core	Date (1998)	Time (UTC +10 hr)	Core depth (mbsf) Top	Bottom	Length (m) Cored	Recovered	Recovery (%)	Section	Length (m) Liner	Curated	Section depth (mbsf) Top	Bottom	Catwalk samples	Comment
180-1118A														
Drilled without coring.			0.0	205.0										Drilled interval
1R	29 July	0405	205.0	214.4	9.4	0.02	0.2							All to paleontology lab
								CC	0.02	0.02	205.00	205.02	PAL	
									0.02	0.02				
2R	29 July	0450	214.4	224.1	9.7	0.04	0.4							
								CC	0.04	0.12	214.40	214.52	HS, PAL	
									0.04	0.12				
3R	29 July	0545	224.1	233.7	9.6	0.21	2.2							
								CC	0.21	0.21	224.10	224.31	HS, PAL	
									0.21	0.21				
4R	29 July	0620	233.7	243.3	9.6	0.27	2.8							
								CC	0.27	0.27	233.70	233.97	HS, PAL	
									0.27	0.27				
5R	29 July	0705	243.3	252.9	9.6	0.40	4.2							
								CC	0.40	0.40	243.30	243.70	PAL, HS	
									0.40	0.40				
6R	29 July	0800	252.9	262.5	9.6	9.11	94.9							
								1	1.00	1.00	252.90	253.90		
								2	1.06	1.06	253.90	254.96	WRSCR	
								3	1.45	1.45	254.96	256.41		
								4	1.50	1.50	256.41	257.91	IW	
								5	1.45	1.45	257.91	259.36	HS	
								6	1.50	1.50	259.36	260.86		
								7	1.03	1.03	260.86	261.89		
								CC	0.12	0.12	261.89	262.01	PAL	
									9.11	9.11				
7R	29 July	0900	262.5	272.1	9.6	3.59	37.4							
								1	1.08	1.08	262.50	263.58		
								2	1.50	1.50	263.58	265.08	HS	
								3	0.84	0.84	265.08	265.92		
								CC	0.17	0.17	265.92	266.09	PAL	
									3.59	3.59				
8R	29 July	0945	272.1	281.7	9.6	8.36	87.1							
								1	1.50	1.50	272.10	273.60		
								2	1.50	1.50	273.60	275.10		
								3	1.50	1.50	275.10	276.60		
								4	1.50	1.50	276.60	278.10	IW	
								5	1.50	1.50	278.10	279.60	HS	
								6	0.64	0.64	279.60	280.24		
								CC	0.22	0.22	280.24	280.46	PAL	
									8.36	8.36				
9R	29 July	1045	281.7	291.4	9.7	6.91	71.2							
								1	1.50	1.50	281.70	283.20		
								2	1.50	1.50	283.20	284.70	HS	
								3	1.50	1.50	284.70	286.20		
								4	1.50	1.50	286.20	287.70		
								5	0.72	0.72	287.70	288.42		

Table T2 (continued).

Core	Date (1998)	Time (UTC +10 hr)	Core depth (mbsf) Top	Core depth (mbsf) Bottom	Length (m) Cored	Length (m) Recovered	Recovery (%)	Section	Length (m) Liner	Length (m) Curated	Section depth (mbsf) Top	Section depth (mbsf) Bottom	Catwalk samples	Comment
								CC	0.19	0.19	288.42	288.61	PAL	
									6.91	6.91				
10R	29 July	1140	291.4	301.0	9.6	6.02	62.7							
								1	1.50	1.50	291.40	292.90	HS	
								2	1.50	1.50	292.90	294.40	IW	
								3	1.50	1.50	294.40	295.90		
								4	1.37	1.37	295.90	297.27		
								CC	0.15	0.15	297.27	297.42	PAL	
									6.02	6.02				
11R	29 July	1225	301.0	310.7	9.7	8.83	91.0							
								1	1.39	1.39	301.00	302.39		
								2	1.48	1.48	302.39	303.87		
								3	1.23	1.23	303.87	305.10	HS	
								4	1.27	1.27	305.10	306.37		
								5	1.29	1.29	306.37	307.66		
								6	1.48	1.48	307.66	309.14		
								7	0.39	0.39	309.14	309.53		
								CC	0.30	0.30	309.53	309.83	PAL	
									8.83	8.83				
12R	29 July	1315	310.7	320.3	9.6	9.10	94.8							
								1	1.06	1.06	310.70	311.76		
								2	1.46	1.46	311.76	313.22		
								3	1.21	1.21	313.22	314.43	IW	
								4	1.50	1.50	314.43	315.93	HS	
								5	1.50	1.50	315.93	317.43		
								6	1.41	1.41	317.43	318.84		
								7	0.75	0.75	318.84	319.59		
								CC	0.21	0.21	319.59	319.80	PAL	
									9.10	9.10				
13R	29 July	1405	320.3	330.0	9.7	9.55	98.5							
								1	1.50	1.50	320.30	321.80		
								2	1.47	1.47	321.80	323.27		
								3	1.50	1.50	323.27	324.77		
								4	1.50	1.50	324.77	326.27	HS	
								5	1.50	1.50	326.27	327.77		
								6	1.50	1.50	327.77	329.27		
								7	0.58	0.58	329.27	329.85	PAL	
									9.55	9.55				
14R	29 July	1450	330.0	339.7	9.7	9.89	102.0							
								1	1.50	1.50	330.00	331.50		
								2	1.14	1.14	331.50	332.64		
								3	1.15	1.15	332.64	333.79		
								4	1.41	1.41	333.79	335.20	IW	
								5	1.40	1.40	335.20	336.60	HS	
								6	1.10	1.10	336.60	337.70		
								7	1.15	1.15	337.70	338.85		
								8	0.78	0.78	338.85	339.63		
								CC	0.26	0.26	339.63	339.89	PAL	
									9.89	9.89				

Table T2 (continued).

Core	Date (1998)	Time (UTC +10 hr)	Core depth (mbsf) Top	Bottom	Length (m) Cored	Recovered	Recovery (%)	Section	Length (m) Liner	Curated	Section depth (mbsf) Top	Bottom	Catwalk samples	Comment
15R	29 July	1540	339.7	349.3	9.6	9.24	96.3							
								1	0.85	0.85	339.70	340.55		
								2	0.89	0.89	340.55	341.44	WRSCR	
								3	1.50	1.50	341.44	342.94		
								4	1.50	1.50	342.94	344.44		
								5	1.42	1.42	344.44	345.86		
								6	1.50	1.50	345.86	347.36		
								7	1.32	1.32	347.36	348.68	HS	
								CC	0.26	0.26	348.68	348.94	PAL	
									9.24	9.24				
16R	29 July	1640	349.3	358.8	9.5	8.80	92.6							
								1	1.40	1.40	349.30	350.70		
								2	1.50	1.50	350.70	352.20		
								3	1.31	1.31	352.20	353.51		
								4	1.50	1.50	353.51	355.01		
								5	1.01	1.01	355.01	356.02	IW	
								6	1.12	1.12	356.02	357.14	HS	
								7	0.77	0.77	357.14	357.91		
								CC	0.19	0.19	357.91	358.10	PAL	
									8.80	8.80				
17R	29 July	1740	358.8	368.2	9.4	8.40	89.4							
								1	1.22	1.22	358.80	360.02		
								2	1.34	1.34	360.02	361.36		
								3	1.50	1.50	361.36	362.86	HS	
								4	1.50	1.50	362.86	364.36		
								5	1.50	1.50	364.36	365.86		
								6	1.34	1.34	365.86	367.20	PAL	
									8.40	8.40				
18R	29 July	1840	368.2	377.8	9.6	6.29	65.5							
								1	1.50	1.50	368.20	369.70		
								2	1.37	1.37	369.70	371.07	IW	
								3	1.41	1.41	371.07	372.48	HS	
								4	1.00	1.00	372.48	373.48		
								5	0.81	0.81	373.48	374.29		
								CC	0.20	0.20	374.29	374.49	PAL	
									6.29	6.29				
19R	29 July	1930	377.8	387.4	9.6	6.42	66.9							
								1	1.40	1.40	377.80	379.20		
								2	1.50	1.50	379.20	380.70		
								3	1.46	1.46	380.70	382.16	HS	
								4	1.50	1.50	382.16	383.66		
								5	0.34	0.34	383.66	384.00		
								CC	0.22	0.22	384.00	384.22	PAL	
									6.42	6.42				
20R	29 July	2025	387.4	396.8	9.4	9.37	99.7							
								1	1.38	1.38	387.40	388.78		
								2	1.44	1.44	388.78	390.22		
								3	1.38	1.38	390.22	391.60		

Table T2 (continued).

Core	Date (1998)	Time (UTC +10 hr)	Core depth (mbsf) Top	Bottom	Length (m) Cored	Recovered	Recovery (%)	Section	Length (m) Liner	Curated	Section depth (mbsf) Top	Bottom	Catwalk samples	Comment
								4	1.45	1.45	391.60	393.05		
								5	1.36	1.36	393.05	394.41		
								6	1.46	1.46	394.41	395.87	HS, IW	
								7	0.70	0.70	395.87	396.57		
								CC	0.20	0.20	396.57	396.77	PAL	
									9.37	9.37				
21R	29 July	2120	396.8	406.3	9.5	7.38	77.7							
								1	1.36	1.36	396.80	398.16		
								2	1.50	1.50	398.16	399.66		
								3	1.50	1.50	399.66	401.16		
								4	1.47	1.47	401.16	402.63		
								5	1.29	1.29	402.63	403.92	HS	
								CC	0.26	0.26	403.92	404.18	PAL	
									7.38	7.38				
22R	29 July	2230	406.3	415.9	9.6	8.83	92.0							
								1	1.39	1.39	406.30	407.69		
								2	1.36	1.36	407.69	409.05		
								3	1.50	1.50	409.05	410.55	HS	
								4	1.38	1.38	410.55	411.93		
								5	1.23	1.23	411.93	413.16	IW	
								6	1.34	1.34	413.16	414.50		
								7	0.42	0.42	414.50	414.92		
								CC	0.21	0.21	414.92	415.13	PAL	
									8.83	8.83				
23R	29 July	2340	415.9	425.6	9.7	7.89	81.3							
								1	1.50	1.50	415.90	417.40		
								2	1.39	1.39	417.40	418.79		
								3	1.24	1.24	418.79	420.03	HS	
								4	1.50	1.50	420.03	421.53		
								5	1.50	1.50	421.53	423.03		
								6	0.50	0.50	423.03	423.53		
								CC	0.26	0.26	423.53	423.79	PAL	
									7.89	7.89				
24R	30 July	0100	425.6	435.2	9.6	9.44	98.3							
								1	1.46	1.46	425.60	427.06	IW	
								2	1.45	1.45	427.06	428.51	HS	
								3	1.47	1.47	428.51	429.98		
								4	1.20	1.20	429.98	431.18		
								5	1.42	1.42	431.18	432.60		
								6	1.43	1.43	432.60	434.03		
								7	0.86	0.86	434.03	434.89		
								CC	0.15	0.15	434.89	435.04	PAL	
									9.44	9.44				
25R	30 July	0220	435.2	444.8	9.6	8.57	89.3							
								1	1.50	1.50	435.20	436.70		
								2	1.28	1.28	436.70	437.98		
								3	1.23	1.23	437.98	439.21	WRSCR	
								4	1.36	1.36	439.21	440.57	HS	

Table T2 (continued).

Core	Date (1998)	Time (UTC +10 hr)	Core depth (mbsf) Top	Core depth (mbsf) Bottom	Length (m) Cored	Length (m) Recovered	Recovery (%)	Section	Length (m) Liner	Length (m) Curated	Section depth (mbsf) Top	Section depth (mbsf) Bottom	Catwalk samples	Comment
								5	1.34	1.34	440.57	441.91		
								6	1.23	1.23	441.91	443.14		
								7	0.49	0.49	443.14	443.63		
								CC	0.14	0.14	443.63	443.77	PAL	
									8.57	8.57				
26R	30 July	0325	444.8	454.4	9.6	5.95	62.0							
								1	1.50	1.50	444.80	446.30		
								2	1.50	1.50	446.30	447.80		
								3	1.19	1.19	447.80	448.99	IW	
								4	1.51	1.51	448.99	450.50	HS	
								CC	0.25	0.25	450.50	450.75	PAL	
									5.95	5.95				
27R	30 July	0510	454.4	463.9	9.5	8.80	92.6							
								1	1.50	1.50	454.40	455.90		
								2	1.37	1.37	455.90	457.27		
								3	1.46	1.46	457.27	458.73		
								4	1.50	1.50	458.73	460.23	HS	
								5	1.45	1.45	460.23	461.68		
								6	1.21	1.21	461.68	462.89		
								CC	0.31	0.31	462.89	463.20	PAL	
									8.80	8.80				
28R	30 July	0635	463.9	473.6	9.7	9.05	93.3							
								1	1.50	1.50	463.90	465.40		
								2	1.46	1.46	465.40	466.86		
								3	1.43	1.43	466.86	468.29		
								4	1.17	1.17	468.29	469.46	IW	
								5	1.39	1.39	469.46	470.85	HS	
								6	1.25	1.25	470.85	472.10		
								7	0.65	0.65	472.10	472.75		
								CC	0.20	0.20	472.75	472.95	PAL	
									9.05	9.05				
29R	30 July	0800	473.6	483.2	9.6	8.96	93.3							
								1	1.47	1.47	473.60	475.07		
								2	1.40	1.40	475.07	476.47		
								3	1.50	1.50	476.47	477.97		
								4	1.27	1.27	477.97	479.24	HS	
								5	1.30	1.30	479.24	480.54		
								6	1.32	1.32	480.54	481.86		
								7	0.56	0.56	481.86	482.42		
								CC	0.14	0.14	482.42	482.56	PAL	
									8.96	8.96				
30R	30 July	0925	483.2	492.9	9.7	9.31	96.0							
								1	1.51	1.51	483.20	484.71		
								2	1.42	1.42	484.71	486.13	IW	
								3	1.47	1.47	486.13	487.60	HS	
								4	1.39	1.39	487.60	488.99		
								5	1.36	1.36	488.99	490.35		
								6	1.22	1.22	490.35	491.57		

Table T2 (continued).

Core	Date (1998)	Time (UTC +10 hr)	Core depth (mbsf) Top	Core depth (mbsf) Bottom	Length (m) Cored	Length (m) Recovered	Recovery (%)	Section	Length (m) Liner	Length (m) Curated	Section depth (mbsf) Top	Section depth (mbsf) Bottom	Catwalk samples	Comment
								7	0.78	0.78	491.57	492.35		
								CC	0.16	0.16	492.35	492.51	PAL	
									9.31	9.31				
31R	30 July	1100	492.9	502.5	9.6	8.70	90.6							
								1	1.44	1.44	492.90	494.34		
								2	1.38	1.38	494.34	495.72		
								3	1.48	1.48	495.72	497.20		
								4	1.42	1.42	497.20	498.62		
								5	1.50	1.50	498.62	500.12		
								6	1.30	1.30	500.12	501.42	HS	
								CC	0.18	0.18	501.42	501.60	PAL	
									8.70	8.70				
32R	30 July	1205	502.5	512.1	9.6	7.20	75.0							
								1	1.48	1.48	502.50	503.98		
								2	1.41	1.41	503.98	505.39	IW	
								3	1.50	1.50	505.39	506.89	HS, WEL	
								4	1.46	1.46	506.89	508.35		
								5	1.25	1.25	508.35	509.60		
								CC	0.10	0.10	509.60	509.70	PAL	
									7.20	7.20				
33R	30 July	1320	512.1	521.8	9.7	9.04	93.2							
								1	1.27	1.27	512.10	513.37		
								2	1.48	1.48	513.37	514.85		
								3	1.43	1.43	514.85	516.28		
								4	1.48	1.48	516.28	517.76		
								5	1.50	1.50	517.76	519.26		
								6	1.06	1.06	519.26	520.32	HS	
								7	0.59	0.59	520.32	520.91		
								CC	0.23	0.23	520.91	521.14	PAL	
									9.04	9.04				
34R	30 July	1435	521.8	531.4	9.6	8.22	85.6							
								1	1.34	1.34	521.80	523.14		
								2	1.37	1.37	523.14	524.51		
								3	1.31	1.31	524.51	525.82	IW	
								4	1.27	1.27	525.82	527.09	HS	
								5	1.40	1.40	527.09	528.49		
								6	1.31	1.31	528.49	529.80		
								CC	0.22	0.22	529.80	530.02	PAL	
									8.22	8.22				
35R	30 July	1550	531.4	541.0	9.6	8.80	91.7							
								1	1.43	1.43	531.40	532.83		
								2	0.92	0.92	532.83	533.75		
								3	0.86	0.86	533.75	534.61	WRSCR	
								4	1.40	1.40	534.61	536.01		
								5	1.46	1.46	536.01	537.47	HS	
								6	1.07	1.07	537.47	538.54		
								7	1.39	1.39	538.54	539.93		

Table T2 (continued).

Core	Date (1998)	Time (UTC +10 hr)	Core depth (mbsf)		Length (m)		Recovery (%)	Section	Length (m)		Section depth (mbsf)		Catwalk samples	Comment
			Top	Bottom	Cored	Recovered			Liner	Curated	Top	Bottom		
								CC	0.27	0.27	539.93	540.20	PAL	
									8.80	8.80				
36R	30 July	1700	541.0	550.7	9.7	8.78	90.5							
								1	1.19	1.19	541.00	542.19		
								2	1.45	1.45	542.19	543.64	IW	
								3	1.31	1.31	543.64	544.95	HS	
								4	1.48	1.48	544.95	546.43		
								5	1.15	1.15	546.43	547.58		
								6	1.45	1.45	547.58	549.03		
								7	0.55	0.55	549.03	549.58		
								CC	0.20	0.20	549.58	549.78	PAL	
									8.78	8.78				
37R	30 July	1810	550.7	560.3	9.6	6.28	65.4							
								1	1.44	1.44	550.70	552.14		
								2	1.34	1.34	552.14	553.48	HS	
								3	1.48	1.48	553.48	554.96		
								4	1.34	1.34	554.96	556.30		
								5	0.47	0.47	556.30	556.77		
								CC	0.21	0.21	556.77	556.98	PAL	
									6.28	6.28				
38R	30 July	1925	560.3	570.0	9.7	8.28	85.4							
								1	1.40	1.40	560.30	561.70		
								2	1.42	1.42	561.70	563.12		
								3	1.43	1.43	563.12	564.55	HS	
								4	1.41	1.41	564.55	565.96		
								5	1.43	1.43	565.96	567.39		
								6	0.95	0.95	567.39	568.34		
								CC	0.24	0.24	568.34	568.58	PAL	
									8.28	8.28				
39R	30 July	2045	570.0	579.6	9.6	8.42	87.7							
								1	1.50	1.50	570.00	571.50	IW	
								2	1.25	1.25	571.50	572.75	HS	
								3	1.38	1.38	572.75	574.13		
								4	1.36	1.36	574.13	575.49		
								5	1.43	1.43	575.49	576.92		
								6	1.33	1.33	576.92	578.25		
								CC	0.17	0.17	578.25	578.42	PAL	
									8.42	8.42				
40R	30 July	2155	579.6	589.2	9.6	5.84	60.8							
								1	1.35	1.35	579.60	580.95		
								2	1.27	1.27	580.95	582.22		
								3	1.50	1.50	582.22	583.72		
								4	1.46	1.46	583.72	585.18	HS	
								CC	0.26	0.26	585.18	585.44	PAL	
									5.84	5.84				
41R	30 July	2310	589.2	598.8	9.6	8.39	87.4							
								1	1.36	1.36	589.20	590.56		
								2	1.36	1.36	590.56	591.92		

Core	Date (1998)	Time (UTC +10 hr)	Core depth (mbsf) Top	Core depth (mbsf) Bottom	Length (m) Cored	Length (m) Recovered	Recovery (%)	Section	Length (m) Liner	Length (m) Curated	Section depth (mbsf) Top	Section depth (mbsf) Bottom	Catwalk samples	Comment
								3	1.45	1.45	591.92	593.37		
								4	1.44	1.44	593.37	594.81	HS	
								5	1.50	1.50	594.81	596.31		
								6	0.99	0.99	596.31	597.30		
								CC	0.29	0.29	597.30	597.59	PAL	
									8.39	8.39				
42R	31 July	0055	598.8	608.4	9.6	9.45	98.4							
								1	1.23	1.23	598.80	600.03		
								2	1.28	1.28	600.03	601.31		
								3	1.26	1.26	601.31	602.57		
								4	1.10	1.10	602.57	603.67	IW	
								5	1.18	1.18	603.67	604.85	HS, WEL	
								6	1.33	1.33	604.85	606.18		
								7	1.18	1.18	606.18	607.36		
								8	0.72	0.72	607.36	608.08		
								CC	0.17	0.17	608.08	608.25	PAL	
									9.45	9.45				
43R	31 July	0235	608.4	618.0	9.6	9.25	96.4							
								1	1.15	1.15	608.40	609.55	HS	
								2	1.46	1.46	609.55	611.01		
								3	1.40	1.40	611.01	612.41		
								4	1.33	1.33	612.41	613.74		
								5	1.28	1.28	613.74	615.02		
								6	1.25	1.25	615.02	616.27		
								7	1.10	1.10	616.27	617.37		
								CC	0.28	0.28	617.37	617.65	PAL	
									9.25	9.25				
44R	31 July	0405	618.0	627.6	9.6	8.83	92.0							
								1	1.50	1.50	618.00	619.50	HS	
								2	1.35	1.35	619.50	620.85		
								3	1.31	1.31	620.85	622.16		
								4	1.30	1.30	622.16	623.46		
								5	1.29	1.29	623.46	624.75		
								6	1.10	1.10	624.75	625.85		
								7	0.45	0.45	625.85	626.30		
								CC	0.53	0.53	626.30	626.83	PAL	
									8.83	8.83				
45R	31 July	0555	627.6	637.2	9.6	8.81	91.8							
								1	1.35	1.35	627.60	628.95		
								2	1.31	1.31	628.95	630.26		
								3	1.18	1.18	630.26	631.44		
								4	1.47	1.47	631.44	632.91		
								5	0.73	0.73	632.91	633.64	WRSCR	
								6	1.02	1.02	633.64	634.66	IW	
								7	0.90	0.90	634.66	635.56	HS	
								8	0.69	0.69	635.56	636.25		
								CC	0.16	0.16	636.25	636.41	PAL	
									8.81	8.81				

Table T2 (continued).

Core	Date (1998)	Time (UTC +10 hr)	Core depth (mbsf) Top	Bottom	Length (m) Cored	Recovered	Recovery (%)	Section	Length (m) Liner	Curated	Section depth (mbsf) Top	Bottom	Catwalk samples	Comment
46R	31 July	0755	637.2	646.8	9.6	9.05	94.3							
								1	1.46	1.46	637.20	638.66		
								2	1.43	1.43	638.66	640.09		
								3	1.45	1.45	640.09	641.54		
								4	1.22	1.22	641.54	642.76		
								5	1.33	1.33	642.76	644.09		
								6	1.30	1.30	644.09	645.39		
								7	0.68	0.68	645.39	646.07	HS	
								CC	0.18	0.18	646.07	646.25	PAL	
									9.05	9.05				
47R	31 July	0920	646.8	656.4	9.6	8.53	88.9							
								1	1.48	1.48	646.80	648.28		
								2	1.37	1.37	648.28	649.65		
								3	1.48	1.48	649.65	651.13		
								4	1.28	1.28	651.13	652.41		
								5	1.25	1.25	652.41	653.66		
								6	1.44	1.44	653.66	655.10	HS	
								CC	0.23	0.23	655.10	655.33	PAL	
									8.53	8.53				
48R	31 July	1055	656.4	666.0	9.6	6.97	72.6							
								1	1.39	1.39	656.40	657.79		
								2	1.50	1.50	657.79	659.29		
								3	1.22	1.22	659.29	660.51	IW	
								4	1.38	1.38	660.51	661.89	HS, WEL	
								5	1.15	1.15	661.89	663.04		
								CC	0.33	0.33	663.04	663.37	PAL	
									6.97	6.97				
49R	31 July	1240	666.0	675.6	9.6	1.95	20.3							
								1	1.20	1.20	666.00	667.20		
								2	0.53	0.53	667.20	667.73	HS	
								CC	0.22	0.22	667.73	667.95	PAL	
									1.95	1.95				
50R	31 July	1355	675.6	685.3	9.7	6.25	64.4							
								1	1.24	1.24	675.60	676.84		
								2	1.36	1.36	676.84	678.20		
								3	1.07	1.07	678.20	679.27	HS	
								4	1.37	1.37	679.27	680.64		
								5	0.94	0.94	680.64	681.58		
								CC	0.27	0.27	681.58	681.85	PAL	
									6.25	6.25				
51R	31 July	1500	685.3	695.0	9.7	2.98	30.7							
								1	0.89	0.89	685.30	686.19	IW	
								2	1.30	1.30	686.19	687.49	HS	
								3	0.67	0.67	687.49	688.16		
								CC	0.12	0.12	688.16	688.28	PAL	
									2.98	2.98				
52R	31 July	1555	695.0	704.7	9.7	0.64	6.6							
								1	0.44	0.44	695.00	695.44	HS	

Table T2 (continued).

Core	Date (1998)	Time (UTC +10 hr)	Core depth (mbsf) Top	Bottom	Length (m) Cored	Recovered	Recovery (%)	Section	Length (m) Liner	Curated	Section depth (mbsf) Top	Bottom	Catwalk samples	Comment
								CC	0.20	0.20	695.44	695.64	PAL	
									0.64	0.64				
53R	31 July	1715	704.7	714.4	9.7	2.82	29.1							
								1	1.40	1.40	704.70	706.10	HS	
								2	1.08	1.08	706.10	707.18		
								CC	0.34	0.34	707.18	707.52	PAL	
									2.82	2.82				
54R	31 July	1835	714.4	724.1	9.7	1.62	16.7							
								1	1.42	1.42	714.40	715.82	HS	
								CC	0.20	0.20	715.82	716.02	PAL	
									1.62	1.62				
55R	31 July	1950	724.1	733.8	9.7	3.02	31.1							
								1	0.87	0.87	724.10	724.97	IW, WEL	
								2	1.25	1.25	724.97	726.22	HS	
								3	0.54	0.54	726.22	726.76		
								CC	0.36	0.36	726.76	727.12	PAL	
									3.02	3.02				
56R	31 July	2120	733.8	743.5	9.7	6.98	72.0							
								1	1.50	1.50	733.80	735.30	HS	
								2	1.47	1.47	735.30	736.77		
								3	0.93	0.93	736.77	737.70	WRSCR	
								4	1.45	1.45	737.70	739.15		
								5	1.18	1.18	739.15	740.33		
								CC	0.45	0.45	740.33	740.78	PAL	
									6.98	6.98				
57R	31 July	2300	743.5	753.1	9.6	6.38	66.5							
								1	1.32	1.32	743.50	744.82		
								2	1.35	1.35	744.82	746.17		
								3	1.47	1.47	746.17	747.64		
								4	1.12	1.12	747.64	748.76	HS	
								5	0.89	0.89	748.76	749.65		
								CC	0.23	0.23	749.65	749.88	PAL	
									6.38	6.38				
58R	1 August	0055	753.1	762.7	9.6	9.07	94.5							
								1	1.34	1.34	753.10	754.44		
								2	1.23	1.23	754.44	755.67		
								3	1.14	1.14	755.67	756.81		
								4	1.50	1.50	756.81	758.31	IW	
								5	1.50	1.50	758.31	759.81	HS, WEL	
								6	1.50	1.50	759.81	761.31		
								7	0.49	0.49	761.31	761.80		
								CC	0.37	0.37	761.80	762.17	PAL	
									9.07	9.07				
59R	1 August	0245	762.7	772.3	9.6	7.82	81.5							
								1	1.29	1.29	762.70	763.99		
								2	1.32	1.35	763.99	765.34	HS	
								3	1.46	1.46	765.34	766.80		
								4	1.32	1.32	766.80	768.12		

Table T2 (continued).

Core	Date (1998)	Time (UTC +10 hr)	Core depth (mbsf) Top	Core depth (mbsf) Bottom	Length (m) Cored	Length (m) Recovered	Recovery (%)	Section	Length (m) Liner	Length (m) Curated	Section depth (mbsf) Top	Section depth (mbsf) Bottom	Catwalk samples	Comment
								5	1.50	1.50	768.12	769.62		
								6	0.69	0.69	769.62	770.31		
								CC	0.24	0.24	770.31	770.55	PAL	
									7.82	7.85				
60R	1 August	0435	772.3	781.9	9.6	2.27	23.6							
								1	1.36	1.36	772.30	773.66	HS	
								2	0.81	0.81	773.66	774.47		
								CC	0.10	0.10	774.47	774.57	PAL	
									2.27	2.27				
61R	1 August	0600	781.9	791.5	9.6	3.72	38.8							
								1	1.28	1.28	781.90	783.18	IW, WEL	
								2	1.28	1.28	783.18	784.46	HS	
								3	0.98	0.98	784.46	785.44		
								CC	0.18	0.18	785.44	785.62	PAL	
									3.72	3.72				
62R	1 August	0730	791.5	801.1	9.6	4.95	51.6							
								1	1.45	1.45	791.50	792.95		
								2	1.17	1.17	792.95	794.12		
								3	1.38	1.38	794.12	795.50		
								4	0.78	0.78	795.50	796.28	HS	
								CC	0.17	0.17	796.28	796.45	PAL	
									4.95	4.95				
63R	1 August	0900	801.1	810.7	9.6	5.86	61.0							
								1	1.18	1.18	801.10	802.28		
								2	1.36	1.36	802.28	803.64		
								3	0.73	0.73	803.64	804.37		
								4	1.13	1.13	804.37	805.50	WRSCR	
								5	1.21	1.21	805.50	806.71	HS	
								CC	0.25	0.25	806.71	806.96	PAL	
									5.86	5.86				
64R	1 August	1035	810.7	820.3	9.6	2.54	26.5							
								1	1.50	1.50	810.70	812.20	IW, HS	
								2	0.76	0.76	812.20	812.96	WEL	
								CC	0.28	0.28	812.96	813.24	PAL	
									2.54	2.54				
65R	1 August	1220	820.3	829.9	9.6	8.13	84.7							
								1	1.43	1.43	820.30	821.73		
								2	1.33	1.33	821.73	823.06	HS	
								3	1.32	1.32	823.06	824.38		
								4	1.30	1.30	824.38	825.68		
								5	1.50	1.50	825.68	827.18		
								6	0.95	0.95	827.18	828.13		
								CC	0.30	0.30	828.13	828.43	PAL	
									8.13	8.13				
66R	1 August	1340	829.9	839.6	9.7	6.24	64.3							
								1	1.50	1.50	829.90	831.40		
								2	1.34	1.34	831.40	832.74		
								3	1.36	1.36	832.74	834.10		

Table T2 (continued).

Core	Date (1998)	Time (UTC +10 hr)	Core depth (mbsf) Top	Core depth (mbsf) Bottom	Length (m) Cored	Length (m) Recovered	Recovery (%)	Section	Length (m) Liner	Length (m) Curated	Section depth (mbsf) Top	Section depth (mbsf) Bottom	Catwalk samples	Comment
								4	1.50	1.50	834.10	835.60		
								5	0.24	0.24	835.60	835.84	HS	
								CC	0.30	0.30	835.84	836.14	PAL	
									6.24	6.24				
67R	1 August	1510	839.6	849.3	9.7	6.38	65.8							
								1	1.29	1.29	839.60	840.89		
								2	1.50	1.50	840.89	842.39	HS, IW, WEL	
								3	1.50	1.50	842.39	843.89		
								4	0.84	0.84	843.89	844.73		
								5	0.77	0.77	844.73	845.50		
								CC	0.48	0.48	845.50	845.98	PAL	
									6.38	6.38				
68R	1 August	1655	849.3	859.0	9.7	5.38	55.5							
								1	1.45	1.45	849.30	850.75	HS, PAL	
								2	1.31	1.31	850.75	852.06		
								3	1.50	1.50	852.06	853.56		
								4	0.97	0.97	853.56	854.53		
								CC	0.15	0.15	854.53	854.68	PAL	
									5.38	5.38				
69R	1 August	1930	859.0	868.7	9.7	3.81	39.3							
								1	1.50	1.50	859.00	860.50		
								2	1.47	1.47	860.50	861.97		
								3	0.65	0.65	861.97	862.62		
								CC	0.19	0.19	862.62	862.81	PAL	
									3.81	3.81				
70R	2 August	0045	868.7	878.4	9.7	2.90	29.9							
								1	1.44	1.41	868.70	870.11	WRSCR	
								2	1.20	1.14	870.11	871.25		
								3	0.26	1.30	871.25	872.55	PAL	
									2.90	3.85				
71R	1 August	0405	878.4	883.2	4.8	0.75	15.6							
								1	0.75	1.28	878.40	879.68		
									0.75	1.28				
72R	2 August	0710	883.2	887.9	4.7	0.81	17.2							
								1	0.81	1.28	883.20	884.48	PAL	
									0.81	1.28				
73R	2 August	1025	887.9	897.5	9.6	1.19	12.4							
								1	1.02	1.50	887.90	889.40	HS	
								2	0.17	0.04	889.40	889.44		
									1.19	1.54				
74R	2 August	1500	897.5	905.6	8.1	2.91	35.9							
								1	1.14	1.44	897.50	898.94		
								2	0.86	1.50	898.94	900.44		
								3	0.91	0.89	900.44	901.33	PAL	
									2.91	3.83				
75R	2 August	1810	905.6	917.0	11.4	2.68	23.5							
								1	1.50	1.50	905.60	907.10		
								2	1.18	1.50	907.10	908.60		

Table T2 (continued).

Core	Date (1998)	Time (UTC +10 hr)	Core depth (mbsf) Top	Core depth (mbsf) Bottom	Length (m) Cored	Length (m) Recovered	Recovery (%)	Section	Length (m) Liner	Length (m) Curated	Section depth (mbsf) Top	Section depth (mbsf) Bottom	Catwalk samples	Comment
								3	0.00	1.13	908.60	909.73		
									2.68	4.13				
76R	2 August	2155	917.0	926.6	9.6	2.32	24.2							
								1	1.50	1.34	917.00	918.34		
								2	0.82	1.50	918.34	919.84		
									2.32	2.84				
				Totals:	721.6	466.21	64.6							

Note: PAL = paleontology; HS = headspace; WRSCR = whole round Screaton; IW = interstitial water; Wel = Wellsbury microbiology.

Table T3. Results of X-ray diffraction analysis of bulk fine-grained sediments, Site 1118. (Continued on next page.)

Core, section, interval (cm)	Depth (mbsf)	Description	XRD identification: major (minor) minerals
180-1118A-			
3R-CC, 4-6	224.14	Silty claystone	Plagioclase, calcite, pyroxene, quartz (illite, amphibole)
4R-CC, 9-11	233.79	Clayey siltstone	Quartz, plagioclase, calcite (pyroxene, k-feldspar, chlorite, chlorite mixed layer, illite, amphibole, pyrite)
5R-CC, 22-23	243.52	Sandstone	Plagioclase, quartz, calcite, pyroxene (chlorite mixed layer, illite, amphibole)
6R-3, 69.5-70	255.65	Volcaniclastic siltstone and claystone	Plagioclase, quartz, calcite, pyroxene, chlorite mixed layer (illite, smectite?, amphibole, pyrite)
7R-3, 25-26	265.33	Silty claystone	Calcite (plagioclase, quartz)
8R-5, 118-120	279.28	Silty claystone	Plagioclase, quartz, calcite, pyroxene (chlorite, smectite?, illite, pyrite)
9R-1, 29.5-30	281.99	Claystone	Plagioclase, quartz, calcite (pyroxene, chlorite mixed layer, smectite?, illite, pyrite)
10R-3, 39-40	294.79	Silty claystone	Plagioclase, calcite (quartz, pyroxene)
11R-1, 11-13	301.11	Clayey siltstone	Plagioclase, calcite (quartz, pyroxene)
13R-1, 6-8	320.36	Silty claystone	Plagioclase (calcite, biotite, quartz, pyroxene)
13R-1, 15-16	320.45	Silty claystone	Plagioclase (quartz)
13R-3, 64-65	232.91	Silty claystone/clayey siltstone	Plagioclase, calcite, quartz (chlorite, smectite?, pyrite)
15R-1, 11-13	339.81	Clayey siltstone	Plagioclase, calcite, pyroxene (dolomite, biotite, illite, chlorite)
16R-4, 29-30	353.80	Silty claystone/calcareous siltstone	Plagioclase, calcite, quartz (chlorite, smectite?, illite, amphibole)
17R-1, 42-44 cm	359.22	Silty claystone	Plagioclase, quartz, calcite, pyroxene (illite, chlorite, pyrite)
18R-3, 137-138	372.44	Silty claystone	Plagioclase, quartz, calcite, pyroxene (illite, chlorite, amphibole, pyrite)
19R-1, 137-138	379.17	Silty claystone	Plagioclase, quartz, pyroxene (calcite, illite, chlorite mixed layer?, amphibole, pyrite)
21R-1, 76-78	397.56	Silty claystone	Plagioclase, quartz, calcite, pyroxene (illite, chlorite, pyrite)
22R-1, 22-23	406.52	Silty claystone	Plagioclase, quartz, pyroxene, amphibole (illite, pyrite)
22R-3, 83-84	409.88	Clayey siltstone	Calcite, plagioclase, quartz, illite, chlorite
23R-5, 79-81	422.32	Silty claystone	Plagioclase, quartz, calcite, pyroxene, illite (chlorite)
24R-1, 32-34	425.92	Clayey siltstone/claystone	Plagioclase, quartz, calcite (chlorite, illite, pyrite)
25R-1, 16-18	435.36	Clayey siltstone/claystone	Plagioclase, calcite, quartz, pyroxene (illite, chlorite, smectite?, pyrite)
25R-6, 111-113	443.02	Silty claystone/clayey siltstone	Plagioclase, illite, quartz, calcite (pyroxene, amphibole)
26R-1, 14-16	444.94	Clayey siltstone	Plagioclase, calcite, quartz (illite, amphibole, pyrite)
27R-4, 68-69	459.41	Silty claystone/clayey siltstone	Plagioclase, calcite, quartz (pyroxene, illite, chlorite, amphibole, pyrite)
28R-4, 102-106	469.31	Siltstone/silty claystone	Plagioclase, quartz, illite (calcite, amphibole, pyroxene, pyrite)
29R-4, 80-81	478.77	Clayey siltstone	Quartz, plagioclase, calcite (chlorite, pyroxene, illite)
30R-3, 85-86	486.98	Clayey siltstone	Plagioclase, calcite, quartz (illite, chlorite, pyrite)
31R-CC, 10-11	501.52	Silty claystone	Plagioclase, quartz, calcite (pyroxene, amphibole, chlorite, illite, pyrite)
32R-3, 36-39	505.75	Silty claystone	Plagioclase, calcite, quartz (illite, smectite?, chlorite, pyroxene, amphibole)
33R-3, 56-60	515.41	Silty claystone	Plagioclase, quartz, calcite (illite, chlorite)
34R-1, 4-5	521.84	Siltstone	Plagioclase, quartz, calcite, pyroxene (smectite?, illite, chlorite)
34R-2, 93-95	524.07	Claystone	Plagioclase, quartz, calcite (chlorite, smectite?)
34R-3, 36-38	524.87	Claystone	Plagioclase, quartz, calcite (pyroxene, chlorite, smectite?, pyrite)
35R-1, 12-13	531.52	Silty claystone	Plagioclase, quartz, calcite (pyroxene, chlorite, smectite?, pyrite)
36R-4, 25-27	545.20	Siltstone-claystone	Quartz, plagioclase, calcite, pyroxene (pyrite, chlorite, illite, smectite?, amphibole)
36R-7, 5-7	549.08	Silty claystone	Plagioclase, calcite, quartz (chlorite, illite, amphibole, pyrite)
37R-5, 2-3	556.32	Siltstone	Calcite, plagioclase, quartz (amphibole, chlorite, smectite?)
38R-1, 49-51	560.79	Silty claystone-clayey siltstone	Calcite, plagioclase, quartz (illite, pyrite, amphibole, chlorite, smectite?)
38R-5, 16-19	566.12	Silty claystone-clayey siltstone	Calcite, quartz, plagioclase (chlorite, smectite?, illite)
39R-1, 38-39	570.38	Silty claystone-clayey siltstone	Quartz, plagioclase, calcite (chlorite, smectite?, illite)
40R-3, 42-43	582.64	Silty claystone-clayey siltstone	Calcite (quartz, plagioclase)
41R-5, 35-36	595.16	Siltstone-clayey siltstone	Plagioclase, quartz, illite, calcite (chlorite)
42R-3, 45-46	601.76	Clayey siltstone	Calcite, plagioclase, quartz (illite, amphibole, chlorite, pyrite)
43R-4, 44-45 cm	612.85	Silty claystone	Calcite, plagioclase, quartz (chlorite, illite)
44R-3, 21-23	621.06	Silty claystone	Calcite, plagioclase, quartz, amphibole (pyrite)
45R-2, 70-71	629.65	Claystone	Calcite, plagioclase, quartz (illite, chlorite, amphibole, pyrite)
46R-4, 83.5-85.5	642.37	Clayey siltstone	Calcite, plagioclase, quartz (illite, chlorite, amphibole)
47R-2, 83-85	649.11	Silty claystone	Plagioclase, calcite, quartz (pyroxene, chlorite, smectite?, illite, pyrite)
48R-1, 85-87	657.25	Silty claystone-clayey siltstone	Plagioclase, calcite, quartz (smectite?, illite, amphibole, pyrite)
49R-1, 103-105	667.03	Silty claystone-clayey siltstone	Calcite, quartz, plagioclase (illite)
50R-1, 75-76	676.35	Silty claystone-claystone	Plagioclase, quartz, pyroxene, calcite, illite
51R-3, 33-34	687.82	Sandstone-claystone	Calcite, plagioclase, quartz (illite, pyrite, amphibole)
53R-1, 123-124	705.93	Sandy siltstone	Plagioclase, calcite, quartz (amphibole, illite, pyrite)
55R-2, 12-14	725.09	Sandy siltstone	Calcite, plagioclase, quartz (illite, pyrite)
56R-3, 42-43	737.19	Silty sandstone	Calcite, plagioclase, quartz (pyrite, illite, amphibole)
57R-5, 64-65	749.40	Silty claystone	Calcite, plagioclase, quartz (amphibole, illite, pyrite)
58R-7, 22-24	761.53	Silty claystone	Calcite, plagioclase, quartz (illite, pyrite, amphibole, chlorite)
59R-3, 9-10	765.43	Silty claystone	Calcite, plagioclase, quartz, illite (pyrite, amphibole, chlorite)
59R-4, 24-25	767.04	Volcaniclastic sandstone-claystone	Quartz, plagioclase, illite, actinolite, calcite (pyrite)
60R-2, 10-12	773.76	Silty claystone-clayey siltstone	Calcite, quartz, plagioclase (illite, pyrite, smectite?)
61R-3, 28-30	784.74	Silty claystone	Calcite, quartz, plagioclase (illite, amphibole, pyrite)
62R-1, 17-19	791.67	Silty claystone-clayey siltstone	Calcite, quartz, plagioclase, illite (amphibole, pyrite)
63R-3, 8-9	803.72	Sandstone-claystone	Calcite, plagioclase, quartz (pyrite, illite)

Table T3 (continued).

Core, section, interval (cm)	Depth (mbsf)	Description	XRD identification: major (minor) minerals
64R-1, 75.5-77	811.46	Silty claystone	Plagioclase, calcite, quartz, illite (pyrite, amphibole)
65R-2, 29-31	822.02	Silty claystone	Calcite, plagioclase, quartz, illite (amphibole, pyrite)
66R-3, 86-88	833.60	Silty claystone	Plagioclase, quartz, calcite (illite, pyrite, amphibole)
67R-CC, 41-42	845.91	Calcareous volcaniclastic sandstone	Calcite, plagioclase, quartz, illite (amphibole)
68R-1, 87-88	850.17	Volcaniclastic sandstone	Calcite, plagioclase, quartz, amphibole, illite
69R-1, 27-28	859.27	Mixed sandstone (calcareous)	Calcite (K-feldspar, plagioclase)
70R-1, 14-15	868.84	Calcareous sandstone	Calcite (quartz, plagioclase)
71R-1, 13-14	878.53	Polymictic breccia	Plagioclase (quartz, K-feldspar, smectite?)

Note: See **"Lithostratigraphy,"** p. 4, for discussion.

Table T4. X-ray fluorescence analyses of dolerites for major elements.

Core, section, interval (cm)	Sample	SiO$_2$	Average	TiO$_2$	Average	Al$_2$O$_3$	Average	Fe$_2$O$_3$	Average	MnO	Average	MgO	Average
180-1118A-													
69R-2, 92-95	1a	49.12		1.89		16.22		14.70		0.13		7.52	
	1b	48.44	48.78	1.86	1.87	15.97	16.09	14.53	14.62	0.13	0.13	7.44	7.48
71R-1, 44-47.5	2a	51.07		1.83		13.52		14.85		0.23		5.89	
	2b	51.47	51.27	1.83	1.83	13.57	13.55	14.96	14.91	0.24	0.23	5.92	5.91
74R-1, 107-110	3a	52.16		1.74		13.12		15.23		0.24		5.94	
	3b	51.49	51.83	1.74	1.74	13.02	13.17	15.41	15.32	0.25	0.25	5.90	5.92
74R-2, 92-95	4a	51.87		1.76		12.80		15.37		0.25		5.48	
	4b	52.10	51.99	1.80	1.78	12.90	12.85	15.54	15.45	0.26	0.25	5.61	5.55
76R-1, 82-84	5a	49.87		1.78		13.33		13.23		0.44		3.48	
	5b	49.90	49.89	1.81	1.79	13.40	13.37	13.37	13.25	0.45	0.45	3.50	3.49
76R-1, 102-105	6a	50.33		1.59		14.30		12.53		0.29		6.28	
	6b	50.55	50.44	1.59	1.59	14.36	14.33	12.55	12.54	0.29	0.29	6.34	6.31
76R-2, 71-75	7a	51.38		1.47		13.81		13.14		0.22		6.80	
	7b	51.71	51.55	1.49	1.48	13.97	13.89	13.31	13.23	0.22	0.22	6.81	6.81

Notes: LOI = loss on ignition. Major element values are in weight percent; a and b = duplicate analyses of the same sample. FeO* = total Fe as FeO.

Table T4 (continued).

Sample	CaO	Average	Na$_2$O	Average	K$_2$O	Average	P$_2$O$_5$	Average	Total	Average	LOI	Average	FeO*/ MgO	Rock type
1a	9.36		1.95		0.15		0.15		101.19		3.14			Dolerite pebble in
1b	9.23	9.29	1.98	1.97	0.15	0.15	0.15	0.15	99.88	100.03	3.14	3.14	1.76	conglomerate of Unit VII
2a	9.76		3.75		0.19		0.14		101.23		3.19			Dolerite
2b	9.83	9.79	3.71	3.73	0.19	0.19	0.14	0.14	101.87	101.55	3.19	3.19	2.27	
3a	9.61		3.07		0.45		0.13		101.70		2.18			Dolerite
3b	9.59	9.60	3.05	3.06	0.44	0.45	0.13	0.13	101.03	101.37	2.18	2.18	2.33	
4a	8.75		3.63		0.22		0.15		100.30		2.68			Dolerite
4b	8.82	8.79	3.61	3.62	0.23	0.23	0.15	0.15	101.02	100.66	2.68	2.68	2.51	
5a	13.56		3.98		0.53		0.19		100.39		9.27			Pegmatite
5b	13.54	13.55	3.99	3.99	0.53	0.53	0.19	0.19	100.68	100.53	9.27	9.27	3.42	segregation
6a	12.11		2.39		0.34		0.12		100.27		2.89			Dolerite
6b	12.14	12.13	2.45	2.32	0.34	0.34	0.12	0.12	100.73	100.50	2.89	2.89	1.79	
7a	10.80		2.51		0.21		0.11		100.45		1.91			Dolerite
7b	10.89	10.85	2.65	2.58	0.21	0.21	0.11	0.11	101.35	100.87	1.91	1.91	1.75	

Table T5. X-ray fluorescence analyses of dolerites for trace elements.

Core, section, interval (cm)	Sample	Nb	Zr	Y	Sr	Rb	Zn	Cu	Ni	Cr	V	Ce	Ba	Rock type
180-1118A-														
69R-2, 92-95	1	8.1	94	23	155	8	104	204	92	102	422	3	0	Dolerite pebble in conglomerate of Unit VII
71R-1, 44-47.5	2	7.8	89	28	148	4	73	58	63	42	401	1	0	Dolerite
74R-1, 107-110	3	7.3	86	27	146	7	95	190	64	41	351	6	3	Dolerite
74R-2, 92-95	4	8.5	97	30	207	4	94	193	55	22	350	7	15	Dolerite
76R-1, 82-84	5	8.2	106	43	125	9	83	106	50	14	361	22	5	Pegmatite segregation
76R-1, 102-105	6	6.5	74	22	151	4	87	166	84	164	346	11	32	Dolerite
76R-2, 71-75	7	5.9	74	21	151	4	87	166	83	163	348	10	30	Dolerite

Note: Trace elements measured in parts per million.

Table T6. Thickness of deformed intervals and types of corresponding structures in cores of Subdomain Ic.
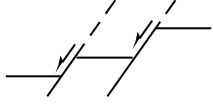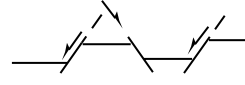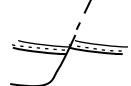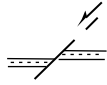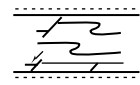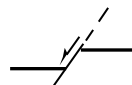
Hole 1118A Core, section	Total thickness (cm)	Thickness of deformed intervals (cm)	Type of structures
10R-4	140	62-73	
11R-1	140	134-138	
11R-4	130	30-34	
12R-5	150	138-145	
18R-4	105	40-46	
24R-3	150	58-65	
27R-1	150	50-58	
28R-5	140	125-135	

Table T7. Stratigraphic distribution of calcareous nannofossils, Hole 1118A. (Continued on next page.)

Core, section, interval (cm)	Depth (mbsf)	Abundance	Preservation	*Calcidiscus leptoporus*	*Calcidiscus macintyrei*	*Ceratolithus rugosus*	*Coccolithus pelagicus*	*Discoaster asymmetricus*	*Discoaster blackstockae*	*Discoaster brouweri*	*Discoaster decorus*	*Discoaster pentaradiatus*	*Discoaster surculus*	*Discoaster tamalis*	*Discoaster variabilis*	*Helicosphaera carteri*	*Helicosphaera sellii*	*Pseudoemiliania lacunosa*	*Reticulofenestra minutula*	*Reticulofenestra pseudoumbilicus*	*Rhabdosphaera clavigera*	*Scyphosphaera apsteinii*	*Sphenolithus abies*	*Syracosphaera histrica*	*Thoracosphaera heimii*	*Thoracosphaera saxea*
180-1118A-																									
1R-CC, 0-2	205.00	C	M	F	R		R			R		r	r			F	R	C	C		R					
2R-CC, 3-4	214.43	A	M	F			F			R		r				F		C	C		R	R			R	
3R-CC, 19-21	224.29	C	M	R		R	R			R						F		F	C		R					
4R-CC, 25-27	233.95	A	M	F			F			R		r				F	R	R	C							
5R-CC, 12-13	243.42	C	M	R						R						R	R	R	C							
6R-CC, 10-12	261.99	A	M	R			F			R		r				F		R	C							
7R-CC, 15-17	266.07	F	M	F	R											F		R	F							
8R-CC, 19-22	280.43	C	M	F			F									F	R	F	C							
9R-CC, 16-19	288.58	C	M	R			F			R						F	R	F	C		R	r				R
10R-CC, 13-15	297.40	C	M	F	R		R			F						F		F								
11R-CC, 17-20	309.70	C	M	R			R			F						R	R	F								
12R-CC, 19-21	319.78	C	M	R	R		R			F						F		F								
13R-7, 57-58	329.84	C	M	R	R		F			F						F		F								
14R-CC, 24-26	339.87			R	R		R			F	r					F		F								
15R-CC, 19-22	348.87	C	M	R			R			F	R					F										
16R-CC, 10-12	358.01	C	M	F	F		R			F	R					C		F						r		
17R-6, 132-134	367.18	C	M	F	F		R			F	F					F		R								
18R-CC, 18-20	374.47	F	M	F			R			R	R					R		R								
19R-CC, 20-22	384.20	C	M	R	R		R			F	F	R				F		R								
20R-CC, 18-20	396.75	C	M	R	R		R			F	F					R		R						r		
21R-CC, 24-26	404.16	C	M	F	R		F			F	F	R				F		R						r		
22R-CC, 19-21	415.11	C	M	F	R		F			F	F	R				F		R				r				
23R-CC, 24-26	423.77	C	M	R						F	R					F										
24R-CC, 13-15	435.02	A	M	F			R			C	F	R				F		F	C						R	
25R-CC, 12-14	443.75	C	M	F	R		R			F	R	R				F		F	C				r	R	R	
26R-CC, 23-25	450.73	C	M	F			R			F	R	R				F		F	C							
27R-CC, 29-31	463.18	F	M				R			R	R	R				R			F							
28R-CC, 18-20	472.93	C	M	F						F	F					F		F	C							R
29R-CC, 12-14	482.54	C	M	R						F	F					F		F	C							
30R-CC, 14-16	492.49	C	M	R			R			F	F					F			C							
31R-CC, 16-18	501.58	C	M				R			F	F					R										
32R-CC, 7-10	509.67	C	M	R						F	F					F										
33R-CC, 20-23	521.11	C	P	R						F	R	R				F										
34R-CC, 19-22	529.99	C	P	R			R			R	R					R										
35R-CC, 25-27	540.18	C	M	F			R			F	F	R				F						r				
36R-CC, 17-20	549.75	C	P	R	R					F	F					F										
37R-CC, 18-21	556.95	C	M	F	R		R			R	F				R	F										
38R-CC, 21-24	568.55	C	M	F	R	R	R			F	F				R	F										
39R-CC, 14-17	578.39	C	M	F	R		R			F	F	R			R	F										
40R-CC, 24-26	585.42	F	M	R						R	F					F			R							
41R-CC, 26-29	597.56	C	M	F	R		R	R		F	F	R				F								R		
42R-CC, 12-17	608.20	A	M	R			F	R		F	F	R		R	R	F			C			R		R		
43R-CC, 26-28	617.63	C	M	R			F			F	R			R	F	F			C				F			
44R-CC, 51-53	626.81	C	M	R			F			F	R			R		F	R		C				R	R		
45R-CC, 14-16	636.39	C	M	R	R		R			F	F					F			C				R			
46R-CC, 16-18	646.23	F	M				R			F	F						F		F				R			
47R-CC, 21-23	655.31	C	M	F			F			F	F					R	F	R	C				F			
48R-CC, 31-33	663.35	F	M	R						F	F					R		R	F				F		R	R
49R-CC, 20-22	667.93	C	M	F	R					F	F			R		F						r	F			
50R-CC, 11-13	681.69			F	R		R			F	F					F	R						R			
51R-CC, 10-12	688.26	C	M	F	R		R			F	F					F						r	R			
52R-CC, 19-20	695.63	R	P							R																
53R-CC, 32-34	707.50	C	M	R			R			F	R					F							R			
54R-CC, 18-20	716.00	C	M	F	R		F			R	F					F							F			
55R-CC, 34-36	727.10			R			R			R	F			R		F							F			
56R-CC, 43-45	740.76			F			F			R	R			R		F						r	F			
57R-CC, 21-23	749.86	C	M	F			R			F	F		R			F							R			
58R-CC, 35-37	762.15	F	M	R	R		R			R	R							R	F							R

Table T7 (continued).

Core, section, interval (cm)	Depth (mbsf)	Abundance	Preservation	Calcidiscus leptoporus	Calcidiscus macintyrei	Ceratolithus rugosus	Coccolithus pelagicus	Discoaster asymmetricus	Discoaster blackstockae	Discoaster brouweri	Discoaster decorus	Discoaster pentaradiatus	Discoaster surculus	Discoaster tamalis	Discoaster variabilis	Helicosphaera carteri	Helicosphaera selli	Pseudoemiliania lacunosa	Reticulofenestra minutula	Reticulofenestra pseudoumbilicus	Rhabdosphaera clavigera	Scyphosphaera apsteinii	Sphenolithus abies	Syracosphaera histrica	Thoracosphaera heimii	Thoracosphaera saxea
59R-CC, 22-24	770.50	F	M	R	R		R			F		R				F		R	C			F		R		R
60R-CC, 8-10	774.55	F	M				R			R		R				F			F				F			
61R-CC, 15-18	785.59	F	G		R		R		R			R				F		R	F				R			
62R-CC, 15-17	796.43	C	M	R	R		F			R		F				F			C				F			
63R-CC, 20-25	806.91	F	M				R			F		F				F		R	F				F			
64R-CC, 26-28	813.22	F	M				R	R		R		R				R			F				F			
65R-CC, 27-30	828.40	C	M	F	R					F		R				F							F			
66R-CC, 28-30	836.12	C	M	F	R	R	F			R		R				F					R		F			
67R-CC, 32-35	845.82	C	M	F	R		R			R		R				F					R		F			
68R-1, 0-1	849.30	C	M	R	R		R			R		R				F		R			R		F			
68R-3, 109-110	853.15	C	M	F	R											F							F			
68R-CC, 14-15	854.67	B																								
69R-CC, 11-12	862.73	B																								

Notes: Abundance (number specimens of a species per field-of-view): A = abundant (10–100); C = common (1–10); F = few (1 per 10 fields of view); R = rare (<1 per 10 fields of view); B = barren. Preservation: G = good; M = moderate; P = poor. Distribution: C = common; F = few; R = rare; r = reworked.

Table T8. Stratigraphic distribution of planktonic foraminifers in Hole 1118A. (Continued on next page.)

Core, section, interval (cm)	Depth (mbsf)	Abundance	Preservation	Candeina nitida	Dentoglobigerina altispira	Dentoglobigerina globosa	Globigerina bulloides	Globigerinella siphonifera	Globigerinita glutinata	Globigerinoides conglobatus	Globigerinoides extremus	Globigerinoides fistulosus	Globigerinoides obliquus	Globigerinoides quadrilobatus	Globigerinoides ruber	Globigerinoides sacculifer	Globigerinoides trilobus	Globorotalia crassaformis	Globorotalia menardii	Globorotalia multicamerata	Globorotalia scitula	Globorotalia tosaensis	Globorotalia truncatulinoides	Globorotalia tumida	Globorotalia tumida flexuosa	Hastigerina pelagica	Neogloboquadrina acostaensis	Neogloboquadrina dutertrei	Neogloboquadrina humerosa	Orbulina suturalis	Orbulina universa	Pulleniatina obliquiloculata	Pulleniatina praecursor	Sphaeroidinella dehiscens	Sphaeroidinella dehiscens s.l.	Sphaeroidinellopsis seminulina	Sphaeroidinellopsis subdehiscens
180-1118A-																																					
1R-CC, 0-2	205.00	A	G					F		A	F	A		A		F		A			A		F	A					A		A	A		A			
2R-CC, 3-4	214.43	A	G							A	A	F		A	A	A	A	A			A		F	A					A			A		A			
3R-CC, 19-21	224.29	A	G				A			F	F	A		A	A	A	A	A			A			A			F		A		F	A		A			
4R-CC, 25-27	233.95	A	G					F		A	F	F		A	A	F	A	F	A		A			A		R			A		F	A		A			
5R-CC, 12-13	243.42	A	G							F	F	R		A	A	R	A		A		A			A					A		F	A		A			
6R-CC, 10-12	261.99	A	G							F	F	A		A	A	F	A	A	A		A	F		A					A		A	A		F			
7R-CC, 15-17	266.07	A	G							A	A	A		A	A	A		A			A			A					A		F	A		A			
8R-CC, 19-22	280.43	A	G							A	A	A		A	A	A		A			F			A		F	F		A		F	A		A			
9R-CC, 16-19	288.58	A	G							A	A	A		A	A	A	A	A			A			A					A		A	A		A			
10R-CC, 13-15	297.40	A	G							F	F	R		A	A	A	A	F	F					F					A		F	F		F			
11R-CC, 17-20	309.70	A	G							A		R	A	A	A	A	A	F	F					F	F				F	R	F	F		F			
12R-CC, 19-21	319.78	A	G									R		F	F		R	F	F		F			F		R			F		R			R			
13R-7, 57-58	329.84	F	G							A			A	A	A	A	A	F	F		R	F		F	F	R			A	F	F	F		F	F		
14R-CC, 24-26	339.87	A	G				R	A	A			R		A	A	A	F	F	R	R	R	F		F	F				A			F		A	F		
15R-CC, 19-22	348.87	F	G				R					R		F	F		F	F	F		R	R		R					F		F	R		F	F		
16R-CC, 10-12	358.01	C	G				F			R		R		F	F		F	R	F		R	R	R	F					F		F	F		F			
17R-6, 132-134	367.18	C	G				R	F	F		R			F	F	F	F	F	R		F			F	F				F		F			F	F		
18R-CC, 18-20	374.47	C	G				R		A		R			A	A	A	A		F					F					F		F	R		F	F		
19R-CC, 20-22	384.20	A	G				F					F		A	A	A		R	F		R		R	F					F		F	F		F	F		
20R-CC, 18-20	396.75	A	G							A		F	A	A	A	A	F	F	F	F	R	F		F					F		F	F		F	F		
21R-CC, 24-26	404.16	R	G											R	R			R						R							R						
22R-CC, 19-21	415.11	C	M									R		A	A	F	A		F		R	F		F					A		R	F		F	F		
23R-CC, 24-26	423.77	A	G	R			F		A		F			A	A		A	R	F			F		F					F		F	F		F	F		
24R-CC, 13-15	435.02	A	G				F			A	A			A	A	F	A	F	A			F		A					A		A	R		R			
25R-CC, 12-14	443.75	A	M				R		F	A	F			A	A	F	A	F	A					A					R		F	R		R			
26R-CC, 23-25	450.73	A	M				F			F	R			A	A			R	A					A					F		A			R			
27R-CC, 29-31	463.18	C	M						F					A	A	R	F		A					A					R		R			R			
28R-CC, 18-20	472.93	F	M				R		R					F	F	R	F	R	F					R					R		F	F		R			
29R-CC, 12-14	482.54	C	M				R	F						F	A		F	R	A					F					F		F	R		R			
30R-CC, 14-16	492.49	C	M						F	A	F				A	R			A					F					A		F	F		R			
31R-CC, 16-18	501.58	F	M					F		F		F			F	R	F		F					F					F		R	R					R
32R-CC, 7-10	509.67	F	G								F				F	R	F	R	F					R					F		R			R		R	R
33R-CC, 20-23	521.11	F	M					F			F	F			F		F		F					R		R			R		R	R		R			
34R-CC, 19-22	529.99	F	G				R	R		R	F			R	F			R	F					R					R		R			R		R	R
35R-CC, 25-27	540.18	R	M								R				R		R		R					R									R				R
36R-CC, 17-20	549.75	F	M								F	R			F	F	F		F			F		F							R			F	F		
37R-CC, 18-21	556.95	C	M					F		F		F			F		F		F			F		R					F		F	F		F	F		
38R-CC, 21-24	568.55	F	M								F			R	F	R	F		F			R		R					F			R		R			
39R-CC, 14-17	578.39	A	G					A		A		F	A	A	A	A		F				F		F					A		F	F		F	F		
40R-CC, 24-26	585.42	C	G							F				F	F		F		F		R	F		F					F		R	F		R			
41R-CC, 26-29	597.56	F	G							F	F	F			F		F		F		R	F		R	R						R			R	R		
42R-CC, 12-17	608.20	A	G		A					A	F	F		A	A	F	A	R	A			A		F					A		A	A		A			
43R-CC, 26-28	617.63	R	P											R		R		R						R								R					
44R-CC, 51-53	626.81	C	M		F					A	A	F		A	A	R	A	R	A					R					F		F	R		R	R		
45R-CC, 14-16	636.39	F	M		F					F	R			F	F			F	F		R			R					R		R	R					
46R-CC, 16-18	646.23	A	G		A					F	F	R		A	A	R	A	A	A			A		A	F		F		A		F	A	R	F	F		
47R-CC, 21-23	655.31	A	M		A							R		F	A		F	R	A				F	A					A		F	R	F	F	F		
48R-CC, 31-33	663.35	C	M		F						F			F	F		F		F		F			F					F		R	F		R			
49R-CC, 20-22	667.93	A	G		A			F			A	R		A	A	R	A	F	F		R			F	F				A		R	A		F	F		
50R-CC, 11-13	681.69	C	M		F			R		F	F	F		F	F		F	R	R		R			R	F	F			R					R	R	R	
51R-1, 71-73	686.01	C	G		F						F	F		F	F	F	F	F	F		F			F	F				F		R	F		F	F		
51R-CC, 10-12	688.26	F	G		R	R					F			F	F	F	F	R	R		R			R	R		R		R		R	R		R	R		
52R-1, 27-30	695.27	C	G		F						F		F	F	F	F	F	F	F		R	R							F		R	R		R			
53R-CC, 32-34	707.50	C	G		F			R		R				F	F	F	F	R	F		R			R					F			R		R		R	
54R-CC, 18-20	716.00	C	G		F		F	R		F	F			F	F	F	F	R	R		R	R		R					F		R	F		R		R	
55R-CC, 34-36	727.10	C	G		F					F	F			F	F	F	F	R	F		R			R					R		R	F		R			R
56R-CC, 43-45	740.76	F	G		F						F			F	F	F	F	R	F		R			R					R		R	F					R
57R-CC, 21-23	749.86	C	G		F			F	F					F	F		F		F					F							F			F	F		
58R-CC, 35-37	762.15	F	M		F					R				F	F	R	F		F					F							F						

Table T8 (continued).

Core, section, interval (cm)	Depth (mbsf)	Abundance	Preservation	Candeina nitida	Dentoglobigerina altispira	Dentoglobigerina globosa	Globigerina bulloides	Globigerinella siphonifera	Globigerinita glutinata	Globigerinoides conglobatus	Globigerinoides extremus	Globigerinoides fistulosus	Globigerinoides obliquus	Globigerinoides quadrilobatus	Globigerinoides ruber	Globigerinoides sacculifer	Globigerinoides trilobus	Globorotalia crassaformis	Globorotalia menardii	Globorotalia multicamerata	Globorotalia scitula	Globorotalia tosaensis	Globorotalia truncatulinoides	Globorotalia tumida	Globorotalia tumida flexuosa	Hastigerina pelagica	Neogloboquadrina acostaensis	Neogloboquadrina dutertrei	Neogloboquadrina humerosa	Orbulina suturalis	Orbulina universa	Pulleniatina obliquiloculata	Pulleniatina praecursor	Sphaeroidinella dehiscens	Sphaeroidinella dehiscens s.l.	Sphaeroidinellopsis seminulina	Sphaeroidinellopsis subdehiscens
59R-CC, 22-24	770.53	C	M		F									F	F	R	F		F					F				F				R		R	R		
60R-CC, 8-10	774.55	C	G		F						R			A		A	F		A									F				F		F		
61R-CC, 15-18	785.59	A	M		A	R								A	A	F		A	A					R				F		R	F	R	R		
62R-CC, 15-17	796.43	C	M		F									F	F		F	R	A									F			R	R	R	R		
63R-CC, 20-25	806.91	C	G		F	F			R				R	A		F	A	R	A					F				F		R	R	F	F	F		
64R-CC, 26-28	813.22	R	P		R														R									R					R			
65R-CC, 27-30	828.40	F	P		R						F			F	F		F	R	R					R				F			R		R			
66R-CC, 28-30	836.12	F	M		F						F			F	F		F	R	R					F	F				R			F	F		F		F
67R-CC, 32-35	845.82	A	M		F				F			F	A	A	A	A	A	R	F						F				F	F		F	F	F	F		
68R-1, 0-1	849.30	C	M		F									F	F	F		R	F					F	F				F	R				F			
68R-1, 135.5-138		C	P		F								F	F	F	F	F	R	F					F	F				F			R	F	F		
68R-2, 129-131		A	M		A								F	A	F	F	A	R	A					A	F				F		F			A		
68R-3, 109-110		A	P		F				R				F	A		R	A		F					F	F				F			R	F	F		F

Notes: Abundance (number of specimens per field of view): A = abundant (2–9); C = common (lower range of abundant); F = few (0.5–1.0); R = rare (1–3 per tray). Preservation: G = good; M = moderate; P = poor.

Table T9. Interstitial water geochemistry, Site 1118.

Core, section, interval (cm)	Depth (mbsf)	pH	Alkalinity (mM)	Salinity	Cl (T) (mM)	Cl (IC) (mM)	SO$_4$ (mM)	Na (mM)	K (mM)	Mg (mM)	Ca (mM)	Ca/Mg	Li (µM)	NH$_4$ (µM)	Sr (µM)	SiO$_2$ (µM)
180-1118A-																
6R-4, 140-150	257.81	8.36	13.059	32.0	561	561	0.5	471	11.1	34.9	2.6	0.07	13	2822	53	349
8R-4, 140-150	278.00	8.36	10.503	32.0	562	566	0.3	472	11.7	35.5	3.0	0.08	15	2719	53	409
10R-2, 140-150	294.30	8.29	9.380	32.0	560	566	0.0	467	12.1	36.5	3.6	0.10	19	2539	57	446
12R-3, 111-121	314.33	8.37	8.526	32.0	560	568	0.9	462	12.4	36.5	4.2	0.11	22	2469	65	433
14R-4, 131-141	335.10	8.26	8.175	32.0	567	564	0.0	460	11.2	37.9	5.4	0.14	24	2119	75	454
16R-5, 91-101	355.92	8.36	4.644	32.0	570	592	0.5	479	10.9	38.4	7.3	0.19	25	2101	72	352
18R-2, 128-137	370.98	8.36	3.650	32.0	565	564	0.0	450	9.5	37.8	9.5	0.25	25	1925	77	433
20R-6, 134-146	395.75	8.41	1.943	32.0	568	573	0.0	446	7.6	38.1	14.4	0.38	29	1834	77	311
22R-5, 112-123	413.05	8.29	1.352	32.0	568	572	0.0	446	6.9	37.0	17.2	0.47	33	1840	74	178
24R-1, 134-146	426.94	8.56	1.356	34.0	568	571	0.3	442	6.6	37.3	20.3	0.54	38	1788	82	193
26R-3, 110-119	448.90	8.42	1.448	33.0	571	576	0.6	444	6.9	36.8	25.0	0.68	32	1586	76	403
28R-4, 107-117	469.36	8.58	2.188	33.0	574	573	0.6	437	6.6	38.1	23.6	0.62	35	1449	75	454
30R-2, 132-142	486.03	8.47	1.287	33.0	571	579	0.4	436	5.6	38.3	24.9	0.65	40	1532	74	283
32R-2, 131-141	505.29	8.51	1.304	33.0	573	583	0.6	434	5.0	37.8	26.1	0.69	49	1479	76	264
34R-3, 116-131	525.67	8.60	0.925	33.0	574	582	0.4	434	4.5	38.0	25.7	0.68	55	1375	79	182
36R-2, 135-145	543.54	8.29	0.992	33.0	576	585	0.5	434	4.1	39.4	24.6	0.62	59	1529	83	217
39R-1, 138-150	571.38	8.54	1.146	33.0	578	589	0.9	442	4.6	39.2	21.5	0.55	61	1743	89	150
42R-4, 98-110	603.55	8.52	1.336	33.0	577	592	0.6	446	5.0	37.6	18.8	0.50	72	1971	109	125
45R-6, 92-102	634.56	8.56	2.540	32.5	573	589	1.2	457	5.8	34.4	15.4	0.45	86	2051	123	234
48R-3, 112-122	660.41	8.32	2.283	32.0	567	582	1.1	456	7.2	30.7	15.2	0.49	107	1999	167	298
51R-1, 74-89	686.04	8.31	2.502	32.0	564	585	0.7	466	9.4	29.1	12.7	0.44	91	2030	218	526
55R-1, 72-87	724.82	8.25	2.794	32.0	562	577	5.3	473	11.5	28.8	11.4	0.40	111	2034	290	659
58R-4, 135-150	758.16	8.28	2.385	32.5	567	585	8.9	474	12.4	27.2	12.5	0.46	126	2047	333	352
61R-1, 113-128	783.03	8.37	6.260	34.0	563	576	11.7	481	12.3	27.5	15.4	0.56	136	2012	417	871
64R-1, 9-21	810.79	8.13	4.180	34.0	552	574	13.1	478	12.4	25.3	18.5	0.73	149	1995	526	822
67R-2, 135-150	842.24	8.32	1.954	34.0	572	576	12.0	481	10.1	24.1	22.0	0.91	148	1886	631	523

Note: Cl (T) = chloride by titration, Cl (IC) = chloride by ion chromatography.

Table T10. Composition of headspace gas in sediments, Site 1118.

Core, section, interval (cm)	Depth (mbsf)	C_1	C_2	C_1/C_2
180-1118A-				
2R-CC, 0-1	214.40	3		
3R-CC, 0-1	224.10	3		
4R-CC, 0-1	233.70	3		
5R-CC, 0-1	243.30	2		
6R-5, 0-2	257.91	1,818		
7R-2, 0-2	263.58	6,497	1	4640
8R-5, 0-2	278.10	14,691	3	4591
9R-2, 0-2	283.20	26,527	5	4912
10R-1, 0-1	291.40	25,218	5	5147
11R-3, 0-2	303.87	39,697	8	5089
12R-4, 0-2	314.43	36,572	7	4942
13R-4, 0-2	324.77	59,235	12	5151
14R-5, 0-2	335.20	40,353	9	4534
15R-7, 130-132	348.66	34,186	8	4119
16R-6, 0-2	356.02	41,363	10	4178
17R-3, 0-2	361.36	40,219	9	4325
18R-3, 0-2	371.07	16,656	5	3399
19R-3, 0-2	380.70	56,706	16	3522
20R-6, 0-2	394.41	40,128	11	3520
21R-5, 0-2	402.63	35,448	11	3313
22R-3, 0-2	409.05	17,204	6	2867
23R-3, 0-2	418.79	30,784	10	3078
24R-2, 0-2	427.06	23,222	9	2524
25R-4, 0-2	439.21	23,826	11	2206
26R-4, 0-2	448.99	62,247	22	2817
27R-4, 0-2	458.73	76,184	28	2702
28R-5, 0-2	469.46	51,821	21	2456
29R-4, 0-2	477.97	39,433	16	2512
30R-3, 0-2	486.13	51,514	20	2538
31R-6, 129-130	501.41	35,083	17	2113
32R-3, 0-2	505.39	37,912	17	2191
33R-6, 0-2	519.26	43,910	18	2453
34R-4, 0-2	525.82	25,611	13	1985
35R-5, 0-2	536.01	22,129	10	2128
36R-3, 0-2	543.64	48,445	25	1915
37R-2, 0-2	552.14	26,160	13	1967
38R-3, 0-2	563.12	98,420	55	1796
39R-2, 0-2	571.50	58,597	35	1669
40R-4, 0-2	583.72	68,873	42	1628
41R-4, 0-2	593.37	28,449	17	1693
42R-5, 0-2	603.67	34,556	21	1677
43R-1, 0-2	608.40	28,927	19	1564
44R-1, 0-2	618.00	30,196	18	1668
45R-7, 0-2	634.66	21,969	12	1831
46R-7, 0-2	645.39	29,268	16	1785
47R-6, 0-1	653.66	21,257	11	1968
48R-4, 0-2	660.51	18,666	9	2051
49R-2, 52-53	667.72	5,430	3	1872
50R-3, 0-1	678.20	8,760	4	2503
51R-2, 0-2	686.19	4,271	1	3285
52R-1, 0-1	695.00	2,001		
53R-1, 0-2	704.70	82		
54R-1, 0-2	714.40	26		
55R-2, 0-2	724.97	19		
56R-1, 0-2	733.80	9		
57R-4, 0-2	747.64	7		
58R-5, 0-2	758.31	4		
59R-2, 0-2	763.99	5		
60R-1, 0-2	772.30	3		
61R-2, 0-2	783.18	5		
62R-4, 0-2	795.50	7		
63R-5, 120-121	806.70	8		
64R-1, 20-21	810.90	3		
65R-2, 0-1	821.73	3		
66R-5, 23-24	835.83	3		
67R-2, 148-150	842.37	3		
68R-1, 0-2	849.30	3		
77R-1, 101-102	888.91	2		

Notes: All concentrations are reported in parts per million by volume. Blanks indicate values below detection limit, except for C_1/C_2 ratio where blanks indicate an undefined value.

Table T11. Calcium carbonate, carbon, nitrogen, and sulfur contents in sediments, Site 1118. (Continued on next page.)

Core, section, interval (cm)	Depth (mbsf)	Inorganic carbon (wt%)	CaCO₃ (wt%)	Organic carbon (wt%)	Total nitrogen (wt%)	C/N	Total sulfur (wt%)
180-1118A-							
3R-CC, 4-5	224.14	0.85	7.05	0.15			0.06
4R-CC, 11-12	233.81	1.94	16.18	0.52			
5R-CC, 21-22	243.51	0.87	7.23	0.32			0.23
6R-3, 70-71	255.66	0.46	3.83	0.73			1.18
7R-3, 24-25	265.32	4.26	35.52	0.21			1.00
8R-5, 77-78	278.87	8.70	72.46	0.09			
8R-5, 118-119	279.28	1.20	10.00	0.35			0.17
9R-1, 30-31	282.00	0.63	5.22	0.62			0.29
9R-5, 29-30	287.99	0.40	3.30	0.18			
10R-3, 40-41	294.80	0.81	6.72	0.07			
11R-1, 11-13	301.11	0.29	2.40	0.14			
13R-1, 6-8	320.36	0.60	5.02	0.19			
13R-1, 15-16	320.45	0.43	3.61	0.22			0.09
13R-3, 64-65	323.91	1.29	10.77	0.19			0.56
14R-2, 3-5	331.53	1.76	14.67	0.23			0.12
15R-1, 11-13	339.81	0.54	4.49	0.23			
16R-4, 28-29	353.79	1.45	12.09	0.11			0.07
17R-1, 42-44	359.22	1.35	11.21	0.24			0.21
18R-3, 137-138	372.44	0.92	7.68	0.17			0.07
19R-1, 137-138	379.17	0.48	3.99	0.17			0.10
21R-1, 76-77	397.56	1.05	8.76	0.10			0.06
22R-1, 22-23	406.52	0.05	0.45	0.08			
22R-3, 82-83	409.87	1.98	16.53	0.23			
23R-5, 79-81	422.32	0.55	4.60	0.12			
24R-1, 32-34	425.92	1.23	10.25	0.14			
25R-1, 16-18	435.36	0.95	7.95	0.30			0.14
25R-6, 111-113	443.02	0.50	4.16	0.13			0.03
26R-1, 14-16	444.94	1.11	9.25	0.15			
27R-4, 67-68	459.40	1.27	10.61	0.11			0.04
28R-4, 102-106	469.31	0.24	2.03	0.11			
29R-4, 80-81	478.77	1.26	10.52	0.09			
30R-3, 85-86	486.98	0.99	8.26	0.32			0.15
31R-CC, 13-15	501.55	0.73	6.08	0.36			0.08
32R-3, 39-41	505.78	0.85	7.05	0.30			0.30
33R-3, 58-60	515.43	1.02	8.51	0.37			0.26
34R-1, 0-1	521.80	0.98	8.16	0.41			0.39
34R-2, 93-95	524.07	0.19	1.56	0.02			0.17
34R-3, 36-38	524.87	1.06	8.85	0.23			0.24
35R-1, 11-12	531.51	0.97	8.07	0.22			0.27
36R-4, 25-27	545.20	1.01	8.41	0.49			0.66
36R-7, 5-7	549.08	0.76	6.34	0.13			0.49
37R-1, 8-10	550.78	1.40	11.63	0.31			0.24
37R-5, 2-3	556.32	1.99	16.59	0.36			0.17
38R-1, 49-51	560.79	1.99	16.56	0.36			0.29
38R-5, 16-19	566.12	2.13	17.70	0.39			0.25
39R-1, 37-38	570.37	1.72	14.30	0.54			0.55
39R-3, 115-116	573.90	0.97	8.08	0.17			0.11
40R-1, 19-21	579.79	1.73	14.37	0.25			0.13
40R-4, 32-34	584.04	3.12	25.97	0.36			0.33
41R-1, 97-99	590.17	2.75	22.92	0.52			0.36
41R-3, 112-115	593.04	1.94	16.19	0.27			
42R-1, 86-88	599.66	3.11	25.93	0.68			0.10
42R-3, 53-53	601.84	1.79	14.90	0.20			0.35
43R-2, 44-46	609.99	4.34	36.19	0.34			0.71
43R-6, 60-62	615.62	0.26	2.20	0.03			0.12
44R-2, 106-108	620.56	1.30	10.85	0.22			0.21
44R-3, 21-23	621.06	3.36	28.00	0.52			0.50
44R-7, 6-8	625.91	2.98	24.78	0.58			0.38
45R-1, 95-96	628.55	3.66	30.45	0.41			0.24
45R-2, 69-70	629.64	3.30	27.47	0.43			0.32
45R-5, 5-6	632.96	3.88	32.35	0.37			
46R-4, 83.5-85.5	642.37	2.30	19.14	0.35			0.16
47R-2, 83-85	649.11	1.23	10.28	0.62			
47R-3, 30-32	649.95	0.16	1.31	0.08	0.02	4	0.13
47R-6, 77-79	654.43	1.27	10.60	0.30			0.26
48R-1, 85-87	657.25	0.72	6.01	0.23			0.29

Table T11 (continued).

Core, section, interval (cm)	Depth (mbsf)	Inorganic carbon (wt%)	CaCO$_3$ (wt%)	Organic carbon (wt%)	Total nitrogen (wt%)	C/N	Total sulfur (wt%)
49R-1, 103-105	667.03	3.09	25.75	0.41			0.20
49R-2, 7-8	667.27	1.91	15.94	0.39			0.43
50R-1, 77-78	676.37	1.11	9.25	0.37			0.50
50R-4, 6-7	679.33	2.89	24.04	0.30	0.02	15	0.23
52R-1, 10-12	695.10	2.64	21.99	0.12			0.15
53R-1, 73-75	705.43	2.96	24.64	0.40			0.25
53R-2, 21-23	706.31	1.08	8.96	0.19			0.26
54R-1, 36-38	714.76	2.27	18.93	0.52			0.35
55R-1, 52-54	724.62	1.23	10.25	0.23			0.27
55R-3, 10-12	726.32	0.87	7.23	0.51			0.22
56R-4, 42-43	738.12	2.78	23.12	0.41			0.14
56R-5, 40-41	739.55	3.52	29.33	0.55			
57R-2, 58-59	745.40	2.74	22.79	0.34			0.21
57R-4, 30-31	747.94	1.03	8.57	0.28			0.28
58R-2, 12-14	754.56	2.56	21.34	0.61			0.44
58R-5, 18-20	758.49	3.19	26.60	0.48			0.17
59R-3, 8-9	765.42	2.84	23.66	0.24	0.02	12	
59R-4, 23-24	767.03	0.54	4.47	0.02			
60R-1, 65-66	772.95	2.89	24.03	0.64			0.35
60R-2, 10-12	773.76	2.98	24.84	0.52			0.37
61R-1, 51-53	782.41	0.57	4.71	0.03			0.21
61R-3, 28-30	784.74	3.21	26.70	0.52	0.03	17	0.17
62R-1, 17-19	791.67	2.60	21.65	0.62			0.26
62R-2, 97-99	793.92	0.57	4.71	0.18			0.10
62R-4, 58-60	796.08	0.85	7.05	0.16			0.42
63R-1, 68-69	801.78	2.45	20.38	0.77			0.37
63R-3, 7-8	803.71	3.66	30.48	0.39			
63R-4, 14-15	804.51	3.35	27.93	0.41			0.28
64R-1, 75.5-77.5	811.46	2.06	17.17	0.36			0.19
66R-1, 117-119	831.07	2.76	23.02	0.41			0.39
66R-3, 123-125	833.97	2.77	23.06	0.10			
67R-1, 41-42	840.01	3.98	33.17	0.21			0.41
67R-5, 40-41	845.13	1.62	13.48	0.06			
68R-1, 86-87	850.16	3.45	28.77	0.11			
68R-2, 41-42	851.16	1.27	10.54				
68R-3, 28-29	852.34	2.24	18.63				
68R-4, 45-46	854.01	10.93	91.06	0.18			
69R-1, 28-29	859.28	9.79	81.54				
69R-2, 17-18	860.67	8.12	67.68	0.06			
69R-3, 30-31	862.27	9.95	82.87				
70R-1, 15-16	868.85	10.06	83.79	0.14			
71R-1, 13-14	878.53	0.05	0.44				
73R-1, 134-135	889.24	0.05	0.45				
74R-3, 30-31	900.74	0.07	0.61				

Note: Blanks indicate values below detection limit, except for C/N ratio where blanks indicate an unde-
fined value.

Table T12. Total bacterial populations and numbers of dividing and divided cells in sediments, Site 1118.

Depth (mbsf)	Total bacterial population (log cells/cm^3)	Dividing and divided cells (log cells/cm^3)
505.39	6.062	4.615
603.67	5.991	4.528
660.51	6.121	4.553
724.81	5.920	4.559
758.31	5.971	4.857
783.02	5.755	4.357
812.20	5.800	4.703
842.23	5.504	4.143

Table T13. Index properties measured in cores, Site 1118. (**See table note.** Continued on next six pages.)

Leg	Site	Hole	Core	Type	Section	Top (cm)	Bottom (cm)	Depth (mbsf)	Water content (bulk)	Water content (dry)	Bulk density (g·cm⁻³)	Dry density (g·cm⁻³)	Grain density (g·cm⁻³)	Porosity (%)	Void ratio
180	1118	A	3	R	CC	10	12	224.20	28.60	40.10	1.85	1.32	2.74	51.70	1.07
180	1118	A	4	R	CC	11	13	233.81	32.30	47.70	1.77	1.20	2.71	55.80	1.26
180	1118	A	5	R	CC	27	29	243.57	29.50	41.70	1.84	1.29	2.74	52.80	1.12
180	1118	A	6	R	1	4	6	252.94	30.50	44.00	1.81	1.26	2.74	54.10	1.18
180	1118	A	6	R	2	2	4	253.92	27.00	37.00	1.90	1.39	2.79	50.20	1.01
180	1118	A	6	R	3	6	8	255.02	32.00	47.10	1.79	1.22	2.75	55.80	1.26
180	1118	A	6	R	4	3	5	256.44	31.80	46.70	1.77	1.21	2.69	55.10	1.23
180	1118	A	6	R	5	5	7	257.96	29.30	41.40	1.84	1.30	2.74	52.50	1.11
180	1118	A	6	R	6	9	11	259.45	27.90	38.60	1.84	1.33	2.66	50.10	1.00
180	1118	A	6	R	7	8	10	260.94	32.50	48.00	1.77	1.20	2.74	56.20	1.29
180	1118	A	7	R	1	13	15	262.63	33.90	51.20	1.74	1.15	2.69	57.40	1.35
180	1118	A	7	R	2	120	122	264.78	34.50	52.70	1.74	1.14	2.74	58.50	1.41
180	1118	A	7	R	3	5	7	265.13	35.80	55.80	1.71	1.10	2.72	59.70	1.48
180	1118	A	8	R	1	65	67	272.75	31.10	45.10	1.80	1.24	2.75	54.70	1.21
180	1118	A	8	R	2	38	40	273.98	27.90	38.60	1.90	1.37	2.82	51.50	1.06
180	1118	A	8	R	3	130	132	276.40	30.20	43.30	1.83	1.27	2.76	53.90	1.17
180	1118	A	8	R	4	111	113	277.71	29.70	42.30	1.84	1.29	2.76	53.30	1.14
180	1118	A	8	R	5	105	107	279.15	35.60	55.40	1.72	1.11	2.75	59.80	1.49
180	1118	A	8	R	6	10	12	279.70	36.50	57.50	1.70	1.08	2.74	60.60	1.54
180	1118	A	9	R	1	56	58	282.26	29.60	42.10	1.81	1.27	2.67	52.40	1.10
180	1118	A	9	R	2	114	116	284.34	32.90	49.00	1.75	1.18	2.69	56.30	1.29
180	1118	A	9	R	3	133	135	286.03	32.00	47.10	1.78	1.21	2.72	55.50	1.25
180	1118	A	9	R	4	146	148	287.66	28.90	40.70	1.85	1.31	2.74	52.10	1.09
180	1118	A	9	R	5	33	35	288.03	23.10	30.00	1.96	1.51	2.70	44.10	0.79
180	1118	A	10	R	1	131	133	292.71	30.10	43.00	1.82	1.27	2.72	53.30	1.14
180	1118	A	10	R	2	59	61	293.49	31.20	45.30	1.80	1.24	2.75	54.90	1.22
180	1118	A	10	R	3	47	49	294.87	29.80	42.40	1.82	1.28	2.71	52.90	1.12
180	1118	A	10	R	4	39	41	296.29	29.70	42.30	1.83	1.28	2.73	53.00	1.13
180	1118	A	11	R	1	88	90	301.88	27.50	37.90	1.87	1.36	2.72	50.20	1.01
180	1118	A	11	R	2	102	104	303.41	33.60	50.60	1.74	1.16	2.71	57.20	1.34
180	1118	A	11	R	3	102	104	304.89	29.50	41.70	1.83	1.29	2.72	52.60	1.11
180	1118	A	11	R	4	81	83	305.91	28.10	39.00	1.86	1.34	2.72	50.90	1.04
180	1118	A	11	R	5	72	74	307.09	26.10	35.30	1.90	1.40	2.72	48.40	0.94
180	1118	A	11	R	6	75	77	308.41	30.70	44.20	1.80	1.25	2.71	53.90	1.17
180	1118	A	11	R	7	24	26	309.38	27.80	38.50	1.86	1.34	2.71	50.50	1.02
180	1118	A	12	R	1	8	10	310.78	25.20	33.70	1.91	1.43	2.69	47.00	0.89
180	1118	A	12	R	2	78	80	312.54	27.30	37.60	1.87	1.36	2.72	50.00	1.00
180	1118	A	12	R	3	91	93	314.13	27.60	38.20	1.86	1.35	2.71	50.30	1.01
180	1118	A	12	R	4	1	3	314.44	27.00	37.00	1.88	1.37	2.71	49.50	0.98
180	1118	A	12	R	5	3	5	315.96	28.80	40.40	1.84	1.31	2.71	51.70	1.07
180	1118	A	12	R	6	1	3	317.44	28.30	39.40	1.84	1.32	2.68	50.80	1.03
180	1118	A	12	R	7	5	7	318.89	31.60	46.30	1.79	1.22	2.74	55.30	1.24
180	1118	A	13	R	1	13	15	320.43	28.80	40.40	1.84	1.31	2.72	51.70	1.07
180	1118	A	13	R	2	28	30	322.08	35.60	55.40	1.72	1.10	2.74	59.70	1.48
180	1118	A	13	R	3	76	78	324.03	27.40	37.80	1.87	1.35	2.71	50.00	1.00
180	1118	A	13	R	4	56	58	325.33	35.10	54.00	1.73	1.12	2.76	59.30	1.46
180	1118	A	13	R	5	3	5	326.30	29.80	42.50	1.81	1.27	2.68	52.70	1.12
180	1118	A	13	R	6	58	60	328.35	29.30	41.50	1.82	1.29	2.68	52.10	1.09
180	1118	A	13	R	7	5	7	329.32	33.70	50.70	1.74	1.16	2.70	57.20	1.34

Table T13 (continued).

Leg	Site	Hole	Core	Type	Section	Top (cm)	Bottom (cm)	Depth (mbsf)	Water content (bulk)	Water content (dry)	Bulk density (g·cm⁻³)	Dry density (g·cm⁻³)	Grain density (g·cm⁻³)	Porosity (%)	Void ratio
180	1118	A	14	R	1	34	36	330.34	33.50	50.40	1.75	1.17	2.73	57.30	1.34
180	1118	A	14	R	2	6	8	331.56	30.30	43.50	1.81	1.26	2.70	53.40	1.15
180	1118	A	14	R	3	5	7	332.69	28.60	40.00	1.85	1.32	2.72	51.50	1.06
180	1118	A	14	R	4	127	129	335.06	28.90	40.60	1.84	1.31	2.72	51.90	1.08
180	1118	A	14	R	5	34	36	335.54	33.30	49.80	1.76	1.17	2.74	57.20	1.34
180	1118	A	14	R	6	108	110	337.68	28.30	39.50	1.85	1.33	2.73	51.30	1.05
180	1118	A	14	R	7	57	59	338.27	31.00	45.00	1.79	1.23	2.69	54.10	1.18
180	1118	A	14	R	8	4	6	338.89	32.90	49.00	1.76	1.18	2.73	56.60	1.31
180	1118	A	15	R	2	26	28	340.81	28.80	40.50	1.83	1.30	2.70	51.60	1.07
180	1118	A	15	R	3	9	11	341.53	31.20	45.40	1.80	1.23	2.73	54.80	1.21
180	1118	A	15	R	4	6	8	343.00	26.40	35.90	1.87	1.38	2.67	48.30	0.94
180	1118	A	15	R	5	6	8	344.50	28.00	38.80	1.86	1.34	2.71	50.70	1.03
180	1118	A	15	R	6	6	8	345.92	32.70	48.60	1.77	1.19	2.74	56.60	1.30
180	1118	A	15	R	7	74	76	348.10	30.60	44.10	1.81	1.26	2.74	54.10	1.18
180	1118	A	16	R	1	4	6	349.34	33.20	49.70	1.75	1.17	2.71	56.80	1.32
180	1118	A	16	R	2	1	3	350.71	29.70	42.20	1.83	1.29	2.73	52.90	1.13
180	1118	A	16	R	3	1	3	352.21	30.10	43.10	1.82	1.27	2.72	53.40	1.15
180	1118	A	16	R	4	1	3	353.52	30.80	44.50	1.80	1.25	2.72	54.20	1.18
180	1118	A	16	R	5	1	3	355.02	31.70	46.30	1.77	1.21	2.67	54.70	1.21
180	1118	A	16	R	6	5	7	356.07	31.30	45.50	1.78	1.22	2.66	54.20	1.18
180	1118	A	16	R	7	16	18	357.30	32.50	48.20	1.76	1.19	2.69	55.90	1.27
180	1118	A	17	R	1	32	34	359.12	31.70	46.40	1.77	1.21	2.69	54.90	1.22
180	1118	A	17	R	2	85	87	360.87	30.80	44.60	1.79	1.24	2.69	54.00	1.17
180	1118	A	17	R	3	22	24	361.58	30.50	43.90	1.81	1.26	2.74	54.00	1.17
180	1118	A	17	R	4	36	38	363.22	32.40	48.00	1.76	1.19	2.70	55.90	1.27
180	1118	A	17	R	5	30	32	364.66	29.10	41.00	1.82	1.29	2.68	51.80	1.07
180	1118	A	17	R	6	49	51	366.35	30.00	42.90	1.81	1.27	2.71	53.20	1.14
180	1118	A	18	R	1	37	39	368.57	29.30	41.50	1.84	1.30	2.74	52.60	1.11
180	1118	A	18	R	2	122	124	370.92	32.40	48.00	1.78	1.20	2.74	56.30	1.29
180	1118	A	18	R	3	70	72	371.77	30.90	44.70	1.80	1.24	2.71	54.20	1.18
180	1118	A	18	R	4	24	26	372.72	32.20	47.50	1.76	1.20	2.68	55.40	1.24
180	1118	A	18	R	5	16	18	373.64	28.50	39.90	1.84	1.31	2.69	51.20	1.05
180	1118	A	19	R	1	31	33	378.11	30.00	42.80	1.81	1.27	2.69	52.90	1.13
180	1118	A	19	R	2	96	98	380.16	22.80	29.50	1.93	1.49	2.60	42.80	0.75
180	1118	A	19	R	3	45	47	381.15	29.50	41.90	1.83	1.29	2.72	52.70	1.11
180	1118	A	19	R	4	3	5	382.19	30.50	43.90	1.80	1.25	2.70	53.60	1.16
180	1118	A	19	R	5	31	33	383.97	31.00	44.80	1.80	1.24	2.72	54.30	1.19
180	1118	A	20	R	1	98	100	388.38	25.90	34.90	1.90	1.41	2.70	48.00	0.92
180	1118	A	20	R	2	21	23	388.99	28.60	40.00	1.84	1.31	2.69	51.20	1.05
180	1118	A	20	R	3	22	24	390.44	26.10	35.30	1.89	1.40	2.70	48.20	0.93
180	1118	A	20	R	4	24	26	391.84	27.40	37.80	1.85	1.34	2.67	49.60	0.99
180	1118	A	20	R	5	77	79	393.82	29.40	41.70	1.82	1.29	2.70	52.40	1.10
180	1118	A	20	R	6	64	66	395.05	31.00	45.00	1.79	1.24	2.71	54.30	1.19
180	1118	A	20	R	7	42	44	396.29	29.10	41.10	1.83	1.30	2.72	52.20	1.09
180	1118	A	21	R	1	81	83	397.61	31.40	45.80	1.80	1.23	2.76	55.20	1.23
180	1118	A	21	R	2	29	31	398.45	29.20	41.20	1.85	1.31	2.76	52.60	1.11
180	1118	A	21	R	3	22	24	399.88	30.00	42.80	1.81	1.27	2.69	52.90	1.12
180	1118	A	21	R	4	32	34	401.48	22.60	29.20	1.97	1.53	2.71	43.60	0.77
180	1118	A	21	R	5	37	39	403.00	33.00	49.20	1.75	1.17	2.67	56.20	1.29

Table T13 (continued).

Leg	Site	Hole	Core	Type	Section	Top (cm)	Bottom (cm)	Depth (mbsf)	Water content (bulk)	Water content (dry)	Bulk density (g·cm⁻³)	Dry density (g·cm⁻³)	Grain density (g·cm⁻³)	Porosity (%)	Void ratio
180	1118	A	22	R	1	4	6	406.34	29.70	42.20	1.83	1.28	2.73	52.90	1.13
180	1118	A	22	R	2	4	6	407.73	25.90	35.00	1.90	1.41	2.71	48.10	0.93
180	1118	A	22	R	3	27	29	409.32	26.20	35.40	1.90	1.40	2.72	48.50	0.94
180	1118	A	22	R	4	4	6	410.59	24.70	32.70	1.94	1.46	2.74	46.60	0.87
180	1118	A	22	R	5	4	6	411.97	26.90	36.80	1.88	1.37	2.71	49.30	0.97
180	1118	A	22	R	6	7	9	413.23	25.50	34.30	1.90	1.41	2.68	47.30	0.90
180	1118	A	22	R	7	10	12	414.60	25.30	33.80	1.92	1.43	2.72	47.30	0.90
180	1118	A	23	R	2	34	36	417.74	26.70	36.50	1.89	1.38	2.72	49.20	0.97
180	1118	A	23	R	3	6	8	418.85	27.70	38.40	1.86	1.34	2.70	50.30	1.01
180	1118	A	23	R	4	6	8	420.09	24.10	31.80	1.93	1.46	2.68	45.40	0.83
180	1118	A	23	R	5	1	3	421.54	29.10	41.10	1.81	1.29	2.66	51.60	1.07
180	1118	A	23	R	6	10	12	423.13	25.20	33.70	1.90	1.42	2.67	46.80	0.88
180	1118	A	24	R	1	9	11	425.69	24.80	33.00	1.93	1.45	2.73	46.80	0.88
180	1118	A	24	R	2	2	4	427.08	25.70	34.50	1.92	1.43	2.74	48.00	0.93
180	1118	A	24	R	3	9	11	428.60	23.00	29.90	1.98	1.52	2.75	44.60	0.80
180	1118	A	24	R	4	3	5	430.01	24.60	32.70	1.92	1.45	2.70	46.30	0.86
180	1118	A	24	R	5	1	3	431.19	25.30	33.80	1.91	1.43	2.71	47.20	0.89
180	1118	A	24	R	6	1	3	432.61	23.80	31.30	2.21	1.68	3.46	51.40	1.06
180	1118	A	24	R	7	1	3	434.04	29.40	41.70	1.82	1.29	2.71	52.40	1.10
180	1118	A	25	R	1	2	4	435.22	29.80	42.40	1.81	1.27	2.68	52.60	1.11
180	1118	A	25	R	2	2	4	436.72	32.90	49.00	1.77	1.19	2.74	56.80	1.31
180	1118	A	25	R	3	2	4	438.00	27.00	36.90	1.87	1.37	2.69	49.30	0.97
180	1118	A	25	R	4	2	4	439.23	29.50	41.90	1.81	1.28	2.68	52.30	1.10
180	1118	A	25	R	5	2	4	440.59	29.90	42.60	1.82	1.28	2.72	53.10	1.13
180	1118	A	25	R	6	2	4	441.93	30.90	44.80	1.79	1.24	2.70	54.20	1.18
180	1118	A	25	R	7	2	4	443.16	29.80	42.50	1.83	1.28	2.73	53.10	1.13
180	1118	A	26	R	1	12	14	444.92	28.60	40.10	1.84	1.31	2.70	51.40	1.06
180	1118	A	26	R	2	2	4	446.32	25.00	33.40	1.91	1.43	2.69	46.70	0.88
180	1118	A	26	R	3	2	4	447.82	31.60	46.10	1.80	1.23	2.77	55.50	1.25
180	1118	A	26	R	4	9	11	449.08	29.30	41.40	1.84	1.30	2.74	52.60	1.11
180	1118	A	27	R	1	12	14	454.52	24.40	32.30	1.92	1.45	2.67	45.70	0.84
180	1118	A	27	R	2	6	8	455.96	25.70	34.50	1.88	1.40	2.64	47.10	0.89
180	1118	A	27	R	3	4	6	457.31	25.90	35.00	1.88	1.39	2.66	47.60	0.91
180	1118	A	27	R	4	2	4	458.75	25.00	33.30	1.92	1.44	2.71	46.80	0.88
180	1118	A	27	R	5	4	6	460.27	25.00	33.40	1.90	1.42	2.65	46.40	0.87
180	1118	A	27	R	6	4	6	461.72	29.40	41.70	1.82	1.28	2.69	52.30	1.10
180	1118	A	28	R	1	88	90	464.78	26.90	36.70	1.87	1.37	2.68	49.00	0.96
180	1118	A	28	R	2	92	94	466.32	24.10	31.70	1.92	1.46	2.65	45.10	0.82
180	1118	A	28	R	3	68	70	467.54	29.90	42.70	1.81	1.27	2.69	52.90	1.12
180	1118	A	28	R	4	40	42	468.69	28.90	40.70	1.82	1.29	2.65	51.30	1.05
180	1118	A	28	R	5	62	64	470.08	24.10	31.70	1.90	1.44	2.61	44.70	0.81
180	1118	A	28	R	6	45	47	471.30	23.10	30.10	1.93	1.49	2.64	43.70	0.78
180	1118	A	28	R	7	6	8	472.16	31.00	44.90	1.78	1.23	2.65	53.80	1.16
180	1118	A	29	R	1	47	49	474.07	27.70	38.40	1.85	1.34	2.69	50.20	1.01
180	1118	A	29	R	2	115	117	476.22	29.80	42.50	1.81	1.27	2.69	52.80	1.12
180	1118	A	29	R	3	104	106	477.51	28.00	38.80	1.84	1.33	2.68	50.30	1.01
180	1118	A	29	R	4	43	45	478.40	23.80	31.20	1.93	1.47	2.66	44.80	0.81
180	1118	A	29	R	5	36	38	479.60	28.00	38.90	1.83	1.32	2.65	50.20	1.01
180	1118	A	29	R	6	8	10	480.62	28.30	39.40	1.83	1.32	2.67	50.60	1.03

Table T13 (continued).

Leg	Site	Hole	Core	Type	Section	Top (cm)	Bottom (cm)	Depth (mbsf)	Water content (bulk)	Water content (dry)	Bulk density (g·cm⁻³)	Dry density (g·cm⁻³)	Grain density (g·cm⁻³)	Porosity (%)	Void ratio
180	1118	A	29	R	7	17	19	482.03	28.30	39.50	1.83	1.31	2.65	50.50	1.02
180	1118	A	30	R	1	99	101	484.19	31.30	45.50	1.78	1.23	2.70	54.50	1.20
180	1118	A	30	R	2	78	80	485.49	28.40	39.80	1.84	1.32	2.69	51.10	1.04
180	1118	A	30	R	3	5	7	486.18	25.00	33.30	1.90	1.43	2.66	46.40	0.87
180	1118	A	30	R	4	40	42	488.00	30.30	43.50	1.80	1.25	2.68	53.30	1.14
180	1118	A	30	R	5	41	43	489.40	28.10	39.10	1.83	1.32	2.66	50.40	1.02
180	1118	A	30	R	6	10	12	490.45	23.30	30.40	1.93	1.48	2.64	43.90	0.78
180	1118	A	30	R	7	27	29	491.84	25.20	33.70	1.88	1.41	2.62	46.20	0.86
180	1118	A	31	R	1	11	13	493.01	24.70	32.80	1.91	1.44	2.66	46.00	0.85
180	1118	A	31	R	2	6	8	494.40	26.20	35.60	1.89	1.39	2.69	48.30	0.93
180	1118	A	31	R	3	62	64	496.34	24.30	32.10	1.92	1.45	2.67	45.50	0.84
180	1118	A	31	R	4	84	86	498.04	24.00	31.50	1.93	1.47	2.67	45.10	0.82
180	1118	A	31	R	5	6	8	498.68	23.70	31.00	1.93	1.48	2.66	44.60	0.81
180	1118	A	31	R	6	102	104	501.14	26.00	35.10	1.90	1.41	2.71	48.10	0.93
180	1118	A	32	R	1	6	8	502.56	26.10	35.40	2.10	1.55	3.35	53.60	1.16
180	1118	A	32	R	2	28	30	504.26	26.10	35.30	1.88	1.39	2.67	48.00	0.92
180	1118	A	32	R	3	35	37	505.74	22.70	29.30	1.93	1.50	2.61	42.80	0.75
180	1118	A	32	R	4	33	35	507.22	34.00	51.60	1.73	1.14	2.67	57.30	1.35
180	1118	A	32	R	5	62	64	508.97	23.90	31.50	1.92	1.46	2.65	44.90	0.82
180	1118	A	33	R	1	48	50	512.58	22.50	29.00	1.95	1.51	2.63	42.70	0.75
180	1118	A	33	R	2	111	113	514.48	23.20	30.20	1.92	1.48	2.62	43.50	0.77
180	1118	A	33	R	3	49	51	515.34	23.90	31.50	1.93	1.47	2.67	45.10	0.82
180	1118	A	33	R	4	10	12	516.38	28.30	39.50	1.83	1.31	2.65	50.60	1.02
180	1118	A	33	R	5	100	102	518.76	25.10	33.50	1.92	1.44	2.72	47.10	0.89
180	1118	A	33	R	6	40	42	519.66	22.90	29.70	1.94	1.49	2.63	43.30	0.76
180	1118	A	33	R	7	17	19	520.49	24.50	32.50	1.91	1.44	2.65	45.70	0.84
180	1118	A	34	R	1	9	11	521.89	24.50	32.40	1.93	1.46	2.71	46.10	0.86
180	1118	A	34	R	2	3	5	523.17	26.50	36.00	1.87	1.38	2.67	48.50	0.94
180	1118	A	34	R	3	25	27	524.76	24.30	32.00	1.92	1.46	2.68	45.60	0.84
180	1118	A	34	R	4	4	6	525.86	24.10	31.70	1.94	1.47	2.71	45.60	0.84
180	1118	A	34	R	5	58	60	527.67	25.50	34.30	1.94	1.45	2.81	48.40	0.94
180	1118	A	34	R	6	14	16	528.63	24.10	31.70	1.94	1.47	2.70	45.60	0.84
180	1118	A	35	R	1	3	5	531.43	26.70	36.40	1.86	1.36	2.64	48.40	0.94
180	1118	A	35	R	4	3	5	534.64	26.03	35.19	1.89	1.40	2.68	47.98	0.92
180	1118	A	35	R	5	3	5	536.04	24.20	32.00	1.93	1.46	2.69	45.70	0.84
180	1118	A	35	R	6	3	5	537.50	22.60	29.20	1.97	1.53	2.70	43.40	0.77
180	1118	A	35	R	7	3	5	538.57	23.10	30.00	1.96	1.51	2.71	44.30	0.79
180	1118	A	36	R	1	6	8	541.06	25.20	33.70	1.86	1.39	2.56	45.70	0.84
180	1118	A	36	R	2	6	8	542.25	22.80	29.50	1.96	1.51	2.67	43.50	0.77
180	1118	A	36	R	3	6	8	543.70	23.80	31.30	1.93	1.47	2.67	44.90	0.82
180	1118	A	36	R	4	6	8	545.01	29.70	42.20	1.81	1.27	2.67	52.40	1.10
180	1118	A	36	R	5	6	8	546.49	25.10	33.50	1.90	1.42	2.65	46.50	0.87
180	1118	A	36	R	6	6	8	547.64	24.60	32.50	1.92	1.45	2.68	46.00	0.85
180	1118	A	36	R	7	9	11	549.12	27.30	37.50	1.84	1.34	2.62	49.00	0.96
180	1118	A	37	R	1	14	16	550.84	25.00	33.30	1.94	1.46	2.76	47.40	0.90
180	1118	A	37	R	2	1	3	552.15	25.40	34.10	1.89	1.41	2.66	46.90	0.89
180	1118	A	37	R	3	5	7	553.53	23.10	30.10	1.95	1.50	2.68	44.00	0.79
180	1118	A	37	R	4	4	6	555.00	23.20	30.20	2.05	1.57	2.94	46.40	0.87
180	1118	A	37	R	5	44	46	556.74	25.40	34.00	2.01	1.50	2.98	49.80	0.99

Table T13 (continued).

Leg	Site	Hole	Core	Type	Section	Top (cm)	Bottom (cm)	Depth (mbsf)	Water content (bulk)	Water content (dry)	Bulk density (g·cm⁻³)	Dry density (g·cm⁻³)	Grain density (g·cm⁻³)	Porosity (%)	Void ratio
180	1118	A	38	R	1	4	6	560.34	24.60	32.60	1.96	1.48	2.80	47.10	0.89
180	1118	A	38	R	2	2	4	561.72	24.20	31.90	1.91	1.45	2.64	45.10	0.82
180	1118	A	38	R	3	2	4	563.14	24.10	31.80	1.93	1.46	2.67	45.40	0.83
180	1118	A	38	R	4	15	17	564.70	25.00	33.30	1.90	1.42	2.65	46.30	0.86
180	1118	A	38	R	5	20	22	566.16	25.60	34.40	1.93	1.44	2.77	48.20	0.93
180	1118	A	38	R	6	9	11	567.48	24.50	32.40	1.88	1.42	2.57	44.90	0.82
180	1118	A	39	R	1	14	16	570.14	23.80	31.30	1.93	1.47	2.68	45.00	0.82
180	1118	A	39	R	2	14	16	571.64	24.50	32.50	1.87	1.41	2.56	44.80	0.81
180	1118	A	39	R	3	44	46	573.19	23.20	30.20	1.98	1.52	2.76	44.90	0.81
180	1118	A	39	R	4	2	4	574.15	23.90	31.30	1.93	1.47	2.67	44.90	0.82
180	1118	A	39	R	5	2	4	575.51	26.70	36.40	1.86	1.37	2.66	48.60	0.95
180	1118	A	39	R	6	2	4	576.94	22.60	29.20	1.95	1.51	2.66	43.10	0.76
180	1118	A	40	R	1	4	6	579.64	22.30	28.60	2.00	1.55	2.75	43.50	0.77
180	1118	A	40	R	2	3	5	580.98	24.10	31.70	1.91	1.45	2.63	44.90	0.82
180	1118	A	40	R	3	27	29	582.49	22.90	29.60	1.92	1.48	2.60	42.90	0.75
180	1118	A	40	R	4	26	28	583.98	22.20	28.50	1.95	1.52	2.63	42.20	0.73
180	1118	A	41	R	1	103	105	590.23	25.00	33.30	1.88	1.41	2.59	45.70	0.84
180	1118	A	41	R	2	83	85	591.39	25.70	34.60	1.88	1.40	2.64	47.10	0.89
180	1118	A	41	R	3	107	109	592.99	26.30	35.70	1.84	1.36	2.58	47.40	0.90
180	1118	A	41	R	4	89	91	594.26	24.80	32.90	1.90	1.43	2.66	46.10	0.86
180	1118	A	41	R	5	88	90	595.69	25.50	34.20	1.88	1.40	2.62	46.60	0.87
180	1118	A	41	R	6	33	35	596.64	24.80	32.90	1.90	1.43	2.64	45.90	0.85
180	1118	A	42	R	1	95	97	599.75	26.70	36.40	1.85	1.35	2.61	48.10	0.93
180	1118	A	42	R	2	101	103	601.04	25.80	34.80	1.88	1.39	2.65	47.40	0.90
180	1118	A	42	R	3	46	48	601.77	25.60	34.30	1.88	1.40	2.65	47.00	0.89
180	1118	A	42	R	4	8	10	602.65	25.90	34.90	1.88	1.40	2.67	47.60	0.91
180	1118	A	42	R	5	113	115	604.80	23.40	30.60	1.94	1.48	2.66	44.30	0.80
180	1118	A	42	R	6	3	5	604.88	23.90	31.50	1.92	1.46	2.66	45.00	0.82
180	1118	A	42	R	7	94	96	607.12	26.50	36.00	1.87	1.38	2.67	48.40	0.94
180	1118	A	42	R	8	50	52	607.86	25.70	34.60	1.86	1.39	2.60	46.80	0.88
180	1118	A	43	R	1	38	40	608.78	25.00	33.30	1.91	1.43	2.68	46.50	0.87
180	1118	A	43	R	2	48	50	610.03	24.80	32.90	1.91	1.44	2.68	46.30	0.86
180	1118	A	43	R	3	32	34	611.33	25.30	33.80	1.90	1.42	2.68	46.90	0.88
180	1118	A	43	R	4	129	131	613.70	25.10	33.60	1.87	1.40	2.59	46.00	0.85
180	1118	A	43	R	5	110	112	614.84	23.70	31.00	1.93	1.47	2.65	44.60	0.80
180	1118	A	43	R	6	57	59	615.59	31.80	46.50	1.72	1.18	2.53	53.50	1.15
180	1118	A	43	R	7	57	59	616.84	24.80	32.90	1.89	1.42	2.61	45.70	0.84
180	1118	A	44	R	3	17	19	621.02	26.20	35.50	1.84	1.36	2.57	47.10	0.89
180	1118	A	44	R	4	37	39	622.53	26.10	35.40	1.74	1.28	2.31	44.30	0.80
180	1118	A	44	R	5	86	88	624.32	27.00	37.10	1.85	1.35	2.64	48.80	0.95
180	1118	A	44	R	6	46	48	625.21	25.90	34.90	1.87	1.39	2.63	47.20	0.89
180	1118	A	44	R	7	3	5	625.88	25.90	35.00	1.87	1.39	2.63	47.30	0.90
180	1118	A	45	R	1	105	107	628.65	25.50	34.20	2.02	1.51	3.04	50.30	1.01
180	1118	A	45	R	2	76	78	629.71	25.90	34.90	1.88	1.39	2.64	47.40	0.90
180	1118	A	45	R	3	6	8	630.32	25.20	33.60	1.90	1.42	2.66	46.60	0.87
180	1118	A	45	R	4	4	6	631.48	24.80	32.90	1.91	1.44	2.67	46.20	0.86
180	1118	A	45	R	5	4	6	632.95	28.00	39.00	1.83	1.32	2.64	50.10	1.01
180	1118	A	45	R	6	4	6	633.68	23.90	31.40	2.00	1.52	2.85	46.60	0.87
180	1118	A	45	R	7	4	6	634.70	24.80	33.00	1.91	1.44	2.67	46.20	0.86

Table T13 (continued).

Leg	Site	Hole	Core	Type	Section	Top (cm)	Bottom (cm)	Depth (mbsf)	Water content (bulk)	Water content (dry)	Bulk density (g·cm⁻³)	Dry density (g·cm⁻³)	Grain density (g·cm⁻³)	Porosity (%)	Void ratio
180	1118	A	46	R	2	4	6	638.70	25.90	34.90	1.90	1.41	2.70	48.00	0.92
180	1118	A	46	R	3	2	4	640.11	25.60	34.50	1.90	1.42	2.70	47.60	0.91
180	1118	A	46	R	4	2	4	641.56	26.20	35.50	1.88	1.39	2.68	48.10	0.93
180	1118	A	46	R	5	2	4	642.78	23.30	30.40	1.96	1.50	2.71	44.50	0.80
180	1118	A	46	R	6	4	6	644.13	24.40	32.20	1.93	1.46	2.70	45.90	0.85
180	1118	A	46	R	7	4	6	645.43	25.90	35.00	1.91	1.42	2.75	48.40	0.94
180	1118	A	47	R	1	2	4	646.82	26.80	36.50	1.87	1.37	2.67	48.80	0.95
180	1118	A	47	R	2	2	4	648.30	23.10	30.00	1.93	1.49	2.63	43.60	0.77
180	1118	A	47	R	3	2	4	649.67	24.90	33.20	1.89	1.42	2.62	45.90	0.85
180	1118	A	47	R	4	2	4	651.15	22.80	29.60	1.95	1.50	2.66	43.40	0.77
180	1118	A	47	R	5	2	4	652.43	24.20	31.90	1.91	1.45	2.64	45.10	0.82
180	1118	A	47	R	6	2	4	653.68	24.70	32.70	1.90	1.43	2.65	45.80	0.85
180	1118	A	48	R	1	2	4	656.42	23.20	30.20	1.94	1.49	2.65	43.90	0.78
180	1118	A	48	R	2	2	4	657.81	23.60	30.90	1.93	1.48	2.67	44.60	0.81
180	1118	A	48	R	3	2	4	659.31	23.40	30.60	1.92	1.47	2.61	43.80	0.78
180	1118	A	48	R	4	2	4	660.53	25.50	34.30	1.89	1.40	2.65	47.00	0.89
180	1118	A	48	R	5	2	4	661.91	30.00	42.80	1.80	1.26	2.66	52.70	1.11
180	1118	A	49	R	1	2	4	666.02	24.30	32.10	1.92	1.45	2.66	45.40	0.83
180	1118	A	49	R	2	2	4	667.22	25.40	34.00	1.89	1.41	2.65	46.80	0.88
180	1118	A	50	R	1	2	4	675.62	31.90	46.80	1.76	1.20	2.65	54.80	1.21
180	1118	A	50	R	2	2	4	676.86	30.20	43.30	1.80	1.26	2.68	53.10	1.13
180	1118	A	50	R	3	2	4	678.22	29.30	41.50	1.81	1.28	2.66	51.90	1.08
180	1118	A	50	R	5	2	4	680.66	29.10	41.10	1.81	1.28	2.65	51.50	1.06
180	1118	A	51	R	1	11	13	685.41	30.10	43.00	1.76	1.23	2.55	51.70	1.07
180	1118	A	51	R	2	12	14	686.31	32.30	47.80	1.76	1.19	2.68	55.60	1.25
180	1118	A	51	R	3	28	30	687.77	29.20	41.30	1.81	1.28	2.66	51.70	1.07
180	1118	A	52	R	1	13	15	695.13	26.80	36.50	1.86	1.36	2.64	48.50	0.94
180	1118	A	53	R	1	17	19	704.87	28.70	40.30	1.82	1.30	2.65	51.10	1.04
180	1118	A	53	R	2	13	15	706.23	28.80	40.50	1.82	1.30	2.66	51.20	1.05
180	1118	A	54	R	1	39	41	714.79	31.10	45.10	1.77	1.22	2.62	53.60	1.16
180	1118	A	55	R	1	58	60	724.68	27.70	38.30	1.84	1.33	2.65	49.70	0.99
180	1118	A	55	R	2	16	18	725.13	29.80	42.40	1.79	1.26	2.62	52.10	1.09
180	1118	A	55	R	3	13	15	726.35	23.70	31.00	1.92	1.47	2.64	44.40	0.80
180	1118	A	56	R	1	52	54	734.32	29.00	40.90	1.81	1.29	2.64	51.30	1.06
180	1118	A	56	R	2	46	48	735.76	27.50	37.90	1.84	1.34	2.64	49.40	0.98
180	1118	A	56	R	3	45	47	737.22	28.00	38.90	1.84	1.32	2.65	50.20	1.01
180	1118	A	56	R	4	38	40	738.08	28.90	40.60	1.82	1.29	2.65	51.20	1.05
180	1118	A	56	R	5	44	46	739.59	27.90	38.70	1.83	1.32	2.64	49.90	1.00
180	1118	A	57	R	1	61	63	744.11	28.80	40.50	1.82	1.30	2.66	51.20	1.05
180	1118	A	57	R	2	62	64	745.44	29.10	41.00	1.80	1.28	2.62	51.20	1.05
180	1118	A	57	R	3	58	60	746.75	29.80	42.50	1.80	1.26	2.64	52.30	1.10
180	1118	A	57	R	4	34	36	747.98	25.70	34.60	1.87	1.39	2.62	47.00	0.89
180	1118	A	57	R	5	67	69	749.43	29.60	42.00	1.79	1.26	2.61	51.70	1.07
180	1118	A	58	R	1	17	19	753.27	29.00	40.90	1.82	1.29	2.66	51.50	1.06
180	1118	A	58	R	3	18	20	755.85	29.10	41.10	1.80	1.28	2.62	51.30	1.05
180	1118	A	58	R	4	16	18	756.97	29.90	42.70	1.80	1.26	2.67	52.70	1.12
180	1118	A	58	R	5	16	18	758.47	22.00	28.20	1.94	1.51	2.58	41.50	0.71
180	1118	A	58	R	6	91	93	760.72	27.50	37.90	1.80	1.30	2.52	48.20	0.93
180	1118	A	58	R	7	19	21	761.50	25.70	34.60	1.88	1.40	2.64	47.10	0.89

Table T13 (continued).

Leg	Site	Hole	Core	Type	Section	Top (cm)	Bottom (cm)	Depth (mbsf)	Water content (bulk)	Water content (dry)	Bulk density (g·cm^{-3})	Dry density (g·cm^{-3})	Grain density (g·cm^{-3})	Porosity (%)	Void ratio
180	1118	A	59	R	1	2	4	762.72	26.90	36.90	1.87	1.37	2.69	49.20	0.97
180	1118	A	59	R	2	2	4	764.01	21.80	28.00	1.98	1.55	2.67	42.20	0.73
180	1118	A	59	R	3	2	4	765.36	24.50	32.40	1.90	1.43	2.62	45.40	0.83
180	1118	A	59	R	4	2	4	766.82	24.70	32.70	2.32	1.75	3.95	55.80	1.26
180	1118	A	59	R	5	2	4	768.14	26.90	36.80	1.86	1.36	2.65	48.80	0.95
180	1118	A	59	R	6	2	4	769.64	24.90	33.10	1.89	1.42	2.62	45.80	0.85
180	1118	A	60	R	1	17	19	772.47	28.50	39.80	1.83	1.31	2.68	51.00	1.04
180	1118	A	60	R	2	6	8	773.72	22.00	28.20	1.96	1.53	2.63	41.90	0.72
180	1118	A	61	R	1	4	6	781.94	20.70	26.10	2.00	1.59	2.67	40.50	0.68
180	1118	A	61	R	2	4	6	783.22	28.90	40.60	1.83	1.30	2.68	51.50	1.06
180	1118	A	61	R	3	4	6	784.50	26.10	35.20	1.88	1.39	2.67	47.90	0.92
180	1118	A	62	R	1	3	5	791.53	26.80	36.70	1.80	1.32	2.50	47.30	0.90
180	1118	A	62	R	2	3	5	792.98	28.90	40.60	1.83	1.30	2.69	51.60	1.07
180	1118	A	62	R	3	3	5	794.15	28.80	40.40	1.83	1.31	2.69	51.50	1.06
180	1118	A	62	R	4	3	5	795.53	27.30	37.60	1.85	1.35	2.66	49.40	0.98
180	1118	A	63	R	1	2	4	801.12	24.50	32.40	1.92	1.45	2.68	45.90	0.85
180	1118	A	63	R	2	2	4	802.30	27.60	38.10	1.85	1.34	2.67	49.80	0.99
180	1118	A	63	R	3	2	4	803.66	28.10	39.10	1.84	1.32	2.68	50.60	1.02
180	1118	A	63	R	4	2	4	804.39	25.30	33.90	1.89	1.41	2.65	46.80	0.88
180	1118	A	63	R	5	2	4	805.52	28.20	39.30	1.81	1.30	2.59	49.90	1.00
180	1118	A	64	R	1	2	4	810.72	26.10	35.30	1.87	1.38	2.65	47.70	0.91
180	1118	A	64	R	2	2	4	812.22	25.60	34.40	1.89	1.41	2.66	47.20	0.89
180	1118	A	65	R	1	26	28	820.56	25.67	34.53	1.88	2.65	1.40	47.19	0.89
180	1118	A	65	R	2	26	28	821.99	24.88	33.11	1.89	2.63	1.42	45.98	0.85
180	1118	A	65	R	3	20	22	823.26	24.59	32.60	1.90	2.64	1.44	45.70	0.84
180	1118	A	65	R	4	27	29	824.65	26.59	36.21	1.86	2.63	1.36	48.20	0.93
180	1118	A	65	R	5	118	120	826.86	26.71	36.45	1.85	2.63	1.36	48.34	0.94
180	1118	A	65	R	6	45	47	827.63	26.95	36.90	1.84	2.61	1.34	48.44	0.94
180	1118	A	66	R	1	121	123	831.11	26.82	36.66	1.87	2.69	1.37	49.06	0.96
180	1118	A	66	R	2	126	128	832.66	22.76	29.46	1.96	2.68	1.51	43.56	0.77
180	1118	A	66	R	3	126	128	834.00	23.10	30.04	1.97	2.72	1.51	44.40	0.80
180	1118	A	66	R	4	127	129	835.37	25.17	33.64	1.91	2.70	1.43	46.99	0.89
180	1118	A	66	R	5	12	14	835.72	24.16	31.86	1.93	2.69	1.47	45.59	0.84
180	1118	A	67	R	1	45	47	840.05	25.31	33.88	1.90	2.67	1.42	46.91	0.88
180	1118	A	67	R	2	46	48	841.35	25.28	33.84	1.91	2.69	1.43	47.09	0.89
180	1118	A	67	R	3	43	45	842.82	24.26	32.03	1.94	2.73	1.47	46.07	0.85
180	1118	A	67	R	4	43	45	844.32	22.60	29.19	1.99	2.74	1.54	43.87	0.78
180	1118	A	67	R	5	48	50	845.21	21.38	27.19	2.04	2.79	1.60	42.54	0.74
180	1118	A	68	R	1	86	88	850.16	17.40	21.07	2.10	2.70	1.73	35.67	0.55
180	1118	A	68	R	2	91	93	851.66	16.33	19.52	2.14	2.72	1.79	34.13	0.52
180	1118	A	68	R	3	43	45	852.49	29.85	42.55	1.79	2.62	1.26	52.15	1.09
180	1118	A	68	R	4	27	29	853.83	7.69	8.33	2.42	2.73	2.23	18.17	0.22
180	1118	A	69	R	1	31	33	859.31	8.51	9.30	2.41	2.75	2.20	19.99	0.25
180	1118	A	69	R	3	40	42	862.37	8.91	9.78	2.38	2.73	2.17	20.70	0.26
180	1118	A	70	R	1	23	25	868.93	11.07	12.45	2.31	2.74	2.06	24.98	0.33
180	1118	A	71	R	1	83	85	879.23	0.35	0.35	2.93	2.95	2.92	0.99	0.01
180	1118	A	72	R	1	67	69	883.87	2.43	2.49	2.78	2.90	2.71	6.57	0.07
180	1118	A	73	R	1	52	54	888.42	0.80	0.80	2.87	2.91	2.85	2.23	0.02
180	1118	A	74	R	2	13	15	899.07	0.73	0.73	2.87	2.91	2.85	2.03	0.02

Note: This table is also available in ASCII format in the TABLES directory.

Table T14. Longitudinal (z) and transverse (x and y) velocities for cores, Site 1118. (**See table note.** Continued on next five pages.)

Leg	Site	Hole	Core	Type	Section	Top (cm)	Bottom (cm)	Depth (mbsf)	x-velocity (m·s⁻¹)	y-velocity (m·s⁻¹)	z-velocity (m·s⁻¹)
180	1118	A	3	R	CC	4	4	224.1	2275	2294	2254
180	1118	A	4	R	CC	14	14	233.8	1968	1950	1965
180	1118	A	5	R	CC	19	19	243.5	2073	2059	2065
180	1118	A	6	R	1	12	12	253.0	1851	1853	1835
180	1118	A	6	R	2	7	7	254.0	1941	1945	1870
180	1118	A	6	R	3	12	12	255.1	1894	1887	1876
180	1118	A	6	R	4	81	81	257.2	1750	1773	1712
180	1118	A	6	R	5	122	122	259.1	1918	1900	1834
180	1118	A	6	R	6	22	22	259.6	1946	1937	1854
180	1118	A	6	R	7	5	5	260.9	1817	1835	1789
180	1118	A	7	R	1	8	8	262.6	1805	1826	1750
180	1118	A	7	R	2	92	92	264.5	1790	1774	1793
180	1118	A	7	R	3	11	11	265.2	1799	1800	1809
180	1118	A	8	R	1	60	60	272.7	1852	1844	1857
180	1118	A	8	R	2	36	36	274.0	2004	1986	1937
180	1118	A	8	R	3	142	142	276.5	1838	1867	1857
180	1118	A	8	R	4	108	108	277.7	1839	1854	1846
180	1118	A	8	R	5	100	100	279.1	1852	1849	1844
180	1118	A	8	R	6	15	15	279.8	1793	1809	1832
180	1118	A	9	R	1	64	64	282.3	1882	1868	1918
180	1118	A	9	R	2	110	110	284.3	1842	1840	1834
180	1118	A	9	R	3	129	129	286.0	1771	1782	1805
180	1118	A	9	R	4	144	144	287.6	1910	1894	1883
180	1118	A	9	R	5	23	23	287.9	1998	2015	1983
180	1118	A	10	R	1	128	128	292.7	1818	1813	1858
180	1118	A	10	R	2	56	56	293.5	1825	1860	1871
180	1118	A	10	R	3	44	44	294.8	1817	1831	1844
180	1118	A	10	R	4	40	40	296.3	1840	1844	1873
180	1118	A	11	R	1	94	94	301.9	1870	1979	2011
180	1118	A	11	R	2	106	106	303.5	1843	1827	1853
180	1118	A	11	R	3	107	107	304.9	1847	1864	1888
180	1118	A	11	R	4	78	78	305.9	1854	1876	1928
180	1118	A	11	R	5	77	77	307.1	1906	1918	1936
180	1118	A	11	R	6	73	73	308.4	1874	1887	1894
180	1118	A	11	R	7	30	30	309.4	1863	1882	1885
180	1118	A	12	R	1	30	30	311.0	1964	1959	1981
180	1118	A	12	R	2	93	93	312.7	1899	1916	1908
180	1118	A	12	R	3	96	96	314.2	1847	1862	1873
180	1118	A	12	R	4	7	7	314.5	1896	1844	1910
180	1118	A	12	R	5	79	79	316.7	1827	1824	1857
180	1118	A	12	R	6	5	5	317.5	1816	1830	1851
180	1118	A	12	R	7	3	3	318.9	1868	1854	1850
180	1118	A	13	R	1	6	6	320.4	1890	1889	1922
180	1118	A	13	R	2	32	32	322.1	1833	1829	1848
180	1118	A	13	R	3	80	80	324.1	1919	1894	1941
180	1118	A	13	R	4	59	59	325.4	1857	1851	1849
180	1118	A	13	R	5	6	6	326.3	1848	1725	1848
180	1118	A	13	R	6	63	63	328.4	1856	1876	1900
180	1118	A	13	R	7	8	8	329.4	1822	1849	1843
180	1118	A	14	R	1	43	43	330.4	1870	1933	1899
180	1118	A	14	R	2	4	4	331.5	2022	2024	2049
180	1118	A	14	R	3	3	3	332.7	1937	1975	1990
180	1118	A	14	R	4	99	99	334.8	1843	1843	1845
180	1118	A	14	R	5	135	135	336.6	1948	1927	1954
180	1118	A	14	R	6	94	94	337.5	1907	1880	1888
180	1118	A	14	R	7	52	52	338.2	1874	1869	1853
180	1118	A	14	R	8	10	10	339.0	1880	1871	1848
180	1118	A	15	R	1	12	12	339.8	1949	1965	1994
180	1118	A	15	R	2	31	31	340.9	1955	1936	1945
180	1118	A	15	R	3	4	4	341.5	1891	1859	1851
180	1118	A	15	R	4	12	12	343.1	1871	1919	1869
180	1118	A	15	R	5	12	12	344.6	1950	1972	1929
180	1118	A	15	R	6	2	2	345.9	1872	1856	1849
180	1118	A	15	R	7	83	83	348.2	1850	1838	1780
180	1118	A	16	R	1	10	10	349.4	1839	1860	1849
180	1118	A	16	R	2	7	7	350.8	1879	1874	1894
180	1118	A	16	R	3	88	88	353.1	1849	1860	1877
180	1118	A	16	R	4	88	88	354.4	1839	1815	1823

Table T14 (continued).

Leg	Site	Hole	Core	Type	Section	Top (cm)	Bottom (cm)	Depth (mbsf)	x-velocity (m·s⁻¹)	y-velocity (m·s⁻¹)	z-velocity (m·s⁻¹)
180	1118	A	16	R	5	83	83	355.8	1948	1958	1918
180	1118	A	16	R	6	2	2	356.0	1805	1926	1913
180	1118	A	16	R	7	21	21	357.4	1858	1851	1871
180	1118	A	17	R	1	23	23	359.0	1800	1802	1778
180	1118	A	17	R	2	82	82	360.8	1841	1849	1852
180	1118	A	17	R	3	28	28	361.6	1796	1802	1810
180	1118	A	17	R	4	42	42	363.3	1823	1824	1853
180	1118	A	17	R	5	37	37	364.7	1831	1843	1832
180	1118	A	17	R	6	55	55	366.4	1808	1792	1804
180	1118	A	18	R	1	42	42	368.6	1808	1844	1854
180	1118	A	18	R	2	119	119	370.9	1812	1840	1869
180	1118	A	18	R	3	65	65	371.7	1773	1777	1786
180	1118	A	18	R	4	32	32	372.8	1802	1789	1835
180	1118	A	18	R	5	19	19	373.7	1827	1831	1879
180	1118	A	19	R	1	32	32	378.1	1818	1859	1838
180	1118	A	19	R	2	90	90	380.1	2146	2121	2013
180	1118	A	19	R	3	43	43	381.1	1827	1829	1853
180	1118	A	19	R	4	8	8	382.2	1801	1798	1798
180	1118	A	19	R	5	5	5	383.7	1866	1868	1839
180	1118	A	20	R	1	115	115	388.6	1906	1941	1931
180	1118	A	20	R	2	37	37	389.2	1950	1939	1950
180	1118	A	20	R	3	18	18	390.4	2199	2204	1994
180	1118	A	20	R	4	28	28	391.9	1930	1944	1911
180	1118	A	20	R	5	86	86	393.9	1925	1910	1901
180	1118	A	20	R	6	69	69	395.1	1837	1833	1805
180	1118	A	20	R	7	39	39	396.3	1822	1864	1705
180	1118	A	21	R	1	78	78	397.6	1847	1875	1837
180	1118	A	21	R	2	23	23	398.4	1847	1844	1812
180	1118	A	21	R	3	31	31	400.0	1820	1828	1822
180	1118	A	21	R	4	36	36	401.5	1825	1859	1834
180	1118	A	21	R	5	32	32	403.0	1925	1917	1911
180	1118	A	22	R	1	23	23	406.5	1947	1923	1834
180	1118	A	22	R	2	44	44	408.1	1928	1898	1834
180	1118	A	22	R	3	44	44	409.5	2064	2034	1970
180	1118	A	22	R	4	25	25	410.8	2074	2065	1978
180	1118	A	22	R	5	61	61	412.5	1962	1940	1965
180	1118	A	22	R	6	1	1	413.2	2005	2018	1914
180	1118	A	22	R	7	1	1	414.5	2006	2009	1991
180	1118	A	23	R	1	55	55	416.5	1945	1937	1944
180	1118	A	23	R	2	55	55	418.0	1932	2018	1902
180	1118	A	23	R	3	81	81	419.6	1976	1955	1917
180	1118	A	23	R	4	112	112	421.2	1988	2071	1978
180	1118	A	23	R	5	67	67	422.2	2055	2064	1967
180	1118	A	23	R	6	17	17	423.2	1922	1930	1954
180	1118	A	24	R	1	31	31	425.9	1942	1958	1925
180	1118	A	24	R	2	12	12	427.2	2040	2047	1994
180	1118	A	24	R	3	52	52	429.0	2023	2039	1964
180	1118	A	24	R	4	23	23	430.2	2225	2016	1949
180	1118	A	24	R	5	27	27	431.5	1980	1986	1930
180	1118	A	24	R	6	38	38	433.0	1963	1975	1934
180	1118	A	24	R	7	15	15	434.2	1886	1866	1870
180	1118	A	25	R	1	17	17	435.4	1890	1996	1864
180	1118	A	25	R	2	119	119	437.9	1852	1847	1875
180	1118	A	25	R	3	107	107	439.1	1863	1857	1853
180	1118	A	25	R	4	9	9	439.3	1923	1816	1860
180	1118	A	25	R	5	113	113	441.7	1819	1816	1805
180	1118	A	25	R	6	12	12	442.0	1961	1959	1936
180	1118	A	25	R	7	17	17	443.3	1871	1898	1890
180	1118	A	26	R	1	15	15	445.0	1916	1891	1775
180	1118	A	26	R	2	81	81	447.1	1984	1973	2037
180	1118	A	26	R	3	81	81	448.6	1924	1906	1916
180	1118	A	26	R	4	3	3	449.0	1979	1955	1935
180	1118	A	27	R	1	35	35	454.8	2002	2005	1978
180	1118	A	27	R	2	52	52	456.4	1917	1915	1871
180	1118	A	27	R	3	68	68	458.0	1938	1967	1839
180	1118	A	27	R	4	16	16	458.9	1901	1918	1895
180	1118	A	27	R	5	33	33	460.6	2092	2112	2039
180	1118	A	27	R	6	85	85	462.5	1959	1943	1826
180	1118	A	28	R	2	85	85	466.3	1975	1982	1928

Table T14 (continued).

Leg	Site	Hole	Core	Type	Section	Top (cm)	Bottom (cm)	Depth (mbsf)	x-velocity (m·s⁻¹)	y-velocity (m·s⁻¹)	z-velocity (m·s⁻¹)
180	1118	A	28	R	4	19	19	468.5	2033	2040	1965
180	1118	A	28	R	6	40	40	471.3	2042	2051	2002
180	1118	A	28	R	7	4	4	472.1	1909	1897	1914
180	1118	A	29	R	1	41	41	474.0	1843	1833	1815
180	1118	A	29	R	2	122	122	476.3	1873	1853	1847
180	1118	A	29	R	3	102	102	477.5	1888	1902	1850
180	1118	A	29	R	4	40	40	478.4	2043	2035	1975
180	1118	A	29	R	5	33	33	479.6	1940	1944	1867
180	1118	A	29	R	6	6	6	480.6	1976	1998	1865
180	1118	A	30	R	1	67	67	483.9	1904	1905	1852
180	1118	A	30	R	2	74	74	485.5	1981	1955	1922
180	1118	A	30	R	3	1	1	486.1	1989	1998	1939
180	1118	A	30	R	4	46	46	488.1	2072	2079	2027
180	1118	A	30	R	5	34	34	489.3	2039	2095	1975
180	1118	A	30	R	5	97	97	490.0	2105	2098	1960
180	1118	A	30	R	6	8	8	490.4	2668	2652	2167
180	1118	A	30	R	7	32	32	491.9	2006	2031	1931
180	1118	A	31	R	1	7	7	493.0	2115	2102	2015
180	1118	A	31	R	2	13	13	494.5	2053	2087	1978
180	1118	A	31	R	3	58	58	496.3	2013	1971	1953
180	1118	A	31	R	4	81	81	498.0	1973	1969	1901
180	1118	A	31	R	5	111	111	499.7	2069	2087	2025
180	1118	A	31	R	5	112	112	499.7	2205	2240	2089
180	1118	A	31	R	6	99	99	501.1	2008	2009	1974
180	1118	A	32	R	1	12	12	502.6	1992	2115	1963
180	1118	A	32	R	2	33	33	504.3	2009	2023	1955
180	1118	A	32	R	3	44	44	505.8	2037	2044	1986
180	1118	A	32	R	4	39	39	507.3	2101	2099	1939
180	1118	A	32	R	5	56	56	508.9	2092	2137	2035
180	1118	A	33	R	1	46	46	512.5	2100	2097	2030
180	1118	A	33	R	2	116	116	514.5	2156	2124	2062
180	1118	A	33	R	3	46	46	515.3	2120	2125	2089
180	1118	A	33	R	4	4	4	516.3	2316	2317	2047
180	1118	A	33	R	5	97	97	518.7	2019	2024	2027
180	1118	A	33	R	6	36	36	519.6	2150	2168	2081
180	1118	A	33	R	7	1	1	520.3	2015	2031	1988
180	1118	A	34	R	1	119	119	523.0	2478	2480	2092
180	1118	A	34	R	2	10	10	523.2	2248	2233	2140
180	1118	A	34	R	2	94	94	524.1	2153	2138	2199
180	1118	A	34	R	3	36	36	524.9	2060	2065	2023
180	1118	A	34	R	4	17	17	526.0	2108	2082	2009
180	1118	A	34	R	5	94	94	528.0	1952	1960	1916
180	1118	A	35	R	1	118	118	532.6	2164	2139	2086
180	1118	A	35	R	2	2	2	532.9	2253	2263	2131
180	1118	A	35	R	3	10	10	533.9	2051	2055	2027
180	1118	A	35	R	4	56	56	535.2	2039	2036	1990
180	1118	A	35	R	5	35	35	536.4	2031	2043	1976
180	1118	A	35	R	5	44	44	536.5	2225	2164	2079
180	1118	A	35	R	6	104	104	538.5	2066	2060	1944
180	1118	A	35	R	7	16	16	538.7	1963	1962	1913
180	1118	A	36	R	1	104	104	542.0	2167	2029	2189
180	1118	A	36	R	2	2	2	542.2	2056	2067	2005
180	1118	A	36	R	3	100	100	544.6	2166	2197	2093
180	1118	A	36	R	4	30	30	545.3	2197	2205	2055
180	1118	A	36	R	5	2	2	546.5	2268	2249	2099
180	1118	A	36	R	6	2	2	547.6	2114	2107	2055
180	1118	A	36	R	7	3.5	3.5	549.1	2116	2091	2009
180	1118	A	36	R	7	41	41	549.4	2064	2098	2026
180	1118	A	37	R	1	28	28	551.0	2268	2296	2296
180	1118	A	37	R	2	36	36	552.5	2016	2019	1881
180	1118	A	37	R	3	4	4	553.5	2166	2152	2053
180	1118	A	37	R	4	42	42	555.0	1989	1989	1928
180	1118	A	37	R	5	2	2	556.3	1986	1991	1983
180	1118	A	38	R	1	9	9	560.4	1956	1954	1930
180	1118	A	38	R	2	7	7	561.8	1991	2000	1951
180	1118	A	38	R	3	17	17	563.3	1974	1988	1915
180	1118	A	38	R	4	12	12	564.7	1987	1977	1941
180	1118	A	38	R	5	17.5	17.5	566.1	1969	1958	1937
180	1118	A	38	R	5	27	27	566.2	1988	1989	1926

Table T14 (continued).

Leg	Site	Hole	Core	Type	Section	Top (cm)	Bottom (cm)	Depth (mbsf)	x-velocity (m·s⁻¹)	y-velocity (m·s⁻¹)	z-velocity (m·s⁻¹)
180	1118	A	38	R	6	4	4	567.4	2007	2002	1929
180	1118	A	39	R	1	38	38	570.4	1941	1991	1987
180	1118	A	39	R	1	45	45	570.5	1993	1998	1949
180	1118	A	39	R	2	18	18	571.7	1978	1969	1908
180	1118	A	39	R	3	49	49	573.2	2110	2079	1978
180	1118	A	39	R	4	59	59	574.7	2117	2108	1985
180	1118	A	39	R	5	1	1	575.5	1923	1993	1937
180	1118	A	40	R	1	19	19	579.8	2026	2022	1984
180	1118	A	40	R	2	19	19	581.1	2168	2187	2045
180	1118	A	40	R	3	22	22	582.4	2017	1997	1988
180	1118	A	40	R	4	33	33	584.1	2034	2016	1948
180	1118	A	41	R	1	97	97	590.2	1915	1885	1913
180	1118	A	41	R	2	79	79	591.4	1938	1937	1841
180	1118	A	41	R	3	118	118	593.1	2094	2107	2040
180	1118	A	41	R	4	81	81	594.2	1948	1987	1925
180	1118	A	41	R	4	86	86	594.2	1950	1948	1919
180	1118	A	41	R	5	83	83	595.6	2045	2018	1927
180	1118	A	42	R	1	112	112	599.9	1986	1998	1958
180	1118	A	42	R	2	107	107	601.1	1921	1940	1886
180	1118	A	42	R	3	22	22	601.5	2413	2425	2177
180	1118	A	42	R	4	5	5	602.6	1937	1915	1884
180	1118	A	42	R	5	117	117	604.8	1950	1956	1923
180	1118	A	42	R	6	6	6	604.9	1971	1957	1893
180	1118	A	42	R	7	60	60	606.8	1929	1951	1893
180	1118	A	42	R	8	48	48	607.8	1945	1928	1886
180	1118	A	43	R	1	36	36	608.8	1915	1929	1876
180	1118	A	43	R	2	44	44	610.0	1918	1915	1864
180	1118	A	43	R	3	38	38	611.4	1945	1926	1892
180	1118	A	43	R	4	127	127	613.7	2601	2604	2315
180	1118	A	43	R	5	115	115	614.9	1999	1928	1916
180	1118	A	43	R	6	54	54	615.6	2015	2027	1945
180	1118	A	43	R	7	55	55	616.8	2028	2004	1916
180	1118	A	44	R	1	98	98	619.0	1997	1972	1974
180	1118	A	44	R	2	109	109	620.6	2521	2508	2267
180	1118	A	44	R	3	22	22	621.1	1958	1959	1888
180	1118	A	44	R	3	38	38	621.2	1971	1963	1882
180	1118	A	44	R	4	43	43	622.6	1949	1960	1903
180	1118	A	44	R	5	92	92	624.4	2117	1971	1919
180	1118	A	44	R	6	42	42	625.2	2029	2066	1932
180	1118	A	44	R	7	8	8	625.9	1998	1985	1952
180	1118	A	45	R	1	95	95	628.6	2048	2006	2001
180	1118	A	45	R	2	97	97	629.9	2039	2044	1971
180	1118	A	45	R	3	4	4	630.3	2022	1998	1935
180	1118	A	45	R	4	8	8	631.5	2220	2320	2049
180	1118	A	45	R	5	6	6	633.0	2200	2242	2084
180	1118	A	45	R	6	6	6	633.7	2085	2156	2050
180	1118	A	45	R	7	9	9	634.8	2056	2064	2026
180	1118	A	45	R	8	25	25	635.8	2050	2076	1921
180	1118	A	46	R	1	81	81	638.0	2130	2126	1991
180	1118	A	46	R	2	2	2	638.7	2036	2056	2016
180	1118	A	46	R	3	43	43	640.5	2033	2059	1995
180	1118	A	46	R	4	84	84	642.4	2154	2163	2060
180	1118	A	46	R	5	6	6	642.8	2003	1997	1961
180	1118	A	46	R	6	76	76	644.9	2022	2006	1913
180	1118	A	46	R	7	14	14	645.5	2039	2025	1955
180	1118	A	47	R	1	88	88	647.7	2051	2051	1977
180	1118	A	47	R	2	83	83	649.1	2632	2082	2016
180	1118	A	47	R	3	31	31	650.0	2678	2432	2476
180	1118	A	47	R	4	12	12	651.3	2030	2057	2009
180	1118	A	47	R	5	57	57	653.0	2134	2103	2091
180	1118	A	47	R	6	57	57	654.2	2286	2269	2089
180	1118	A	48	R	1	87	87	657.3	2421	2387	2176
180	1118	A	48	R	2	5	5	657.8	2116	2162	2034
180	1118	A	48	R	3	69	69	660.0	2218	2275	2064
180	1118	A	48	R	4	30	30	660.8	2190	2143	2169
180	1118	A	48	R	5	12	12	662.0	2128	2117	2046
180	1118	A	49	R	1	103	103	667.0	2177	2178	2057
180	1118	A	49	R	2	2	2	667.2	2099	2093	2031
180	1118	A	50	R	1	76	76	676.4	2032	1992	1910

Table T14 (continued).

Leg	Site	Hole	Core	Type	Section	Top (cm)	Bottom (cm)	Depth (mbsf)	x-velocity (m·s⁻¹)	y-velocity (m·s⁻¹)	z-velocity (m·s⁻¹)
180	1118	A	50	R	2	113	113	678.0	1831	1845	1797
180	1118	A	50	R	3	81	81	679.0	1955	1946	1854
180	1118	A	50	R	4	7	7	679.3	2040	2016	2018
180	1118	A	50	R	5	7	7	680.7	2024	2030	2034
180	1118	A	51	R	1	9	9	685.4	1990	1995	1940
180	1118	A	51	R	2	18	18	686.4	2026	2022	1913
180	1118	A	51	R	3	33	33	687.8	2044	2035	1969
180	1118	A	52	R	1	11	11	695.1	2079	2094	2042
180	1118	A	53	R	1	14	14	704.8	1970	1974	1934
180	1118	A	53	R	2	22	22	706.3	2033	2025	2029
180	1118	A	54	R	1	36	36	714.8	2030	2033	1935
180	1118	A	55	R	1	54	54	724.6	2019	2043	1943
180	1118	A	55	R	2	14	14	725.1	2070	2070	1989
180	1118	A	55	R	3	12	12	726.3	2086	2081	2017
180	1118	A	56	R	1	57	57	734.4	2085	2101	1991
180	1118	A	56	R	2	44	44	735.7	2076	2076	1987
180	1118	A	56	R	3	43	43	737.2	2103	2112	1986
180	1118	A	56	R	4	43	43	738.1	2081	2089	1981
180	1118	A	56	R	5	42	42	739.6	2121	2113	1998
180	1118	A	57	R	1	56	56	744.1	1954	2056	1978
180	1118	A	57	R	2	5	5	744.9	2107	2109	1992
180	1118	A	57	R	3	55	55	746.7	2071	2080	1973
180	1118	A	57	R	4	31	31	748.0	2003	2016	1938
180	1118	A	57	R	5	65	65	749.4	2084	2082	1959
180	1118	A	58	R	1	14	14	753.2	2069	2078	1993
180	1118	A	58	R	2	14	14	754.6	1990	2053	1945
180	1118	A	58	R	3	16	16	755.8	2020	2076	1959
180	1118	A	58	R	4	21	21	757.0	2031	2049	1961
180	1118	A	58	R	5	21	21	758.5	2131	2128	1988
180	1118	A	58	R	6	88	88	760.7	2043	2093	2021
180	1118	A	58	R	7	24	24	761.6	2024	2043	1943
180	1118	A	59	R	1	80	80	763.5	2112	2008	2117
180	1118	A	59	R	2	46	46	764.5	1982	1978	1929
180	1118	A	59	R	3	9	9	765.4	2083	2090	2010
180	1118	A	59	R	4	24	24	767.0	1956	1935	1921
180	1118	A	59	R	5	9	9	768.2	2076	2100	1992
180	1118	A	59	R	6	54	54	770.2	2099	2090	1958
180	1118	A	60	R	1	64	64	772.9	2186	2170	2001
180	1118	A	60	R	2	10	10	773.8	2229	2237	2089
180	1118	A	61	R	1	51	51	782.4	2224	2164	2185
180	1118	A	61	R	2	110	110	784.3	1773	1807	1817
180	1118	A	61	R	3	29	29	784.8	2101	2128	2060
180	1118	A	62	R	1	116	116	792.7	2132	2139	2021
180	1118	A	62	R	2	98	98	793.9	1903	1904	1879
180	1118	A	62	R	3	72	72	794.8	2080	2085	1978
180	1118	A	62	R	4	58	58	796.1	2086	2121	2017
180	1118	A	63	R	1	68	68	801.8	1955	2069	2082
180	1118	A	63	R	2	68	68	803.0	1956	1929	1904
180	1118	A	63	R	3	7	7	803.7	1767	2158	1975
180	1118	A	63	R	4	13	13	804.5	2157	2159	2066
180	1118	A	63	R	5	30	30	805.8	2121	2105	2079
180	1118	A	64	R	1	76	76	811.5	2111	2139	2032
180	1118	A	64	R	2	37	37	812.6	2167	2151	2082
180	1118	A	65	R	1	30	30	820.6	2187	2182	2042
180	1118	A	65	R	2	30	30	822.0	2189	2221	2079
180	1118	A	65	R	3	26	26	823.3	2167	2175	2069
180	1118	A	65	R	4	23	23	824.6	2198	2194	2078
180	1118	A	65	R	5	119	119	826.9	2150	2174	2053
180	1118	A	65	R	6	50	50	827.7	2187	2192	2082
180	1118	A	66	R	1	119	119	831.1	2237	2208	2119
180	1118	A	66	R	2	124	124	832.6	2236	2243	2232
180	1118	A	66	R	3	124	124	834.0	2280	2277	2126
180	1118	A	66	R	4	122	122	835.3	2219	2223	2168
180	1118	A	66	R	5	9	9	835.7	2242	2252	2172
180	1118	A	67	R	1	42	42	840.0	2229	2238	2127
180	1118	A	67	R	2	43	43	841.3	2233	2228	2149
180	1118	A	67	R	3	40	40	842.8	2226	2243	2199
180	1118	A	67	R	4	39	39	844.3	2313	2357	2278
180	1118	A	67	R	5	41	41	845.1	2332	2421	2311

Table T14 (continued).

Leg	Site	Hole	Core	Type	Section	Top (cm)	Bottom (cm)	Depth (mbsf)	x-velocity (m·s⁻¹)	y-velocity (m·s⁻¹)	z-velocity (m·s⁻¹)
180	1118	A	68	R	1	87	87	850.2	2394	2405	2341
180	1118	A	68	R	2	91	91	851.7	2377	2377	2363
180	1118	A	68	R	3	28	28	852.3	3158	2974	2854
180	1118	A	68	R	4	44	44	854.0	3223	3355	3314
180	1118	A	69	R	1	28	28	859.3	4652	4595	4415
180	1118	A	69	R	2	16	16	860.7	3742	3982	3769
180	1118	A	69	R	3	30	30	862.3	4294	5285	4950
180	1118	A	70	R	1	15	15	868.9	3861	3938	3776
180	1118	A	71	R	1	84	84	879.2	6068	6190	6190
180	1118	A	71	R	1	84	84	879.2	6068	6190	6190
180	1118	A	72	R	1	68	68	883.9	5407	5187	5354
180	1118	A	72	R	1	68	68	883.9	5407	5187	5354
180	1118	A	73	R	1	53	53	888.4	5676	5886	5904
180	1118	A	73	R	1	53	53	888.4	5676	5886	5904
180	1118	A	74	R	2	14	14	899.1	5912	6006	5944
180	1118	A	74	R	2	14	14	899.1	5912	6006	5944

Note: This table is also available in ASCII format in the **TABLES** directory.

Table T15. Thermal conductivity values in cores, Site 1118. (**See table note.** Continued on next five pages.)

Leg	Site	Hole	Core	Type	Section	Top interval (cm)	Bottom interval (cm)	Top depth (mbsf)	Bottom depth (mbsf)	Middle depth (mbsf)	Thermal conductivity (W·m^{-1}·°C^{-1})	Thermal conductivity average (W·m^{-1}·°C^{-1})
180	1118	A	3	R	CC	16	18	224.3	224.3	224.3	1.113	
180	1118	A	3	R	CC	16	18	224.3	224.3	224.3	1.105	1.11
180	1118	A	4	R	CC	17	19	233.9	233.9	233.9	1.307	
180	1118	A	4	R	CC	17	19	233.9	233.9	233.9	1.254	1.28
180	1118	A	5	R	CC	16	18	243.5	243.5	243.5	1.162	
180	1118	A	5	R	CC	16	18	243.5	243.5	243.5	1.138	1.15
180	1118	A	6	R	2	35	39	254.3	254.3	254.3	1.284	
180	1118	A	6	R	2	35	39	254.3	254.3	254.3	1.233	1.26
180	1118	A	6	R	4	20	22	256.6	256.6	256.6	1.148	
180	1118	A	6	R	4	20	22	256.6	256.6	256.6	1.261	
180	1118	A	6	R	4	20	22	256.6	256.6	256.6	1.251	1.22
180	1118	A	6	R	6	65	67	260.0	260.0	260.0	1.053	
180	1118	A	6	R	6	65	67	260.0	260.0	260.0	1.059	
180	1118	A	6	R	6	65	67	260.0	260.0	260.0	1.065	1.06
180	1118	A	7	R	1	3	5	262.5	262.6	262.5	1.086	
180	1118	A	7	R	1	3	5	262.5	262.6	262.5	0.934	1.01
180	1118	A	7	R	3	3	5	265.1	265.1	265.1	1.031	
180	1118	A	7	R	3	3	5	265.1	265.1	265.1	0.986	1.01
180	1118	A	8	R	2	44	46	274.0	274.1	274.1	1.155	
180	1118	A	8	R	2	44	46	274.0	274.1	274.1	1.154	1.15
180	1118	A	8	R	4	106	108	277.7	277.7	277.7	1.152	
180	1118	A	8	R	4	106	108	277.7	277.7	277.7	1.191	1.17
180	1118	A	8	R	6	5	7	279.7	279.7	279.7	1.029	
180	1118	A	8	R	6	5	7	279.7	279.7	279.7	0.993	1.01
180	1118	A	9	R	2	66	68	283.9	283.9	283.9	1.191	
180	1118	A	9	R	2	66	68	283.9	283.9	283.9	1.092	1.14
180	1118	A	9	R	4	130	132	287.5	287.5	287.5	1.036	
180	1118	A	9	R	4	130	132	287.5	287.5	287.5	1.010	1.02
180	1118	A	10	R	2	25	29	293.2	293.2	293.2	1.109	
180	1118	A	10	R	2	25	29	293.2	293.2	293.2	0.916	1.01
180	1118	A	10	R	4	59	61	296.5	296.5	296.5	1.066	
180	1118	A	10	R	4	59	61	296.5	296.5	296.5	1.081	1.07
180	1118	A	11	R	2	118	121	303.6	303.6	303.6	1.042	
180	1118	A	11	R	2	118	121	303.6	303.6	303.6	1.036	1.04
180	1118	A	11	R	4	32	37	305.4	305.5	305.4	1.105	
180	1118	A	11	R	4	32	37	305.4	305.5	305.4	1.006	1.06
180	1118	A	11	R	6	70	71	308.4	308.4	308.4	1.121	
180	1118	A	11	R	6	70	71	308.4	308.4	308.4	1.117	1.12
180	1118	A	12	R	2	103	110	312.8	312.9	312.8	1.064	
180	1118	A	12	R	2	103	110	312.8	312.9	312.8	1.074	1.07
180	1118	A	12	R	4	9	15	314.5	314.6	314.6	1.020	
180	1118	A	12	R	4	9	15	314.5	314.6	314.6	1.031	1.03
180	1118	A	12	R	6	8	15	317.5	317.6	317.5	1.043	
180	1118	A	12	R	6	8	15	317.5	317.6	317.5	1.010	1.03
180	1118	A	13	R	2	63	70	322.4	322.5	322.5	0.993	
180	1118	A	13	R	2	63	70	322.4	322.5	322.5	1.118	
180	1118	A	13	R	2	63	70	322.4	322.5	322.5	1.029	1.05
180	1118	A	13	R	4	3	8	324.8	324.9	324.8	1.177	
180	1118	A	13	R	4	3	8	324.8	324.9	324.8	1.014	1.10
180	1118	A	13	R	6	1	3	327.8	327.8	327.8	1.061	
180	1118	A	13	R	6	1	3	327.8	327.8	327.8	1.055	
180	1118	A	13	R	6	1	3	327.8	327.8	327.8	0.942	1.02
180	1118	A	14	R	2	2	8	331.5	331.6	331.6	1.079	
180	1118	A	14	R	2	2	8	331.5	331.6	331.6	1.240	1.16
180	1118	A	14	R	4	123	127	335.0	335.1	335.0	1.032	
180	1118	A	14	R	4	123	127	335.0	335.1	335.0	1.049	1.04
180	1118	A	14	R	6	9	18	336.7	336.8	336.7	1.038	
180	1118	A	14	R	6	9	18	336.7	336.8	336.7	1.001	1.02
180	1118	A	14	R	8	58	60	339.4	339.5	339.4	1.154	
180	1118	A	14	R	8	58	60	339.4	339.5	339.4	1.026	
180	1118	A	14	R	8	58	60	339.4	339.5	339.4	1.046	1.08
180	1118	A	15	R	2	37	38	340.9	340.9	340.9	1.019	
180	1118	A	15	R	2	37	38	340.9	340.9	340.9	0.984	1.00
180	1118	A	15	R	4	43	45	343.4	343.4	343.4	1.054	
180	1118	A	15	R	4	43	45	343.4	343.4	343.4	1.060	1.06
180	1118	A	15	R	6	17	20	346.0	346.1	346.0	1.053	

Table T15 (continued).

Leg	Site	Hole	Core	Type	Section	Top interval (cm)	Bottom interval (cm)	Top depth (mbsf)	Bottom depth (mbsf)	Middle depth (mbsf)	Thermal conductivity (W·m⁻¹·°C⁻¹)	Thermal conductivity average (W·m⁻¹·°C⁻¹)
180	1118	A	15	R	6	17	20	346.0	346.1	346.0	1.030	1.04
180	1118	A	16	R	2	102	105	351.7	351.8	351.7	1.121	
180	1118	A	16	R	2	102	105	351.7	351.8	351.7	1.083	1.10
180	1118	A	16	R	4	130	135	354.8	354.9	354.8	1.045	
180	1118	A	16	R	4	130	135	354.8	354.9	354.8	1.009	1.03
180	1118	A	16	R	6	11	16	356.1	356.2	356.2	1.144	
180	1118	A	16	R	6	11	16	356.1	356.2	356.2	1.212	1.18
180	1118	A	17	R	2	76	79	360.8	360.8	360.8	0.981	
180	1118	A	17	R	2	76	79	360.8	360.8	360.8	1.054	1.02
180	1118	A	17	R	4	126	129	364.1	364.2	364.1	1.118	
180	1118	A	17	R	4	126	129	364.1	364.2	364.1	1.150	1.13
180	1118	A	17	R	6	39	44	366.3	366.3	366.3	1.122	
180	1118	A	17	R	6	39	44	366.3	366.3	366.3	1.113	1.12
180	1118	A	18	R	2	46	49	370.2	370.2	370.2	1.164	
180	1118	A	18	R	2	46	49	370.2	370.2	370.2	1.127	1.15
180	1118	A	18	R	4	22	27	372.7	372.8	372.7	1.109	
180	1118	A	18	R	4	22	27	372.7	372.8	372.7	1.109	1.11
180	1118	A	19	R	2	19	24	379.4	379.4	379.4	1.152	
180	1118	A	19	R	2	19	24	379.4	379.4	379.4	1.127	1.14
180	1118	A	19	R	4	71	79	382.9	383.0	382.9	1.182	
180	1118	A	19	R	4	71	79	382.9	383.0	382.9	1.250	1.22
180	1118	A	20	R	2	33	39	389.1	389.2	389.1	1.046	
180	1118	A	20	R	2	33	39	389.1	389.2	389.1	1.115	1.08
180	1118	A	20	R	4	46	50	392.1	392.1	392.1	1.130	
180	1118	A	20	R	4	46	50	392.1	392.1	392.1	1.173	1.15
180	1118	A	20	R	6	93	99	395.3	395.4	395.4	1.107	
180	1118	A	20	R	6	93	99	395.3	395.4	395.4	0.910	1.01
180	1118	A	21	R	2	20	27	398.4	398.4	398.4	1.148	
180	1118	A	21	R	2	20	27	398.4	398.4	398.4	1.107	1.13
180	1118	A	21	R	4	75	79	401.9	402.0	401.9	1.037	
180	1118	A	21	R	4	75	79	401.9	402.0	401.9	1.027	1.03
180	1118	A	22	R	2	13	17	407.8	407.9	407.8	1.300	
180	1118	A	22	R	2	13	17	407.8	407.9	407.8	1.223	1.26
180	1118	A	22	R	4	6	8	410.6	410.6	410.6	1.108	
180	1118	A	22	R	4	6	8	410.6	410.6	410.6	1.068	1.09
180	1118	A	22	R	6	42	45	413.6	413.6	413.6	1.229	
180	1118	A	22	R	6	42	45	413.6	413.6	413.6	1.189	1.21
180	1118	A	23	R	2	4	7	417.4	417.5	417.5	1.159	
180	1118	A	23	R	2	4	7	417.4	417.5	417.5	1.147	1.15
180	1118	A	23	R	4	0	2	420.0	420.1	420.0	1.072	
180	1118	A	23	R	4	0	2	420.0	420.1	420.0	1.055	1.06
180	1118	A	23	R	6	0	5	423.0	423.1	423.1	1.181	
180	1118	A	23	R	6	0	5	423.0	423.1	423.1	1.213	
180	1118	A	23	R	6	0	5	423.0	423.1	423.1	1.186	1.19
180	1118	A	24	R	2	9	14	427.2	427.2	427.2	1.292	
180	1118	A	24	R	2	9	14	427.2	427.2	427.2	1.129	
180	1118	A	24	R	2	9	14	427.2	427.2	427.2	1.177	1.20
180	1118	A	24	R	4	21	27	430.2	430.3	430.2	1.220	
180	1118	A	24	R	4	21	27	430.2	430.3	430.2	1.136	1.18
180	1118	A	24	R	6	25	35	432.9	433.0	432.9	1.204	
180	1118	A	24	R	6	25	35	432.9	433.0	432.9	1.178	1.19
180	1118	A	24	R	1	36	40	426.0	426.0	426.0	1.172	
180	1118	A	24	R	1	36	40	426.0	426.0	426.0	1.210	1.19
180	1118	A	24	R	3	46	49	429.0	429.0	429.0	1.246	
180	1118	A	24	R	3	46	49	429.0	429.0	429.0	1.239	1.24
180	1118	A	24	R	5	29	31	431.5	431.5	431.5	1.150	
180	1118	A	24	R	5	29	31	431.5	431.5	431.5	1.111	1.13
180	1118	A	24	R	7	60	62	434.6	434.7	434.6	1.322	
180	1118	A	24	R	7	60	62	434.6	434.7	434.6	1.042	1.18
180	1118	A	25	R	2	33	38	437.0	437.1	437.1	1.052	
180	1118	A	25	R	2	33	38	437.0	437.1	437.1	1.009	1.03
180	1118	A	25	R	4	28	33	439.5	439.5	439.5	1.031	
180	1118	A	25	R	4	28	33	439.5	439.5	439.5	1.021	
180	1118	A	25	R	4	28	33	439.5	439.5	439.5	1.039	1.03
180	1118	A	25	R	6	13	16	442.0	442.1	442.1	1.135	
180	1118	A	25	R	6	13	16	442.0	442.1	442.1	1.167	1.15
180	1118	A	26	R	2	71	77	447.0	447.1	447.0	1.056	

Table T15 (continued).

Leg	Site	Hole	Core	Type	Section	Top interval (cm)	Bottom interval (cm)	Top depth (mbsf)	Bottom depth (mbsf)	Middle depth (mbsf)	Thermal conductivity (W·m⁻¹·°C⁻¹)	Thermal conductivity average (W·m⁻¹·°C⁻¹)
180	1118	A	26	R	2	71	77	447.0	447.1	447.0	1.077	1.07
180	1118	A	26	R	4	6	9	449.1	449.1	449.1	1.171	
180	1118	A	26	R	4	6	9	449.1	449.1	449.1	1.011	
180	1118	A	26	R	4	6	9	449.1	449.1	449.1	1.025	1.07
180	1118	A	26	R	3	65	71	448.5	448.5	448.5	1.075	
180	1118	A	26	R	3	65	71	448.5	448.5	448.5	1.113	1.09
180	1118	A	27	R	2	29	39	456.2	456.3	456.2	1.192	
180	1118	A	27	R	2	29	39	456.2	456.3	456.2	1.192	1.19
180	1118	A	27	R	4	52	59	459.3	459.3	459.3	1.086	
180	1118	A	27	R	4	52	59	459.3	459.3	459.3	1.074	1.08
180	1118	A	27	R	6	75	78	462.4	462.5	462.4	1.168	
180	1118	A	27	R	6	75	78	462.4	462.5	462.4	1.028	1.10
180	1118	A	27	R	1	7	11	454.5	454.5	454.5	1.153	
180	1118	A	27	R	1	7	11	454.5	454.5	454.5	1.114	1.13
180	1118	A	27	R	3	19	26	457.5	457.5	457.5	1.155	
180	1118	A	27	R	3	19	26	457.5	457.5	457.5	1.135	1.15
180	1118	A	27	R	5	7	15	460.3	460.4	460.3	1.148	
180	1118	A	27	R	5	7	15	460.3	460.4	460.3	1.160	
180	1118	A	27	R	5	7	15	460.3	460.4	460.3	1.146	1.15
180	1118	A	28	R	2	50	57	465.9	466.0	465.9	1.055	
180	1118	A	28	R	2	50	57	465.9	466.0	465.9	1.081	1.07
180	1118	A	28	R	4	55	59	468.8	468.9	468.9	1.084	
180	1118	A	28	R	4	55	59	468.8	468.9	468.9	1.033	1.06
180	1118	A	28	R	6	28	34	471.1	471.2	471.2	1.207	
180	1118	A	28	R	6	28	34	471.1	471.2	471.2	1.224	1.22
180	1118	A	29	R	2	44	51	475.5	475.6	475.5	1.115	
180	1118	A	29	R	2	44	51	475.5	475.6	475.5	1.075	1.10
180	1118	A	29	R	4	50	56	478.5	478.5	478.5	1.208	
180	1118	A	29	R	4	50	56	478.5	478.5	478.5	1.201	1.20
180	1118	A	29	R	6	51	57	481.1	481.1	481.1	0.931	
180	1118	A	29	R	6	51	57	481.1	481.1	481.1	1.116	1.02
180	1118	A	30	R	2	120	125	485.9	486.0	485.9	1.181	
180	1118	A	30	R	2	120	125	485.9	486.0	485.9	1.167	1.17
180	1118	A	30	R	4	51	57	488.1	488.2	488.1	1.228	
180	1118	A	30	R	4	51	57	488.1	488.2	488.1	1.170	1.20
180	1118	A	30	R	6	107	114	491.4	491.5	491.5	1.277	
180	1118	A	30	R	6	107	114	491.4	491.5	491.5	1.274	1.28
180	1118	A	31	R	2	70	79	495.0	495.1	495.1	1.161	
180	1118	A	31	R	2	70	79	495.0	495.1	495.1	1.178	1.17
180	1118	A	31	R	4	79	86	498.0	498.1	498.0	1.233	
180	1118	A	31	R	4	79	86	498.0	498.1	498.0	1.221	1.23
180	1118	A	31	R	6	0	12	500.1	500.2	500.2	1.201	
180	1118	A	31	R	6	0	12	500.1	500.2	500.2	1.224	1.21
180	1118	A	32	R	2	124	132	505.2	505.3	505.3	1.204	
180	1118	A	32	R	2	124	132	505.2	505.3	505.3	1.223	1.21
180	1118	A	32	R	4	139	144	508.3	508.3	508.3	1.219	
180	1118	A	32	R	4	139	144	508.3	508.3	508.3	1.239	1.23
180	1118	A	33	R	2	0	7	513.4	513.4	513.4	1.231	
180	1118	A	33	R	2	0	7	513.4	513.4	513.4	1.224	1.23
180	1118	A	33	R	4	136	144	517.6	517.7	517.7	1.231	
180	1118	A	33	R	4	136	144	517.6	517.7	517.7	1.361	
180	1118	A	33	R	4	136	144	517.6	517.7	517.7	1.329	1.31
180	1118	A	33	R	6	100	107	520.3	520.3	520.3	1.099	
180	1118	A	33	R	6	100	107	520.3	520.3	520.3	1.105	1.10
180	1118	A	34	R	2	10	17	523.2	523.3	523.3	1.118	
180	1118	A	34	R	2	10	17	523.2	523.3	523.3	1.128	1.12
180	1118	A	34	R	4	21	25	526.0	526.1	526.1	1.426	
180	1118	A	34	R	4	21	25	526.0	526.1	526.1	1.167	
180	1118	A	34	R	4	21	25	526.0	526.1	526.1	1.143	1.25
180	1118	A	34	R	6	1	3	528.5	528.5	528.5	1.247	
180	1118	A	34	R	6	1	3	528.5	528.5	528.5	1.108	1.18
180	1118	A	35	R	2	67	73	533.5	533.6	533.5	1.214	
180	1118	A	35	R	2	67	73	533.5	533.6	533.5	1.114	1.16
180	1118	A	35	R	4	6	12	534.7	534.7	534.7	1.192	
180	1118	A	35	R	4	6	12	534.7	534.7	534.7	1.169	1.18
180	1118	A	35	R	6	10	18	537.6	537.7	537.6	1.209	
180	1118	A	35	R	6	10	18	537.6	537.7	537.6	1.200	1.20

Table T15 (continued).

Leg	Site	Hole	Core	Type	Section	Top interval (cm)	Bottom interval (cm)	Top depth (mbsf)	Bottom depth (mbsf)	Middle depth (mbsf)	Thermal conductivity (W·m^{-1}·°C^{-1})	Thermal conductivity average (W·m^{-1}·°C^{-1})
180	1118	A	36	R	2	81	85	543.0	543.0	543.0	1.076	
180	1118	A	36	R	2	81	85	543.0	543.0	543.0	1.116	1.10
180	1118	A	36	R	4	27	31	545.2	545.3	545.2	1.077	
180	1118	A	36	R	4	27	31	545.2	545.3	545.2	1.100	1.09
180	1118	A	36	R	6	8	13	547.7	547.7	547.7	1.115	
180	1118	A	36	R	6	8	13	547.7	547.7	547.7	1.103	1.11
180	1118	A	37	R	2	2	10	552.2	552.2	552.2	1.165	
180	1118	A	37	R	2	2	10	552.2	552.2	552.2	1.142	1.15
180	1118	A	37	R	4	2	10	555.0	555.1	555.0	1.190	
180	1118	A	37	R	4	2	10	555.0	555.1	555.0	1.182	1.19
180	1118	A	37	R	1	18	22	550.9	550.9	550.9	1.147	
180	1118	A	37	R	1	18	22	550.9	550.9	550.9	1.149	1.15
180	1118	A	37	R	3	5	9	553.5	553.6	553.6	1.155	
180	1118	A	37	R	3	5	9	553.5	553.6	553.6	1.118	1.14
180	1118	A	38	R	2	137	141	563.1	563.1	563.1	1.249	
180	1118	A	38	R	2	137	141	563.1	563.1	563.1	1.173	1.21
180	1118	A	38	R	4	48	52	565.0	565.1	565.1	1.263	
180	1118	A	38	R	4	48	52	565.0	565.1	565.1	1.129	1.20
180	1118	A	38	R	6	21	27	567.6	567.7	567.6	1.171	
180	1118	A	38	R	6	21	27	567.6	567.7	567.6	1.198	1.18
180	1118	A	39	R	1	5	9	570.1	570.1	570.1	1.120	
180	1118	A	39	R	1	5	9	570.1	570.1	570.1	1.099	1.11
180	1118	A	39	R	3	35	41	573.1	573.2	573.1	1.194	
180	1118	A	39	R	3	35	41	573.1	573.2	573.1	1.182	1.19
180	1118	A	39	R	5	34	39	575.8	575.9	575.9	1.268	
180	1118	A	39	R	5	34	39	575.8	575.9	575.9	1.151	1.21
180	1118	A	39	R	6	9	14	577.0	577.1	577.0	1.205	
180	1118	A	39	R	6	9	14	577.0	577.1	577.0	1.201	1.20
180	1118	A	40	R	2	15	20	581.1	581.2	581.1	1.213	
180	1118	A	40	R	2	15	20	581.1	581.2	581.1	1.194	1.20
180	1118	A	40	R	4	32	37	584.0	584.1	584.1	1.132	
180	1118	A	40	R	4	32	37	584.0	584.1	584.1	1.192	1.16
180	1118	A	41	R	2	119	126	591.8	591.8	591.8	1.178	
180	1118	A	41	R	2	119	126	591.8	591.8	591.8	1.161	1.17
180	1118	A	41	R	4	102	108	594.4	594.5	594.4	1.214	
180	1118	A	41	R	4	102	108	594.4	594.5	594.4	1.220	1.22
180	1118	A	41	R	6	0	8	596.3	596.4	596.4	1.231	
180	1118	A	41	R	6	0	8	596.3	596.4	596.4	1.159	1.20
180	1118	A	42	R	2	41	46	600.4	600.5	600.5	1.231	
180	1118	A	42	R	2	41	46	600.4	600.5	600.5	1.213	1.22
180	1118	A	42	R	4	9	16	602.7	602.7	602.7	1.152	
180	1118	A	42	R	4	9	16	602.7	602.7	602.7	1.147	1.15
180	1118	A	42	R	6	24	34	605.1	605.2	605.1	1.156	
180	1118	A	42	R	6	24	34	605.1	605.2	605.1	1.084	1.12
180	1118	A	42	R	8	0	6	607.4	607.4	607.4	1.254	
180	1118	A	42	R	8	0	6	607.4	607.4	607.4	1.237	1.25
180	1118	A	43	R	2	33	38	609.9	609.9	609.9	1.320	
180	1118	A	43	R	2	33	38	609.9	609.9	609.9	1.262	
180	1118	A	43	R	2	33	38	609.9	609.9	609.9	1.252	1.28
180	1118	A	43	R	4	11	19	612.5	612.6	612.6	1.199	
180	1118	A	43	R	4	11	19	612.5	612.6	612.6	1.216	1.21
180	1118	A	43	R	6	24	34	615.3	615.4	615.3	1.171	
180	1118	A	43	R	6	24	34	615.3	615.4	615.3	1.184	1.18
180	1118	A	44	R	2	97	107	620.5	620.6	620.5	1.127	
180	1118	A	44	R	2	97	107	620.5	620.6	620.5	1.163	1.15
180	1118	A	44	R	4	81	89	623.0	623.1	623.0	1.107	
180	1118	A	44	R	4	81	89	623.0	623.1	623.0	1.128	1.12
180	1118	A	44	R	6	20	26	625.0	625.0	625.0	1.181	
180	1118	A	44	R	6	20	26	625.0	625.0	625.0	1.170	1.18
180	1118	A	45	R	2	74	80	629.7	629.8	629.7	1.086	
180	1118	A	45	R	2	74	80	629.7	629.8	629.7	1.085	1.09
180	1118	A	45	R	4	20	26	631.6	631.7	631.7	1.033	
180	1118	A	45	R	4	20	26	631.6	631.7	631.7	1.064	1.05
180	1118	A	45	R	6	20	29	633.8	633.9	633.9	1.197	
180	1118	A	45	R	6	20	29	633.8	633.9	633.9	1.207	1.20
180	1118	A	45	R	8	56	61	636.1	636.2	636.1	1.209	
180	1118	A	45	R	8	56	61	636.1	636.2	636.1	1.172	1.19

Table T15 (continued).

Leg	Site	Hole	Core	Type	Section	Top interval (cm)	Bottom interval (cm)	Top depth (mbsf)	Bottom depth (mbsf)	Middle depth (mbsf)	Thermal conductivity (W·m^{-1}·°C^{-1})	Thermal conductivity average (W·m^{-1}·°C^{-1})
180	1118	A	46	R	2	6	10	638.7	638.8	638.7	1.138	
180	1118	A	46	R	2	6	10	638.7	638.8	638.7	1.077	1.11
180	1118	A	46	R	4	20	26	641.7	641.8	641.8	1.207	
180	1118	A	46	R	4	20	26	641.7	641.8	641.8	1.203	1.21
180	1118	A	46	R	6	22	26	644.3	644.4	644.3	1.185	
180	1118	A	46	R	6	22	26	644.3	644.4	644.3	1.132	
180	1118	A	46	R	6	22	26	644.3	644.4	644.3	1.161	1.16
180	1118	A	47	R	2	19	21	648.5	648.5	648.5	1.055	
180	1118	A	47	R	2	19	21	648.5	648.5	648.5	1.117	1.09
180	1118	A	47	R	4	2	5	651.2	651.2	651.2	1.207	
180	1118	A	47	R	4	2	5	651.2	651.2	651.2	1.204	1.21
180	1118	A	47	R	6	91	94	654.6	654.6	654.6	1.106	
180	1118	A	47	R	6	91	94	654.6	654.6	654.6	1.063	1.08
180	1118	A	47	R	1	75	79	647.6	647.6	647.6	1.183	
180	1118	A	47	R	1	75	79	647.6	647.6	647.6	1.162	1.17
180	1118	A	48	R	1	134	139	657.7	657.8	657.8	1.142	
180	1118	A	48	R	1	134	139	657.7	657.8	657.8	1.125	1.13
180	1118	A	48	R	3	97	102	660.3	660.3	660.3	1.106	
180	1118	A	48	R	3	97	102	660.3	660.3	660.3	1.065	
180	1118	A	48	R	3	97	102	660.3	660.3	660.3	1.101	1.09
180	1118	A	48	R	5	50	55	662.4	662.4	662.4	1.288	
180	1118	A	48	R	5	50	55	662.4	662.4	662.4	1.203	1.25
180	1118	A	49	R	1	6	10	666.1	666.1	666.1	1.041	
180	1118	A	49	R	1	6	10	666.1	666.1	666.1	1.092	1.07
180	1118	A	49	R	2	17	22	667.4	667.4	667.4	1.073	
180	1118	A	49	R	2	17	22	667.4	667.4	667.4	1.018	1.05
180	1118	A	50	R	2	76	80	677.6	677.6	677.6	0.954	
180	1118	A	50	R	2	76	80	677.6	677.6	677.6	0.936	0.95
180	1118	A	50	R	4	8	16	679.4	679.4	679.4	1.162	
180	1118	A	50	R	4	8	16	679.4	679.4	679.4	1.175	1.17
180	1118	A	51	R	2	21	27	686.4	686.5	686.4	1.038	
180	1118	A	51	R	2	21	27	686.4	686.5	686.4	1.063	1.05
180	1118	A	51	R	3	52	57	688.0	688.1	688.0	0.994	
180	1118	A	51	R	3	52	57	688.0	688.1	688.0	0.952	0.97
180	1118	A	51	R	1	31	34	685.6	685.6	685.6	1.123	
180	1118	A	51	R	1	31	34	685.6	685.6	685.6	1.144	1.13
180	1118	A	52	R	1	0	6	695.0	695.1	695.0	0.933	
180	1118	A	52	R	1	0	6	695.0	695.1	695.0	0.903	0.92
180	1118	A	53	R	1	0	12	704.7	704.8	704.8	1.086	
180	1118	A	53	R	1	0	12	704.7	704.8	704.8	1.078	1.08
180	1118	A	53	R	2	26	37	706.4	706.5	706.4	1.118	
180	1118	A	53	R	2	26	37	706.4	706.5	706.4	1.131	1.12
180	1118	A	54	R	1	68	80	715.1	715.2	715.1	1.051	
180	1118	A	54	R	1	68	80	715.1	715.2	715.1	1.033	1.04
180	1118	A	55	R	1	4	11	724.1	724.2	724.2	1.057	
180	1118	A	55	R	1	4	11	724.1	724.2	724.2	1.092	1.07
180	1118	A	55	R	3	1	9	726.2	726.3	726.3	1.054	
180	1118	A	55	R	3	1	9	726.2	726.3	726.3	1.061	1.06
180	1118	A	56	R	2	10	20	735.4	735.5	735.5	1.102	
180	1118	A	56	R	2	10	20	735.4	735.5	735.5	1.109	
180	1118	A	56	R	2	10	20	735.4	735.5	735.5	1.104	1.11
180	1118	A	56	R	4	26	38	738.0	738.1	738.0	1.174	
180	1118	A	56	R	4	26	38	738.0	738.1	738.0	1.191	1.18
180	1118	A	57	R	2	0	15	744.8	745.0	744.9	1.149	
180	1118	A	57	R	2	0	15	744.8	745.0	744.9	1.156	1.15
180	1118	A	57	R	4	0	10	747.6	747.7	747.7	1.101	
180	1118	A	57	R	4	0	10	747.6	747.7	747.7	1.131	1.12
180	1118	A	58	R	2	52	66	755.0	755.1	755.0	1.257	
180	1118	A	58	R	2	52	66	755.0	755.1	755.0	1.212	1.23
180	1118	A	58	R	4	120	134	758.0	758.2	758.1	1.282	
180	1118	A	58	R	4	120	134	758.0	758.2	758.1	1.228	
180	1118	A	58	R	4	120	134	758.0	758.2	758.1	1.241	1.25
180	1118	A	58	R	6	78	86	760.6	760.7	760.6	1.137	
180	1118	A	58	R	6	78	86	760.6	760.7	760.6	1.154	1.15
180	1118	A	59	R	2	48	51	764.5	764.5	764.5	1.139	
180	1118	A	59	R	2	48	51	764.5	764.5	764.5	1.110	1.12
180	1118	A	59	R	4	75	82	767.6	767.6	767.6	1.157	

Table T15 (continued).

Leg	Site	Hole	Core	Type	Section	Top interval (cm)	Bottom interval (cm)	Top depth (mbsf)	Bottom depth (mbsf)	Middle depth (mbsf)	Thermal conductivity (W·m⁻¹·°C⁻¹)	Thermal conductivity average (W·m⁻¹·°C⁻¹)
180	1118	A	59	R	4	75	82	767.6	767.6	767.6	1.153	1.16
180	1118	A	60	R	1	1	5	772.3	772.4	772.3	1.155	
180	1118	A	60	R	1	1	5	772.3	772.4	772.3	1.102	1.13
180	1118	A	61	R	1	30	40	782.2	782.3	782.3	1.128	
180	1118	A	61	R	1	30	40	782.2	782.3	782.3	1.126	1.13
180	1118	A	61	R	2	22	27	783.4	783.5	783.4	1.096	
180	1118	A	61	R	2	22	27	783.4	783.5	783.4	1.092	1.09
180	1118	A	61	R	3	90	97	785.4	785.4	785.4	1.085	
180	1118	A	61	R	3	90	97	785.4	785.4	785.4	1.155	1.12
180	1118	A	62	R	1	8	12	791.6	791.6	791.6	0.955	
180	1118	A	62	R	1	8	12	791.6	791.6	791.6	0.958	0.96
180	1118	A	62	R	3	67	70	794.8	794.8	794.8	1.065	
180	1118	A	62	R	3	67	70	794.8	794.8	794.8	1.085	1.08
180	1118	A	63	R	4	0	4	804.4	804.4	804.4	1.192	
180	1118	A	63	R	4	0	4	804.4	804.4	804.4	1.081	1.14
180	1118	A	63	R	2	72	74	803.0	803.0	803.0	1.103	
180	1118	A	63	R	2	72	74	803.0	803.0	803.0	1.013	1.06
180	1118	A	64	R	2	33	37	812.5	812.6	812.6	1.165	
180	1118	A	64	R	2	33	37	812.5	812.6	812.6	1.139	1.15
180	1118	A	65	R	2	79	92	822.5	822.7	822.6	1.197	
180	1118	A	65	R	2	79	92	822.5	822.7	822.6	1.193	1.20
180	1118	A	65	R	4	119	130	825.6	825.7	825.6	1.223	
180	1118	A	65	R	4	119	130	825.6	825.7	825.6	1.133	
180	1118	A	65	R	4	119	130	825.6	825.7	825.6	1.200	
180	1118	A	65	R	4	119	130	825.6	825.7	825.6	1.208	1.19
180	1118	A	66	R	2	116	122	832.6	832.6	832.6	1.107	
180	1118	A	66	R	2	116	122	832.6	832.6	832.6	1.176	
180	1118	A	66	R	2	116	122	832.6	832.6	832.6	1.145	1.16
180	1118	A	66	R	4	67	79	834.8	834.9	834.8	1.208	
180	1118	A	66	R	4	67	79	834.8	834.9	834.8	1.180	1.19
180	1118	A	67	R	2	55	64	841.4	841.5	841.5	1.195	
180	1118	A	67	R	2	55	64	841.4	841.5	841.5	1.136	
180	1118	A	67	R	2	55	64	841.4	841.5	841.5	1.177	1.17
180	1118	A	67	R	4	30	38	844.2	844.3	844.2	1.163	
180	1118	A	67	R	4	30	38	844.2	844.3	844.2	1.217	1.19
180	1118	A	68	R	1	27	34	849.6	849.6	849.6	1.386	
180	1118	A	68	R	1	27	34	849.6	849.6	849.6	1.360	1.37
180	1118	A	68	R	2	84	91	851.6	851.7	851.6	1.305	
180	1118	A	68	R	2	84	91	851.6	851.7	851.6	1.368	1.34
180	1118	A	68	R	3	75	85	852.8	852.9	852.9	1.381	
180	1118	A	68	R	3	75	85	852.8	852.9	852.9	1.422	1.40
180	1118	A	68	R	4	48	54	854.0	854.1	854.1	2.045	
180	1118	A	68	R	4	48	54	854.0	854.1	854.1	1.982	
180	1118	A	68	R	4	48	54	854.0	854.1	854.1	1.971	2.00
180	1118	A	69	R	1	49	56	859.5	859.6	859.5	1.830	
180	1118	A	69	R	1	49	56	859.5	859.6	859.5	1.855	
180	1118	A	69	R	1	49	56	859.5	859.6	859.5	1.850	1.85
180	1118	A	69	R	3	53	62	862.5	862.6	862.5	1.862	
180	1118	A	69	R	3	53	62	862.5	862.6	862.5	1.800	1.83
180	1118	A	70	R	1	67	72	869.4	869.4	869.4	1.584	
180	1118	A	70	R	1	67	72	869.4	869.4	869.4	1.566	1.58
180	1118	A	71	R	1	2	7	878.4	878.5	878.4	1.443	
180	1118	A	71	R	1	2	7	878.4	878.5	878.4	1.735	1.59
180	1118	A	72	R	1	3	8	883.2	883.3	883.3	1.410	
180	1118	A	72	R	1	3	8	883.2	883.3	883.3	1.544	1.48
180	1118	A	73	R	1	61	66	888.5	888.6	888.5	1.977	
180	1118	A	73	R	1	61	66	888.5	888.6	888.5	1.808	
180	1118	A	73	R	1	61	66	888.5	888.6	888.5	1.900	
180	1118	A	73	R	1	61	66	888.5	888.6	888.5	1.941	1.91
180	1118	A	74	R	1	85	90	898.4	898.4	898.4	1.909	
180	1118	A	74	R	1	85	90	898.4	898.4	898.4	2.004	
180	1118	A	74	R	1	85	90	898.4	898.4	898.4	2.003	1.97
180	1118	A	74	R	3	14	22	900.6	900.7	900.6	1.595	
180	1118	A	74	R	3	14	22	900.6	900.7	900.6	1.937	
180	1118	A	74	R	3	14	22	900.6	900.7	900.6	1.859	1.80

Note: This table is also available in ASCII format in the TABLES directory.

Table T16. Summary of logging operations, Site 1118.

	Logging		Mudline depth (mbrf)		Pipe depth (mbsf)		Logged interval (mbsf)	
Run	Tool string	Pass	Drill pipe	Wireline	Drill pipe	Wireline	Bottom	Top
1	Triple combo	Down	2315.4	2315.5	98.6	102.6	891.1	–94
1	Triple combo	Up	2315.4	2311.4	98.6	99.6	891.1	–67
2	FMS-sonic	Up 1	2315.4	2313.9	98.6		892	799.7
2	FMS-sonic	Up 2	2315.4	2313.7	98.6	98.4	891.4	66.9

Table T17. Break times, transit times, depths, and interval velocities for each station occupied during the VSP experiment.

Station	Depth (mbsf)	Hydrophone break time (ms)	Geophone break time (ms)	Transit time (ms)	Interval velocity (m·s⁻¹)
20	121.0	73.72	1685.57	1611.85	1732.2
19	146.1	73.73	1700.07	1626.34	1672.2
18	176.1	73.70	1717.98	1644.28	1806.1
17	206.1	73.67	1734.56	1660.89	1949.3
16	236.1	73.61	1749.89	1676.28	1857.6
15	266.1	72.73	1765.16	1692.43	1808.3
14	296.1	72.76	1781.78	1709.02	1914.5
13	326.1	72.69	1797.38	1724.69	1789.3
12	356.0	74.44	1815.84	1741.40	1921.8
11	386.0	74.60	1831.61	1757.01	1856.9
10	416.1	76.50	1849.72	1773.22	1903.6
9	446.1	75.39	1864.37	1788.98	2455.0
8	476.1	76.24	1877.44	1801.20	1570.4
7	505.2	75.26	1894.99	1819.73	4013.0
6	536.1	76.51	1903.94	1827.43	1505.0
5	566.2	76.51	1923.94	1847.43	1934.0
4	596.1	76.42	1939.31	1862.89	1929.3
3	626.1	76.40	1954.84	1878.44	2953.9
2	656.2	75.54	1964.17	1888.63	1959.5
1	686.1	75.44	1979.33	1903.89	

Table T18. A comparison of VSP check-shot data with depth estimates derived from physical properties and logging measurements.

VSP depth (mbsf)	VSP TWT* (ms)	VSP TWT† (ms bsf)	Predicted depth (m)	Error (m)
121.1	3232.6	140.6	120.95	–0.05
146.1	3261.6	169.6	145.84	–0.26
176.1	3297.5	205.5	177.45	1.35
206.1	3330.7	238.7	207.58	1.48
236.1	3361.4	269.4	238.81	2.71
266.1	3393.7	301.7	267.00	3.90
296.1	3426.9	334.9	301.33	5.23
326.1	3458.2	366.2	331.48	5.38
356.0	3491.6	399.6	363.37	7.37
386.0	3522.8	430.8	393.05	7.05
416.1	3555.2	463.2	425.09	8.99
446.1	3586.7	494.7	455.90	9.80
476.1	3611.1	519.1	479.80	3.70
505.2	3648.2	556.2	517.55	12.35
536.1	3663.5	571.6	533.75	–2.35
566.2	3703.6	611.6	576.03	9.83
596.1	3734.5	642.5	608.90	12.80
626.1	3765.5	673.5	641.34	15.24
656.2	3785.9	693.9	662.94	6.74
686.1	3816.4	724.4	694.44	8.34

Notes: * = VSP transit time corrected for the geometry of the experiment, and converted to two-way traveltime (TWT) for direct comparison to the MCS data. † = VSP transit time converted to two-way time below seafloor (bsf). Predicted depth is calculated from the velocity-depth function derived from physical properties and logging measurements.